



THE THERMAL CONE PENETRATION TEST POTENTIALS IN SOIL INVESTIGATION

Kevin Emmanuel Alain Berthet





MSc in Geo-Engineering

MSc thesis

“The Thermal Cone Penetration Test Potentials in Soil Investigation”

Kevin Emmanuel Alain Berthet

4748948

Delft University of Technology

Geo-Engineering

Dr Ir. P.J. Vardon

TU Delft

Dr Ir. W. Broere

TU Delft

Ir. K. Reinders

TU Delft

Dr Ir. M. Murali

Fugro

Preface

This thesis is written as the final requirement of the Master Science, Civil Engineering Geo-Engineering at the Technical University of Delft. The research was conducted in 8 and a half months from February to October 2019, with the collaboration between the Technical University of Delft and Fugro Offshore Nederland B.V. The supervision research project was led by Dr Ir. P.J. Vardon, Dr Ir. W. Broere and Ir. K. J. Reinders from the Technical University of Delft, and by Dr. Ir. M. Murali from Fugro.

Fugro is one of the world's leading service providers with high experience in acquisition and interpretations of geological, geophysical and geotechnical data necessary for designing building in the safest and most sustainable, efficient manner offshore as well as onshore projects.

The research described in this thesis report proposed one of the first steps undertaken in the research of the potentials of temperature sensor added on Cone Penetrometer. With the rapid growth of offshore wind turbine projects and geothermal projects, more insight is requested in thermal soil engineering parameters. Previous research proved the potential of the Thermal Cone Penetrometer Test to determine the thermal conductivity and initial temperature of soils through temperature decay tests (Akrouch *et al.*, 2016; Vardon *et al.*, 2018). This project aims to investigate the possible potentials of the T-CPT to improve soil characterisation during site investigation.

The research project would not have been achievable without the help received from different persons. First, I would like to thank my committee for helping with precious guidance and important recommendations. Secondly, I would like to address a particular acknowledgement to the project chairman, Associate Professor Phil Vardon, for his involvement and the high interest he showed in supervising this project. Thirdly, I would like to thank especially Dr Ir. W. Broere for his time, his scientific knowledge and the precise observations he provided along with the research project. Finally, I would like to thank Dr Ir. M. Murali for introducing and supervising me as well as J. Peuchen and all the people I interacted with during this project at Fugro.

Most importantly, none of this could have been achieved without my family and friends. Especially to my parents and my sister, it would be an understatement to say that, as a family. Every time I doubted, they did not let me give up and I am extremely grateful for their unconditional support. This research project stands as a testament to your unconditional encouragement and devotion.

Abstract

The widely used cone penetration test (CPT) allows in-situ measurements of soil behaviour during continuous penetration. The traditional sensors incorporated in a cone penetrometer are for measuring cone resistance, sleeve friction, pore pressure, and inclination. Many supplementary sensors have been studied and tried in research settings and in practice. Examples are sensors for natural gamma radiation, electrical resistivity and time domain reflectometry. None have made it to routine practice.

As an introduction to the thermal cone penetration test, this thesis presents a review of CPT add-on sensors that (1) allow continuous penetration at 20 mm/s, (2) considered robust, i.e. have no external moving parts, (3) offer potential for broad geotechnical value, i.e. not limited to special applications only. The review considers recent advances in electronics, sensor technology, and data processing systems.

The Thermal Cone Penetration test (T-CPT) was introduced by Akrouch (2016) using temperature decay test to determine the soil thermal conductivity. An improved interpretation model was proposed by Vardon (2018) and validated via an in-situ testing programme (Vardon *et al.*, 2018). The T-CPT records temperature variations during continuous penetration depending on different factors such as soil type (grain size), soil strength, and thermal properties of soils. In this report, the potentials of the thermal cone penetration test prototype developed and used by Fugro are investigated during continuous penetration conditions in order to determine the possible dependencies between the soil engineering properties and the T-CPT measurements.

Table of Contents

| | |
|--|----------|
| THE THERMAL CONE PENETRATION TEST POTENTIALS IN SOIL INVESTIGATION | I |
| PREFACE..... | IV |
| ABSTRACT..... | V |
| TABLE OF CONTENTS..... | VI |
| LIST OF FIGURES..... | X |
| LIST OF TABLES..... | XIII |
| LIST OF APPENDICES..... | XIV |
| LIST OF ABBREVIATIONS..... | XV |
| 1. INTRODUCTION | 1 |
| 1.1. General Introduction | 1 |
| 1.2. Motivations | 1 |
| 1.3. Project Relevance | 1 |
| 1.4. Research Question and Objectives Statement | 2 |
| 1.5. Research Approach and Strategy | 2 |
| 1.5.1. Introduction | 2 |
| 1.5.2. Research approach..... | 3 |
| 1.5.3. Research strategy..... | 3 |
| 1.6. Reading The Report | 4 |
| 2. STATE OF THE ART OF THE CONE PENETRATION TEST..... | 5 |
| 2.1. Introduction | 5 |
| 2.2. CPTu Principle..... | 5 |
| 2.3. Add-On Sensors Table | 9 |

| | |
|---|-----------|
| 3. LITERATURE REVIEW | 12 |
| 3.1. Literature Review Introduction..... | 12 |
| 3.2. Mechanical Principles Occurring During Cone Penetration | 12 |
| 3.2.1. Failure mechanisms in clay & sand | 12 |
| 3.2.2. Thinly layered soil influences on the cone resistance, q_c , recorded during CPT | 17 |
| 3.2.3. General mechanical interactions between the cone penetrometer and the soil | 20 |
| 3.3. Thermal Principles Occurring During Cone Penetration | 24 |
| 3.3.1. General introduction of the thermal soil properties | 24 |
| 3.3.2. Correlations between thermal soil properties, soil type and porosity | 25 |
| 3.3.3. General thermal interactions between the cone penetrometer and the soil | 28 |
| 3.4. Thermal Tests Introductions | 29 |
| 3.4.1. Thermal probe test equipment and test procedure | 29 |
| 3.4.2. T-CPT equipment and test procedure | 30 |
| 3.5. Temperature Decay Tests Interpretation models | 30 |
| 3.5.1. Akrouh proposed temperature decay interpretation model | 30 |
| 3.5.2. Vardon proposed temperature decay interpretation model | 31 |
| 3.6. Literature Review Summary | 33 |
| 4. RESEARCH METHODOLOGY | 34 |
| 4.1. Introduction | 34 |
| 4.1.1. Aims | 34 |
| 4.1.2. Investigations programme | 34 |
| 4.2. Simplified Solution | 35 |
| 4.2.1. Assumptions used for the simplified solution | 35 |
| 4.2.2. Proposed simplified solution | 35 |
| 4.2.3. Simplified solution sensitivity analysis | 37 |
| 4.3. Research Methodology Workflow | 38 |
| 4.3.1. Numerical investigation workflows | 38 |
| 4.3.2. Database analysis workflow | 40 |
| 5. NUMERICAL MODELLING INVESTIGATION | 41 |
| 5.1. General Introduction | 41 |
| 5.2. 2D Axisymmetric FEM Comsol Model | 41 |
| 5.2.1. 2D FE simplified model | 42 |
| 5.2.2. Numerical analysis programme | 43 |
| 5.3. Temperature Features Dependencies Investigations | 44 |
| 5.3.1. Sensitivity analysis programme | 44 |

| | | |
|-------------|---|-----------|
| 5.3.2. | Heat source estimation | 44 |
| 5.3.3. | Cone tip temperature dependencies observations | 46 |
| 5.3.4. | Cone temperature sensitivity analysis conclusions | 53 |
| 5.4. | T-CPT Temperature Behaviour Investigations In Thinly-Layered Soil | 55 |
| 5.4.1. | Thinly layered soil investigation programme | 55 |
| 5.4.2. | Sand/Clay multi-layer system investigation observations | 58 |
| 5.4.3. | Multi-layer system conclusions..... | 60 |
| 5.5. | Numerical Modelling Investigation Conclusions | 61 |
| 5.5.1. | Sensitivity analyses conclusions | 61 |
| 5.5.2. | Soil parameters prediction potential | 61 |
| 5.5.3. | T-CPT Thin-layered soil detection & characterisation potential | 61 |
| 6. | DATABASE ANALYSIS | 62 |
| 6.1. | Hollandse Kust Noord Project..... | 62 |
| 6.2. | Fugro Site Investigation | 62 |
| 6.2.1. | Geological setting..... | 65 |
| 6.2.2. | HKN Wind Farm Zone soil units | 65 |
| 6.3. | Database Research | 67 |
| 6.3.1. | General database research introduction | 67 |
| 6.3.2. | Available In-Situ & Laboratory tests database used | 67 |
| 6.3.3. | Database analysis methodology | 68 |
| 6.4. | Database Analysis Results & Interpretations | 71 |
| 6.4.1. | T-CPT initial temperature gradient, $\nabla(T)_{\text{initial}}$: | 71 |
| 6.4.2. | T-CPT maximum temperature difference, $\Delta(T)_{\text{max}}$: | 73 |
| 6.4.3. | $\Delta(T)_{\text{max}}$ vs Laboratory tests | 75 |
| 6.4.4. | $\Delta(T)_{\text{max}}$ vs SCPT | 78 |
| 6.5. | Additional Database Analysis | 79 |
| 6.5.1. | T-CPT initial temperature gradient, $\nabla(T)_{\text{initial}}$: | 79 |
| 6.5.2. | T-CPT maximum cone tip temperature difference, $\Delta(T)_{\text{max}}$: | 81 |
| 6.5.3. | Maximum cone tip temperature vs Particle Size Distribution: | 82 |
| 6.6. | Database Analyses Conclusions | 83 |
| 7. | DISCUSSION..... | 86 |
| 7.1. | Numerical Modelling Investigation..... | 86 |
| 7.1.1. | Sensitivity analysis of homogenous soil | 86 |
| 7.1.2. | Multi-layer model | 86 |
| 7.1.3. | FE numerical model limitations | 87 |
| 7.2. | Database Analysis..... | 88 |

| | | |
|---------------|---|-----|
| 8. | CONCLUSIONS & RECOMMENDATIONS | 90 |
| 8.1. | Conclusions On The T-CPT Potentials & Limitations | 90 |
| 8.2. | Recommendations & Future Work | 91 |
| 8.2.1. | Recommendations for future numerical modelling investigations | 91 |
| 8.2.2. | Recommendations on the database results | 91 |
| 9. | REFERENCES | 92 |
| APPENDIX I | ADD-ON SENSORS FOR CONE PENETRATION TESTING | 99 |
| APPENDIX II | THERMAL SOIL ENGINEERING PARAMETER VALUES IN FUNCTION OF THE SOIL TYPE & SOIL POROSITY ACCORDING TO FAROUKI (1981) | 116 |
| APPENDIX III | SIMPLIFIED CONE TIP / SOIL HEAT TRANSFER ANALYTICAL SOLUTION | 118 |
| APPENDIX IV | HKN SITE T-CPT PROFILES | 119 |
| APPENDIX V | $\nabla(T)_{\text{INITIAL}}$ VS Q_T REGRESSION RESIDUALS INVESTIGATION | 131 |
| APPENDIX VI | $\nabla(T)_{\text{INITIAL}}$ VS F_S REGRESSION RESIDUALS INVESTIGATION | 134 |
| APPENDIX VII | $\Delta(T)_{\text{MAX}}$ VS Q_T REGRESSION RESIDUALS INVESTIGATION | 137 |
| APPENDIX VIII | $\Delta(T)_{\text{MAX}}$ VS F_S REGRESSION RESIDUALS INVESTIGATION | 142 |
| APPENDIX IX | $\Delta(T)_{\text{MAX}}$ VS LABORATORY & SCPT TESTS REGRESSION INVESTIGATION | 147 |
| APPENDIX X | $\Delta(T)_{\text{MAX}}$ VS LABORATORY TESTS REGRESSION INVESTIGATION FROM ADDITIONAL DATABASE | 151 |
| APPENDIX XI | CONC TIP RESISTANCE, Q_T , VS PARTICLE SIZE DISTRIBUTION | 154 |
| APPENDIX XII | SLEEVE FRICTION, F_S , VS PARTICLE SIZE DISTRIBUTION | 155 |

List of Figures

| | |
|--|----|
| Figure 1: Piezocone penetrometer layout (Tom Lunne, Peter K. Robertson, 1997)..... | 5 |
| Figure 2: Cone manufacturing and operating tolerances (Conshohocken, 1996) | 6 |
| Figure 3: Penetrometer design configurations: (a) Electronic Friction-type, (b) Type 1 Piezocone, (c) Standard 10-cm ² Type 2 Piezocone, and (d) 15-cm ² Type 2 (Conshohocken, 1996) | 6 |
| Figure 4: Soil disturbance during cone penetration (Silva and Bolton, 2004) adapted from Muromachi work (Muromachi, 1981)..... | 13 |
| Figure 5: Typical failure surfaces for sand and clay | 13 |
| Figure 6: Sand displacement under cone penetration from Arshad's work (2014) | 14 |
| Figure 7: Failure surface development (Lubking, 1997)..... | 15 |
| Figure 8: Failure shape features in sand in function of the cone diameter and the internal friction angle based on Prandtl's theory (Douwes Dekker, 1984)..... | 16 |
| Figure 9: Relative density & Horizontal stress effects on the cone tip resistance (Houlsby and Hitchman, 1988)..... | 16 |
| Figure 10: Flasher bed deposit example (van der Linden, 2016)..... | 17 |
| Figure 11: Compilation of penetration analyses for dense sand layers ($D_R = 90\%$) of different thicknesses interbedded in soft clay ($s_u = 20$ kPa) from Ahmadi (2005)..... | 18 |
| Figure 12: Compilation of penetration analyses for loose sand layers ($D_R = 30\%$) of different thicknesses interbedded in soft clay ($s_u = 150$ kPa) from Ahmadi (2005)..... | 19 |
| Figure 13: Mechanical cone penetrometer & soil interaction | 20 |
| Figure 14: Particle size effect on the interface friction angle for a rusted steel interface, after Han et al.(2018) | 21 |
| Figure 15: Interface roughness effect on the interface friction angle at critical state after Han et al.(2018): | 22 |
| Figure 16: critical-state friction angle ratio δ_{cs}/ϕ_{cs} vs mean particle size D_{50} for uniform sands and graded sands after Han et al.(2018)..... | 22 |
| Figure 17: Computed thermal conductivities & volumetric heat capacities as a function of the soil density, Vardon (2019)..... | 26 |

| | |
|--|----|
| Figure 18: Volumetric heat capacity vs thermal conductivity (Vardon, 2019)..... | 26 |
| Figure 19: Thermal interaction between the cone tip and the soil | 28 |
| Figure 20: Thermal needle probe (left) & T-CPT cone penetrometer (right) from Vardon (2018) | 29 |
| Figure 21: Sensitivity analysis performed on the simplified solution..... | 37 |
| Figure 22: Cone tip temperature features numerical investigation workflow | 38 |
| Figure 23: Cone tip temperature behaviour in thinly layered soils workflow | 39 |
| Figure 24: Database analysis workflow | 40 |
| Figure 25: Model simplified geometry..... | 42 |
| Figure 26: Estimated heat source, H_s , as a function of the cone resistance, q_c , with applying a low δ/ϕ ratio of 0.60 in green, a median δ/ϕ ratio of 0.65 in black, and a high δ/ϕ ratio of 0.70 in red, and with assuming the ϕ increasing with the cone resistance | 45 |
| Figure 27: Temperature behaviour for different Sand/Clay fraction | 47 |
| Figure 28: Temperature behaviour for different Sand/Clay fraction | 47 |
| Figure 29: Temperature behaviour for different Sand/Clay fraction | 48 |
| Figure 30: Temperature behaviour for pure sand, $q_c = 5$ MPa and mean δ/ϕ ratio value = 0.65 .. | 49 |
| Figure 31: Temperature behaviour for pure sand, $q_c = 10$ MPa and mean δ/ϕ ratio value = 0.65 | 49 |
| Figure 32: Temperature behaviour for pure sand, $q_c = 30$ MPa and mean δ/ϕ ratio value = 0.65 | 50 |
| Figure 33: Interface friction angle uncertainty effect..... | 51 |
| Figure 34: Interface friction angle uncertainty effect..... | 51 |
| Figure 35: Interface friction angle uncertainty effect..... | 52 |
| Figure 36: Maximum temperature difference vs cone resistance for different Sand/Clay fraction & fixed porosity, $n = 0.4$ and mean δ/ϕ ratio value = 0.65 | 54 |
| Figure 37: Maximum temperature difference vs cone resistance for pure sand and mean δ/ϕ ratio value = 0.65 | 54 |
| Figure 38: Multi-layers system thermal behaviour 8 cm Sand/Clay..... | 58 |

| | |
|--|----|
| Figure 39: Multi-layers system thermal behaviour 15 cm Sand/Clay..... | 59 |
| Figure 40: Multi-layers system thermal behaviour 30 cm Sand/Clay..... | 59 |
| Figure 41: HKN site overview & site location (Fugro Netherlands Marine, 2019)..... | 62 |
| Figure 42: T-CPT profile example | 68 |
| Figure 43: HKN21 T-CPT profile & investigation markers | 69 |
| Figure 44: $\nabla(T)_{\text{initial}}$ vs q_t plot | 72 |
| Figure 45: $\nabla(T)_{\text{initial}}$ vs f_s plot | 72 |
| Figure 46: $\Delta(T)_{\text{max}}$ vs q_t plot..... | 74 |
| Figure 47 $\Delta(T)_{\text{max}}$ vs f_s plot | 74 |
| Figure 48: $\Delta(T)_{\text{max}}$ vs D_{50} | 76 |
| Figure 49: $\Delta(T)_{\text{max}}$ vs D_{60} | 76 |
| Figure 50: $\Delta(T)_{\text{max}}$ vs Clay Percentage | 77 |
| Figure 51: $\Delta(T)_{\text{max}}$ vs Sand Percentage | 77 |
| Figure 52: $\Delta(T)_{\text{max}}$ vs Small Strain Shear Modulus G_0 obtained from SCPT | 78 |
| Figure 53: $\nabla(T)_{\text{initial}}$ vs q_t for the additional database | 79 |
| Figure 54: $\nabla(T)_{\text{initial}}$ vs f_s for the additional database | 80 |
| Figure 55: $\Delta(T)_{\text{max}}$ vs q_t for the additional database..... | 81 |
| Figure 56: $\Delta(T)_{\text{max}}$ vs f_s for the additional database | 81 |
| Figure 57: $\Delta(T)_{\text{max}}$ vs D_{50} for the additional database | 82 |
| Figure 58: $\Delta(T)_{\text{max}}$ vs D_{60} for the additional database | 82 |
| Figure 59: $\Delta(T)_{\text{max}}$ plotted on Robertson's SBT Chart..... | 83 |

List of Tables

| | |
|--|----|
| Table 1: Perceived applicability of CPTu for deriving engineering soil parameters | 7 |
| Table 2: Thermal properties of soil components at 20°C and 1 atm (Wijk, 1963) | 24 |
| Table 3: Parameters used for uniform layer system investigation | 56 |
| Table 4: Parameters used for multi-layer system investigation | 57 |
| Table 5: HKN Wind Farm Zone In-Situ test programme (Netherlands Enterprise Agency, 2019) | 63 |
| Table 6: HKN Wind Farm Zone Laboratory test programme (Netherlands Enterprise Agency, 2019)..... | 64 |
| Table 7: HKN Wind Farm Zone soil units stratigraphy from Fugro Report (Fugro Netherlands Marine, 2019) | 66 |
| Table 8: $\Delta(T)_{\max}$ vs Particle Size Distribution regression results..... | 75 |
| Table 9: $\Delta(T)_{\max}$ vs Soil Type Percentage regression results | 75 |
| Table 10: Temperature features & CPT measurements (q_t, f_s) correlations summary | 84 |
| Table 11: T-CPT measurements & soil parameters direct correlations summary | 84 |
| Table 12: Comparison of the observed correlation between mean grain size, the temperature measurements and the classical CPT measurements..... | 88 |
| Table 13: Regression analyses between mean grain size, the temperature measurements and the classical CPT measurements for the HKN site | 89 |

List of Appendices

| | | |
|---------------|--|-----|
| APPENDIX I | ADD-ON SENSORS FOR CONE PENETRATION TESTING | 99 |
| APPENDIX II | THERMAL SOIL ENGINEERING PARAMETER VALUES IN FUNCTION OF THE SOIL TYPE & SOIL POROSITY ACCORDING TO FAROUKI (1981) | 116 |
| APPENDIX III | SIMPLIFIED CONE TIP / SOIL HEAT TRANSFER ANALYTICAL SOLUTION | 118 |
| APPENDIX IV | HKN SITE T-CPT PROFILES | 119 |
| APPENDIX V | $\nabla(T)_{\text{INITIAL}}$ VS Q_T REGRESSION RESIDUALS INVESTIGATION | 131 |
| APPENDIX VI | $\nabla(T)_{\text{INITIAL}}$ VS F_S REGRESSION RESIDUALS INVESTIGATION | 134 |
| APPENDIX VII | $\Delta(T)_{\text{MAX}}$ VS Q_T REGRESSION RESIDUALS INVESTIGATION | 137 |
| APPENDIX VIII | $\Delta(T)_{\text{MAX}}$ VS F_S REGRESSION RESIDUALS INVESTIGATION | 142 |
| APPENDIX IX | $\Delta(T)_{\text{MAX}}$ VS LABORATORY & SCPT TESTS REGRESSION INVESTIGATION..... | 147 |
| APPENDIX X | $\Delta(T)_{\text{MAX}}$ VS LABORATORY TESTS REGRESSION INVESTIGATION FROM ADDITIONAL DATABASE | 151 |
| APPENDIX XI | CONC TIP RESISTANCE, Q_T , VS PARTICLE SIZE DISTRIBUTION | 154 |
| APPENDIX XII | SLEEVE FRICTION, F_S , VS PARTICLE SIZE DISTRIBUTION..... | 155 |

List of Abbreviations

CPT:

Cone Penetration Test.

CPTu:

Cone Penetration Test with pore water pressure measurement, piezocone test.

T-CPT:

Cone Penetration Test with cone tip temperature measurement, temperature decay test.

Cone resistance, q_c :

The force acting on the cone, Q_c , divided by the projected area of the cone, A_c .

Corrected cone resistance, q_t :

The cone resistance q_c corrected for pore water pressure effect:

$$q_t = q_c + u_2 (1 - a_n)$$

Cone area ratio, a_n :

The ratio between the cross-sectional area of the cell or shaft, A_n , and the projected area of the cone, A_c :

$$a_n = \frac{A_n}{A_c}$$

Sleeve friction, f_s :

The frictional force acting on the friction sleeve, F_s , divided by the sleeve friction surface area, A_s :

$$f_s = \frac{F_s}{A_s}$$

Net cone resistance, q_n :

The total vertical stress, σ_{v0} , subtracted from the corrected cone resistance, q_t :

$$q_n = q_t - \sigma_{v0}$$

Net pore pressure, Δ_u :

The equilibrium pore pressure, u_0 , subtracted from the measured pore pressure, u_2 :

$$\Delta_u = u_2 - u_0$$

Normalised cone resistance, Q_t :

The cone resistance expressed in a non-dimensional form, and taking into account of the stress changes in-situ:

$$Q_t = \left(\frac{q_t - \sigma_{v0}}{\sigma'_{v0}} \right)$$

Normalised cone resistance, Q_{tn} :

The cone resistance expressed in a non-dimensional form, and taking into account the stress changes in-situ, and where the stress exponent (n) varies with soil type:

$$Q_{tn} = \left(\frac{q_t - \sigma_{v0}}{P_{a2}} \right) \left(\frac{P_a}{\sigma'_{v0}} \right)^n$$

$$n = 0.381 \cdot I_c + 0.05 \cdot \left(\frac{\sigma'_{v0}}{p_a} \right) - 0.15$$

Pore pressure, u_1 , u_2 and u_3 :

u_1 : measured on the cone

u_2 : measured just behind the cone

u_3 : measured just behind the sleeve friction.

Pore pressure ratio, B_q :

The net pore pressure normalised to the net cone resistance, q_n :

$$B_q = \frac{\Delta_u}{q_n}$$

Friction ratio, R_f :

The ratio between the sleeve friction, f_s , and the corrected cone resistance, q_t , expressed as a percentage:

$$R_f = \left(\frac{f_s}{q_t} \right) * 100\%$$

1. Introduction

1.1. General Introduction

Geotechnical engineers use many different tests, in-situ as well as in laboratory to derive engineering soil parameters important for safe and efficient design of structures. The **Cone Penetration Test (CPT)** is the most used soil in-situ test around the world. Its success is due to its reliability, low disturbances to the site (not significantly destructive compared to borehole), low operation cost and fast execution. In the past decades, a great number of CPT add-on sensors have been implemented in order to derive other engineering soil parameters, most of them did not make it to routine practice. The piezo-cone penetrometer test (CPTu) is the only add-on sensor which made it to routine practice. Recently, a new add-on sensor has been introduced by Fugro. A temperature sensor is incorporated in the cone tip. The research was carried out on the derivation of the thermal conductivity of soil during halted penetration of the cone penetrometer and by analysing the temperature decay of the soil tested. The method has been proposed and validated by Vardon (2018). More recent research proved the similar process was not applicable for the heat capacity determination of soil.

1.2. Motivations

This research aims to investigate the temperature sensor added-on a cone penetrometer probe potential in adding more insight to better characterise soils during the site investigation. As heat is generated on the cone tip due to the induced friction during the continuous penetration depending on the cone tip resistance (force applied recorded during the cone penetration), and on the soil characteristics (stiffness, in-situ stresses, density, interface friction angle, grain size, and grain size distribution). It is expected that the heat generated from the soil/cone friction is an indicator of the mechanical soil/cone behaviour related to other soil engineering parameters that could potentially be estimated using the T-CPT in future site investigations.

1.3. Project Relevance

The relevance of the work aimed for this project should fulfil both the academic and industry level; increasing the insight of soil behaviour as well as the accuracy and robustness of soil investigations. The proposal layout consists of the state-of-the-art of CPT add-on sensors that have been implemented up to now, including their potentials and limitations. A focus is made on the T-CPT add-on sensor, followed by a literature review on thermal soil properties and heat transfer occurring during the CPT. A simplified solution, based on several assumptions are presented to capture the general picture of the physic taking place during the cone penetration on a thermal and mechanical point of views. This is followed by a 2D numerical **Finite Element (FE)** model using the FE software Comsol 5.2 to improve the accuracy of the computation and to explore the T-CPT potentials based on sensitivity analysis. Eventually, an investigation is undertaken on possible existing correlations between soil properties/type and the T-CPT measurements collected during

site investigations by Fugro. This last step concludes the research project undertaken in the T-CPT potentials in soil investigation.

1.4. Research Question and Objectives Statement

The aim of this research is to investigate the possible correlations that can be derived analysing the T-CPT measurements which could improve the soil behaviour understanding and the soil type characterisation. The research project of this master thesis aims to answer the following main research question:

Can T-CPT data (cone tip temperature, cone tip resistance, sleeve friction) obtained during continuous penetration be used to improve soil investigation?

Which can be answered by answering the following sub-questions:

-Cone recorded temperature profiles present distinctive features. Therefore, can these features be a function of soil properties?

-Can a correlation between the temperature profile and the soil properties be derived from a database including in-situ tests, laboratory tests and from a numerical model?

-Can the recorded temperature gradient during continuous penetration give more information about the soil type/behaviour?

-Can the recorded temperature difference between the temperature and the initial temperature of the soil, give more information about the soil type?

The main research objectives consist of learning and understanding the heat exchange occurring between the cone tip and the soil. Moreover, a second main objective could be described as correlating the cone tip temperature variation recorded during continuous cone penetration with engineering soil parameters involved in the heat exchange to estimate the T-CPT potential in improving the soil characterisation based on the cone tip temperature evolution and the other CPT measurements.

1.5. Research Approach and Strategy

1.5.1. Introduction

The research approach of this project consists of modelling the heat transfer process occurring between the cone tip and the soil during the penetration of the cone penetrometer. This is of use to investigate the different dependencies of the temperature measurement features and if soil engineering parameters can be derived from the cone tip temperature evolution recorded during a T-CPT. To do so, actual T-CPT field tests from the Hollandse Kust Noord Project is provided by Fugro.

1.5.2. Research approach

The research approach proposed for this project is to observe the relationships between temperature measurements and soil engineering parameters. The investigation is one of brief since no research has been made on this particular subject. The research must, therefore, involve a certain number of in-situ field data and laboratory data to conclude on any existing potential correlations. Elements from other research could be used to complement the reliability and/or scientific basement of this project such as previous studies related to CPT, thermal soil properties, and interface friction angle. This research is stated as valid in order to process through the project. Another important point to make is the Finite Element software Comsol 5.2 is used to model and analyse heat transfer occurring between the cone tip and the soil during the cone penetration.

1.5.3. Research strategy

To answer the research question and fulfil the research objectives, the project is undertaken respecting the following research strategy:

- State-of-the-art of CPTu & CPT add-on sensors
- Literature study on T-CPT
- Research Methodology including a simplified solution of the heat transfer between the cone tip and the soil
- Numerical Modelling Investigation on the T-CPT potentials using a 2D FE numerical model of the heat transfer between the cone tip and the soil
- Analysis of available database

The state-of-the-art on CPTu practices and CPT add-on sensors is provided as requested by Fugro. This constitutes a base for the paper that will be proposed and presented for the 6th International Conference on Geotechnical and Geophysical Site Characterization that will take place in Budapest on September 2020 by Fugro. Then, a focus is made on the mechanical and thermal interactions occurring during cone penetration and the most recent advancement on the T-CPT as a literature review.

This is followed by the research methodology adopted for answering the research question. The research methodology includes a first approach to the mechanical and thermal interactions with a simplified solution of the heat transfer created making crude assumptions and simplifications to capture the main heat transfer phenomena occurring during the cone penetration. Thenceforth, a 2D FE numerical model of the heat transfer between the cone tip and soil during cone penetration is undertaken using the FE method software Comsol 5.2. This aims to mimic the penetration of the cone to new soil material with more accuracy and reliability than the proposed simplified solution. The numerical model consists of a 2D axisymmetric model considering a realistic but moderately simplified geometry, interior air-filled voids of the Thermal Cone Penetrometer prototype used in the field data acquisition.

1.6. Reading The Report

The report is delivered in different parts, the first chapter consists of the introduction of the thesis report, enumerating the different objectives and research questions of the MSc Thesis. The second chapter consists of a review introducing the different CPT add-on sensors, summarising the probe design, the measured and/or derived physical properties, the advantages and limitations of each add-on sensor. The third chapter is the literature review. The fourth chapter introduces to the readers the research implementation, detailing the methodology and strategy adopted and the assumptions made on the heat transfer occurring during the cone penetration. The fifth chapter details the numerical modelling investigations undertaken, detailing the proposed numerical models, and giving the results obtained with the author's interpretations. The sixth chapter consists of the analysis of data obtained from two different site investigations provided by Fugro. The seventh chapter is composed of the discussion of the numerical modelling investigations and the database analyses. The last chapter of the report presents the main conclusions of the research, answering the research questions and answering the T-CPT potentials in soil investigation. Additionally, the recommendations for future work are addressed in this last chapter concluding the report.

2. State of the Art of the Cone Penetration Test

2.1. Introduction

This chapter covers in detail the principle and potential of classic piezocone penetration test (CPTu). In addition to the thesis research, a review on CPT add-on sensors is presented, including each CPT add-on sensors the penetration mode required for measuring, the soil characteristics and parameters measured and derived, the probe design and the test procedure, and the advantages and limitations of each CPT add-on sensors. This review is implemented in Appendix I and is used as a base by Fugro for the 6th International Conference on Geotechnical and Geophysical Site Characterization, which will be given in Budapest, in September 2020.

2.2. CPTu Principle

The Cone Penetration Test (CPT) is considered as one of the most used tools for in situ for soil investigation in geotechnical engineering. The CPT principle is a simple procedure defined in the ASTM D5778 – 12 (Conshohocken, 1996), which consists of a penetrometer cone tip with a 60° angle and a projected cone based area (A_c) of 10 cm^2 (or 15 cm^2 , depending on the cone model) penetrating through the soil at a constant penetration test of 20 mm/s (Figure 1). During the cone penetrometer penetration, the force applied on the conical point required to penetrate the soil is recorded by electrical methods at different resolution (20 to 10 mm interval readings) depending on the maximal resolution capacity of the cone penetrometer used. The cone resistance, q_c , is often used directly in soil characterization and obtained dividing the recorded force by the cone base area (A_c). The second measurement made during CPT via a friction sleeve present directly behind the cone tip. As the force applied on the cone tip, the force exerted on the sleeve is measured by electrical methods. The sleeve friction resistance, f_s , is obtained by dividing the measured axial force exerted on the sleeve by the surface area of the sleeve friction, A_{ft} of 150 cm^2 for a 10 cm^2 cone (225 cm^2 for a 15 cm^2 cone).

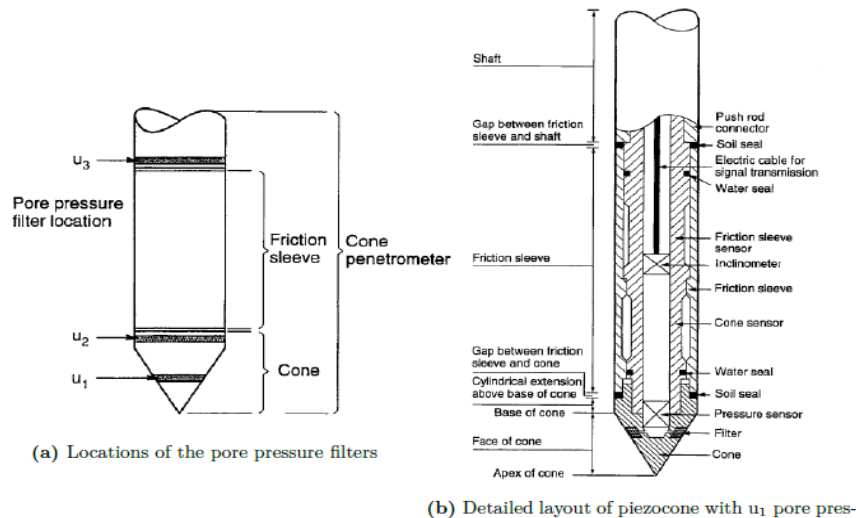


Figure 1: Piezocone penetrometer layout (Tom Lunne, Peter K. Robertson, 1997)

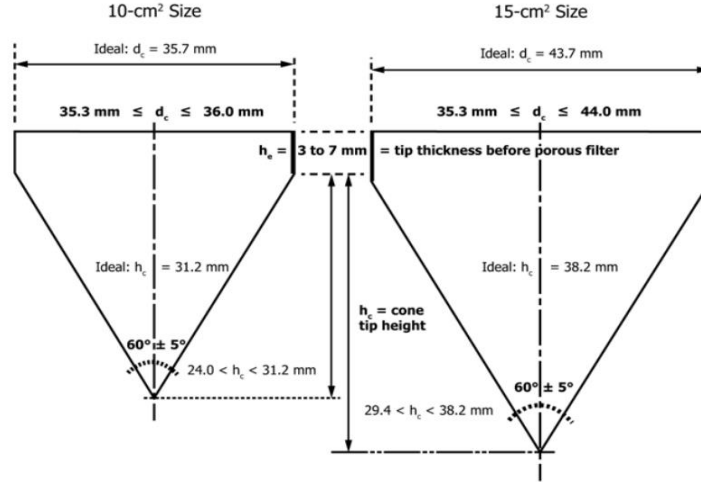


Figure 2: Cone manufacturing and operating tolerances (Conshohocken, 1996)

Nowadays, recording the pore water pressure at the u_2 location (Figure 2) during the continuous cone penetration using an electronic pressure transducer as an add-on sensor on the classic CPT has become a common practice, and is commonly called piezocone penetration test (CPTu). The record of the pore pressure offers several advantages such as allowing the correction of the pore water pressure acting on the cone geometry during the continuous cone penetration, mainly to correct and normalize the cone tip resistance used for soil characterisation (especially in soft clays and silts). Additionally, CPTu can be used for a to determine the soil permeability and increase the soil type identification reliability by halting the cone penetration at the desired depth and recording the pore pressure decay over time (pore pressure dissipation test).

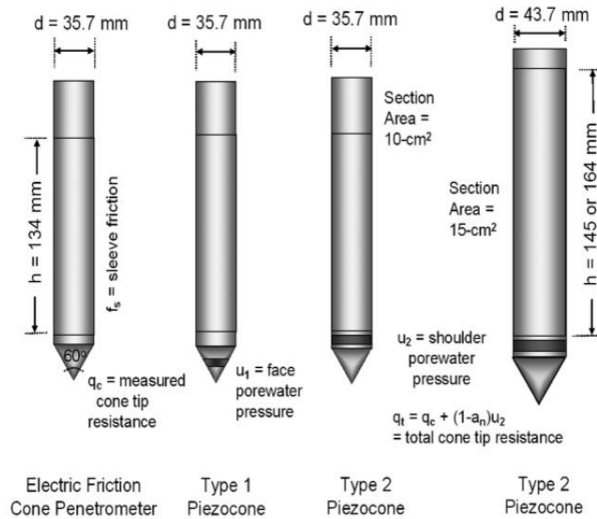


Figure 3: Penetrometer design configurations: (a) Electric Friction-type, (b) Type 1 Piezocone, (c) Standard 10-cm² Type 2 Piezocone, and (d) 15-cm² Type 2 (Conshohocken, 1996)

Inclinometers are also included in modern cones to record the vertical deviation of the cone penetrometer during penetration. The vertical deviation should not exceed 2 degrees and a check should be made on pushrods straightness. This check is of great use to avoid any damage to equipment and to assess the verticality of the tests.

The classical CPT sensors are for measuring cone resistance, q_c , sleeve friction, f_s , pore pressure, u , and inclination. These measurements are commonly used in order to identify the soil type during site investigation using Soil Behaviour Type charts (Tom Lunne, Peter K. Robertson, 1997; Robertson, 2010). Additionally, a great number of semi-empirical correlations have been developed to estimate engineering geotechnical soil parameters from the traditional sensors incorporated in a cone penetrometer. These semi-empirical correlations allow Geotechnical engineers to estimate geotechnical soil parameters important for designing such as the soil density (and relative density for sandy soil), the over-consolidation ratio, the friction angle, the permeability, the undrained shear strength, the coefficient of consolidation, some stiffness soil parameters and others. The different reliabilities for each correlation depend on the type of soil and are presented by Robertson (2010; 2016).

Table 1: Perceived applicability of CPTu for deriving engineering soil parameters
(Robertson and Cabal, 2010)

| Soil Type | D_r | ψ | K_0 | OCR | S_t | s_u | ϕ' | E, G^* | M | G_0^* | k | c_h |
|-------------|-------|--------|-------|-----|-------|-------|---------|----------|-----|---------|-----|-------|
| Sand | 2-3 | 2-3 | | 5 | | | 2-3 | 2-3 | 2-3 | 2-3 | 3 | 3-4 |
| Clay | | | 2 | 1 | 2 | 1-2 | 4 | 2-4 | 2-3 | 2-4 | 2-3 | 2-3 |

Reliability scale: 1 = high, 2=high to moderate, 3=moderate, 4=moderate to low, 5=low, blank=no applicability, *=improved with Seismic sensor.

Where:

| | | | |
|----------|------------------------------|-----------|----------------------------|
| D_r : | Relative density | ϕ' : | Friction angle |
| Ψ : | State parameter | E: | Young's stiffness modulus |
| K_0 : | In-situ stress ratio | G: | Shear strain modulus |
| OCR: | Over consolidation ratio | M: | Compressibility |
| S_t : | Sensitivity parameter | G_0 : | Small strain shear modulus |
| s_u : | Undrained shear strength | k: | Permeability |
| c_h : | Coefficient of consolidation | | |

Apart from the piezometer probe, multiples sensors have been implemented without making it to routine practice. Aside from the research question, an exhaustive review of existing CPT add-on sensors was undertaken in order to index any major add-on sensors developed to date. The paper consists of reviewing and introducing the CPT probes (the test procedure, the soil characteristics measured and derived, the advantages and possible limitations of each CPT sensor developed up today), respecting the following conditions: (1) continuous penetration at 20 mm/s, (2) robust, have no external moving parts, and (3) offer the potential for broad geotechnical value, not only limited to special applications only. The review considers recent advances in electronics, sensor technology and data processing systems and is included in Add-On Sensors for Cone Penetration Testing. The following list of CPT add-on sensors have been investigated:

- Acoustic Sensor (Microphone)
- Video Sensor (VisCPT)
- Electrical Resistivity Sensor (ERT & CRP)
- Time Domain Reflectometry Sensor (TDR)
- Radioisotope Sensors (NM & ND)
- Multi-Friction & Multi-Piezo-Friction Sensors (MPFP)
- Temperature Sensor (Thermocouples & T-CPT)
- Magnetometer Sensor (MagCone)
- Optical Fiber Sensors (FO)
- pH & Redox Potential Sensors
- Laser-Induced Fluorescence Sensor (LIF)
- Integrated Optoelectronic Chemical Sensor

2.3. Add-On Sensors Table

| Add-on Sensor | | Penetration Mode | Soil Characteristics | | Available Literature |
|--|--|------------------|--|--|--|
| | | | Measured | Derived | |
| Acoustic (Microphone) | | Continuous | -Acoustic Emission Activity [kHz] | -Stratigraphy Transition -Changes in Relative Density | Villet (1981), Muromachi (1981), Tringale (1982), Massarsch (1986), Menge (1995), Houlsby (1998), Mao (2018) |
| Video (VisCPT) | | Continuous | -Direct Soil Observation | -Stratigraphy Transition -Clay Fissure Detection -Clay & Sand Seam Detection -Particle Size Analysis -Soil Contaminant | Raschke (1997), Hryciw (1998) |
| Electrical Resistivity Sensors | Electrical Resistivity Tomography (ERT) | Halted | -Soil Resistivity -Pore Water Resistivity | -Porosity -Density | Zuidberg (1988), Campanella (1993) |
| | Cone Resistivity Penetrometer (CRP) | Continuous | -Soil Electrical Resistivity | -Subsurface Spatial Variation -Thin Soil Layering Detection -Sand Dilatancy Characteristics -Relative Density -Soil Contaminant (acidic & NAPL spills) | Campanella (1993), Yoon (2009, 2011) |
| Time-Domain Reflectometry (TDR) | | Halted | -Permittivity -Soil Electrical Conductivity | -Water Content -Dry density -Porosity -Spatial Distribution of The Volumetric Water Content | Upadhyaya (1982), Nozaki (1990), Lightner (1995), Vaz (2001), Yu (2004), Chen (2010), Miyamoto (2012) |

| Add-on Sensor | | Penetration Mode | Soil Characteristics | | Available Literature |
|--|----------------------|---|---|---|--|
| | | | Measured | Derived | |
| Multi-Piezo-Friction Sensor (MPFP) | | Continuous | -Friction On Texturized Sleeve -Pore Pressure | -Soil Type Classification | Hebeler (2018) |
| pH, Electrical Conductivity & Redox Potential Sensor (ORP or ChemiCone) | | Halted Continuous for the pH sensor only | -Electron & Hydrogen ions activity -pH -Electrical conductivity | -Soil Oxidation -Soil Contaminants (acid & base spills) | Olie (1992), Bratton (1996; 1998), Woeller (1991) |
| Magnetometer (MagCone) | | Continuous | -Magnetic Field | -Unexploded Bomb Detection (UXB/UXO), -Existing Underground Structures Detection (driving depth of pile foundations, sheet pile lengths, the position of anchors & power cables) | Zhang (2007), Wiertsema & Partners (2016), Gouda Geo-Equipment BV (2019), |
| Radioisotope Sensors (NM & ND) | | Halted | -Radioactive Energy Photons Dissipation -Soil Atomic Density | -Density -Porosity -Water Content -Stratigraphy Transition -Liquefaction Potential | Marton (1988), Sully (1988), Shibata (1992; 1994), Mimura (1995), Jia (2013, 2019) |
| Temperature Sensors | Thermocouples | Halted | -Temperature Variations | -Soil Chemical Activity (Methane Generation & Biological activity) -Permafrost Depth | Woeller (Woeller <i>et al.</i> , 1991), Burns (1998) |
| | T-CPT | Halted | -Temperature Decay | -Thermal Conductivity -Initial Soil Temperature | Akrouch (Akrouch <i>et al.</i> , 2016), Vardon (Vardon, 2018; Vardon <i>et al.</i> , 2018) |

| Add-on Sensor | Penetration Mode | Soil Characteristics | | Available Literature |
|--|------------------|---|--|---|
| | | Measured | Derived | |
| Fiber Optic (FO) | Continuous | -Cone Resistance with High-Frequency (500 Hz) & Lower Temperature Sensitivity | -Thin Soil Layers Better Detected | Looijen (2018) |
| Laser-Induced Fluorescence Sensor (LIF) | Continuous | -Soil Fluorescence | -Soil Contaminants: Petroleum Hydrocarbons & Aromatic Hydrocarbons | Lin (1995), Burns (Burns and Mayne, 1998), Rossabi (2000), Pepper (2002), Kurup (2006; 2007, 2017), Appelo (2018) |
| Integrated Optoelectronic Chemical Sensor | Continuous | -In-situ Chemical Concentration by Wave Interference | -Soil Contaminants: Ammonia, pH & BTEX | Burns (Burns and Mayne, 1998), Mccall (2018) |
| Gamma Radiation & Neutron Sensors (RadCone) | Halted | -In-situ Uranium Detection By Na(Tl) Crystal Detector | -Radioactive Soil Contaminants | Marton (Marton <i>et al.</i> , 1988), Morgan (1998), Diego (2001), |

3. Literature Review

3.1. Literature Review Introduction

Thermal properties of soils and heat flow conditions are of importance in many engineering and geothermal projects. Situations, where heat transfer takes place, are numerous, such as road designs, airfields, buildings in cold region or high-power electricity cables, where high heat dissipation is advantageous, or for pipelines carrying high-viscosity fluids, for which the viscosity increases with the decrease of temperature. Commonly, the thermal conductivity of soils used to be measured using a thermal needle probe. This probe has its own limitations due to its fragile design and the time-consumption of the test, which make the test unpopular for in-situ offshore purposes especially. The use of a thermal cone offers several advantages, such as the in-situ measurements of the thermal properties of soil during a cone penetration test (CPT) in great depth without external tool (thermal needle probe), the shorter duration of the T-CPT (less than one hour) compared to thermal needle probe test (approximately 25 hours), no need of external heat source since the heat is generated by the soil-cone friction during the cone penetration. The T-CPT gives all the information usually derived from a regular CPT along with a measure of the soil thermal conductivity (requiring to halt the cone penetration to execute a temperature decay test). Further research is required on the interpretation of the maximum temperature difference reached and of the temperature gradient recorded during a continuous cone penetration test to investigate the T-CPT potential on improving soil characterisation by deriving other soil parameters involved in the heat transfer such as the thermal soil conductivity, the volumetric heat capacity and the bulk density parameters using the T-CPT data (cone tip temperature, cone tip resistance, sleeve friction).

3.2. Mechanical Principles Occurring During Cone Penetration

Investigating the mechanism developing during cone penetration is the first step to understanding the frictional phenomenon occurring between the soil and the cone penetrometer at the origin of the heat transfer between the soil and the cone tip that could be characterised by the temperature sensor added on the cone tip (T-CPT). The theory of Prandtl is used as a base for the different failure mechanisms occurring for different types of soil.

3.2.1. Failure mechanisms in clay & sand

As the cone penetrometer is pushed through the soil, the soil experiences different types of strain. Depending on the zone in which the soil considered is located relative to the cone tip, large plastic strains to elastic strains can occur as defined in Figure 4 by Muromachi (Muromachi, 1981) and adapted by Silva and Bolton (2004). The failure mechanism occurring during the cone penetration differs for sand and clay since the failure surfaces are thought to be depending on the soil strength and stiffness which differs significantly for sandy soil and clayey soil. Sand failure surfaces are assumed to be characterised by logarithmic spirals with curved lines to the cone penetrometer rod. This typical failure surface is assumed to be due to the frictional characteristics of sandy soils (Meyerhof, 1974, 1983; Lubking, 1997). In contrast, clay failure surfaces are assumed to be rather circular with a significantly smaller area of influence (Smits, 1977).

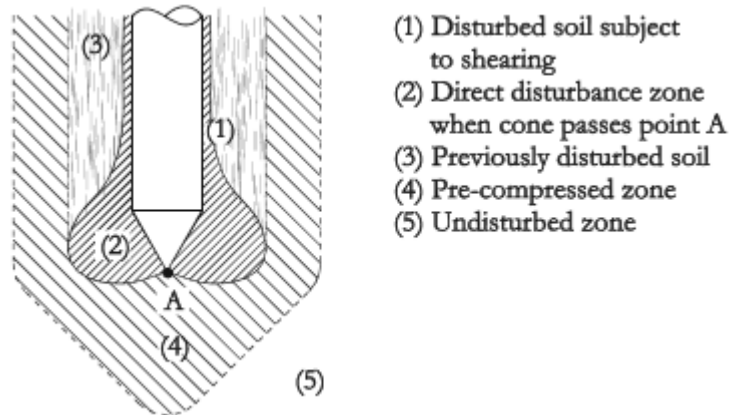


Figure 4: Soil disturbance during cone penetration (Silva and Bolton, 2004) adapted from Muromachi work (Muromachi, 1981)

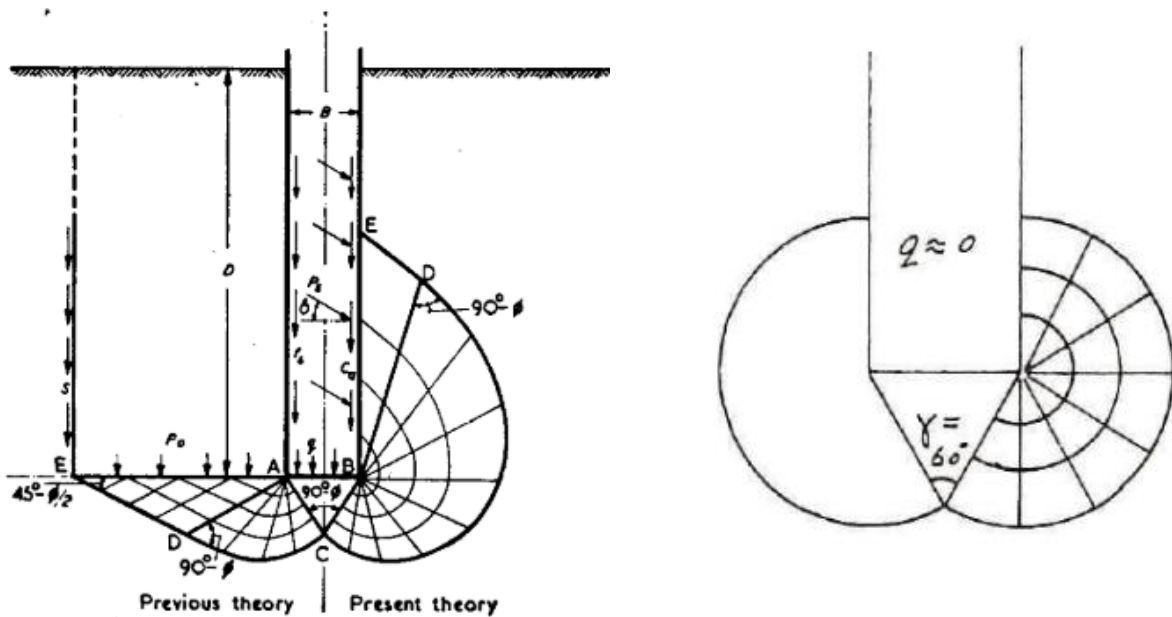


Figure 5: Typical failure surfaces for sand and clay

Recent research made on the investigation of the cone penetration mechanism using image correlation technique (DIC) were conducted and presented in Arshad's work (2014). The DIC technique used allows tracking soil displacement during cone penetration. The investigation was undertaken for sand at a different depth relative to the cone diameter (d_{cone}) with a relative density of 85%. Figure 6 shows the experiment results for the different depths. Firstly, at ground level, the failure shape formation is distinctly respecting the failure mechanism derived from the theory of Prandtl. As the cone penetrometer reaches greater depth in the sand, the overall displacement field becomes more vertical and the sand grains neighbouring the cone tip undergo particle crushing. This suggests that the failure mechanism is a function of the stress level.

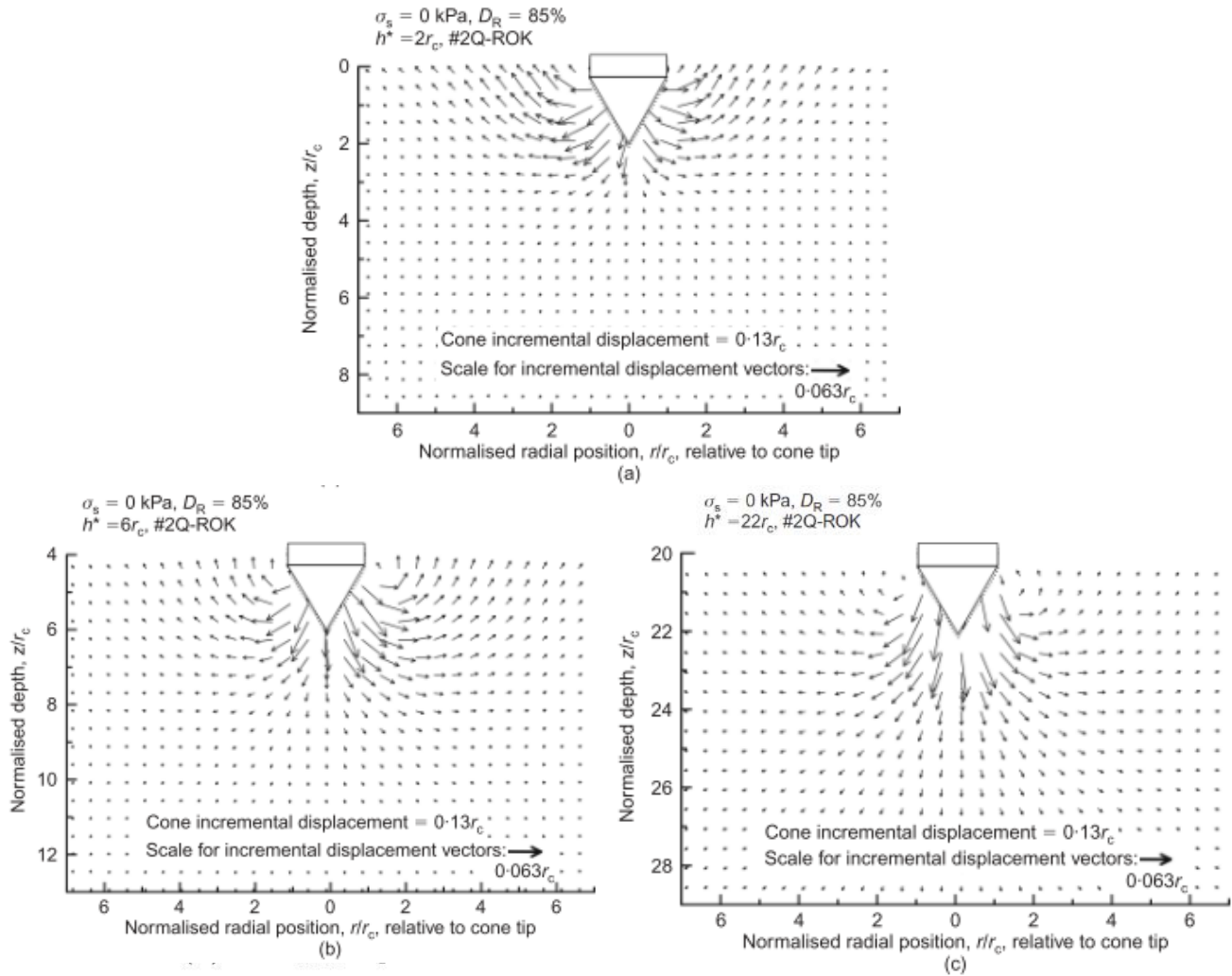


Figure 6: Sand displacement under cone penetration from Arshad's work (2014)
(a) At ground level, (b) at $3 d_{cone}$ depth, (c) at $11 d_{cone}$ depth

These experimental observations are in agreement with several authors' researched who attended and proposed failure surface development and critical depth characterising the maximum cone resistance recordable. In sandy soil, the failure surface around the cone penetrometer evolves depending on the cone diameter, the maximum cone tip resistance at critical depth or the internal friction angle depending on the author.

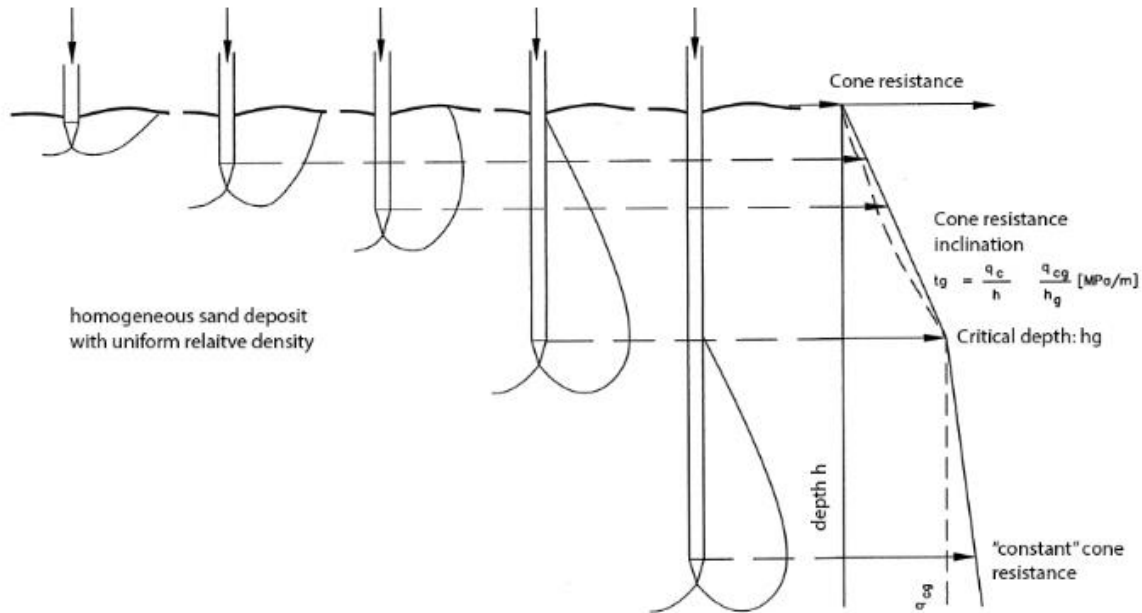


Figure 7: Failure surface development (Lubking, 1997)

The magnitude of the failure surface and its influence is thought to be mainly a function of the internal friction angle for sandy soil. Large angle of internal friction induces large dilatancy angle resulting in dilative answer due to shearing of the sand under penetration. Due to the dilative response of sands with high internal friction angle and high relative density, the area which undergoes shearing is then greater. This results in critical depth value to be larger for sands with higher internal friction angle and relative density (Lubking, 1997). The same logic is thought to be applicable regarding the horizontal plane magnitude as showed in Figure 8, with the failure shape features increasing with higher values of internal friction angle (Douwes Dekker, 1984).

Past research demonstrated that the cone resistance measured during cone penetration is influenced mainly by the horizontal stress and the relative density of the soil (Houlsby and Hitchman, 1988; M M Ahmadi and Robertson, 2005). These research proved the small effect of the vertical stress on the cone resistance measured over the important effect of the horizontal stress and the relative density that were concluded to be the main parameters affecting the cone tip resistance measured during a cone penetration test. Additionally, the cone tip resistance measured was also proved to be more influenced by the soil resistance below the cone tip than above (M M Ahmadi and Robertson, 2005).

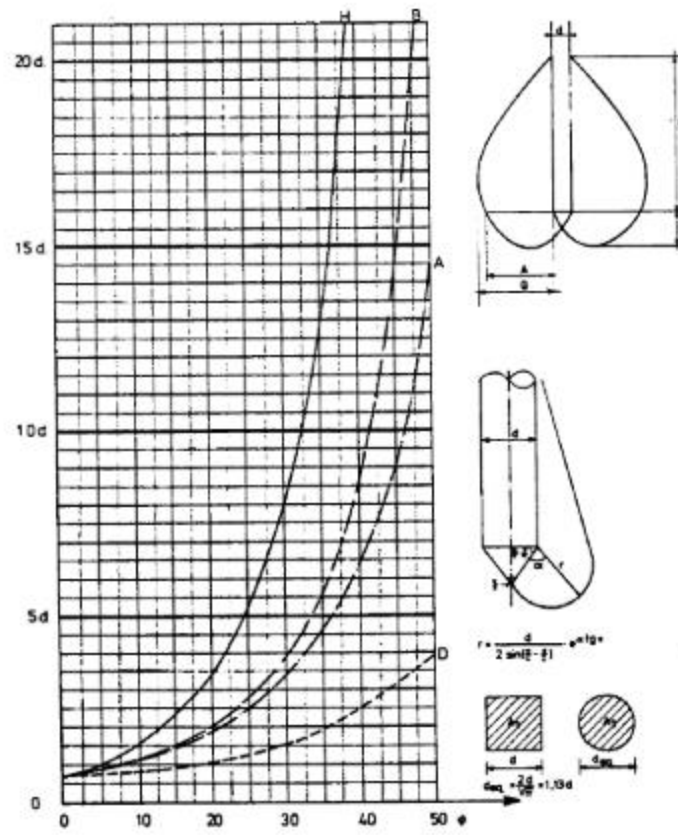


Figure 8: Failure shape features in sand in function of the cone diameter and the internal friction angle based on Prandtl's theory (Douwes Dekker, 1984)

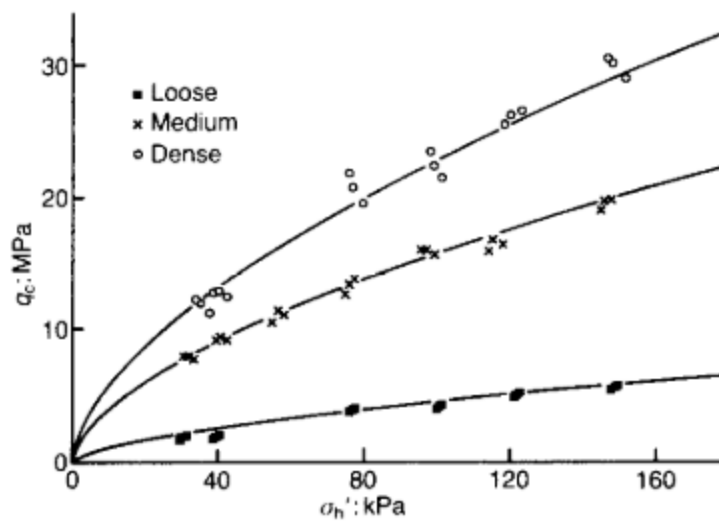


Figure 9: Relative density & Horizontal stress effects on the cone tip resistance (Houlsby and Hitchman, 1988)

3.2.2. Thinly layered soil influences on the cone resistance, q_c , recorded during CPT

Thin layers of clay/silt material can be encountered in sand deposits (Figure 10). This type of deposit is usually known as ‘flasher bed’. This deposit is characterised by the intercalation of thin layers of sand (10 to 300 mm) and thin clay/silt layers (3 to 15 mm). Due to the layers’ thickness, it is challenging to accurately estimate the true characteristics of those thin layers using cone penetrometer tests. Moreover, the challenge consists of classifying those layers and the influences of the intercalation on the sand liquefaction potentials (van der Linden, 2016).

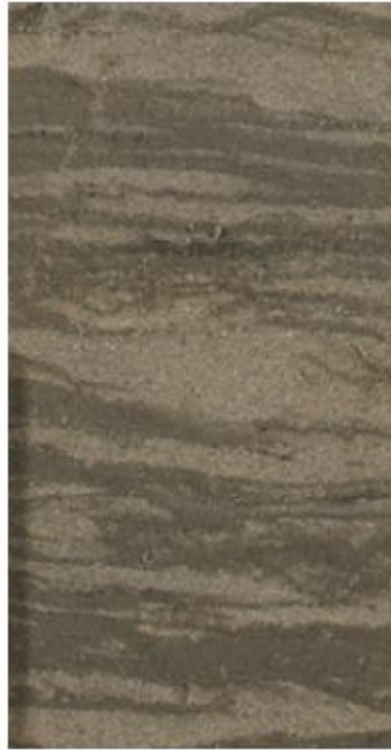


Figure 10: Flasher bed deposit example (van der Linden, 2016)

Ahmadi’s work (2005) demonstrated the parameters affecting the interface influence distance and the CPT measurement encountered in thinly layered soils. This investigation was undertaken using parametric numerical modelling and the simple Mohr-Coulomb elastic-plastic model. The main results obtained from the penetration analyses are presented in Figure 11 & Figure 12. The main results of Ahmadi’s research are the identification of the parameters influencing the cone tip resistance recorded during a cone penetration test.

The research demonstrated that the void ratio (or porosity), the relative density as well as the stresses (horizontal and vertical) especially influence the cone tip measurements in thin-layers soil. As can be seen, the cone tip resistance, q_c , is more influenced by the strength of the layer above. Consequently, the distance over which a cone penetrometer senses an interface is a function of the soil strength and the soil stiffness below the interface. The in-situ effective vertical stress was demonstrated to be of very small influence as it plays a minor role in the cone resistance and in the interface influence distance. On the contrary, the in-situ effective horizontal stress was found to play a major role in the cone tip resistance and the interface influence as several previous research demonstrated it. The cone tip resistance increases as the in-situ effective horizontal stress increases as well.

In conclusion of Ahmadi's work (2005), the cone tip resistance and interface influence distance is most significantly a function of both the relative density, D_R , as well as the in-situ effective horizontal stress, σ'_H , for dense sand. Therefore, the higher the soil strength and stiffness of the sand, the greater the correction applied on the cone tip resistance should be. The interface influence distance was found to be a function of the difference in soil strength and stiffness between the two different soil layers. This last observation results in the interface influence distance increasing as the difference in soil strength and stiffness increase between the different layers.

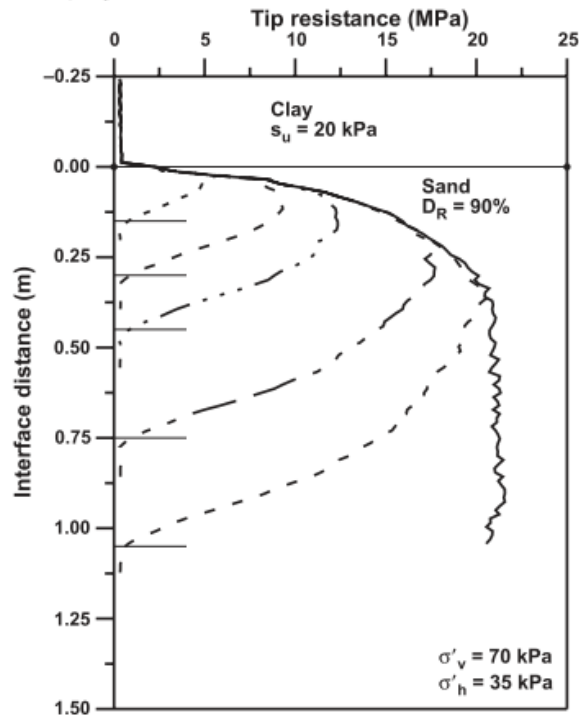


Figure 11: Compilation of penetration analyses for dense sand layers ($D_R = 90\%$) of different thicknesses interbedded in soft clay ($s_u = 20$ kPa) from Ahmadi (2005)

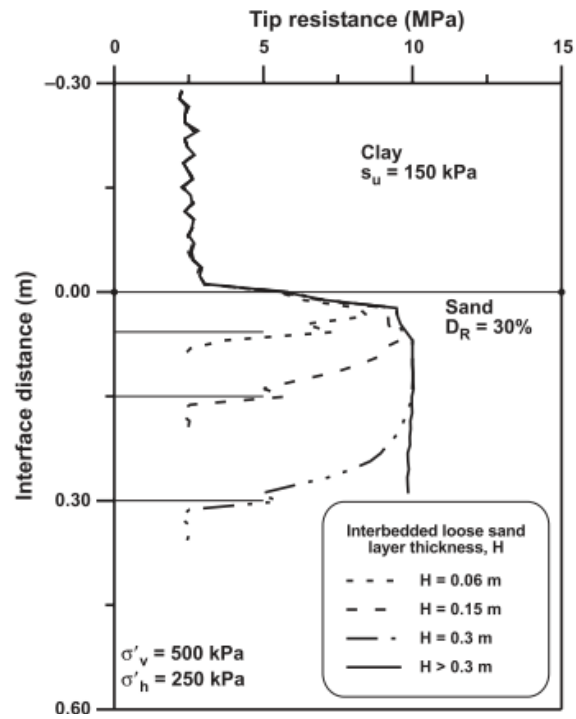


Figure 12: Compilation of penetration analyses for loose sand layers ($D_R = 30\%$) of different thicknesses interbedded in soft clay ($s_u = 150$ kPa) from Ahmadi (2005)

3.2.3. General mechanical interactions between the cone penetrometer and the soil

The soil interacts in different ways with the cone penetrometer due to the force, F_c , applied on the cone penetrometer (Figure 13). Pushing through the soil by applying a force F_c on the cone penetrometer results in the development of reaction forces, F_{RH} and $F_{R, soil}$, from the soil normal to the application surfaces of the cone tip. This can be seen as the resistance of the soil to the cone penetration. From the sliding occurring between the cone surfaces and the soil-grains friction is generated. The friction force resulting from the soil/cone interaction is characterised by the force applied on the cone and the coefficient of friction, μ . The coefficient of friction, μ , can be defined as the ratio between the shear force and the normal force, or more simply expressed as follows:

$$\mu = \tan(\delta) \quad (1)$$

where δ_s is the interface soil-steel friction angle, with a maximum value being the peak angle of internal friction of the soil, ϕ_u (Potyondy, 1961). Potyondy results suggest the interface frictional angle between dense saturated sand and smooth steel surface to be equal to 0.64 times the internal friction angle of the sand considered. Whereas the interface friction angle between clayey soil and smooth steel surface was observed to be equal to 0.55 times the internal friction angle of the clay considered. Other experimental research was undertaken by Han et al. (2018) show the sand and steel interface friction angle varies between 0.53 to 0.70 for a smooth steel surface. The fluctuation was investigated looking at the different effects of the particle size, the shear surface roughness and the sand gradation.

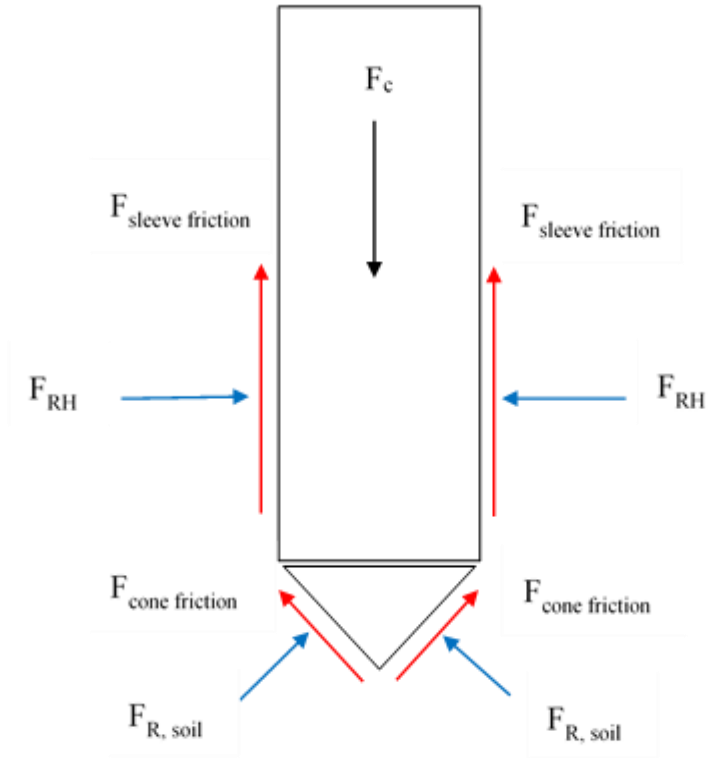


Figure 13: Mechanical cone penetrometer & soil interaction

For the particle size, it was observed that the internal friction angle, ϕ_{cs} , and the interface friction angle δ_{cs} , are a function of the particle size and the shape of the sand. Figure 14 presents experimental results from Han et al. (Han *et al.*, 2018) showing that the interface friction angle, δ_{cs} , decreases with an increase of particle size (D_{50}). Additionally, sands presenting more rounded and spherical particle packing morphology tend to develop lower internal and interface friction angles at the critical state than sands characterised by sharp angular particles. The ratio between the interface friction and the internal friction angles, δ_{cs}/ϕ_{cs} , occurs to be independent of the sand packing morphology. Although the δ_{cs}/ϕ_{cs} ratio decreases with an increase of the sand particle size for the same surface roughness (Figure 14).

Figure 15 shows evidence that the interface roughness effect on the δ_{cs}/ϕ_{cs} ratio and the major role that it plays in the interface shear strength. An apparent trend is noticeable of increasing δ_{cs}/ϕ_{cs} ratio with respect to an increase of normalized interface roughness independently to the sand packing morphology and grain size.

The sand gradation effect on the δ_{cs}/ϕ_{cs} ratio was also investigated by Han et al. (Han *et al.*, 2018). The experiment results suggest that sand particle interlocking develop faster at the shear interface as the interface roughness increases for uniformly graded sand with shearing occurring in the sand sample resulting in the interface friction angle mobilisation of the sand (Figure 16). Whereas, for well-graded sands, it is suggested that smaller sand grains ease rolling and sliding of bigger sand grains leading in altering the kinetics shearing process (Han *et al.*, 2018).

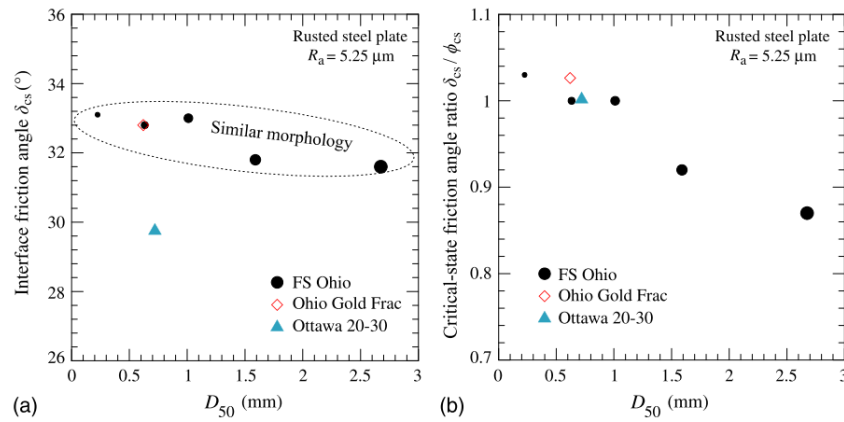


Figure 14: Particle size effect on the interface friction angle for a rusted steel interface, after Han et al.(2018)

- (a) interface friction angle δ_{cs} at critical state vs mean particle size D_{50} ;
- (b) critical-state friction angle ratio δ_{cs}/ϕ_{cs} vs mean particle size D_{50} .

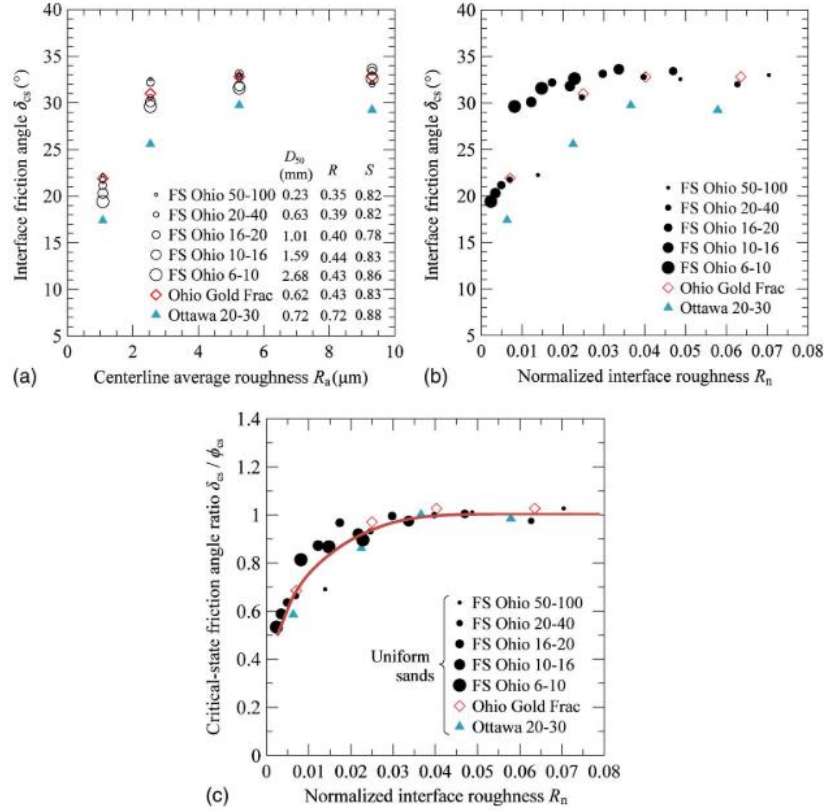


Figure 15: Interface roughness effect on the interface friction angle at critical state after Han et al.(2018):

- (a) interface friction angle δ_{cs} at critical state versus centreline average roughness R_a ;
- (b) interface friction angle δ_{cs} at critical state versus normalized interface roughness R_n ;
- (c) critical-state friction angle ratio δ_{cs}/ϕ_{cs} versus normalized interface roughness R_n .

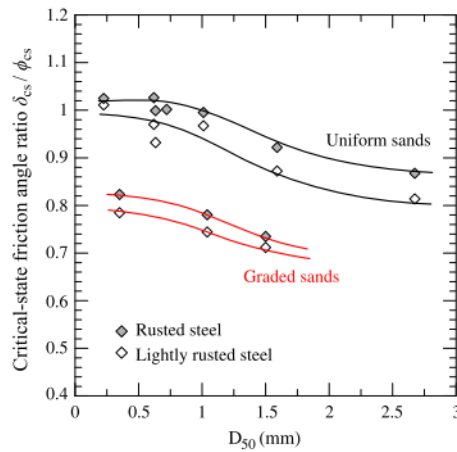


Figure 16: critical-state friction angle ratio δ_{cs}/ϕ_{cs} vs mean particle size D_{50} for uniform sands and graded sands after Han et al.(2018).

As a result, the friction resulting from the mechanical Cone/Soil interaction is of high complexity and depends on a multitude of factors such as the interface surface roughness, the soil stiffness, the relative density, the dilatancy angle, the particle size distribution and the in-situ stresses (Potyondy, 1961; Han *et al.*, 2018). The friction generated results in energy that is dissipated in the form of heat which induces heat transfer to take place between the cone penetrometer and the soil during the cone penetration.

3.3. Thermal Principles Occurring During Cone Penetration

3.3.1. General introduction of the thermal soil properties

High stresses tend to develop around the cone tip during the penetration of the cone penetrometer into the soil. Soils are composed of a multitude of material that can be defined into three main components that are soil particles, water and gas, with each of these components having different thermal properties. A summary of the main thermal parameters for the main soil components is presented in Table 2 (Wijk, 1963). Thermal conductivity, λ , is the ability of a material to conduct heat. Specific heat capacity, c_p , is the measure of heat required to increase the material's temperature by 1°C, the volumetric heat capacity, C , is also very often used in an engineering context, being the product of the specific heat capacity and the density, ρ , of the material. The soil-cone interaction leads to complex thermo-hydro-mechanical process not fully understood yet. However, the heat transfer mechanisms in the soil are well known, divided into conduction, convection and radiation. Convection heat transfer is defined as the transfer of energy between a moving fluid and a solid material. Radiation heat transfer is defined as the energy transfer in electromagnetic form. Conduction heat transfer is defined as the transfer of energy by means of molecular excitement within a material due to a change in temperature. Some simplifications of the heat transfer mechanisms in soil occurring during cone penetration test can be made. In soils, the radiation heat transfer mechanism can be neglected since it contributes to less than 1% of the whole heat transfer (Rees *et al.*, 2000). Convection heat transfer plays a significant role in the overall heat transfer mechanism when groundwater flow conditions exist or for highly permeable soils such as gravels (Haigh, 2008). Therefore, conduction heat transfer is the most relevant heat transfer process occurring in soils and well captured by Fourier's law (Fourier, 1822).

Table 2: Thermal properties of soil components at 20°C and 1 atm (Wijk, 1963)

| Material | Density ρ (g/cm ³) | λ (W/m · K) | c_p (J/g · K) | C (J/cm ³ · K) | α (10 ⁻³ cm ² /s) |
|----------------------------------|-------------------------------------|---------------------|-----------------|-----------------------------|--|
| Quartz | 2.65 | 8.4 | 0.73 | 1.924 | 43 |
| Many soil minerals ^a | 2.65 | 2.9 | 0.73 | 1.924 | 15 |
| Soil organic matter ^a | 1.30 | 0.25 | 1.92 | 2.510 | 1.0 |
| Water | 1.00 | 0.6 | 4.14 | 4.184 | 1.42 |
| Air | 0.0012 | 0.026 | 1.004 | 0.0012 | 0.21 |

^aApproximate average values.

3.3.2. Correlations between thermal soil properties, soil type and porosity

Research put in evidence that the relative fractions of various soil constituents influence the effective value of the effective soil thermal conductivity. However, the effective thermal conductivity of the soil also depends on the spatial distribution of the soil constituents relative to each other. For water-saturated soils, the sensitivity of the effective thermal conductivity to variations in microstructure is low. This suggests that the geometric mean equation is the best representative mean to determine water-saturated soils and can be determined using the equation (2) (Farouki, 1981).

$$k_{soil} = \left(\prod k_{solid}^{(1-n)f_{solid}} \right) \left(k_{water}^{nS} \cdot k_{air}^{n(1-S)} \right) \quad (2)$$

In which n is the porosity, f_{solid} is the fraction by volume of solid (referring to the different solid soil components such as quartz (sand), silt, clay and peat), S corresponds to the degree of saturation. For saturated soil, the contribution of the air term can be reasonably neglected.

Whereas the heat capacity is a volumetric property. Therefore, the following weighted arithmetic mean can be used according to Farouki (1981):

$$C_{soil} = (1 - n) \sum f_{solid} \cdot C_{solid} + n \cdot S \cdot C_{water} + n(1 - S)C_{air} \quad (3)$$

The influences of the density and the solid fraction on the thermal conductivity and the volumetric heat capacity were investigated by Vardon (2019) using both weighted arithmetic mean and geometric mean equations. Figure 17 shows the influence of the sand/clay fraction for saturated soil, it was observed that the sand/clay fraction is of small importance for the heat capacity, it seems that the heat capacity is rather influenced by the bulk density, decreasing as the volume of water increase. Unlike the heat capacity, the thermal conductivity is greatly affected by the sand/clay fraction ratio.

In consequence, a strong correlation between heat capacity and thermal conductivity of soils was observed. Figure 18 shows the high dependency of the heat capacity on the porosity value and therefore the density of the soil. Whereas, the thermal conductivity is greatly affected by the sand/clay fraction, especially for porous material for which the sand/clay fraction greatly affects the thermal conductivity value by reducing it significantly.

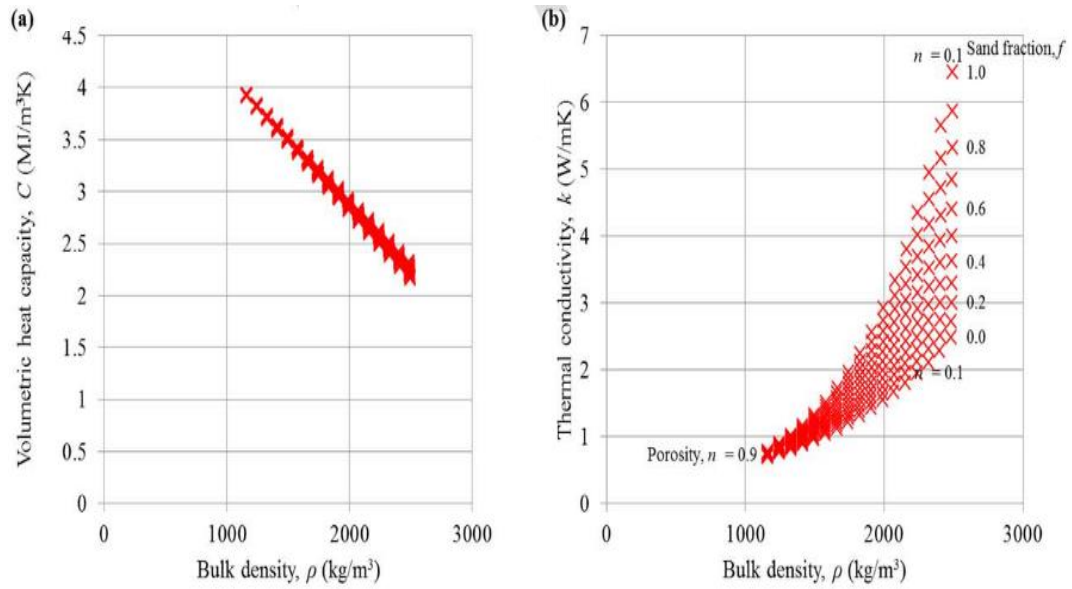


Figure 17: Computed thermal conductivities & volumetric heat capacities as a function of the soil density, Vardon (2019)

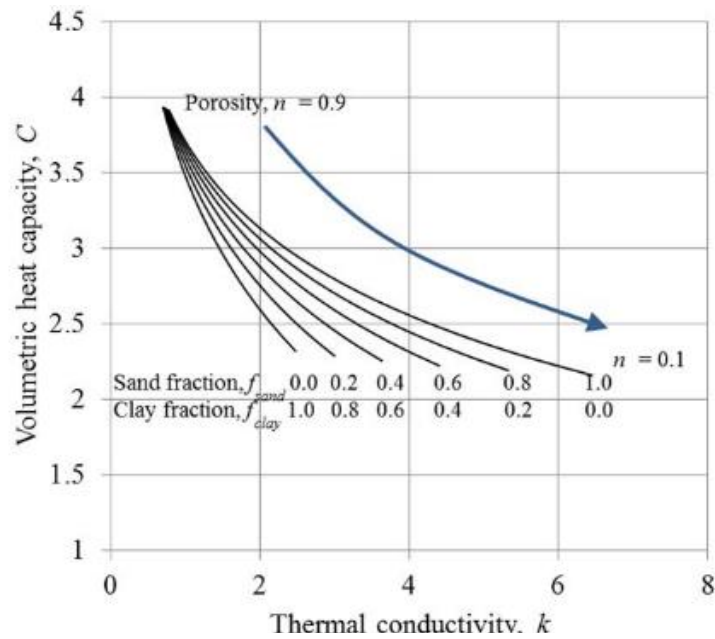


Figure 18: Volumetric heat capacity vs thermal conductivity (Vardon, 2019)

As a result, the heat capacity interpretation model unreliability using the T-CPT temperature decay test procedure, the potentials of correlations based on continuous CPT measurement were investigated. Vardon (2019) proposed a method to estimate the heat capacity and thermal conductivity of soils based on classical CPTu measurements.

Using the classical CPTu measurements and the existing correlations between them, soil index, porosity and soil type fraction (P.K. Robertson and Cabal, 2010; Peter K. Robertson and Cabal, 2010; Lengkeek, Arny; de Greef, J.; Joosten, 2018), Vardon proposed a procedure to estimate heat capacity and thermal conductivity of soils (Vardon, 2019). The resulting method was then used using CPTu measurements and then confronted with laboratory tests. This heat capacity determination method was found to be significantly more reliable as the heat capacity is mainly fluctuating with changes in soil density. However, the thermal conductivity was found being not accurate and should be corrected from site to site. It is thought that this is due to the complexity in estimating the sand and clay ratio based on CPTu measurements. Additionally, the expression for determining the thermal conductivity used by Vardon (2019) and given by Farouki (1981) does not account for the particle size, which is thought to be of important matter for coarse soils since demonstrated by Haigh's work (2008).

3.3.3. General thermal interactions between the cone penetrometer and the soil

As previously mentioned, due to the friction induced by the cone penetration, heat is mainly being generated on the cone tip surface and the sleeve friction surface. The heat transfer occurring between the soil and the cone tip is governed by the first law of thermodynamics (i.e. conservation of energy). The equation was first derived from Fourier's law (Fourier, 1822) and can be written in the following form assuming no mass transfer or radiation:

$$\rho c_p \frac{\partial T}{\partial t} - \nabla \cdot (\lambda \nabla T) = \dot{q}_v \quad (4)$$

where \dot{q}_v is the volumetric heat source, ρ the density of the material, c_p the specific heat capacity of the material and λ the thermal conductivity of the material.

Hence, the heat generated from the friction is diffused through the cone and the soil (Figure 19). The cone tip temperature recorded during a continuous penetration is, therefore, the heat source induced by means of friction minus the heat diffused into the soil. The heat generated on the sleeve friction is assumed to be insignificant compared to the heat-induced by friction at the cone tip. Additionally, assuming that the low ratio of steel/void inside the cone between the cone tip and the sleeve friction allow simplifying the problem assuming limited heat transfer between the cone tip and the rest of the cone penetrometer.

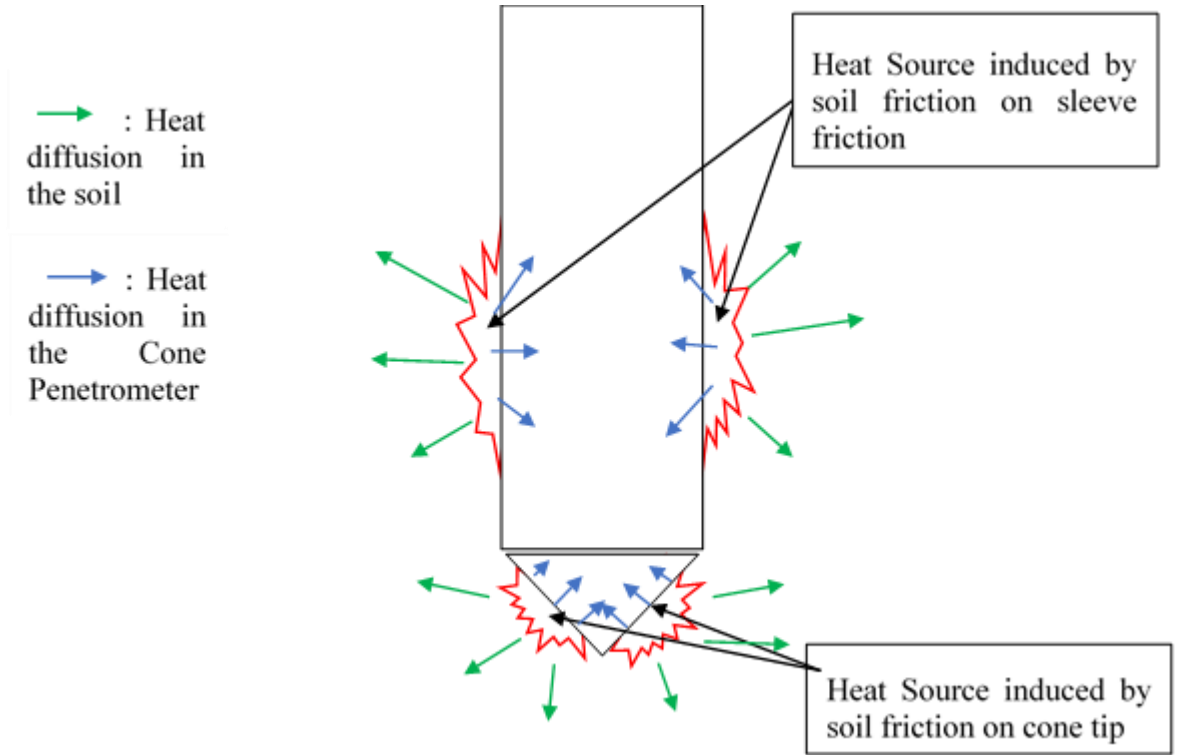


Figure 19: Thermal interaction between the cone tip and the soil

3.4. Thermal Tests Introductions

The thermal cone penetration test was introduced by Akrouch (2016) as an in-situ test useful to determine thermal properties of soil as an alternative to the thermal needle probe test (ASTM, 2014). Temperature sensors have been used by industry for decades, the use was mainly to measure in-situ temperatures. The cone typically heats up during the cone penetration (ISO, 2012). Heat is generated by friction between the soil and the cone, and therefore the heat increase must dissipate to measure the in-situ temperature. By recording the temperature dissipation, new perspectives for the cone penetration test applications were introduced. Indeed, the temperature dissipation provides valuable information to derive the thermal properties of soil, such as the thermal conductivity or the heat capacity. The interpretation method for deriving thermal conductivity introduced by Akrouch (2016) is based on empirical approaches and equation fitting. Using the similitude between excess pore pressure dissipation equation and thermal dissipation equation. However, a new interpretation model method was developed by Vardon (2018), this method presents the advantages to be a more theoretical approach resulting in a robust derivation of thermal conductivity of the soil.

3.4.1. Thermal probe test equipment and test procedure

The thermal needle probe (ASTM, 2014) is used for both laboratory and in-situ tests to derive the thermal conductivity of the soil. The thermal conductivity is determined based on the principle that heat dissipates radially with the application of a constant heat (heat source). The heating phase can be used as well as the cooling phase to derive the thermal conductivity of the soil. The thermal needle probe test results use an interpretation model based on the assumption of a line source solution (Carslaw and Jaeger, 2003). The thermal needle is designed to be as thin as possible to satisfy, as much as possible the assumption of an infinitely thin line source used in the interpretation model (Figure 20). The thinness of the needle is restricted to be sufficiently robust. However, this is a clear limitation of the test in-situ since strong soil layer, and deep penetration tests are not possible using the thermal needle probe. Moreover, the thermal needle test is pushed separately from the CPT cone, increasing significantly the operation time required and test's cost.

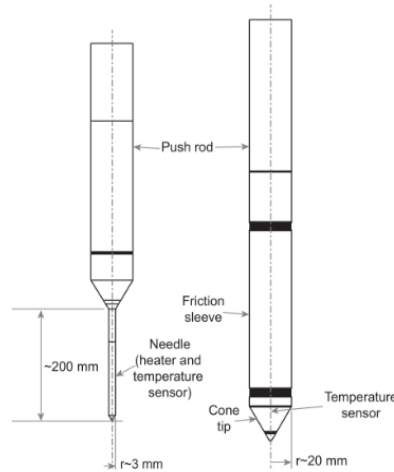


Figure 20: Thermal needle probe (left) & T-CPT cone penetrometer (right) from Vardon (2018)

3.4.2. T-CPT equipment and test procedure

The T-CPT probe includes a temperature sensor on the cone tip of the CPT (Figure 20). To date, two different T-CPT prototypes have been deployed and used. Both cones have a radius of 18 mm, the T-CPT prototypes developed by Fugro. The location of the temperature sensor installed on the probe differs as well as the internal voids (the second cone presenting a smaller void close to the cone tip). The T-CPT Cone Prototype 1 has its temperature sensor located above the cone tip, further away from the outer diameter of the probe than the T-CPT Prototype 2. The T-CPT Cone Prototype 2 has its temperature sensor located closer to the cone tip and its outer surface.

The T-CPT consists of pushing the cone penetrometer through the soil and continuously measuring the cone resistance, sleeve friction, pore pressure as well as the temperature. At a selected temperature, the cone penetration is stopped, and the dissipation of the heat generated during the cone penetration is recorded (no heat source required). The temperature dissipation is carried out until the interpretation model can give a good result, or until no change in temperature is observed. This thesis presents work undertaken in order to interpret the data obtained during continuous penetration of the thermal cone penetrometer.

3.5. Temperature Decay Tests Interpretation models

3.5.1. Akrouh proposed temperature decay interpretation model

Akrouh introduced in 2016 the thermal cone dissipation cone test (T-TCT). The results of the test showed a high potential even though the interpretation model proposed is empirically based on the similitudes between the advective water flow and the thermal conductivity (mass balance and energy balance). With the inclusion of this assumption, Akrouh proposed to estimate the thermal conductivity and diffusivity with the following expressions:

$$\lambda \approx \frac{1}{(A * t_{50})^B} \quad (5)$$

$$\alpha \approx \frac{T_{50} * a^2 * \chi}{t_{50}} \quad (6)$$

With A, B, and χ unitless parameters determined from the calibration of the TCT results. The interpretation model followed the following methodology: (a) in-situ TCT tests and soil samples extracted at the tested locations for laboratory testing purposes; (b) a numerical model was used to evaluate the calibration parameters; (c) results of the TCT tests were compared to the soil thermal properties measured from laboratory tests. Regarding the estimation of maximum temperature, the model uses a hyperbolic curve to fit the data to determine a theoretical value, and estimate the t_{50} used to derive the thermal properties of soil. Regardless of the simplifications made, and the empirical essence of the method, the interpretation model was seen to be able to give reasonable thermal properties values within the limited number of tests undertaken.

3.5.2. Vardon proposed temperature decay interpretation model

Vardon (2018; 2018) proposed a more theoretical interpretation model based on axisymmetric conditions and assuming that the dominant heat transfer process is the conduction. The model allows the derivation of (bulk) thermal properties of soil such as heat conductivity, k , and heat volumetric capacity, C . Three different developed one-dimensional asymmetrical analytical solutions have been used in Vardon research (Carslaw and Jaeger, 2003; Jaeger, 2011):

- “a. an instantaneous heat release along with a line inside an infinite medium
- b. an instantaneous heat release along the surface of a cylinder inside an infinite medium
- c. a perfectly conducting cylinder inside an infinite medium with an initial temperature different to that of the surrounding medium” Vardon (2018)

Vardon (2018; 2018) demonstrated that the three different analytical solutions lead to the same solution for the thermal conductivity, considering log timescale ($>100s$ for most soils) and a small radius (radius of the CPT cone).

$$k = f_{TC} \frac{S(T_{max} - T_0)}{4\pi[t(T - T_0)]} \text{ (Data – based method)} \quad (7a)$$

$$k = f_{TC} \frac{S(T_{max} - T_0)}{4\pi e^{i_T}} \text{ (Graphical method)} \quad (7b)$$

where f_{TC} is a factor included for calibration of the T-CPT cone; $S = c_{p,steel} * \rho_{steel} * A_{steel}$ is the heat content/release per length per degree; c_p is the specific heat capacity; ρ is the density; A is the cross-sectional area of the T-CPT cone; subscript ‘steel’ attributes properties relevant to steel; T_{max} is the maximum recorded temperature; T_0 is the initial ground temperature; T is the temperature at the current time; and t is time. The parameter i_T is the y-intercept (i_T) from a tangent drawn in the linear portion of an $\ln(T - T_0) - \ln(t)$ plot – that is when the time is large. Factor f_{TC} is included to allow for voids within the cone and the location of the sensor within the cone.

A check was made on the method since the solution converges after a sufficient time, more exactly when the gradient of the $\ln(T - T_0) - \ln(t)$ plot is equal to -1. According to Vardon’s work (2018), the equations (7a & 7b) are theoretically equal and allow the determination of the thermal conductivity of soil using either Thermal CPT data directly or by plotting the data in an $\ln(T - T_0) - \ln(t)$ plot. The method requires the initial temperature (T_0), which can be determined in two different ways. The first is by waiting until the heat generated by the cone penetration has dissipated; the second is by using the following equation:

$$T_0 = \frac{t_1 T_1 - t_2 T_2}{t_1 - t_2} \quad (8)$$

Two different solutions (9a & 9b) for the volumetric heat capacity of the soil are also proposed by Vardon (Vardon, 2018), based on the assumption that only the third of the analytical solutions represents the temperature well in the short term where the heat capacity is of greater impact.

$$C = \rho c_p = f_{HC} \left(\frac{dT_{norm}}{d\sqrt{t}} \Big|_{t \rightarrow 0} \frac{S}{4r_{CPT}} \right)^2 \frac{1}{\pi k} \text{ (Data – based method)} \quad (9a)$$

$$C = \rho c_p = f_{HC} \left(grad_T \frac{S}{4r_{CPT}} \right)^2 \frac{1}{\pi k} \text{ (Graphical method)} \quad (9b)$$

f_{HC} is the cone T-CPT calibration factor, r_{CPT} the radius of the cone, and $grad_T$ the gradient at the origin of a $T_{norm} - \sqrt{t}$ plot (Vardon, 2018):

$$T_{norm} = \frac{T_{max} - T}{T_{max} - T_0} \quad (10)$$

Full detailed of the assumptions and derivations are provided by Vardon (2018).

Vardon proposed a validation on his interpretation method. This validation consisted of 1D axisymmetric numerical analysis. The determination of calibration factor f_{TC} was undertaken using a two-dimensional asymmetrical numerical analysis. No calibration factor f_{HC} was possible due to the lack of field data. Both numerical analyses were undertaken using Comsol v5.2. The verification of the interpretation model was made on the main three final purposes of the Thermal CPT, that are the determination of the in-situ temperature, of the thermal conductivity, and of the heat capacity. To do so, calibration factors f_{TC} and f_{HC} were set up equal to unity.

3.6. Literature Review Summary

The literature review presented aimed to present the different interactions (mechanical and thermal) occurring between the cone tip and the soil by presenting the main conclusion addressed by researchers over the past few years on cone penetration failure mechanism, interface friction, thermal soil properties and dependencies over soil type fraction as well as porosity of water-saturated soils. Additionally, the main results obtained from previous research on the T-CPT were presented and summarised.

The interpretation model proposed by Akrouch (2016) introduced the potential of the T-CPT test to estimate thermal soil properties recording temperature decay at halted cone penetration. The lack of theoretical background of this proposed model was overcome by the recent interpretation model proposed by Vardon (2018). Using Vardon model, the thermal CPT shows good potential in determining point thermal conductivity value at selected depths in sandy soils using temperature decay recording. However, the thermal CPT requires the penetration to generate a temperature rise superior to 1°C to calculate the realistic thermal conductivity of the soil. This condition may not be possible in soft soils, and clayey soils have not been yet validated, constituting so far the main limitations of the Thermal cone penetrometer test. Despite the reliability of the thermal conductivity model, the heat capacity determination model based on T-CPT temperature decay test proposed by Vardon (2018) showed large scatter and lack of robustness.

Further research showed that the heat capacity should be determined using the usual CPT measurements (q_c , f_s and u). This last proposed interpretation model seems to be more robust and gives more reliable values for the heat capacity which is directly correlated to the soil density and porosity and not that affected by the sand/clay fraction ratio. This model needs to be confirmed with further practices to confirm its robustness and reliability, especially for the thermal conductivity determination model which seems to lack of reliability, requiring corrections from site to site. To date, the potential of the thermal CPT explored was essentially oriented towards determining the thermal properties of soil with the different interpretation models previously introduced. However, no research has been undertaken on the thermal soil behaviour to the Cone Penetration Test and its potential. Therefore, the research focuses on thermal soil behaviour during the CPT and its potential for improving soil characterisation.

4. Research Methodology

4.1. Introduction

4.1.1. Aims

The aims of the research are to address answers on the potentials of the T-CPT by understanding the mechanical/thermal interactions occurring between the cone penetrometer and the soil. The thermal interactions were studied in detail and represent the main focus of the thesis project with the investigations of the T-CPT potentials regarding the soil characterisation. Although the thermal interactions result from mechanical interactions, those were not investigated in detail in this project, only a crude investigation was made to estimate the resulting heat generated by friction.

4.1.2. Investigations programme

The framework of the research is divided into three different parts. The first part was the review on the CPT add-on sensors. Parts of the review were used and included in the previous chapters, and the full review is available in Appendix I.

The second part consists of exploring T-CPT potentials. From the literature review, thanks to Farouki's work (1981), it was stated that for fully saturated soils, the thermal soil properties such as the bulk density the thermal conductivity and the specific heat capacity are a function of the soil composition (sand and clay fraction) and the soil porosity (Appendix II). Therefore, those relationships are used to study the heat transfer occurring between the cone tip and the soil in order to conclude on the T-CPT potentials in determining the soil properties involved in the heat transfer. To do so, the mechanical interactions are shortly studied in order to give a crude estimation of the expected heat source as well as low and top boundary values of the heat source resulting from the friction between the cone tip and the soil as a function of the cone tip resistance. Finite Element Method model is used to conclude on the T-CPT potentials in soil engineering parameters estimation and in thin-layers soils detection and characterisation.

The last part of this project consists of the analysis of The Hollandse Kust Noord (HKN) project database provided by Fugro in which the T-CPT has been deployed significantly. The laboratory test results matching with the T-CPT profiles are analysed as well as the possible potentials of the T-CPT in predicting soil engineering parameters are presented and discussed. Along with the thesis project, an additional database was provided by Fugro from a different site to be studied according to the results obtained from the analysis of the HKN database.

4.2. Simplified Solution

4.2.1. Assumptions used for the simplified solution

In order to understand the temperature features recorded during cone penetration, a simple model was proposed to capture the heat transfer logic observed on in-situ tests. To do so, multiple numbers of assumptions were made to simplify the problem but respecting as much as possible the physics occurring between the cone tip and the soil during cone penetration. The following assumptions were made for the elaboration of this simplified model:

- 1D axisymmetric (half of the geometry is studied)
- Homogenous soil, Thermal soil properties and soil density set as constant
- Fully saturated ($S_r = 100\%$)
- Conduction heat transfer is the most relevant heat transfer process occurring in soils and well captured by Fourier's law (Fourier, 1822)
- Steel is infinitely conductive compared to soil
- Cone tip is a full volume of steel
- Heat diffusion mainly horizontal (assuming no vertical diffusion in the soil during the cone penetration)
- Soil temperature is always reinitialised to the initial soil temperature
- No heat diffusion into the CPT rod
- The heat-induced by friction on the sleeve friction is not considered

4.2.2. Proposed simplified solution

The aims of this proposed simplified solution are, firstly, to mimic the mechanical and thermal interactions occurring between the cone tip and the soil. Secondly, the simplified solution aims to estimate the temperature changes in the cone tip by setting up the soil thermal properties. This allows a preliminary investigation of the parameter influences (soil properties, the force applied on the cone, heat resulting from friction). Following the first law of thermodynamics, the general equation in term of energy can be expressed for the heat transfer occurring between the cone tip and the soil as follows:

$$\dot{E}_{source} - \dot{E}_{cone} - \dot{E}_{soil} = 0 \quad (11)$$

Rearranging the equation to express the energy in the cone:

$$\dot{E}_{cone} = \dot{E}_{source} - \dot{E}_{soil} \quad (12)$$

where \dot{E}_{cone} is the energy diffused into the cone tip, \dot{E}_{source} is the energy source induced by the friction of the soil on the cone tip lateral area surface, and \dot{E}_{soil} the energy diffused into the soil in kJ/s.

The heat source is estimated as follows:

$$F_{fc} = \mu \cdot q_c \cdot A_c \cdot \cos(60^\circ) [kN/linear\ meter] \quad (13)$$

Then the energy source is estimated by multiplying the force of friction by the distance of sliding in one second, v , which is equal to the inclined distance of the cone tip sheared in one second:

$$v = \frac{v_{cone\ penetration}}{\cos(0.5 \cdot 60^\circ)} \left[\frac{m}{s} \right] \quad (15)$$

$$\dot{E}_{source} = F_{fc} \cdot v \left[\frac{kJ}{s} \right] \quad (16)$$

Then the energy diffused in the soil is estimated as follows:

$$\dot{E}_{soil} = \lambda_{soil} \cdot A/2 \cdot F_{diffusion} \cdot (T_{cone} - T_{0,soil}) \quad (17)$$

$$A = \pi \cdot r_{cone} \cdot h_{cone} [m^2] \quad (18)$$

where h_{cone} is the height of the cone tip, A is the lateral surface area of the cone tip which corresponds to the surface in contact on which heat transfer occurs, and $F_{diffusion}$ is a factor of diffusion allowing to take into account the distance of influence of the heat conduction in the soil and the heat storage capacity of the soil (resistance). To estimate a realistic value of $F_{diffusion}$ including the effect of the soil density and the specific heat capacity of the soil, the parameter $F_{diffusion}$ was calibrated in such a way that the cone tip temperature matches with the data (for a cone resistance of 1 MPa, the cone temperature increase of 1°). This led to the first approximation of the radius of influence $F_{diffusion}$ as a function of the soil density and the soil specific heat capacity:

$$F_{diffusion} = \frac{1}{\frac{8}{C_{V,soil}} \cdot 10^{-3}} [m] \quad (19)$$

$$C_{V,soil} = c_{p,soil} \cdot \rho_{soil} [MJ/m^3K] \quad (20)$$

Finally, the cone tip temperature can be determined as follows:

$$T_{cone}^{t+1} = T_{cone}^t + \frac{\dot{E}_{cone}}{\left(\rho_{cone} \cdot c_{p,cone} \cdot \frac{1}{2} \cdot Volume_{cone} \right)} [K] \quad (21)$$

4.2.3. Simplified solution sensitivity analysis

A sensitivity analysis was performed on the cone tip temperature evolution depending on the different input parameters established for the simplified solution elaboration for a better understanding of the dependencies of the different temperature recording features (Appendix III).

Figure 21 presents the main conclusion of the crude sensitivity analysis conducted. As can be seen, the initial slope of the cone tip temperature seems to be dominated by the in-situ stresses represented by the cone tip resistance in this case. It was observed that other soil engineering parameters such as the soil friction angle and therefore the interface friction angle coefficient play an important role as well. Regarding the thermal soil properties (thermal conductivity and heat capacity), their effects were better observed on the depth required to reach the maximum temperature and on the maximum temperature reached. Moreover, the soil density plays an essential role in the maximum cone tip temperature reachable, since the soil density is directly influencing the heat transfer. This is due to the decrease of heat volumetric capacity as the soil density increases (Farouki, 1981). The soil density influences on the heat transfer can also be observed on the soil thermal diffusivity, which increases as the volumetric heat capacity decreases (specific heat capacity multiplied by the soil density) for a given thermal conductivity.

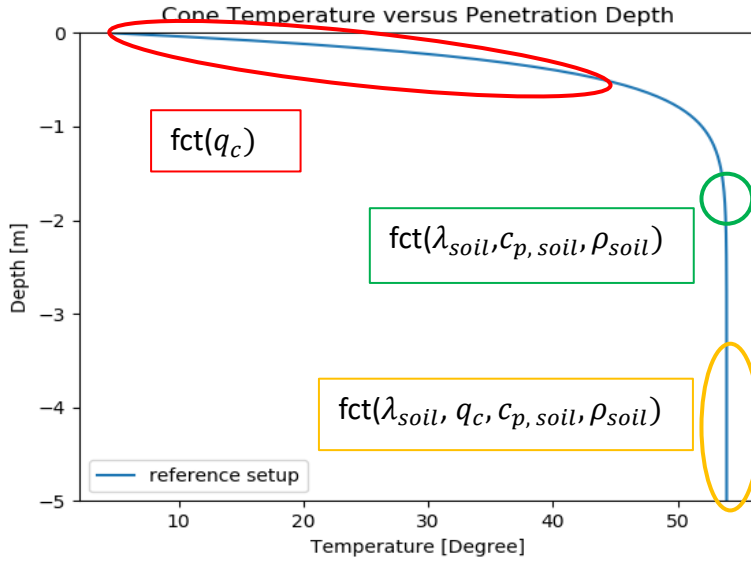


Figure 21: Sensitivity analysis performed on the simplified solution

4.3. Research Methodology Workflow

The observations and conclusions made using the simplified solution give a first direction for the research to implement in order to investigate and answer the T-CPT potentials in improving soil characterisation during soil investigation. The following research methodology workflow is proposed and used for answering the research questions and fulfil the research objectives and is based on the results of the simplified solution presented above.

4.3.1. Numerical investigation workflows

The numerical investigation programme is made of several investigations that aim to give a better understanding of the magnitude effect of the different parameters affecting the cone tip temperature. To do so the numerical investigation programme is subdivided into two different parts.

The first part attempts to validate the conclusions addressed using the simplified solution and to investigate the potential of the T-CPT in determining soil type for a given heat source as well as the soil parameters involved in the heat transfer. The uncertainties of the heat source estimation are also investigated to get a first impression of the potentials of the T-CPT. Therefore, the first part of the investigation programme starts with assuming the relationships between thermal material properties, density and porosity given by Farouki (1981). These relationships are included in Appendix II and assumed to be representative of the effective thermal soil properties. Then, based on the method proposed in the simplified solution, a simple method is proposed to estimate the heat source in function of the cone resistance. A 2D axisymmetric FE model is proposed and used to conclude on the different dependencies and associated magnitude of the cone tip temperatures features observed in-situ and on the T-CPT potentials in estimating soil properties involved in the heat transfer (Figure 22).

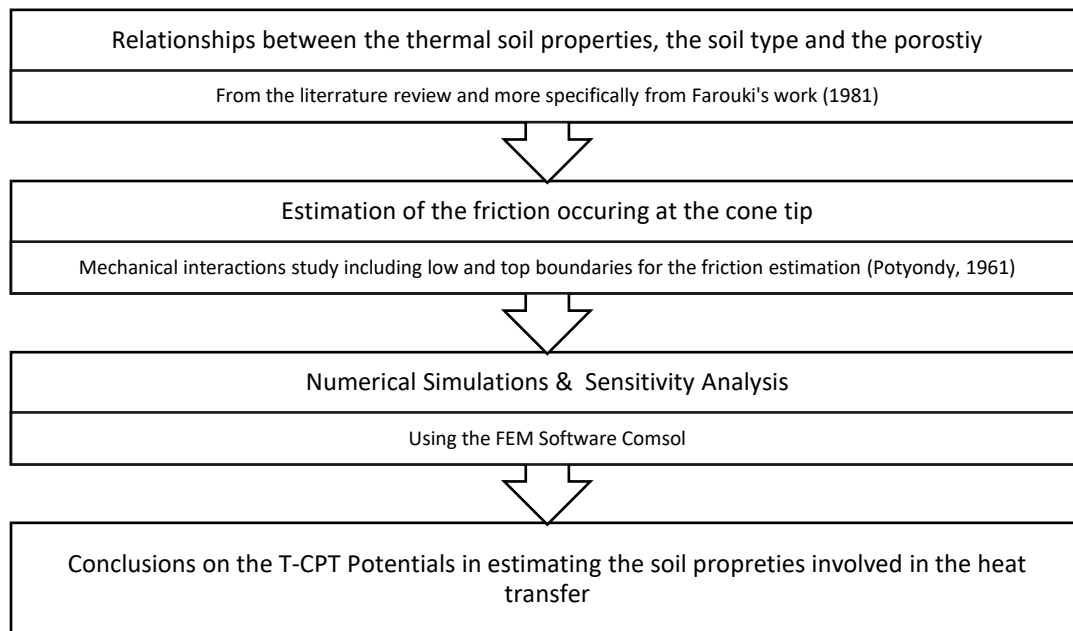


Figure 22: Cone tip temperature features numerical investigation workflow

The second part of the numerical investigation consists of studying the cone tip temperature behaviour in thinly layered soil. The numerical investigation follows the workflow presented in Figure 23 and aims to understand better the effect of high vertical soil variability on the cone tip temperature. Eventually, the results of this numerical investigation are of use to conclude on the potential of the T-CPT in detecting thin soil strata and in characterising them.

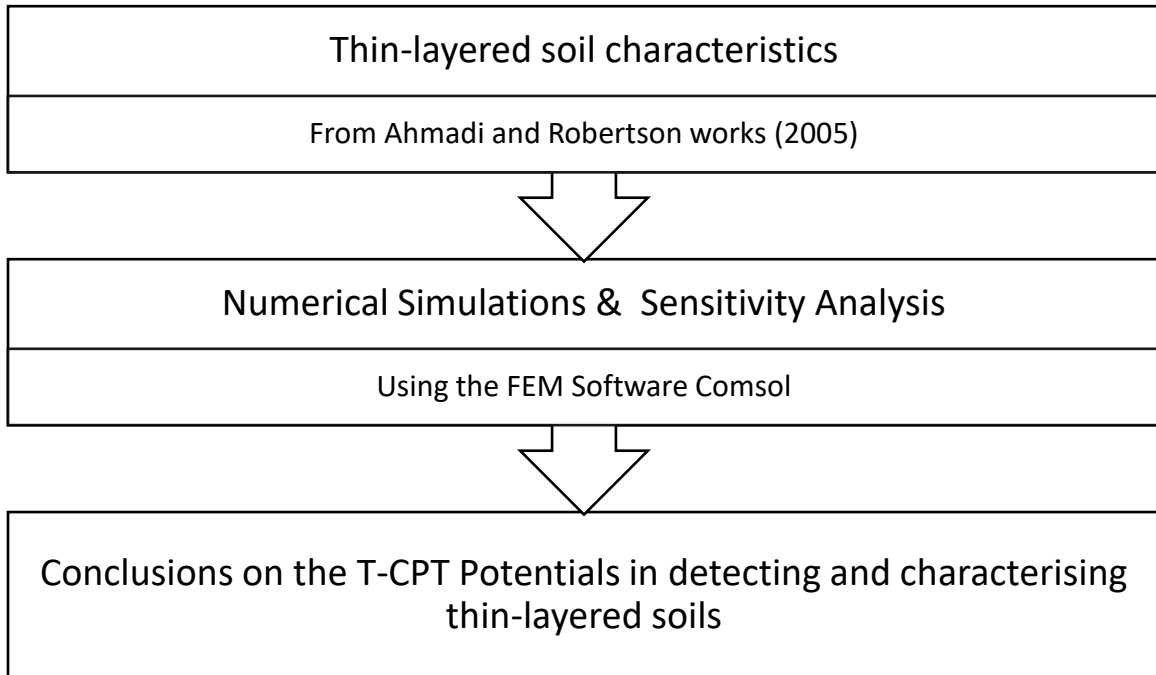


Figure 23: Cone tip temperature behaviour in thinly layered soils workflow

4.3.2. Database analysis workflow

The database analysis aims to find possible relationships between soil parameters obtained from laboratory tests and the different temperature features observed during the recording of the cone temperature during cone penetration. The database analysis includes the analysis and filtering of a large number of different laboratory tests and the comparison to the different temperature features. The database analyses are undertaken on the Hollandse Kust Noord (HKN) project as well as on another site kept private by Fugro. The database analyses follow the workflow presented in Figure 24.

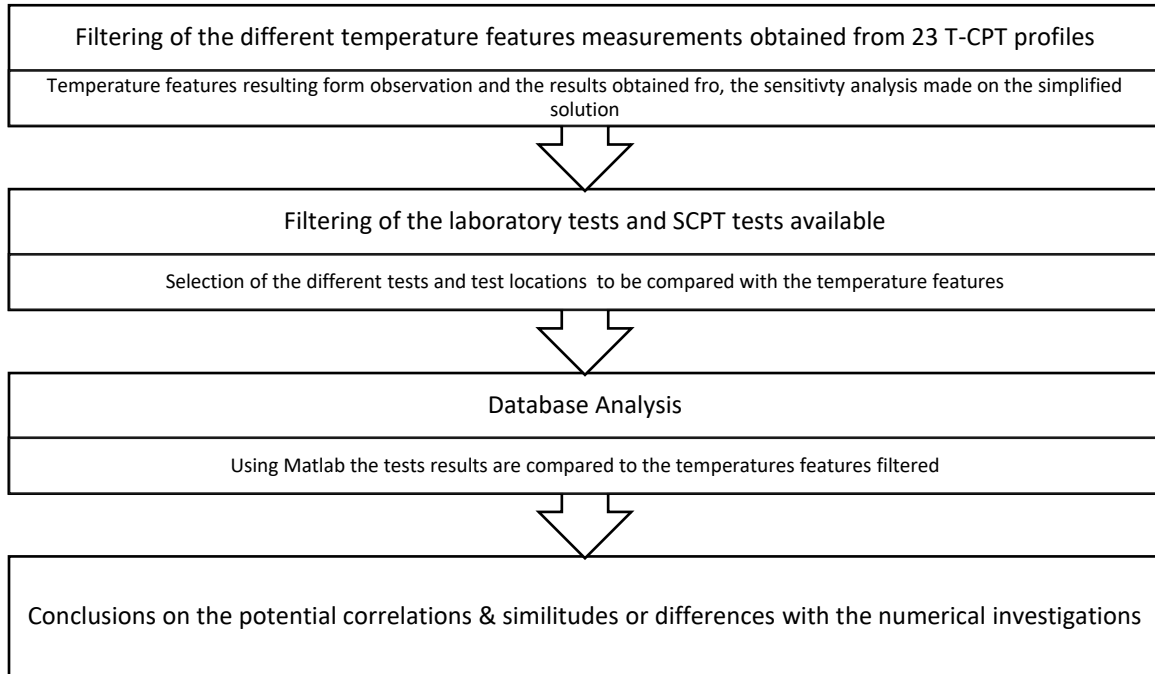


Figure 24: Database analysis workflow

5. Numerical Modelling Investigation

5.1. General Introduction

The Numerical Modelling Investigation consists of exploring the thermal behaviour recorded via the T-CPT as temperature measurements, its potentials and limitations to improve soil characterisation. Previously, a simplified solution was proposed, using the basic thermodynamic laws to mimic the cone tip and soil interactions observed during the cone penetration. A preliminary sensitivity analysis was performed on this simplified approach to determine the dependency of temperature measurement. The numerical modelling investigation consists of the elaboration of a finite element method model capturing the heat transfer occurring between the cone tip and the soil. Firstly, using the FEM software Comsol, sensitivity analyses were performed to check the validity of the conclusions made on dependencies of the temperature measurement features using the simplified solution. Secondly, an investigation is performed on the potential of the T-CPT measurements in predicting engineering soil parameters involved in the heat transfer within the limit of the friction estimation accuracy. Thirdly, the ability of the T-CPT in detecting thin layered soil is investigated and the potential of estimating characteristic engineering soil properties by means of heat transfer was evaluated. Additionally, the performance of the T-CPT in detecting thin-layers is determined by comparison with current different methods used by industry.

5.2. 2D Axisymmetric FEM Comsol Model

The numerical model consists of a 2D axisymmetric model considering a realistic but moderately simplified geometry, interior air-filled voids of the Thermal cone penetrometer prototype used in the field data acquisition, which is later used to validate the interpretations derived from the simplified proposed solution. Moreover, this numerical model is then used to investigate the different dependencies of the temperature measurement features observed in-situ as well as to conclude on the potential of the T-CPT. The finite element mesh used in the 2D numerical model is a 5000 three-noded triangular elements mesh, refined around the cone penetrometer, and especially around the tip of the cone. The domain selected is used to avoid any influences on the results from any geometrical and material boundaries. The air-filled voids are removed from the numerical analysis due to the low heat conduction of air. The cone penetration is simulated by applying a heat source resulting from the friction generated due to the sliding and rolling of the soil grains on the cone tip surface during the cone penetration.

5.2.1. 2D FE simplified model

A simplified geometry is proposed to model the heat transfer occurring during cone penetration. This simplified geometry is necessary since the FE model made using the software Comsol does not include mechanical deformation and therefore is not able to replicate the vertical motion of soil at the cone tip. This results in the loss of contact between the soil and cone tip as well as the loss of soil heated due to the heat source applied. This is due to the inability of the model to deal with the interaction between the cone tip and the soil being heated and moved vertically. Therefore, Figure 25 presents the simplified geometry adopted for a standard cone penetrometer (36 mm diameter). The simplified geometry respects the expected volumetric quantity of the true cone tip. The numerical investigations were undertaken with the following specificities:

- Initial Cone and Soil Temperature set to 283.5 Kelvin
- Heat Source applied between the cone tip surface and the soil
- 2D axisymmetric problem
- Top boundaries set as open temperature boundaries for both the cone penetrometer and the soil
- Soil lower boundary set as fixed temperature boundary (283.5 Kelvin)
- Vertical motion applied to the soil with a 2 cm/s to match with the standard penetration rate of the standard cone penetrometer test
- The cone penetrometer and the soil are set as a solid in which the thermodynamic laws are applied

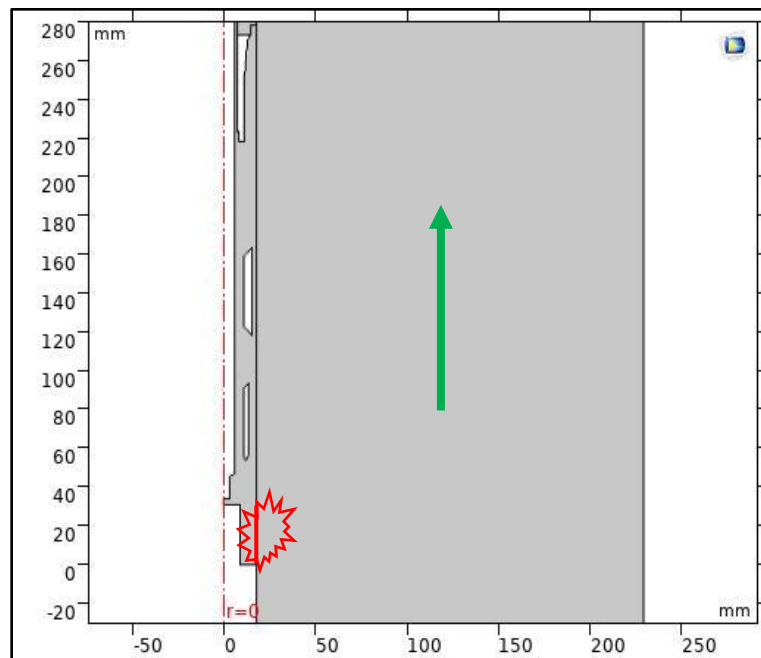


Figure 25: Model simplified geometry

5.2.2. Numerical analysis programme

Different studies are undertaken using 2D FEM model proposed. Firstly, a parametric study is performed to investigate the influences on the heat exchange of the heat source and the soil properties (density, initial temperature, thermal properties). The results are then compared with the results obtained from the simplified solution and conclusions are addressed on the dependencies of the temperature measurement features. The heat transfer in pure sand is investigated more deeply, respecting the relationships linking bulk soil density, heat capacity and thermal conductivity to soil type fraction as well as the porosity using Farouki's research (1981). This is of use to determine the potential of the T-CPT to determine soil parameters involved in the heat transfer occurring between the cone tip and the soil during cone penetration. The models are also used to investigate heat transfer occurring in thin-soil layers and to observe the response as well as the eventual decay of the temperature sensor, varying the heat source value.

5.3. Temperature Features Dependencies Investigations

5.3.1. Sensitivity analysis programme

The sensitivity analysis programme consists of the investigation of the thermal behaviour of the cone tip resulting from heat transfer occurring between the cone tip and the soil during cone penetration. The cone temperature evolution is thought to be a function of the friction occurring between the cone tip and the soil as well as the heat transfer as presented with the simplified solution previously introduced. By estimating the heat source (and its low and high bounds) induced by the friction arising between the cone tip and the soil, the sensitivity analysis attends to investigate the temperature feature's dependencies and to answer the research question: "Can the recorded temperature features be used to estimate soil parameters involved in the heat transfer occurring between the cone tip and the soil?". To do so, a simplified estimation of the heat source used as an input parameter for the FE model is proposed. Secondly, the effects of soil composition on the temperature feature are investigated as well (in term of Sand and Clay fraction). Finally, the temperature features dependencies are then investigated for pure sand for a large range of porosity. All in all, these investigations attempt to answer the questions raised regarding the T-CPT potentials for improving soil characterisation.

5.3.2. Heat source estimation

As mentioned in section 5.3.1, the heat source is an important input for the use of the FE numerical model presented using the FEM software Comsol. Using the results found by Potyondy (1961) and by Han (2018) presented in section 3.2.3, a similar logic is used for the simplified solution. The friction occurring between the cone tip and the soil is estimated such as:

The coefficient of friction, μ , is estimated based on Potyondy work (1961):

$$\mu = \tan(\delta) = \tan(0.64 \cdot \phi_u) \quad (22)$$

The force of friction, F_{fc} , is estimated as follows:

$$F_{fc} = \mu \cdot q_c \cdot A_c \cdot \cos(60^\circ) [kN/linear\ meter] \quad (23)$$

Then the heat source is estimated by multiplying the force of friction by the lateral area of the cone and by the distance of sliding in one second, v , which is equal to the inclined distance of the cone tip sheared in one second:

$$v = \frac{v_{cone\ penetration}}{\cos(0.5 \cdot 60^\circ)} \left[\frac{m}{s} \right] \quad (24)$$

Resulting in estimating the Heat Source such as:

$$Heat_{source} = F_{fc} \cdot A_{cone,lateral} \cdot v \left[\frac{W}{m^2} \right] \quad (25)$$

Where $A_{cone,lateral}$ is the lateral area of a cone of 36 mm of diameter:

$$A_{cone,lateral} = \pi \cdot r_{cone} \cdot \frac{r_{cone}}{\cos(60^\circ)} [m^2] \quad (26)$$

Assuming that the equation linking the effective friction angle and the cone resistance given by Kulhawy and Mayne (1990) is representative and valid, the Heat Source was estimated with low and high boundaries (Figure 26).

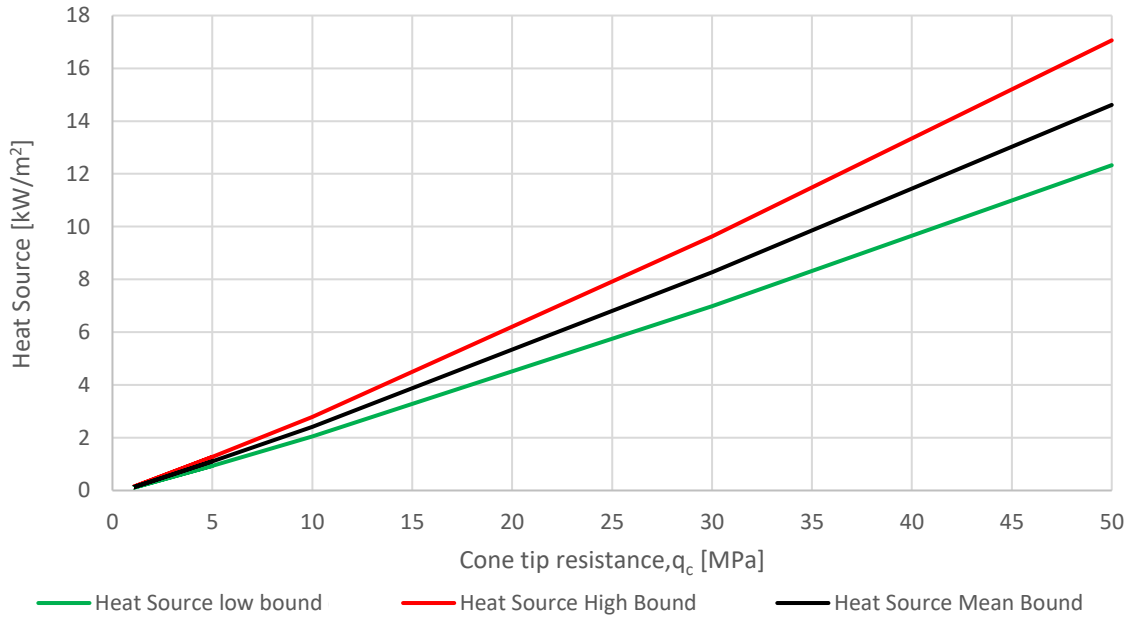


Figure 26: Estimated heat source, H_s , as a function of the cone resistance, q_c , with applying a low δ/ϕ ratio of 0.60 in green, a median δ/ϕ ratio of 0.65 in black, and a high δ/ϕ ratio of 0.70 in red, and with assuming the ϕ increasing with the cone resistance

Recalling that the friction and resulting heat source was studied and estimated in a simplistic fashion in order to focus on the heat transfer occurring between the cone tip and the soil. A better investigation of the soil parameters involved in the interface friction angle and the friction in general as well as the relationships linking the soil internal friction angle with the cone resistance would be recommended for further work. Although, it is thought and assumed that the presented method gives reasonable heat source estimation in the function of the cone resistance for sandy soils since good matches are found between the maximum temperature computed using this method and the one observed in-situ.

5.3.3. Cone tip temperature dependencies observations

The soil properties such as the soil bulk density, the specific heat capacity and the thermal conductivity were computed respecting the Farouki's equations (1981) previously presented in section 3.3.2. The different combinations of soil properties used for the different numerical investigations can be found in Appendix II.

Sand & Clay Fraction Influences:

The first investigation undertaken was performed on the different thermal properties for the diverse values of Sand/Clay fraction for a fixed porosity, $n = 0.4$. The sand fraction decreases from a maximal fraction set to 100% to 0% by increments of 10%. The numerical investigation is done for three different values of heat source, corresponding to three different values of cone resistance (5, 10 and 30 MPa) using a median δ/ϕ ratio value equal to 0.65 (Potyondy, 1961; Han *et al.*, 2018). The results are presented in Figure 27, Figure 28 and Figure 29. It can be observed that the Sand/Clay fraction has a limited effect on the maximum cone temperature. In Figure 27, for a heat source estimated with a cone resistance set equal to 5 MPa, the maximum temperature difference at the cone tip between pure clay and pure sand is lower than 1 Kelvin (maximum cone tip temperature for pure clay = 286.84 Kelvin, maximum cone tip temperature for pure sand = 285.98 Kelvin). The same behaviour is observed for higher values of heat source (Figure 28 & Figure 29), the cone tip temperature increases as the heat source increases for all Sand/Clay fraction investigated, and the cone tip maximum temperature difference observed between pure clay and pure sand increases as well proportionally to the heat source (1.87 Kelvin of cone tip temperature difference for a heat source estimated with $q_c = 10$ MPa and 6.48 Kelvin of cone tip temperature difference for a heat source estimated with $q_c = 30$ MPa). From visual observation, it can be seen that the initial slope of the cone tip temperature does not change as a function of the Sand/Clay fraction but does change as a function of the applied heat source.

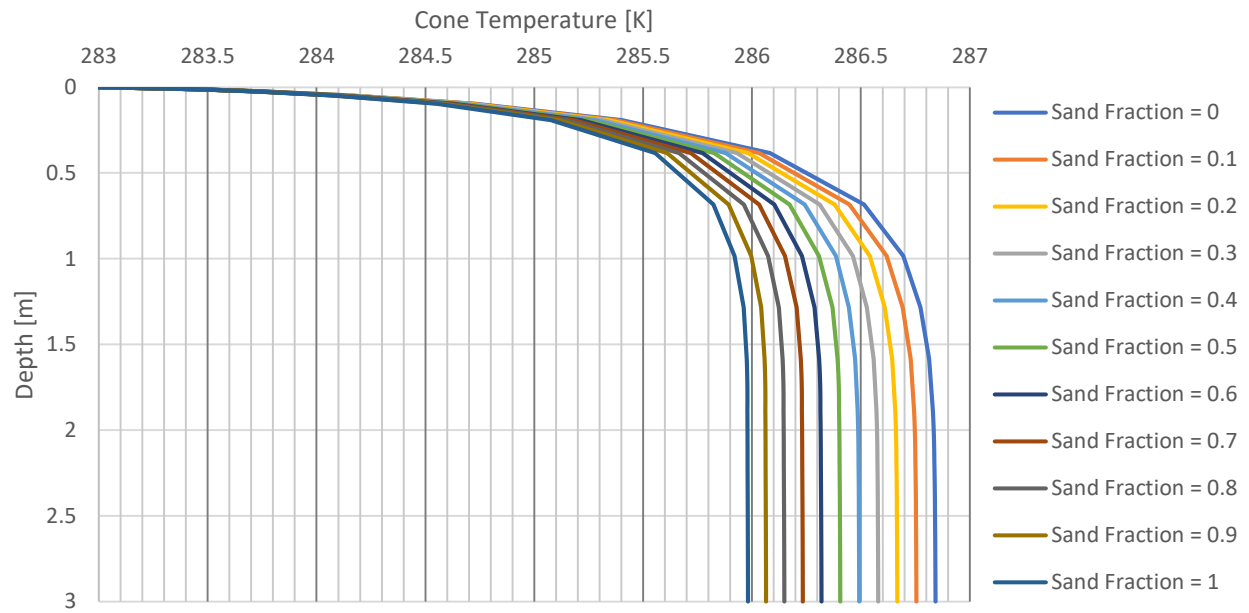


Figure 27: Temperature behaviour for different Sand/Clay fraction porosity , $n = 0.4$, $q_c = 5$ MPa and mean δ/ϕ ratio value = 0.65

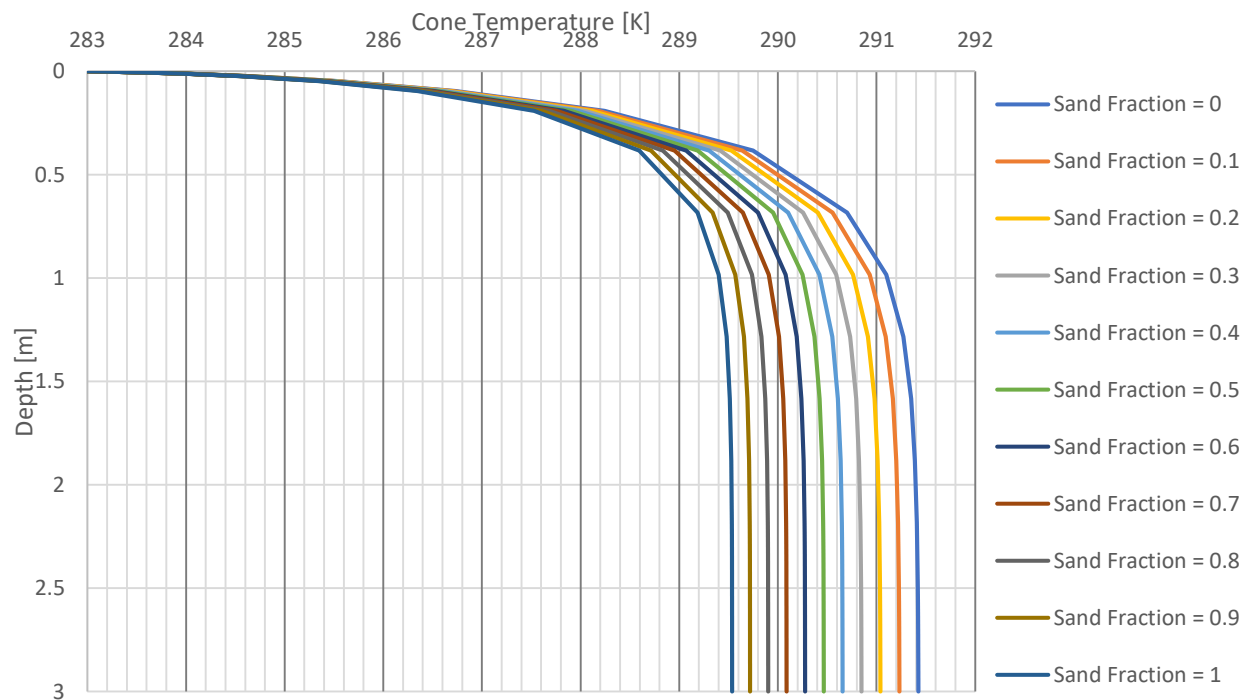


Figure 28: Temperature behaviour for different Sand/Clay fraction porosity , $n = 0.4$, $q_c = 10$ MPa and mean δ/ϕ ratio value = 0.65

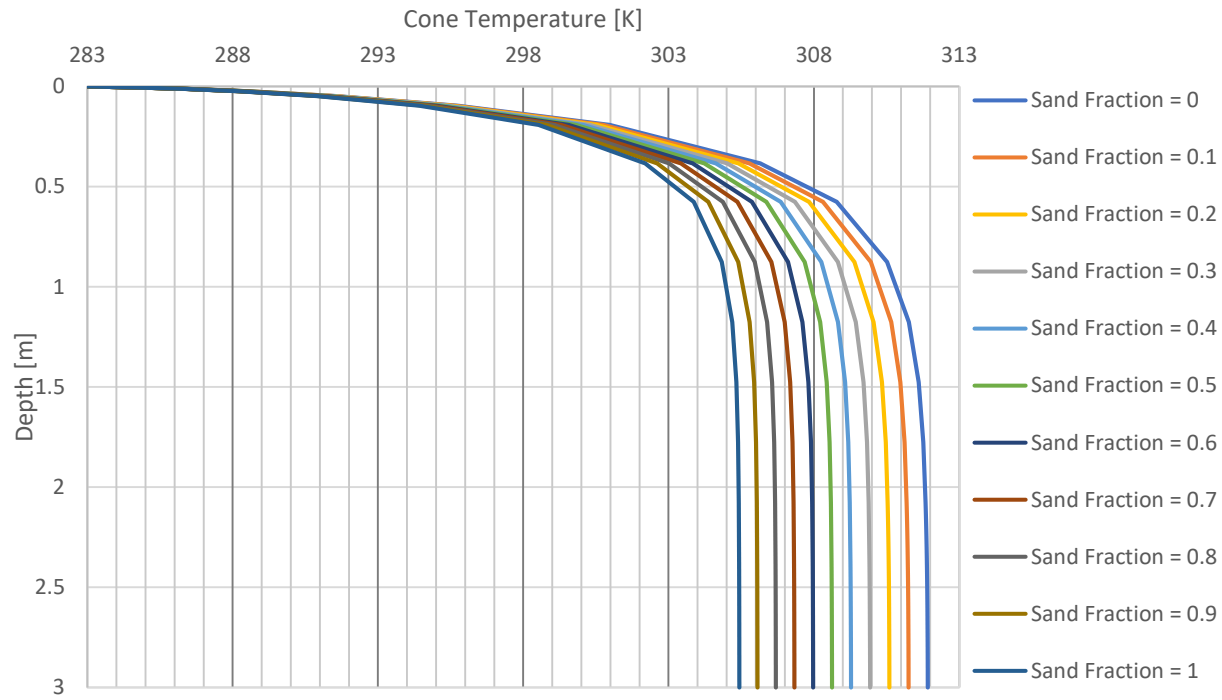


Figure 29: Temperature behaviour for different Sand/Clay fraction porosity , $n = 0.4$, $q_c = 30$ MPa and mean δ/ϕ ratio value = 0.65

Porosity Influences For Pure Sand:

The sand porosity influences on the cone temperature were investigated for the heat source values than the ones used in the previous numerical investigations. The results are presented in Figure 30, Figure 31 and Figure 32. For each different applied heat source, the initial slope of the cone tip temperature does not appear to be influenced by the sand porosity and the associated sand soil properties such as the bulk density, the specific heat capacity and the thermal conductivity (Appendix II). However, the maximum cone tip temperature is significantly affected by the sand porosity as the thermal conductivity and volumetric heat capacity and more generally the thermal diffusivity is affected by the sand porosity. It can be seen that this logic is respected by the model and lower porosity values result in lower maximum cone tip temperature due to the increase of thermal diffusivity of the sand with a decrease of porosity. Moreover, the porosity influence on the maximum cone tip temperature appears to be non-linear as the maximum cone tip temperature reduces more for high porosity values than for low porosity values. Different maximum cone tip temperature differences between pure sand with a porosity of 0.1 and 0.9 were found, 1.52 Kelvin for a heat source resulting from a $q_c = 5$ MPa, 4.97 Kelvin for a heat source resulting from a $q_c = 10$ MPa and 14.91 Kelvin for a heat source resulting from a $q_c = 30$ MPa.

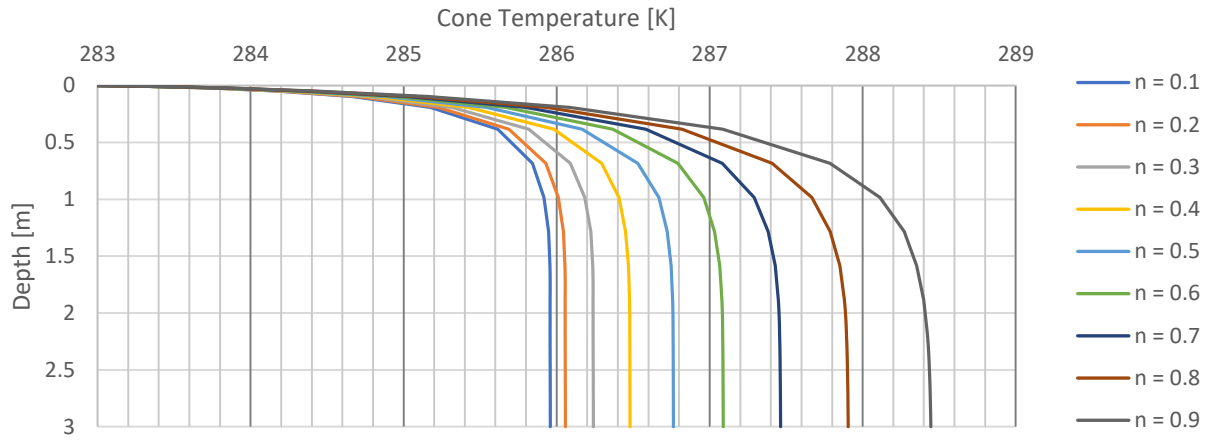


Figure 30: Temperature behaviour for pure sand, $q_c = 5$ MPa and mean δ/ϕ ratio value = 0.65

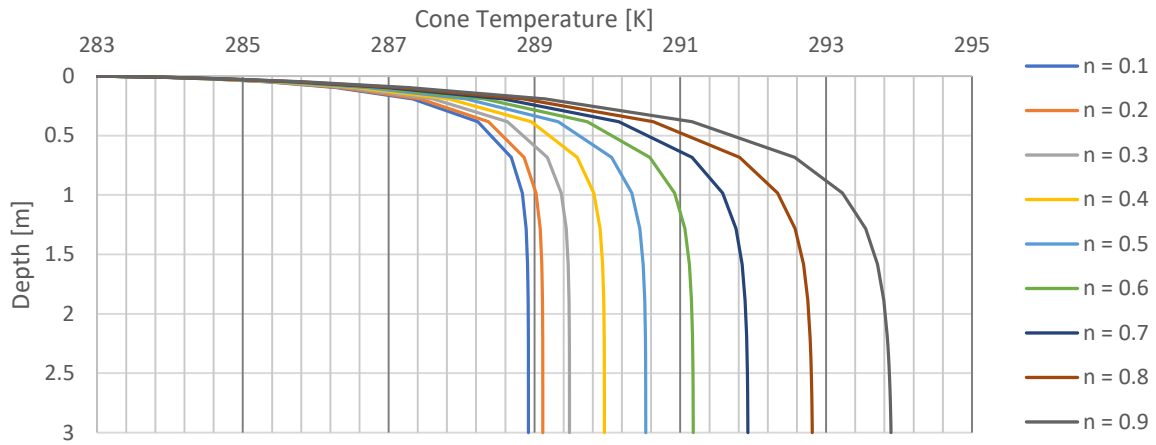


Figure 31: Temperature behaviour for pure sand, $q_c = 10$ MPa and mean δ/ϕ ratio value = 0.65

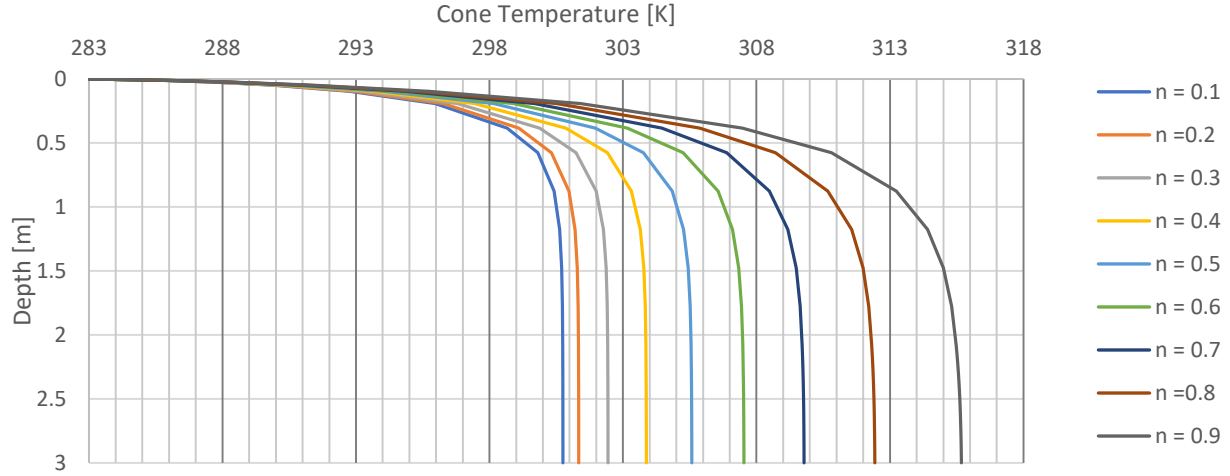


Figure 32: Temperature behaviour for pure sand, $q_c = 30$ MPa and mean δ/ϕ ratio value = 0.65

Interface and Internal Friction Angle Ratio Influences:

As the estimated heat source is determined using the interface friction angle ratio between the cone tip made of steel and the soil, the influences of the interface friction angle were investigated in order to estimate the T-CPT potentials in determining the soil properties involved in the heat transfer (bulk density, specific heat capacity and thermal conductivity). As previously mentioned, the ratio between interface friction angle between sand and steel as well as the sand internal friction angle, δ/ϕ , is generally accepted to be equal to 0.64 (Potyondy, 1961). However, recent research demonstrated the higher complexity in predicting the δ/ϕ ratio, and different δ/ϕ ratio values were found for different sands, ranging from 0.53 to 0.70 and depending on different parameters mentioned in section 3.2.3 (Han *et al.*, 2018). Therefore, the δ/ϕ ratio influences on the heat source estimation and the resulting maximum cone tip temperature for a pure sand with a fixed porosity value set to $n = 0.4$ were investigated using a low bound $\delta/\phi = 0.60$, a mean $\delta/\phi = 0.65$ and a high bound $\delta/\phi = 0.70$.

The numerical investigation results on the δ/ϕ ratio influences are presented in Figure 30, Figure 31 & Figure 32. From the numerical investigation results, the high influences of the δ/ϕ ratio on the cone tip temperature development are clearly visible. The δ/ϕ ratio value is significantly affecting the maximum cone tip temperature value. The δ/ϕ ratio bounds resulted in different maximum cone tip temperature depending on the cone resistance selected and the resulting estimated heat source. It can be seen that the maximum cone tip difference between the low and high bounds of δ/ϕ ratio increases with an increase of cone resistance. The maximum cone tip difference between the low and high δ/ϕ ratio bounds varies from 1.16 Kelvin for a $q_c = 5$ MPa, 2.32 Kelvin for a $q_c = 10$ MPa, to 6.96 Kelvin for a $q_c = 30$ MPa.

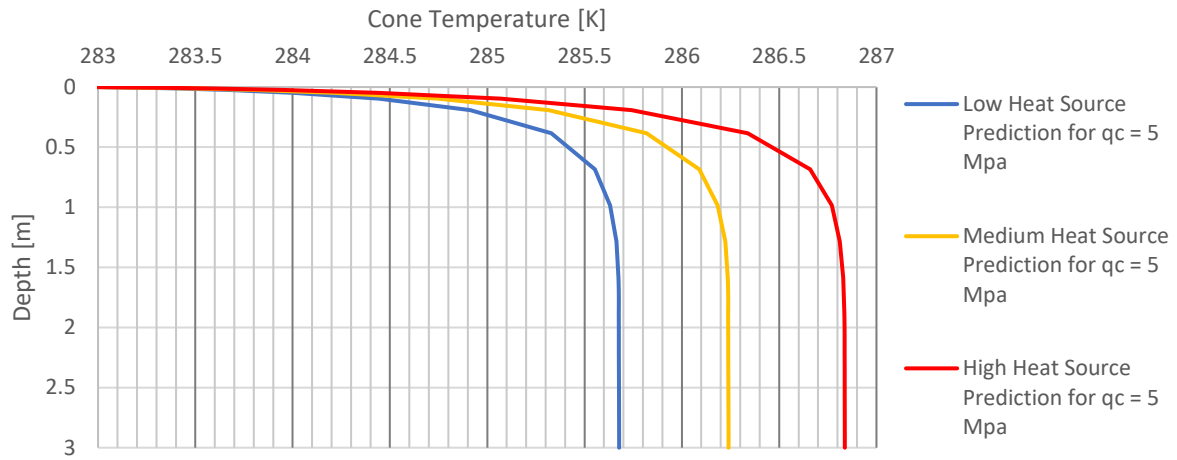


Figure 33: Interface friction angle uncertainty effect
 $n = 0.3$ & $q_c = 5$ MPa, low δ/ϕ ratio value = 0.50, median δ/ϕ ratio value = 0.65 and high δ/ϕ ratio value = 0.70

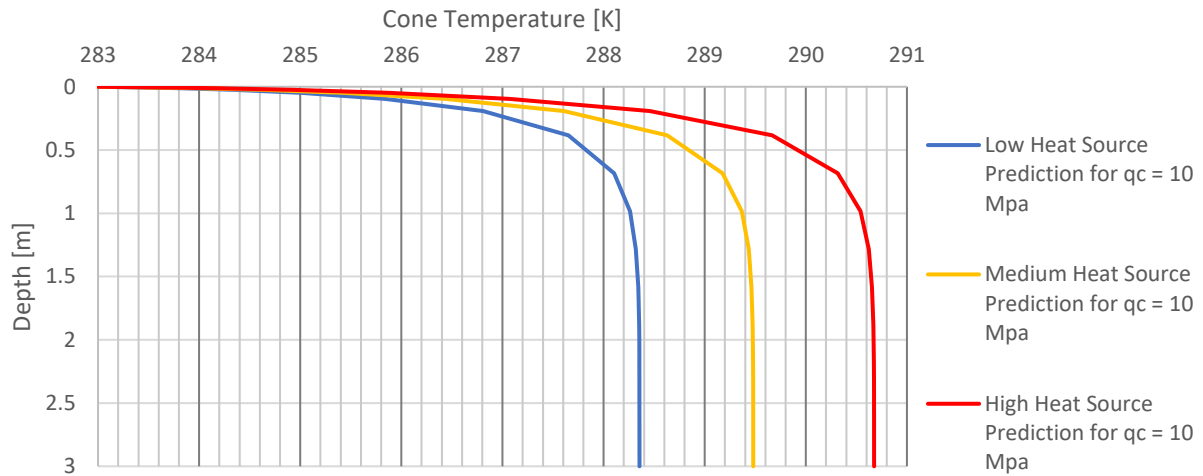


Figure 34: Interface friction angle uncertainty effect
 $n = 0.3$ & $q_c = 10$ MPa, low δ/ϕ ratio value = 0.50, median δ/ϕ ratio value = 0.65 and high δ/ϕ ratio value = 0.70

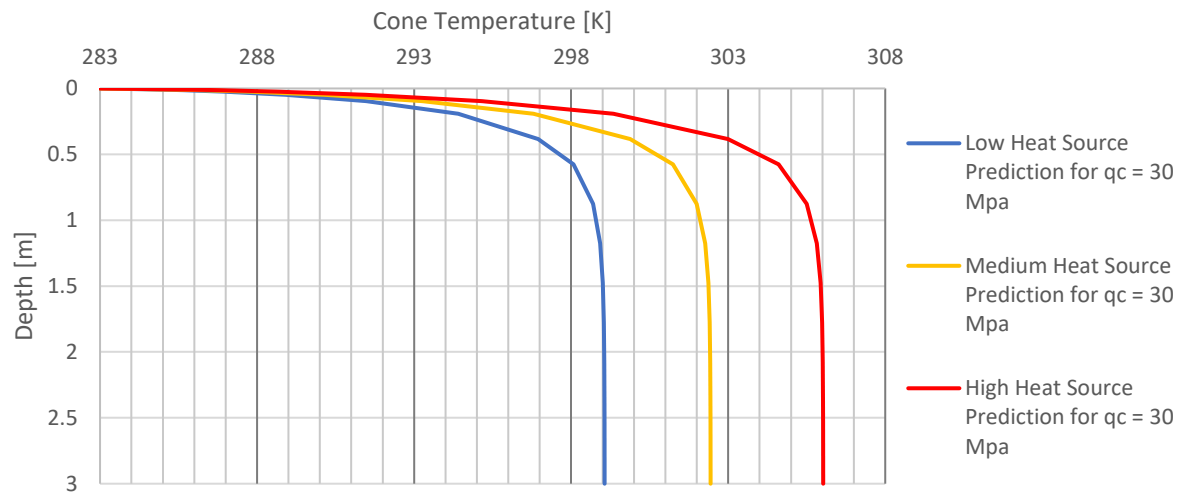


Figure 35: Interface friction angle uncertainty effect
 $n = 0.3$ & $q_c = 30$ MPa, low δ/ϕ ratio value = 0.50, median δ/ϕ ratio value = 0.65 and high δ/ϕ ratio value = 0.70

5.3.4. Cone temperature sensitivity analysis conclusions

From the observations previously made, several conclusions can be addressed on the cone temperature behaviour and dependencies. Firstly, the conclusions addressed on temperature features presented using the simplified solution were respected and observed with using the 2D FE numerical model presented. The initial slope of the cone tip temperature is concluded to be mainly a function of the stress applied on the cone tip. Moreover, the maximum cone tip temperature value is concluded to be a function of the different soil parameters involved in the heat transfer, but mainly a function of the stress applied, the δ/ϕ ratio value and the resulting heat source.

Figure 36 presents the maximum cone tip temperature in function of the cone resistance and assuming a mean δ/ϕ ratio value of 0.65 for the soil of varying Sand/Clay fraction at a fixed porosity value of 0.4. Figure 37 presents the maximum temperature in function of the cone resistance and assuming a mean δ/ϕ ratio value of 0.65 for pure sand at different porosity values.

In real situations, the sand porosity is known to be varying from 0.4 for loose sand to 0.2 for dense sand. In consequence, the influences of the soil properties on the heat transfer for pure sand with a porosity varying between 0.2 and 0.4 does not significantly affect the heat transfer and the maximum cone temperature reached as only 2 degrees of difference is observed between a dense sand with a porosity set to 0.2 and a looser sand with a porosity set to 0.4 for the highest heat source resulting from a $q_c = 30$ MPa assuming a mean δ/ϕ ratio value of 0.65. The maximum cone temperature difference is even lower for lower cone resistance. Additionally, the high complexity in estimating the δ/ϕ ratio value and small variation in the δ/ϕ ratio value showed that the resulting heat source affects the maximum cone temperature with a greater impact than the soil properties affect the heat transfer. In consequence, from those observations and the conclusions addressed, it is concluded that the T-CPT offers minor potentials in determining soil properties involved in the heat transfer occurring between the cone tip and the soil. Therefore, the friction is concluded to be of greater influence and to play a major role in the heat transfer, which could potentially be investigated in further work to get valuable information on the sand properties affecting the δ/ϕ ratio value such as the particle size, or the sand gradation.

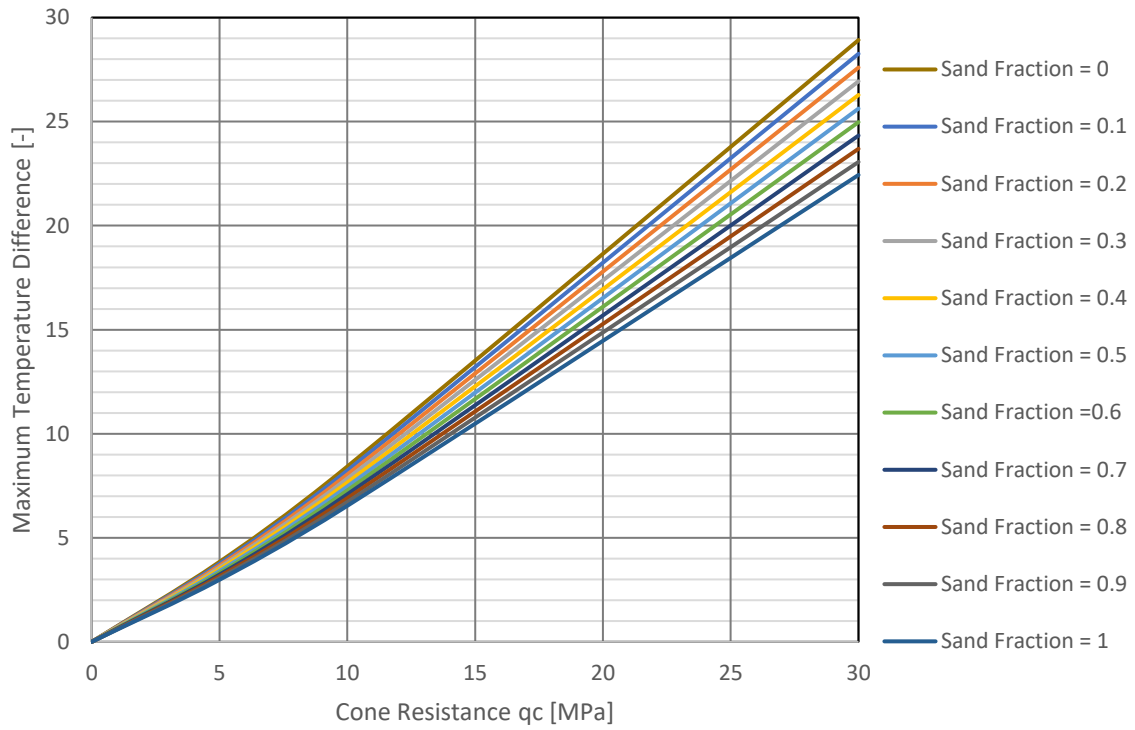


Figure 36: Maximum temperature difference vs cone resistance for different Sand/Clay fraction & fixed porosity, $n = 0.4$ and mean δ/ϕ ratio value = 0.65

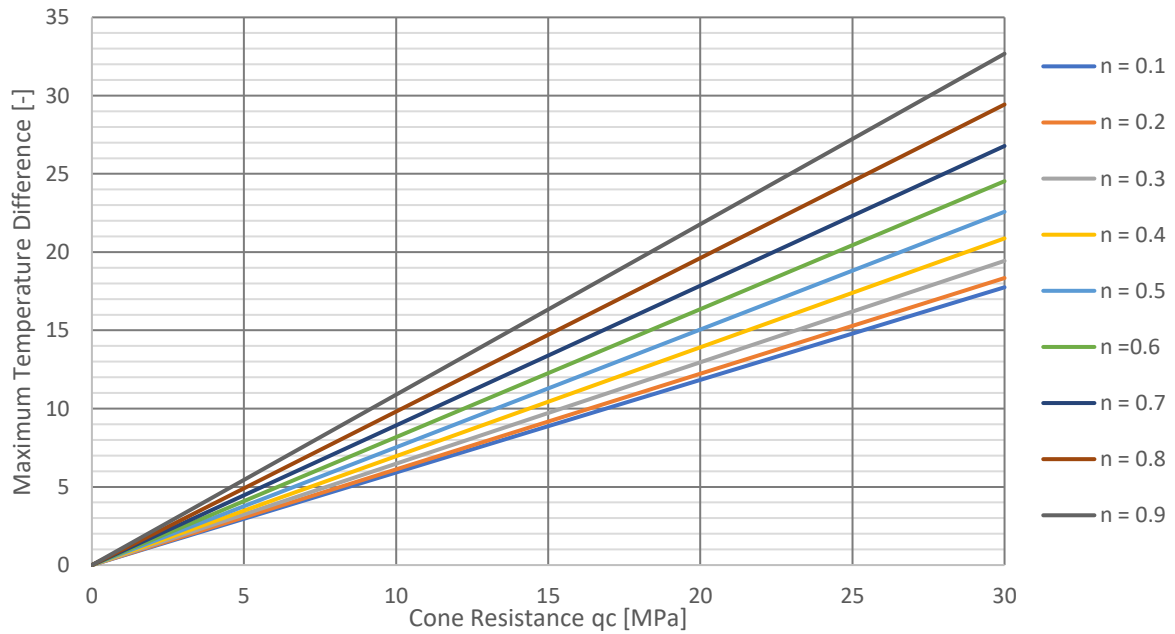


Figure 37: Maximum temperature difference vs cone resistance for pure sand and mean δ/ϕ ratio value = 0.65

5.4. T-CPT Temperature Behaviour Investigations In Thinly-Layered Soil

The last investigation conducted aims to investigate the thermal behaviour of the T-CPT in thinly-layered soils. The temperature sensor is thought to be compared to the cone resistance recording due to the time necessary to dissipate heat in soils. Therefore, the impact of multi-thinly layered soils is of interest in order to get a better understanding of the different factors influencing the temperature features recorded by the T-CPT during cone penetration and to get a better idea of the T-CPT application potentials.

5.4.1. Thinly layered soil investigation programme

In order to investigate the T-CPT temperature behaviour in thinly-layered soil, an investigation programme was proposed (section 4.3.1). To capture the general physical behaviour, the applied heat source in thin layer systems was estimated based on the cone resistance recorded during cone penetration in thinly layered soils. It is well established by numerical and experimental research (Ahmadi and Robertson, 2005; van der Linden, 2016) that the cone resistance recorded by the CPT is influenced by a number of factors such as the characteristic strength value of the different soil layers, the thickness and the cone-diameter. More precisely, the past research demonstrated that the cone resistance recorded by the CPT in thin-layered soils is influenced by the high soil vertical variability (section 3.2.2). The cone resistance measurement was found to be influenced by the soil above and below the cone tip, resulting in an overestimation of the characteristic cone resistance in soft soils, whereas the characteristic cone resistance of stiff soils is generally highly underestimated. Following Ahmadi and Robertson observations (2005), the same impact of the multi-layer systems on the cone resistance computed was assumed as valid, and therefore, the impact was then applied on the resulting heat source values. Table 3 & Table 4 summarise the soil parameters and heat sources applied used for the different uniform and multi-layer systems investigated.

Additionally, another FE numerical model was generated in order to respect the thin multi-layer geometry and their associated soil properties involved in the heat transfer arising between the cone tip and the soil. To do so, thin soil layers of 1 mm of thickness were implemented in the previous FE numerical model on the soil area in contact with the cone tip. Using periodic functions, the soil bulk density, the specific heat capacity, the thermal conductivity and the heat source soil parameters are then changing for each millimetre of soil depending on the layer thickness and the cone penetration rate (0.02 m/s). This is of use to mimic the cone penetration in thinly layered soils and to observe the general behaviour of the cone tip temperature recorded in such soil stratigraphy.

Table 3: Parameters used for uniform layer system investigation

| Layering System | Parameters | Soil Type | |
|-----------------|--|-----------|--------|
| | | Clay | Sand |
| Soil Parameters | Bulk density [kg/m^3] | 1988.8 | 2161.1 |
| | Volumetric Heat Capacity [$\text{MJ}/\text{m}^3 \cdot \text{K}$] | 2.93 | 2.60 |
| | Thermal Conductivity [$\text{W}/\text{m} \cdot \text{K}$] | 1.54 | 3.81 |
| Uniform Layer | Characteristic Cone Resistance, $q_{c, \text{char}}$ [MPa] | 0.33 | 22 |
| | Characteristic Heat Source, $H_{S, \text{char}}$ [W/m^2] | 750 | 56400 |

Table 4: Parameters used for multi-layer system investigation

| | | | |
|---------------|---|------|--------|
| 8 cm | Modified Cone Resistance, $q_{c, mod}$ [MPa] | 0.5 | 2.5 |
| | Modified Heat Source, $H_{S, mod}$ [W/m ²] | 1280 | 6410 |
| 15 cm | Modified Cone Resistance, $q_{c, mod}$ [MPa] | 0.5 | 5 |
| | Modified Heat Source, $H_{S, mod}$ [W/m ²] | 1280 | 10980 |
| 30 cm | Modified Cone Resistance, $q_{c, mod}$ [MPa] | 0.5 | 10 |
| | Modified Heat Source, $H_{S, mod}$ [W/m ²] | 1280 | 256450 |
| 50 cm | Modified Cone Resistance, $q_{c, mod}$ [MPa] | 0.5 | 12.5 |
| | Modified Heat Source, $H_{S, mod}$ [W/m ²] | 1280 | 35900 |
| 75 cm | Modified Cone Resistance, $q_{c, mod}$ [MPa] | 0.5 | 16 |
| | Modified Heat Source, $H_{S, mod}$ [W/m ²] | 1280 | 47440 |
| 100 cm | Modified Cone Resistance, $q_{c, mod}$ [MPa] | 0.5 | 22 |
| | Modified Heat Source, $H_{S, mod}$ [W/m ²] | 1280 | 66800 |

5.4.2. Sand/Clay multi-layer system investigation observations

The different multi-layer thickness models gave the same thermal behaviour. For every set up tested, it can be observed that the maximum temperature observed in the previous configuration with uniform soil layer is not reached. Using the multi-layer numerical model, the temperature equilibrium between the heat generated by means of friction arising between the cone tip and the soil during cone penetration is not reached after 3 m of simulated cone penetration for a multi-layer system as thin as 8 cm. This is thought to be mainly due to the arising of the heat source in the sand layers inducing the cone tip temperature to rise even if the sand is a more thermally conductive material than the clay. For all cases, the cone temperature obtained for the multi-layer system is lower than the cone temperature obtained for a uniform sand layer resulting from a reduced heat source using the same cone tip resistance value as used for the multi-layer system.

For all multi-layer configurations (Figure 38, Figure 39 & Figure 40), it can be observed that the cone tip temperature increases to a higher value than the maximum temperature value expected for a uniform clay layer. However, the cone tip temperature obtained is always lower than a uniform sand layer using the same cone tip resistance than the cone tip resistance assumed for the sand layer within the multi-layer system. It can be observed that for thinner multi-layer configuration, the cone tip temperature is not reaching the temperature obtained for a uniform clay or a uniform sand layer using the same heat source parameters. Moreover, as the multi-layer system gets thinner and thinner, the cone tip temperature tends to average over a fixed temperature. Similarly, the thicker the multi-layer system, the larger the temperature fluctuation observed.

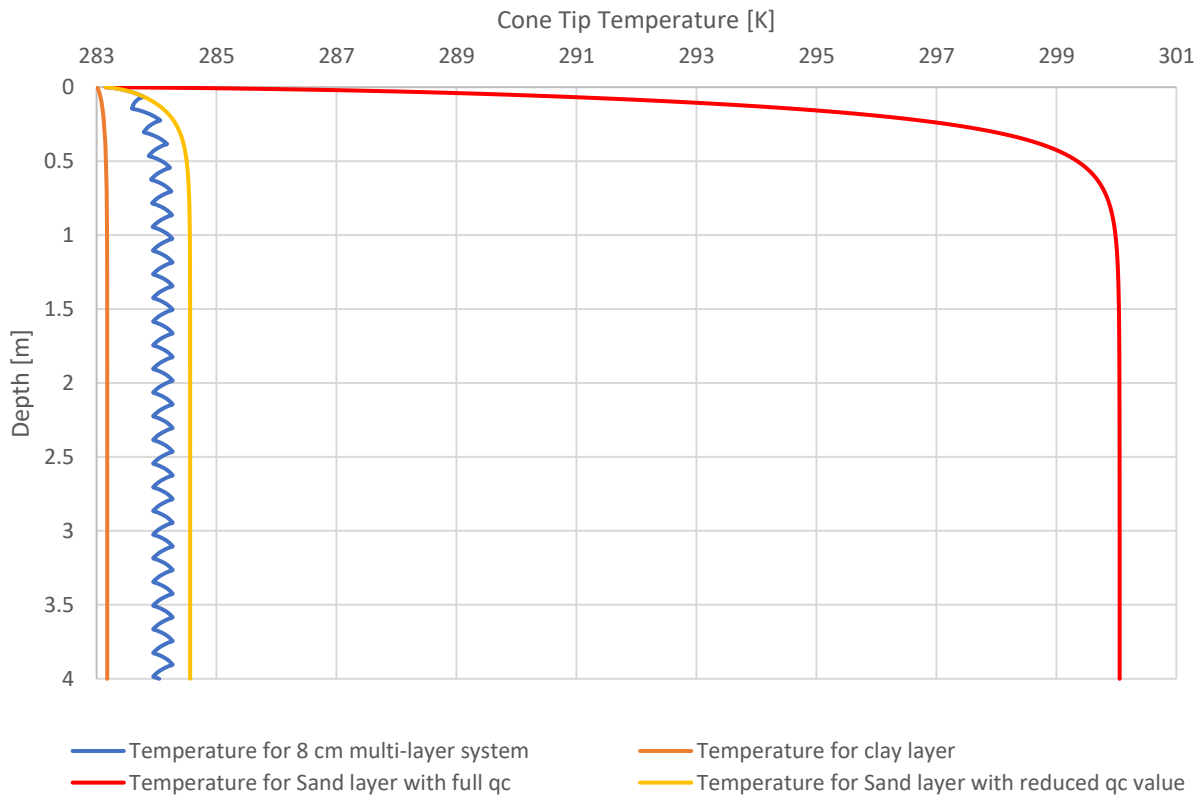


Figure 38: Multi-layers system thermal behaviour 8 cm Sand/Clay

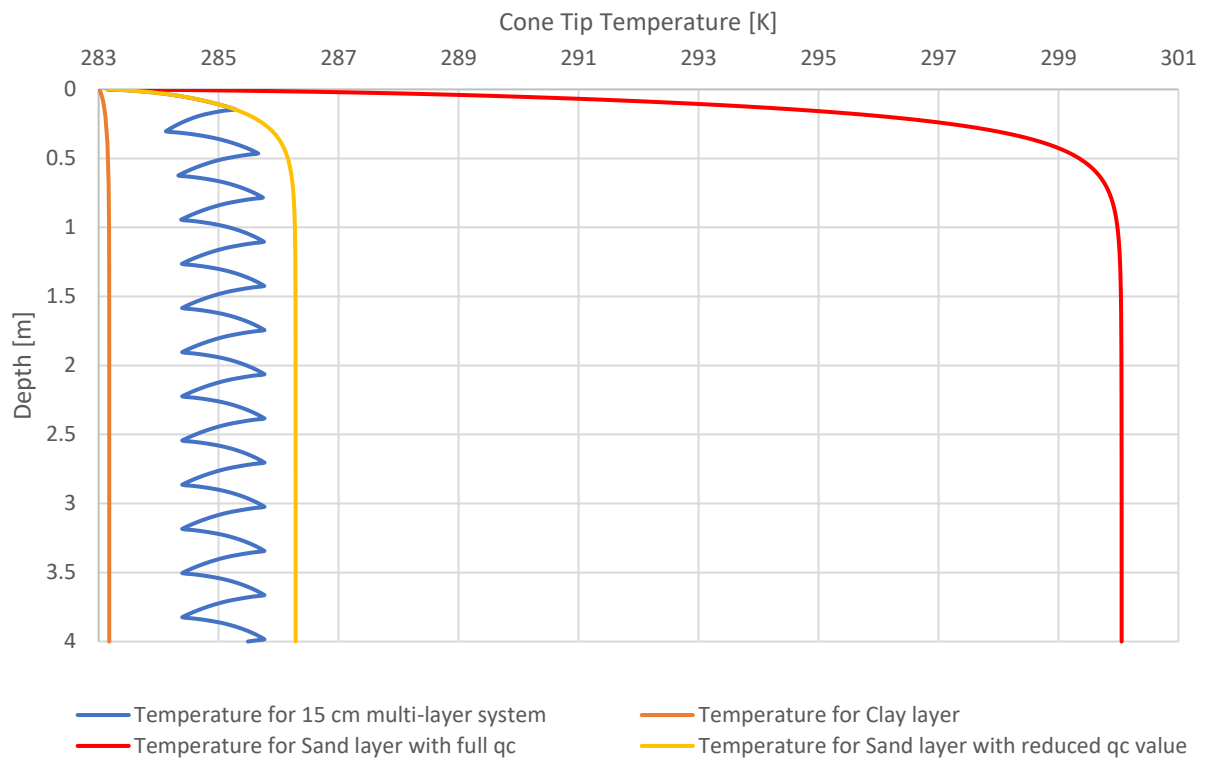


Figure 39: Multi-layers system thermal behaviour 15 cm Sand/Clay

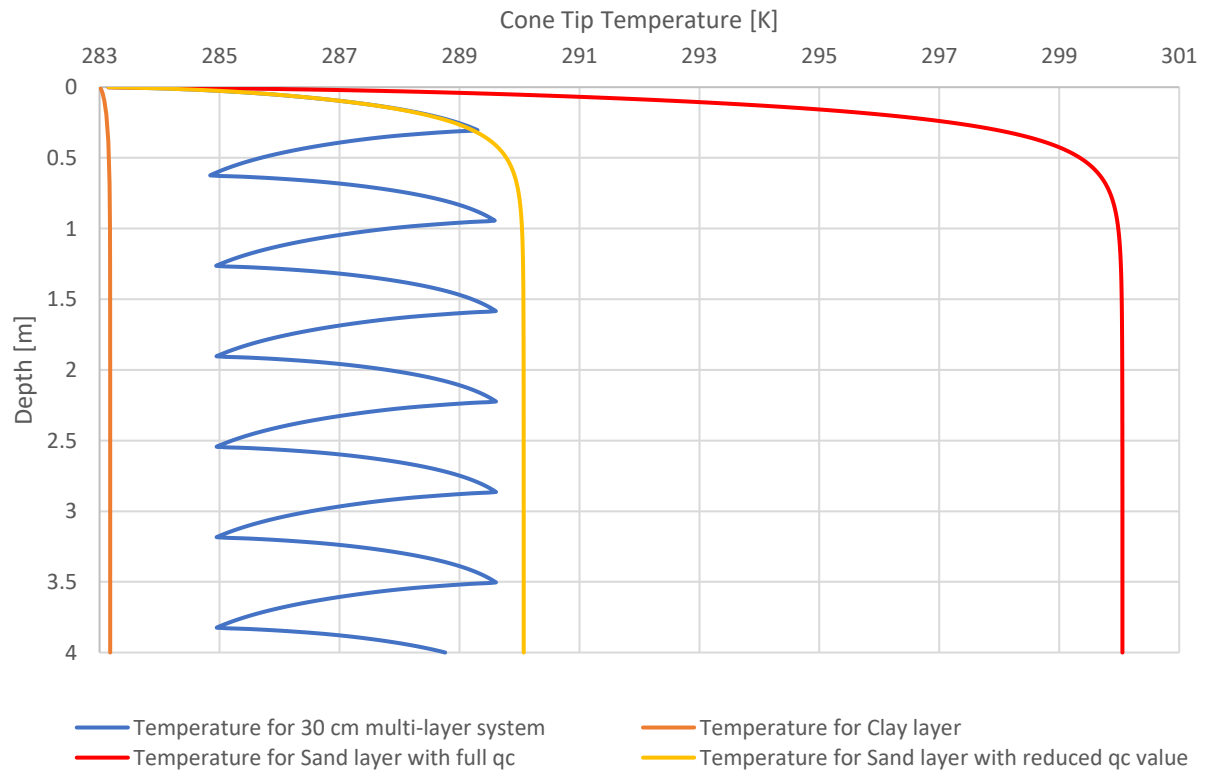


Figure 40: Multi-layers system thermal behaviour 30 cm Sand/Clay

5.4.3. Multi-layer system conclusions

Based on the observations made on the numerical modelling investigations previously presented, the following conclusions can be addressed on the thermal behaviour of multi-layer systems. The cone tip temperature in multi-layer systems is significantly influenced by the layer thickness and its resulting cone tip resistance. Due to the lower diffusivity characteristic value of clayey soils (specific heat capacity, thermal conductivity and soil bulk density), the heat generated by friction in the sandy layers is not dissipated as fast as it would be in a sand layer. In consequence, the minimum cone tip temperature reached in the clay layers increases as the thickness and the assumed cone resistance of the sand increase as well. This illustrates the heat dissipation delay occurring in the cone tip which affects the thermal sensor answer. Therefore, the thermal sensor can record an increase in temperature due to an increase in cone tip resistance with good reliability. However, when a softer layer is encountered, the time required for the cone tip to dissipate the heat previously generated is too important to reach the expected cone tip temperature for the clay layer. From the set of soil parameters used for the multi-layer system investigation (Table 3), it can be concluded that the thermal conductivity and the heat source applied are the main parameters affecting the heat transfer during the cone penetration as both soil parameters, the specific heat capacity and soil bulk density, do not differ significantly.

Finally, the thermal behaviours observed for the different set of multi-layers proved the dissimilarities of the temperature features that could be recorded for homogeneous soils or thin-layer soils. The cone temperature evolution is thought to be, mainly affected by the heat source resulting from friction, the thickness of the layers and the resulting heat transfer occurring in each different soil layer and the different thermal conductivity of the different soils encountered.

5.5. Numerical Modelling Investigation Conclusions

5.5.1. Sensitivity analyses conclusions

The sensitivity analyses performed allowed to address multiple of conclusions on the soil behaviour and the temperature measurements were undertaken using a T-CPT. The assumptions made regarding the dependencies of the initial slope of the cone temperature and of the maximum cone temperature value from the crude sensitivity analysis performed using the simplified solution proposed previously in the Research Methodology chapter were also observed using the 2D axisymmetric FE numerical model. The initial slope cone tip temperature is concluded to be mainly controlled by the stress and therefore by the heat resulting from the friction between to cone tip and the soil. The maximum cone tip temperature is concluded to be mainly controlled by the stress and the resulting heat source but secondarily by the soil porosity and by the thermal soil properties resulting from the porosity value and soil type (Sand/Clay fraction).

5.5.2. Soil parameters prediction potential

In consequence of the numerical investigations performed, it is concluded that the T-CPT offers a low potential to predict the soil parameters involved in the heat transfer arising between the cone tip and the soil. The maximum cone tip temperature is concluded to be mainly a function of the stress applied as well as the mechanical soil properties affecting the δ/ϕ ratio and therefore the resulting friction.

5.5.3. T-CPT Thin-layered soil detection & characterisation potential

The numerical investigations undertook with multi-layer soil system showed the different thermal behaviour of the cone tip interacting with soils of high vertical variability. The T-CPT potentials in characterising multi-layer soils are concluded to be poor since the uncertainties on the heat source prediction are large as was demonstrated all along with this chapter. It is expected that the temperature variation of the cone tip would not be as sharp as the temperature variation obtained using the numerical model due to the progressive change of the soil parameters and the friction. Considering the delay affecting the thermal sensor recording, the thinly layered soils are concluded to be better detected using a pore pressure sensor. The numerical investigations proposed was one of brief and more extensive study should be undertaken in order to fully conclude on this aspect of the T-CPT potentials with in-situ testing on sites offering the opportunity to deploy the T-CPT and such soil strata.

6. Database Analysis

6.1. Hollandse Kust Noord Project

The Hollandse Kust Noord (HKN) project was initiated by the Netherlands Enterprise Agency (Rijksdienst Voor Ondernemend Nederland, RVO). The HKN project consists of 700 MW offshore wind turbine project which is part of the Dutch Government roadmap towards offshore wind power development. The HKN Wind Farm Zone site is located ten nautical miles off the west coast of the Netherlands (Figure 41). To do so, Fugro was requested to perform a geotechnical site investigation of the HKN Wind Farm Zone. The first aim of the geotechnical survey is to validate the geological model resulting from the geophysical investigation. Secondly, the secondary objectives of the geotechnical survey are to determine the soil engineering properties required for the wind farm engineering design (Netherlands Enterprise Agency, 2019).

6.2. Fugro Site Investigation

The geotechnical site investigation executed by Fugro was associated to a laboratory testing programme to validate and update the geological/geophysical model for the HKN Wind Farm Zone project, to determine the variability in seabed conditions (vertical and lateral variation), and to provide geotechnical data to process the design of wind farm foundation elements (Fugro Netherlands Marine, 2019). The In-Situ tests list and Laboratory tests list is provided in Table 5 and Table 6.

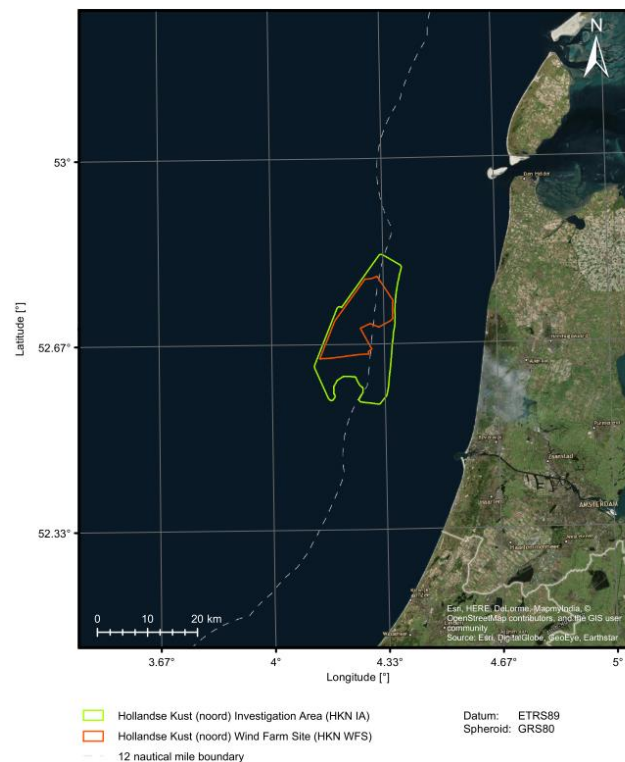


Figure 41: HKN site overview & site location (Fugro Netherlands Marine, 2019)

Table 5: HKN Wind Farm Zone In-Situ test programme (Netherlands Enterprise Agency, 2019)

| In-Situ Test Type | Test Quantity |
|--|----------------------|
| Seafloor CPTs <i>At 78 different locations, depths ranging from 2.1 m to 53.0 m below seafloor.</i> | 85 |
| Seafloor Seismic CPTs <i>At 21 different locations, depths ranging from 2.9 m to 52.9 m below seafloor.</i> | 28 |
| Seafloor Temperature CPTs <i>At 23 different locations, depths ranging from 1.0 m to 7.5 m below seafloor.</i> | 24 |
| Pore Pressure Dissipation Tests <i>At 38 different locations, at selected depths using a CPTu probe.</i> | 72 |
| Boreholes <i>At 28 different locations, depths ranging from 60 m to 80 m below seafloor. The boreholes included downhole sampling & seismic cone penetration testing</i> | 31 |

Table 6: HKN Wind Farm Zone Laboratory test programme (Netherlands Enterprise Agency, 2019)

| Laboratory Test Type | Test Quantity |
|--|---------------|
| Particle Size Analysis <i>Sieving and pipette</i> | 570 |
| Particle Density <i>Pycnometer</i> | 235 |
| Min & Max-Dry Unit Weight | 123 |
| Atterberg Limits | 95 |
| Permeability Test | 69 |
| Unit Weight Tests | 1685 |
| Thermal Conductivity <i>Temperature decay tests</i> | 28 |
| Transient Plane Heat Source | 22 |
| Electrical Resistivity | 27 |
| Microscopy Photography | 109 |
| Carbonate Content | 192 |
| Organic Content <i>Dichromate oxidation (198) and mass loss on ignition (61)</i> | 259 |
| Pore Water Salinity | 27 |
| Triaxial Tests | 122 |
| Ring Shear Tests <i>Soil-Soil (57) & Soil-Steel (105) Interfaces</i> | 162 |
| Compressibility Tests | 21 |

6.2.1. Geological setting

After the site investigation, Fugro concluded on the geological setting, specific to the site used as a database for this thesis. Fugro conclusions on the geological setting are available in Fugro report (Fugro Netherlands Marine, 2019). As previously stated (Figure 41), the HKN Wind Farm Zone site is situated in the southern North Sea, 18.5 km from the Dutch Coastline. The geological development of the current southern North Sea basin dates to the mid-Palaeozoic, resulting from a long and complex history of basin subsidence, occasionally stopped by tectonic uplift and erosion episodes. Three glacial periods affected the HKN Wind Farm Zone site location, each of them separated by interglacial periods (Elsterian Glaciation, Holsteinian Interglacial, Saalian Glaciation, Eemian Interglacial, Weichselian Glaciation, and Holocene). The HKN Wind Farm Site is characterized by soil top layers consisting of Holocene clay-rich deposits of the Naaldwijk Formation overlain by transgressive sand of the Southern Bight Formation (Fugro Netherlands Marine, 2019).

6.2.2. HKN Wind Farm Zone soil units

The geotechnical survey was conducted along with the geological and geophysical study. The geotechnical data obtained from the geotechnical survey campaign was used to validate the geological model and correlated soil layers and geological features expected. The crossed-investigations resulted in a geological ground model in which four main soil units were defined (Table 7). Both soil units A & B were deposited in shallow marine to coastal plain environments during the Holocene period and consists of the most common top layers on the HKN Wind Farm Zone site. The two other soil units (C & D) were deposited during a number of different glacial and interglacial episodes of the Pleistocene period (Fugro Netherlands Marine, 2019; Netherlands Enterprise Agency, 2019).

Table 7: HKN Wind Farm Zone soil units stratigraphy from Fugro Report (Fugro Netherlands Marine, 2019)

| Unit | Depth to Base of Unit [m Lowest Astronomical Tide] | Thickness Range [m] | Soil Description |
|-------------|---|--------------------------------|--|
| DS | 23 to 29 | 0 to 3.5 | -Medium dense to very dense silica fine to coarse SAND, with traces of organic matter |
| A | 20 to 30 | <1 to 13 | -Medium dense to very dense silica fine to medium SAND, with shells and shell fragments |
| B | 21 to 43 | 0 to 19 | -Medium dense to very dense, silica, fine to medium SAND, with shells and shell fragments, occasionally thin laminae with shell fragments & -High strength to very high strength silty, slightly sandy to sandy non-calcareous to calcareous CLAY and/or SILT, with shells and shell fragments |
| C | 22 to 70 | 1 to 41 | -Medium dense to very dense slightly silty to silty, silica to calcareous silica, fine to medium SAND |
| D | >65 | >43 | -Medium dense to very dense, slightly silty to very silty, silica to calcareous silica, fine to medium SAND, with thin laminae to medium beds of clay and silt & -High strength to very high strength calcareous to non-calcareous CLAY, with thin to thick laminae of sand |

6.3. Database Research

6.3.1. General database research introduction

The database analysis performed aimed to confront the temperature features and the classical CPT measurements recorded using a T-CPT probe to an extensive list of laboratory and In-Situ tests in order to observe any possible correlations and existing relationships between soil engineering parameters and temperature measurements. The T-CPT programme set by Fugro includes 24 T-CPT, approximately 6 m deep below the seafloor. The first meter of T-CPT data was disregarded for numerous reasons such as the unreliability of the T-CPT measurements and the extreme variability of the first meter of the top layer. The CPT measurements and borehole samples in the 6 first meter of soil present the evidence of the soil units A, B and C previously presented (See section: HKN Wind Farm Zone soil units, and Table 7). Consequently, the database was mainly performed on Holocene dense to very dense, silica sand to silty sand, presenting high variability with occasional layers of clayish material.

6.3.2. Available In-Situ & Laboratory tests database used

For the site considered, 24 T-CPT were conducted. The T-CPT were all conducted following the same procedure: they all recorded the cone resistance, the sleeve friction and the temperature recorded by the sensor placed inside the CPT, they are approximately 6 m below ground level, the penetration was halted every meter to record the temperature decay. 21 SCPTs were done nearby the T-CPT locations (within 5 m away from the T-CPT), giving average values of the soil shear modulus over 50 cm every meter. As a result of the shallow penetration depth set for the T-CPT programme, a reduced database was extracted to filter the relevant SCPT and laboratory tests.

Fugro undertook different laboratory tests for the site currently considered. The Testing Plan made is composed of Particle Size Distribution, Density tests, Particle Density, Triaxial tests, Ring-Shear tests, Thermal Conductivity and Heat Capacity tests, Oedometer tests, Age Dating, Permeability tests, Microscopy analysis, Electrical Resistivity tests (Table 6). The tests were undertaken using samples taken from the neighbour boreholes (within 5 m away from the T-CPT).

6.3.3. Database analysis methodology

The Laboratory Database is filtered with respect to the T-CPT available. Since the T-CPT are all approximately 6 m deep, only the laboratory and in-situ tests in this range of depth are considered. The previous investigations and conclusions made (See chapter: Numerical Modelling Investigation) suggested investigating the database when the maximal cone tip temperature difference, $\Delta(T)_{\max}$, is reached. Therefore, a filter is applied to the temperature difference to select the data points of matters, which is when the $\Delta(T)_{\max}$ is reached (and therefore no change in temperature is observed).

The temperature difference is determined using the temperature recorded subtracted by the initial soil temperature derived using T-CPT point method (Vardon *et al.*, 2018) and by interpolating between the intervals. The T-CPT profiles are presented in HKN Site T-CPT Profiles. The T-CPT profiles include the cone resistance, the friction, the soil index (I_{sbt}), the initial soil temperature determined using Vardon method, the temperature difference in green and the maximum temperature difference in red (Figure 42). The second temperature measurement used in the database analysis is the gradient of temperature (temperature difference between two points divided by the depth difference, which is 2 cm).

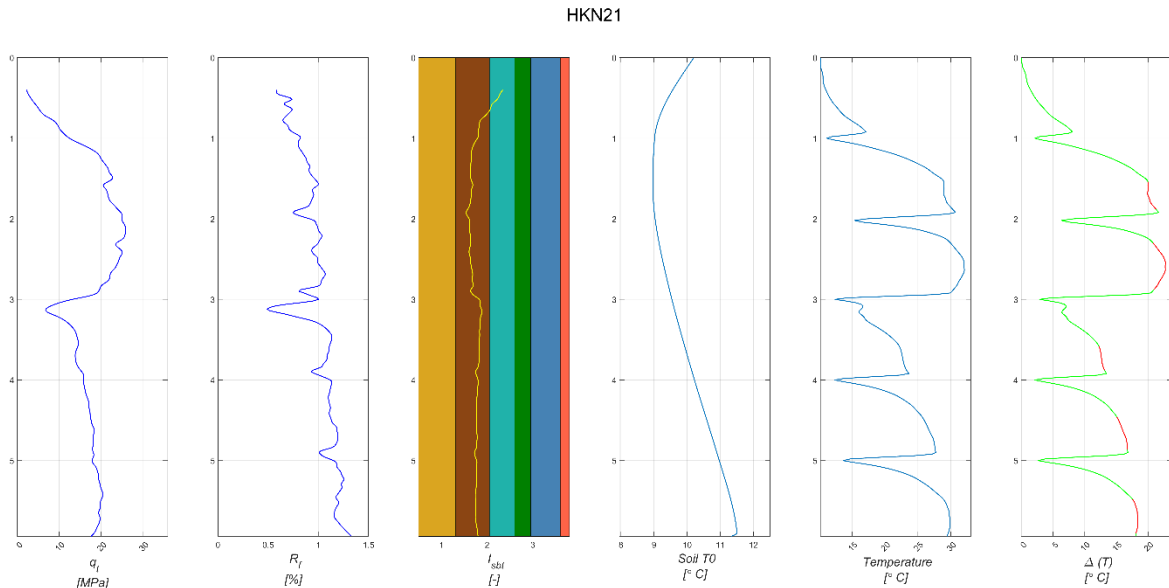


Figure 42: T-CPT profile example

Initial Temperature Slope Investigation:

The first investigation was done at the start of each cone penetration interval (areas circled in blue in Figure 43), where the temperature increase is important, the halted penetration due to the temperature decay tests were undertaken to determine the soil thermal conductivity. Linear regressions were undertaken for the gradient of temperature, $\nabla(T)_{\text{initial}}$, vs the cone tip resistance and the sleeve friction, followed by an analysis of the residuals with respect to following laboratory and in-situ tests: Particle Size Distribution, Density tests, Particle Density, Triaxial tests, Thermal Conductivity and Heat Capacity tests, Microscopy analysis, SCPT tests.

Maximum Temperature Difference Investigation:

The second investigation undertook consists of comparing the classical CPT measurements (q_c , f_s) with the maximum temperature difference, $\Delta(T)_{\text{max}}$, once the maximum temperature difference is reached (areas in red on the temperature difference presented on each T-CPT profile, see Figure 43). Linear regressions were also undertaken for the maximum temperature difference, $\Delta(T)_{\text{max}}$, vs the cone tip resistance and the sleeve friction, followed by an analysis of the residuals with respect to laboratory and in-situ tests previously listed. Additionally, an investigation consisting of analysing the possible correlation between the same list of laboratory and in-situ tests with the temperature measurements (Temperature difference & gradient of temperature) is proposed.

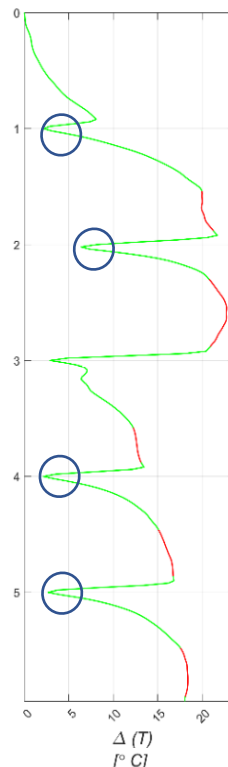


Figure 43: HKN21 T-CPT profile & investigation markers

Regression Analysis Methodology:

The regression analysis was done using Linear and Nonlinear least-squares methods depending on the mathematic shape of the trends observed (Mathworks, 2019). Regression analysis is generally characterised by the regression equation coefficients, the residuals and the regression's fit. Mathematically, the residual, for a specific predictor value, is the difference between the response value y and the predicted response value \hat{y} , resulting from the regression analysis and the equation's coefficients determination and depending on the best fitting mathematical expression (linear or exponential expressions were used for the database analysis). The residuals for the Linear and Nonlinear least-squares methods were calculated using the following equation:

$$r_i = y_i - \hat{y}_i \quad (22)$$

The summed square of residuals for the Linear and Nonlinear least-squares methods is given by:

$$S = \sum_{i=1}^n r_i^2 = \sum_{i=1}^n (y_i - \hat{y}_i)^2 \quad (23)$$

where n is the number of data points included in the fit and S is the sum of squares error estimate.

Laboratory & In-Situ Tests List:

The following list of tests was used to analyse the possible existing correlations between the temperature measurements and the soil engineering characteristics:

- Particle Size Distribution tests
- Unit Weight tests
- Particle Density tests
- Triaxial tests
- Thermal Conductivity tests
- Heat Capacity tests
- Microscopy analysis
- SCPT tests.

6.4. Database Analysis Results & Interpretations

The investigations focus on the two different temperature features observed on the cone tip temperature profile previously introduced, which are the initial temperature slope and the maximum cone tip temperature. For both temperature features, the gradient of temperature and the cone tip temperature are plotted against the classical CPT measurements (q_t & f_s). Regression analysis and the resulting residuals are investigated using the laboratory test results and the SCPT results available. Finally, direct analysis of the maximum temperature difference of the cone tip is performed to investigate any possible correlations between the cone tip temperature evolution and the soil characteristics.

6.4.1. T-CPT initial temperature gradient, $\nabla(T)_{\text{initial}}$:

$\nabla(T)_{\text{initial}}$ vs q_t :

The rate of temperature increase between two CPT point measurements (temperature gradient, $\nabla(T)_{\text{initial}}$) recorded by the T-CPT after restarting the cone penetration (the penetration was halted every meter for temperature decay test) is investigated to validate the statements made in section 4, regarding the dependencies of the initial temperature slope observed in-situ and in the numerical analysis. The database analysis shows that the strongest dependencies between temperature measurements and classical CPT measurements are for the cone tip resistance, q_t (Figure 44).

The regression analysis performed for the $\nabla(T)_{\text{initial}}$ vs q_t plots resulted in high R-Squared value (0.85), which demonstrates the high dependency of $\nabla(T)_{\text{initial}}$ on the in-situ stresses previously suggested by the numerical analysis performed. The investigation conducted on the possible dependencies between the regression residuals and the previously listed tests did not show any strong relationships (Figure 44). This was expected since the results obtained from the simplified solution proposed suggested a high-stress dependency between the $\nabla(T)_{\text{initial}}$ and the cone tip resistance, q_t . The residuals obtained from the regression analysis did not include any noticeable relationships, only D_{50} and D_{60} present visible trends. However, both R-Squared values are low ($R^2 = 0.29$ for D_{50} and $R^2 = 0.36$ for D_{60}).

$\nabla(T)_{\text{initial}}$ vs f_s :

The $\nabla(T)_{\text{initial}}$ was then compared to the sleeve friction, f_s , recorded by the T-CPT. The correlation observed in Figure 45 suffers from larger scatter than the trend previously observed comparing the $\nabla(T)_{\text{initial}}$ and the cone tip resistance. The regression analysis presents low R-Squared value (0.69). One of the reasons that could explain the weaker correlation observed between the $\nabla(T)_{\text{initial}}$ and f_s could be the weaker robustness of the sleeve friction measurements compared to the cone tip resistance measurements as well as the fact that the heat is generated by the friction occurring at the cone tip surface. However, the scatter could be explained by the possible higher sensitivity of the sleeve friction to different soil feature. Therefore, investigations on the regression residuals were also performed (Figure 45). The residuals investigation resulted in only weak trends on the Particle Size Distribution for D_{50} and D_{60} with best results obtained for the $\nabla(T)_{\text{initial}}$ residuals regression analysis ($R^2 = 0.54$ for D_{50} and $R^2 = 0.52$ for D_{60}).

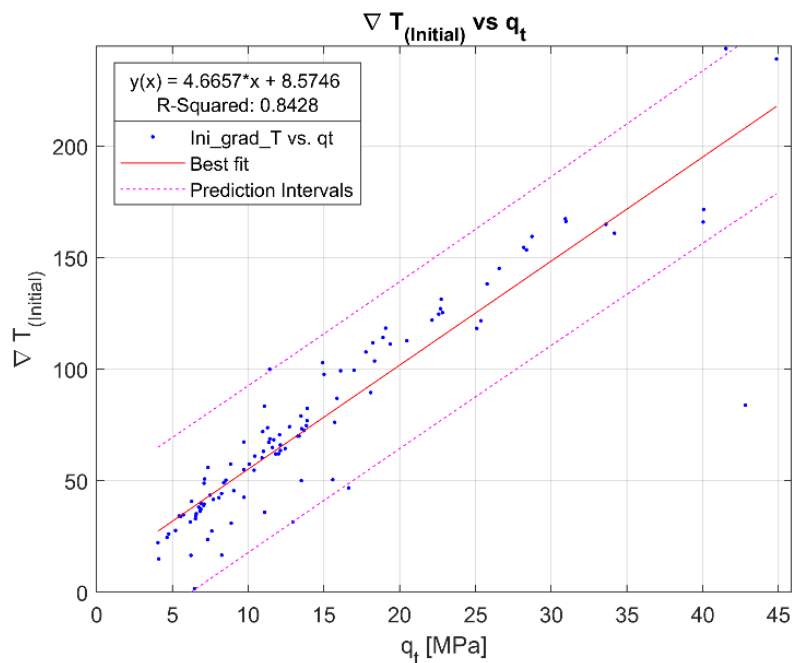


Figure 44: $\nabla(T)_{\text{initial}}$ vs q_t plot

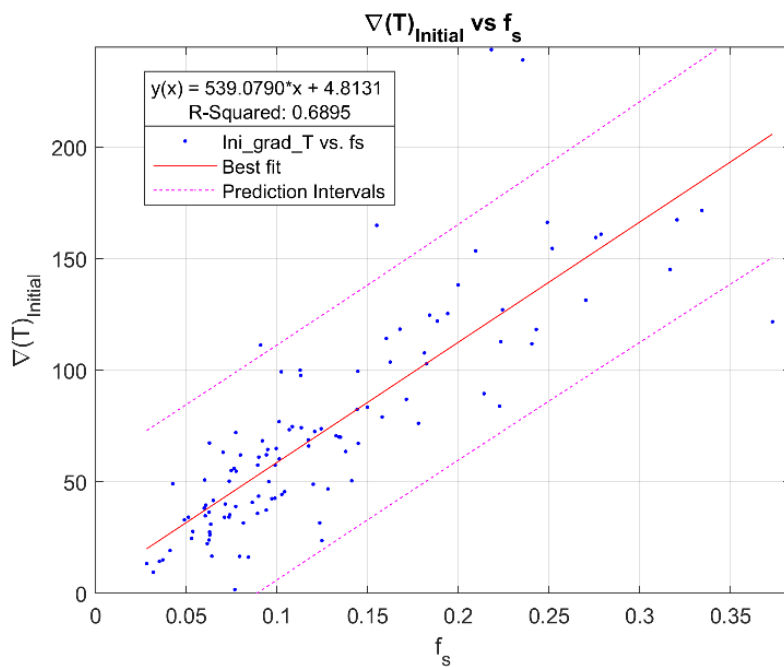


Figure 45: $\nabla(T)_{\text{initial}}$ vs f_s plot

6.4.2. T-CPT maximum temperature difference, $\Delta(T)_{\max}$:

$\Delta(T)_{\max}$ vs q_t :

The dependency between the $\Delta(T)_{\max}$ and the cone resistance, q_t was analysed. As previously explained, the temperature difference recorded by the T-CPTs is filtered to only consider the data points for which the maximum temperature difference is reached.

The $\Delta(T)_{\max}$ vs q_t plot (Figure 46) presents a strong correlation between the cone tip resistance and the temperature difference when filtering the data with an R-Squared value of 0.97. This strong correlation between cone resistance and temperature difference suggests a strong relationship between the in-situ the temperature recorded and the in-situ stress of the soil, responsible for the friction generating the heat recorded. The scatters were investigated by plotting the residuals of the regression analysis against the laboratory and in-situ tests previously listed.

The results do not show any strong correlations that could explain the scatters (Appendix VII). Especially, no correlations were observed concerning the main soil parameters influencing the heat transfer (soil density, heat capacity and thermal conductivity). Some trends can be observed for the heat capacity, the thermal diffusivity and the residuals. However, the lack of filtered data for the heat capacity, the thermal conductivity and the thermal diffusivity does not allow to make any conclusions on the possible correlations. It is suggested that the scatters are functions of too many soil parameters, hiding the possible dependencies between the temperature difference scatter magnitudes and the considered soil parameters.

$\Delta(T)_{\max}$ vs f_s :

The second parameters dependency considered is the $\Delta(T)_{\max}$ versus the sleeve friction, f_s . The $\Delta(T)_{\max}$ vs f_s plot (Figure 47) shows a weaker dependency (compared to $\Delta(T)_{\max}$ vs q_t dependency observed previously) of the maximum temperature difference to the sleeve friction with an R-Squared value of 0.79. The larger scatter observed compared to the $\Delta(T)_{\max}$ vs q_t regression presented previously could be partially explained by the larger uncertainties related to the sleeve friction measurement accuracy.

An investigation was also undertaken on the $\Delta(T)_{\max}$ vs f_s residuals by confronting the residuals to the list of laboratory and in-situ tests previously presented. Weak correlations were found with an approximate R-Squared value of 0.40 for each of the different diameter of the Particle Size Distribution (Appendix VIII). It can be observed that the residual values are increasing as the Particle Size Distribution (PSD) is increasing, which suggests that the maximum temperature difference is a function of the sleeve friction, induced by the in-situ horizontal stress and the PSD.

No other correlations were observed investigating the other laboratory and in-situ tests (Appendix VIII). However, this could be due to the lack of data, or to the multiple factor dependency of the residuals hiding the possible existing relationships between the regression residuals and the soil parameters.

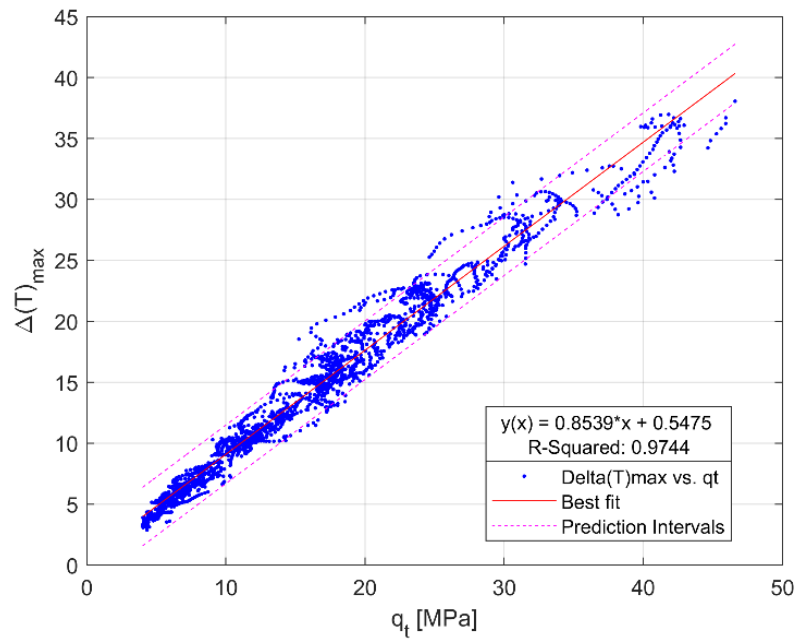


Figure 46: $\Delta(T)_{\max}$ vs q_t plot

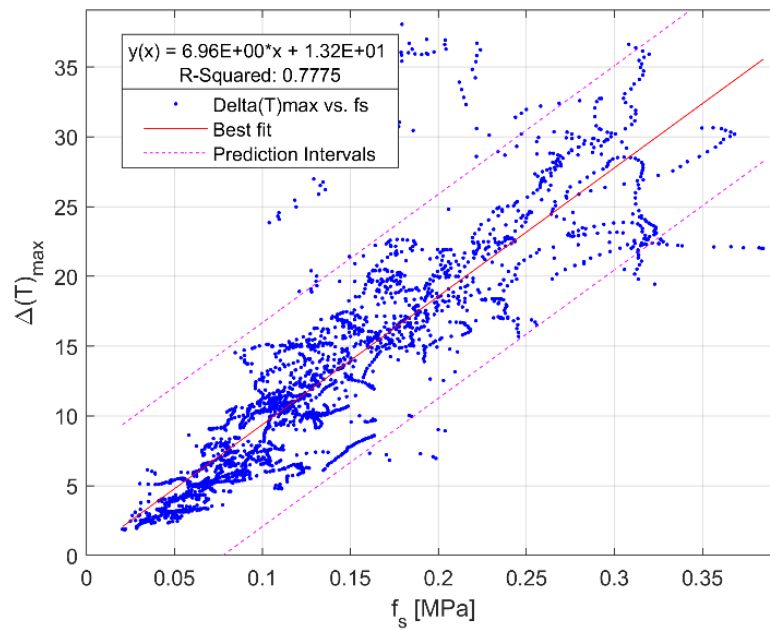


Figure 47 $\Delta(T)_{\max}$ vs f_s plot

6.4.3. $\Delta(T)_{\max}$ vs Laboratory tests

In order to avoid the factors that possibly affected the previous investigations, the $\Delta(T)_{\max}$ was plotted directly against the laboratory tests and the SCPT tests available. The results found in Figure 48 and Figure 49 confirmed the previous results as the PSD is a function of the $\Delta(T)_{\max}$. The regressions' fit value is varying depending on the particle size percentage considered (Table 8), going from an R-squared value of 0.37 with a visible trend but suffering from the largest scatter for D_{10} , to an R-Squared value of 0.77 with a clear trend and the smallest scatter for D_{60} .

Table 8: $\Delta(T)_{\max}$ vs Particle Size Distribution regression results

| Particle Size Distribution | R-Squared |
|----------------------------|-----------|
| D₁₀ | 0.37 |
| D₅₀ | 0.74 |
| D₆₀ | 0.77 |
| D₉₀ | 0.63 |

The soil type percentage distribution was also considered. The possible relationship between the $\Delta(T)_{\max}$ and the soil composition in terms of percentage of clay, silt, fines and sand was then investigated. The results presented in Figure 50 and Figure 51 suggest strong correlations between soil type composition and the maximum temperature difference, with the regression's good fit summarised in Table 9. The results respect the logic as the percentage of fines (clay and silt) decreases exponentially as the $\Delta(T)_{\max}$ increases. The opposite logic is respected with the sand percentage which increases exponentially as the $\Delta(T)_{\max}$ increases.

Table 9: $\Delta(T)_{\max}$ vs Soil Type Percentage regression results

| Soil Type Percentage | R-Squared |
|----------------------|-----------|
| Clay | 0.94 |
| Silt | 0.79 |
| Fines | 0.91 |
| Sand | 0.91 |

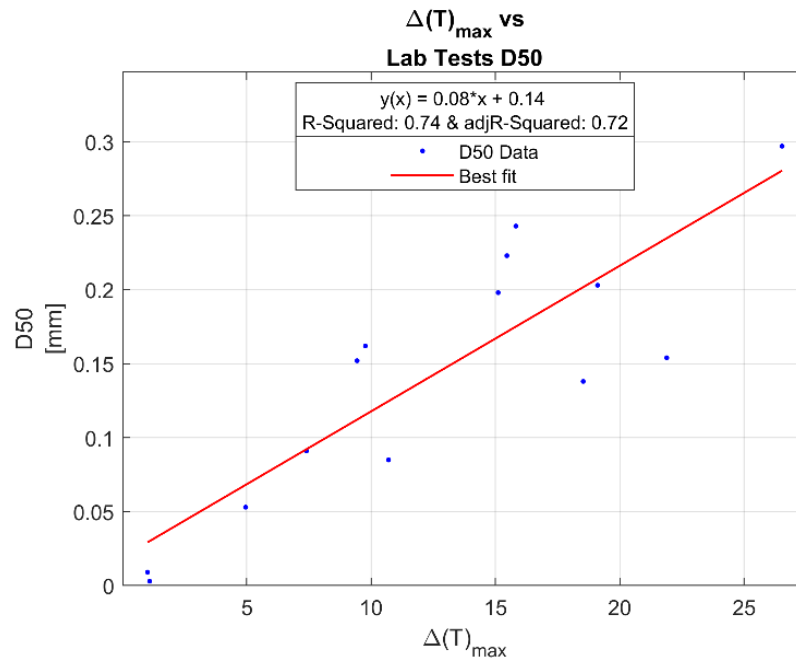


Figure 48: $\Delta(T)_{\max}$ vs D_{50}

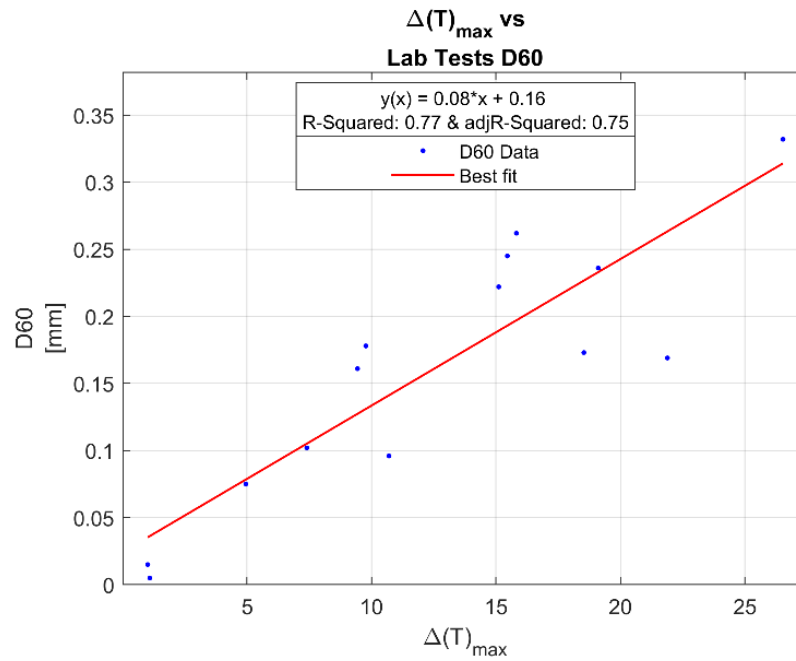


Figure 49: $\Delta(T)_{\max}$ vs D_{60}

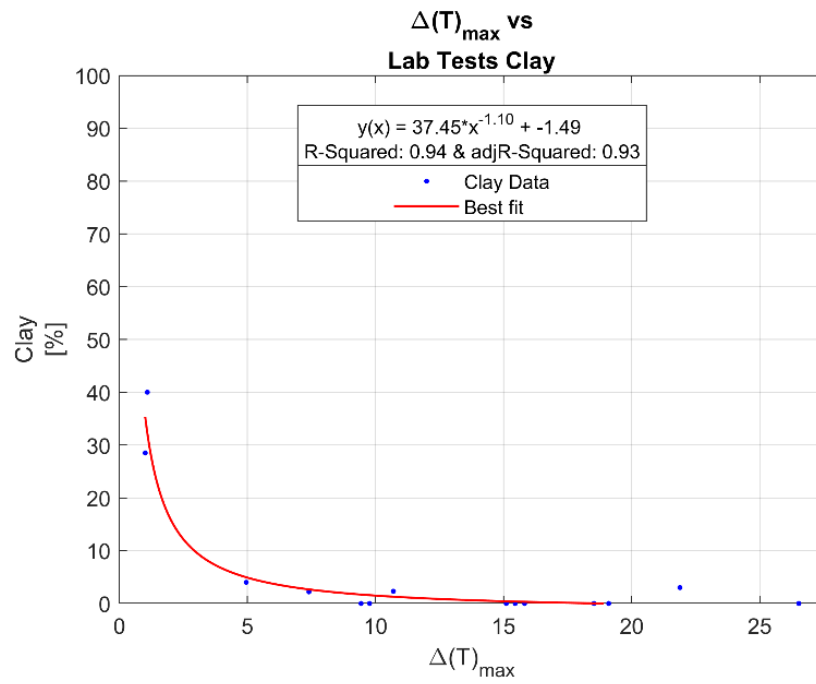


Figure 50: $\Delta(T)_{\max}$ vs Clay Percentage

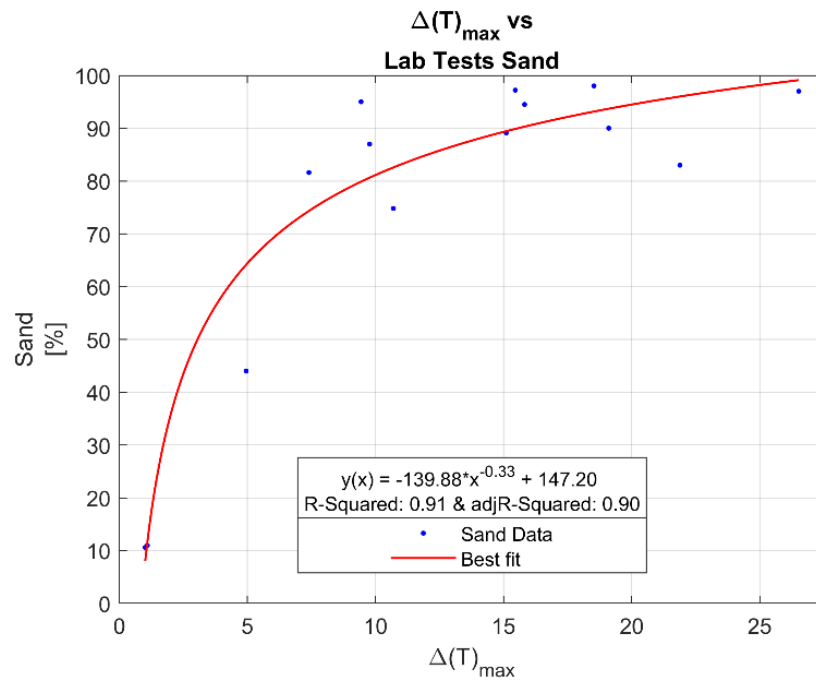


Figure 51: $\Delta(T)_{\max}$ vs Sand Percentage

6.4.4. $\Delta(T)_{\max}$ vs SCPT

Since the previous research suggested that the change of temperature is mainly induced by in-situ stress. The soil stiffness was thought to be an interesting soil parameter to investigate. A number of SCPT are available to the investigation with respect to the T-CPT database. In Figure 52, the shear modulus obtained from SCPT increases as the $\Delta(T)_{\max}$ increases. The origin of the large scatter of the regression could be the procedure of the SCPT, which consist of seismic measurements between two geophones that are 0.50 m spaced to each other.

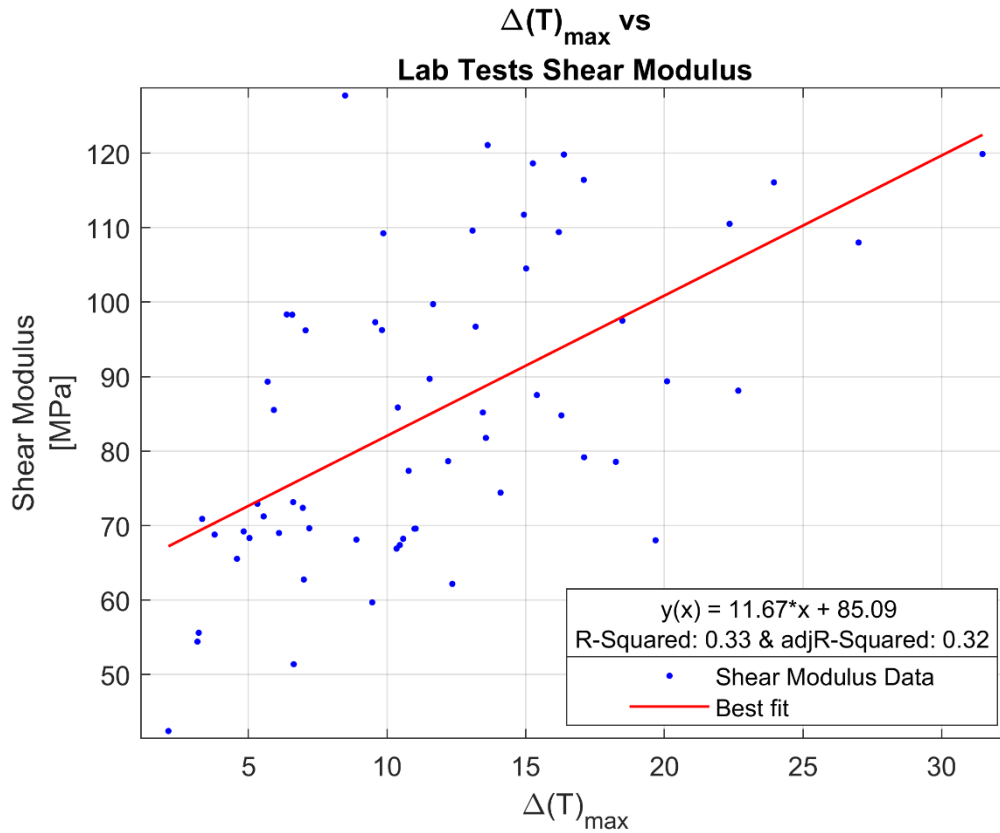


Figure 52: $\Delta(T)_{\max}$ vs Small Strain Shear Modulus G_0 obtained from SCPT

6.5. Additional Database Analysis

An additional database was provided by Fugro along with the research project. The project location is kept private by Fugro. Therefore, no information is given regarding the exact site location. This additional database analysis focuses on the positive results found in the HKN database analysis. The initial slope of temperature is therefore analysed as well as the maximum cone tip temperature difference with classical CPT measurements (q_c , f_s). Additionally, the maximum cone tip temperature difference is compared to the particle size distribution tests in order to confirm the results found for the HKN site.

6.5.1. T-CPT initial temperature gradient, $\nabla(T)_{\text{initial}}$:

The analysis undertaken on the initial temperature gradient, $\nabla(T)_{\text{initial}}$, for the additional database considering the usual CPT measurements (q_t , f_s) is in adequation with the results found in the HKN database analysis. The trend observed for the initial temperature gradient vs the cone resistance (Figure 53) suffers from smaller scatter than the initial temperature gradient vs the sleeve friction (Figure 54). Therefore, it is assumed that the initial temperature gradient is mainly a function of the cone tip resistance, q_c .

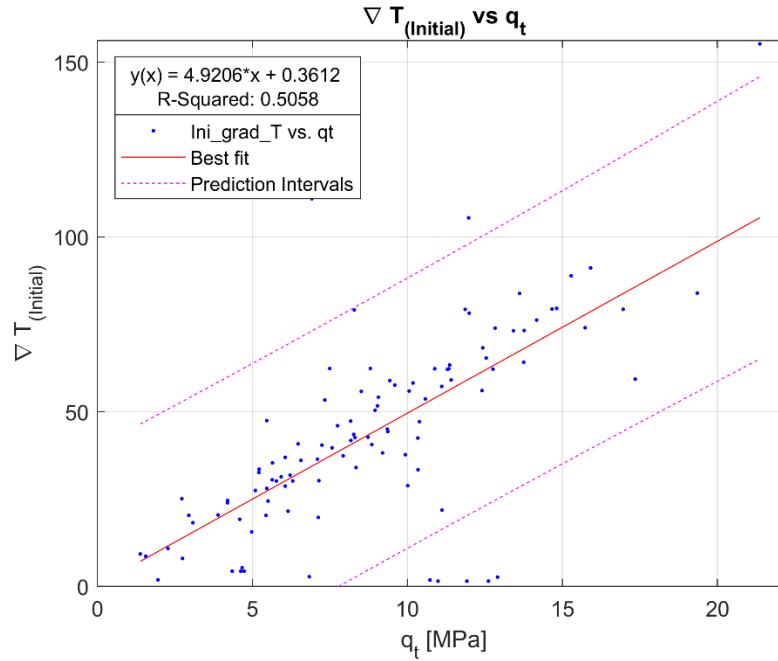


Figure 53: $\nabla(T)_{\text{initial}}$ vs q_t for the additional database

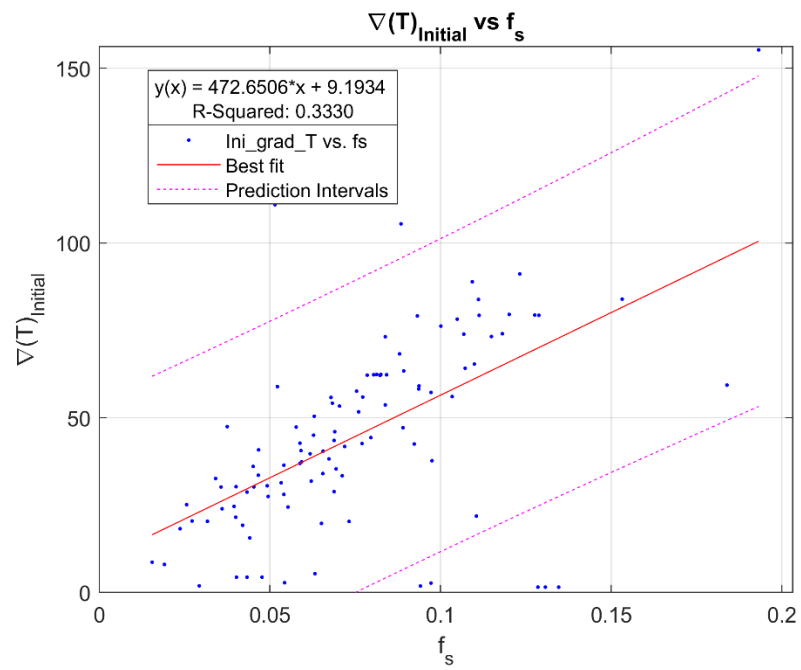


Figure 54: $\nabla(T)_{\text{Initial}}$ vs f_s for the additional database

6.5.2. T-CPT maximum cone tip temperature difference, $\Delta(T)_{\max}$:

The analysis undertaken on the maximum cone tip temperature difference, $\Delta(T)_{\max}$, for the additional database considering the usual CPT measurements (q_t, f_s) is also in adequation with the results found for the HKN database analysis. Figure 55 and Figure 56 show that strong relationships observed for the HKN database between the maximum cone tip temperature difference and the CPT measurements (q_t, f_s) are also observed for a different site. The maximum cone tip temperature difference is therefore thought to be mainly a function of the cone resistance

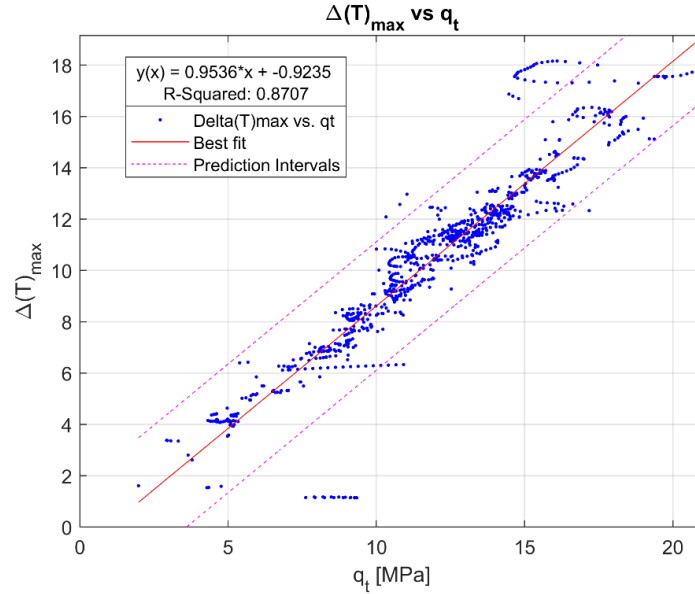


Figure 55: $\Delta(T)_{\max}$ vs q_t for the additional database

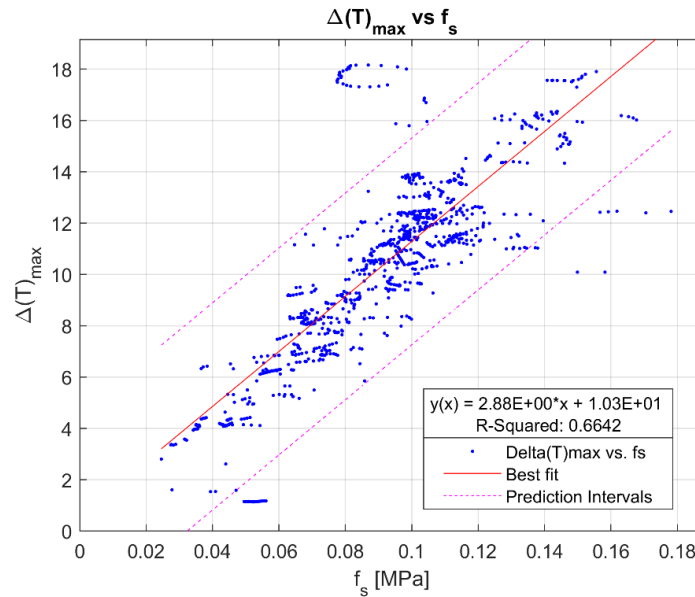


Figure 56: $\Delta(T)_{\max}$ vs f_s for the additional database

6.5.3. Maximum cone tip temperature vs Particle Size Distribution:

Regarding the analysis of the maximum cone tip temperature difference, here as well the same results were found for the additional database than for the HKN database analysis (Appendix X). The maximum cone tip temperature difference, $\Delta(T)_{\max}$, was found to increase as the particle size of the soil increases, with the best trends found for D_{50} and D_{60} as can be seen in Figure 57 and Figure 58.

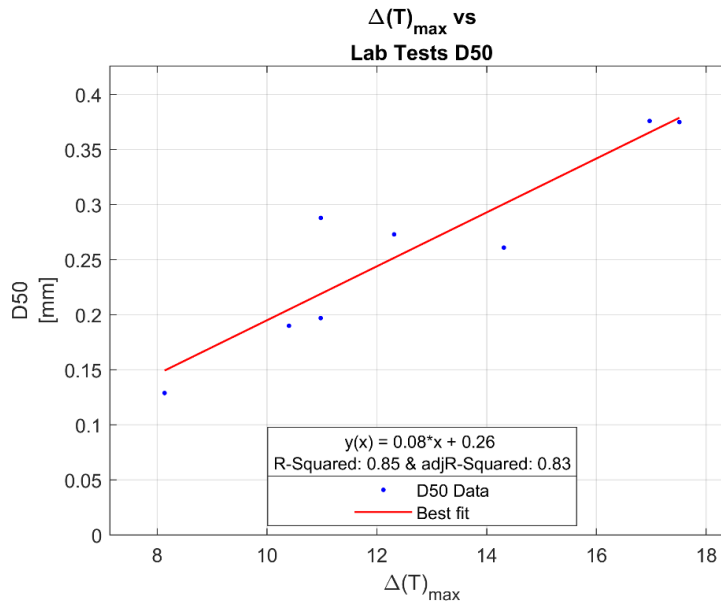


Figure 57: $\Delta(T)_{\max}$ vs D_{50} for the additional database

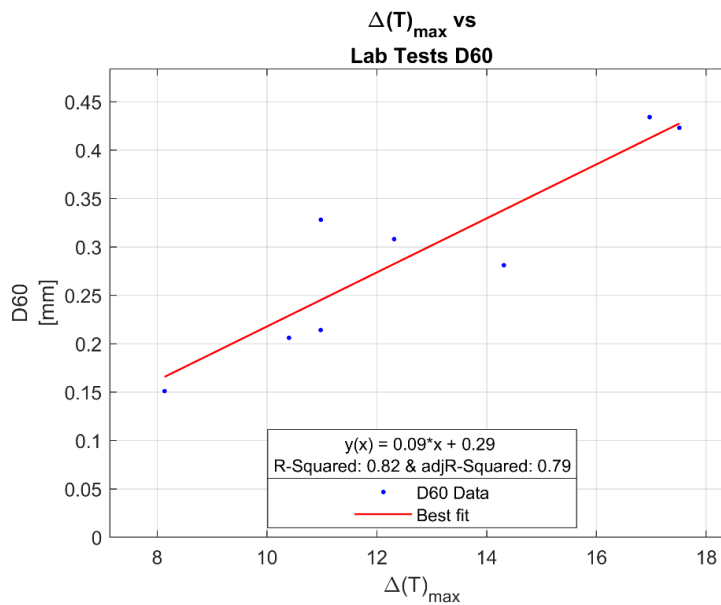


Figure 58: $\Delta(T)_{\max}$ vs D_{60} for the additional database

6.6. Database Analyses Conclusions

The database analyses performed on different sites provide important insight into the possible relationships between the temperature measurements recorded using T-CPT and the classical CPT measurements (cone tip resistance, q_t , and sleeve friction, f_s). Figure 59 presents the maximum cone tip temperature difference plotted on Robertson's Soil Behaviour Type chart for the HKN database. Looking at Figure 59, it can be concluded that the maximum cone tip temperature difference is mainly a function of the cone tip resistance, q_c . The maximum cone tip temperature difference can be split into two different soil behaviour according to Robertson's Soil Behaviour Type chart. The first one is the sand contractive zone, for which the maximum cone tip temperature difference ranges between 0 to 10. The second one is the sand dilative zone, for which the maximum cone tip temperature difference ranges from 10 to 40°C. Further research should be undertaken on the cone tip thermal behaviour with the dilative/contractive behaviour of sandy soils in order to assess the T-CPT potentials to increase the sand characteristics' insight. Table 10 summarises the important relationships observed for the HKN site database and the additional database provided by Fugro. As can be seen, the strongest dependencies are observed between the temperature features and the cone tip resistance measurements. This correlates with the assumptions previously made in the section in the chapter: Research Methodology, stating that the heat generated by friction occurred mostly around the cone tip and that the heat generated was mainly stress-dependent. Therefore, the temperature features recorded seem to capture well, with respect to the area of interests, the in-situ stress variability observed.

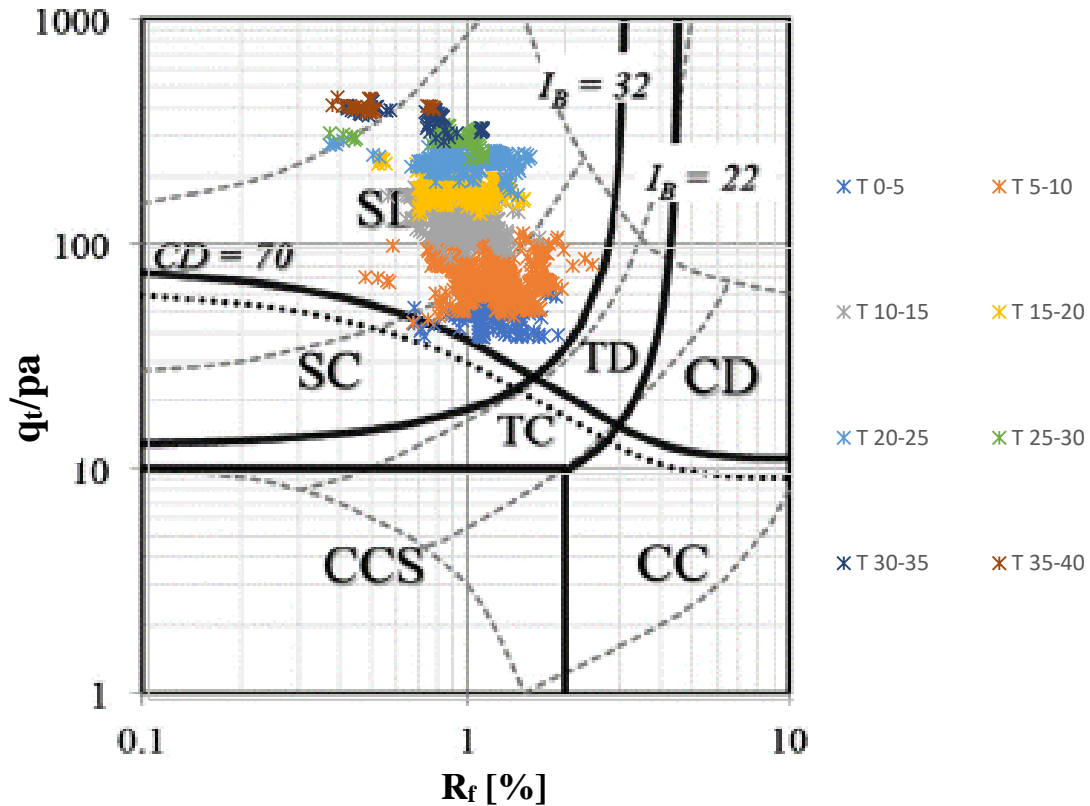


Figure 59: $\Delta(T)_{\max}$ plotted on Robertson's SBT Chart

The analysis of the regression's residuals did not succeed in the observation of a strong correlation between residuals and soil features that could have explained the scatter observed. Only weak trends were observed for the D_{50} and D_{60} values obtained from Particle Size Distribution for the following regressions' residuals: $\nabla(T)_{\text{initial}}$ vs q_t , and $\nabla(T)_{\text{initial}}$ vs f_s . These results suggest that the residuals are dependent on numerous soil parameters, resulting in no significant relationships.

Table 10: Temperature features & CPT measurements (q_t, f_s) correlations summary

| | R-Squared Value | |
|---------------------------------------|-----------------|-----------------|
| | HKN Site | Additional Site |
| $\nabla(T)_{\text{initial}}$ vs q_t | 0.86 | 0.50 |
| $\nabla(T)_{\text{initial}}$ vs f_s | 0.68 | 0.33 |
| $\Delta(T)_{\text{max}}$ vs q_t | 0.97 | 0.87 |
| $\Delta(T)_{\text{max}}$ vs f_s | 0.79 | 0.66 |

Table 11 summarises the main results and allows a direct comparison between the Particle Size Distribution characteristics and the maximum cone tip temperature difference, $\Delta(T)_{\text{max}}$. It can be seen that the maximum cone tip temperature difference presents a strong relationship with the soil Particle Size Distribution and soil type content. The investigations undertaken on the soil unit weight suggested no dependency with the different temperature measurements features, suggesting that for the database analysed, the soil type content is a direct factor of the maximum cone tip temperature difference, $\Delta(T)_{\text{max}}$. This seems to be aligned with the previous research made on soil friction, with friction increasing as sand soil content increases.

Table 11: T-CPT measurements & soil parameters direct correlations summary

| $\Delta(T)_{\text{max}}$ vs: | R-Squared Value | |
|------------------------------|-----------------|-----------------|
| | HKN Site | Additional Site |
| D_{10} | 0.37 | 0.65 |
| D_{50} | 0.74 | 0.85 |
| D_{60} | 0.77 | 0.82 |
| D_{90} | 0.63 | 0.56 |

The database available did not allow to perform a complete analysis of the thermal soil parameters (heat capacity, thermal conductivity and thermal diffusivity). This is due to the restrictive numbers of laboratory tests and in-situ thermal conductivity tests (T-CPT temperature decay tests) matching with the zone of interests described in the Database Research section of the Database Analysis chapter. Over the twenty thermal tests undertaken in the geotechnical tests programme (Table 5 & Table 6), only 2 to 4 values are available and matching for each thermal tests. Consequently, no serious and robust regression analysis could be performed on what was initially set as the main research objective of this thesis.

The same lack of data was encountered for the friction angle parameter, which was assumed and set as an important parameter affecting the heat generation in the model proposed (Appendix III). Moreover, the regression analysis results performed on the soil unit weight did not give correlations with the temperature measurements. It could be explained by the quality of the unit weight tests, and/or the high vertical and horizontal variability, affecting the possible pieces of evidence of the relationship between temperature measurements and soil unit weight.

7.1. Numerical Modelling Investigation

The numerical investigation results in few major findings answering the research questions of this thesis project which are discussed in this section. The results obtained from the FE numerical analyses give a better understanding of the heat transfer occurring between the soil and the cone tip. The dependencies of the temperature measurement features were identified with success, with the initial slope of the cone temperature being highly influenced by the applied heat source. The maximum cone tip temperature, on the other hand, is influenced by the soil properties involved in the heat transfer such as the bulk density, the specific heat capacity and the thermal conductivity of the soil.

7.1.1. Sensitivity analysis of homogenous soil

Moreover, the contribution of the soil properties involved in the heat transfer was analysed and their low influences were to the maximum cone tip temperature development were observed during cone penetration, relative to the impact of the friction. This observations and conclusions allow answering the main research question of this thesis by stating that the T-CPT offers limited potential in determining the soil properties involved in the heat transfer occurring during the cone penetration. As a result, the mechanical and geometrical properties of sand influencing the friction, and therefore the resulting heat source, were observed and concluded to have greater influences on the cone tip temperature features than the soil thermal properties.

7.1.2. Multi-layer model

The investigation performed on thinly layered soil shows the atypical cone tip temperature behaviour differing from the cone tip behaviour observed for homogeneous soil layer. It was observed that thinly layered soils do not allow the full dissipation of heat generated in the sandy layers, which is a result of the low dissipation potential of the T-CPT compared to its ability to track increases of stresses generating frictional heat. Here as well, the uncertainties in predicting the frictional heat source result in stating the T-CPT potential in detecting and characterising of thinly layered soil as rather limited.

7.1.3. FE numerical model limitations

The performed numerical analysis did not include a deep and complete study of the mechanical interactions between the soil and the cone penetrometer. The numerical analysis was limited to heat transfer study by application of heat source between the cone tip and the soil. In addition to these limitations, the model proposed is an analogy of a cone penetrometer. Due to the focus on the thermal exchange and the disregard of the mechanical interactions occurring during cone penetration, no deformation theories were implemented in the numerical model. Consequently, the geometry of the cone tip had to be modified to a hollow cylinder, respecting the volumetric quantity of the true cone tip. In consequence, the results obtained from the numerical investigations were used to quantify the magnitude of influence of the different parameters involved in the friction and the heat transfer occurring between the cone tip and the soil during cone penetration.

Another limitation of the model results in the difference between the initial temperature gradients observed using the FE numerical model and the values observed in-situ. Greater initial temperature gradients were observed in-situ, resulting in reaching the asymptotic maximum temperature difference in shorter time in-situ than numerically for a given soil. This could be explained by two different possibilities: The numerical model was run applying a constant heat source, and consequently a constant cone resistance. However, it is well established that the cone tip resistance recorded on-field is influenced by the soil below and above the cone penetrometer, and therefore by the stresses applied in-situ on the cone tip. Therefore, the observed initial temperature gradient is thought to keep increasing as the cone resistance increases. Additionally, as the cone resistance reduces due to the influences of the soil below the cone and due to the time required to dissipate heat, transitional temperature features can be confused for maximum temperature value. Secondly, the absence of mechanical interactions between the cone tip and the soil of the FE numerical model could explain the difference in behaviour. It is suggested that as the cone penetrometer advances in the soil, it influences the soil underneath to a certain distance (Ahmadi and Robertson, 2005; van der Linden, 2016), pre-compressing the drained soils such as sand would result in a friction force not constant but increasing until reaching a maximum value, the critical state strength under normally consolidated conditions, which is a function of the soil type, grain size, and soil strength resistance. At certain stress level, the particle crushing phenomenon is expected to occur for sands, which might result in a different mechanical friction behaviour resulting in heat being generated by the friction and crushing arising between the soil particles (Falagush *et al.*, 2015). Also, the numerical investigations were not considering the surface of contact effects on the thermal conductivity and therefore on the heat diffusivity (Haigh, 2008).

7.2. Database Analysis

The database analysis performed on two different sites demonstrated a strong correlation between the initial temperature gradient as well as the maximum cone tip temperature difference and the classical CPT measurements (q_c, f_s). These observations reinforce the assumptions made stating the cone tip temperature being mainly influenced by the confinement stresses experienced by the soil at the cone tip. The database analysis presented a good match between the maximum cone tip temperature difference and the particle size distribution which follows the conclusions given in the numerical analysis chapter, stating the maximum cone tip temperature being influenced mainly by the soil texture (particle packing morphology) and strength.

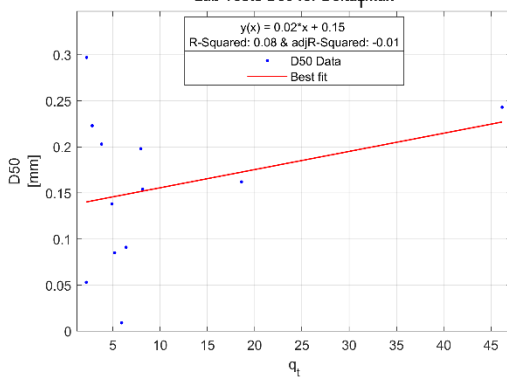
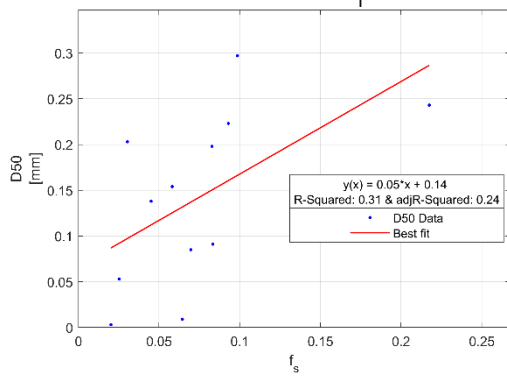
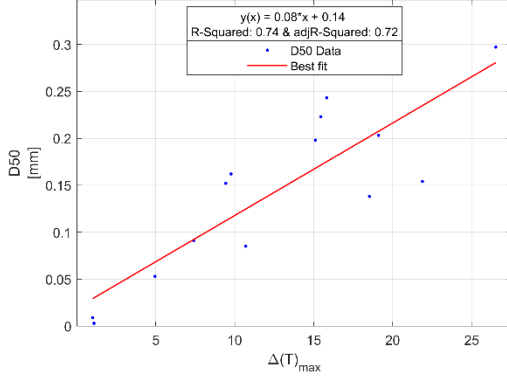
Table 12 and Table 13 present the different regression analysis results between classical CPT measurements (q_c, f_s), the different temperature features and the D_{50} values obtained from particle size distribution tests. It is clearly seen that the sleeve friction is more related to the grain size than the cone resistance is as advanced by Hebelier (2018). The D_{50} values were found to be better correlated to the maximum cone tip temperature difference, $\Delta(T)_{\max}$. This is in agreement with the conclusions given after the numerical modelling investigations, stating the maximal cone tip temperature difference to be highly influenced by the stresses as well as the particle size, gradation and the internal friction angle as Potyondy (1961) and Han (2018) showed pieces of evidence on the dependencies of the δ/ϕ ratio on those soil parameters. However, the maximum induced friction and therefore the maximum cone tip temperature difference, $\Delta(T)_{\max}$, may not allow predicting the full range of particle size distribution. It is thought that the relationships found between temperature measurements and Particle Size Distribution test are highly site-specific, with a strong dependency on the in-situ stresses (vertical and horizontal), deposit age, over consolidation ratio as well as the stiffness. Therefore, additional in-situ tests and research should be done on different site locations to check and validate the correlations found as results of the regression analysis performed on the two databases provided by Fugro.

The potential of the T-CPT in determining the particle size must also be interpreted in term of how relevant the potential and the associated limitations of the T-CPT can be used by industry. The main limitations of the T-CPT are the absence of control on the temperature development, the fact that only the maximal cone tip temperature is of interest. As a result of these limitations, the potential of the T-CPT and its usability is judged as limited.

Table 12: Comparison of the observed correlation between mean grain size, the temperature measurements and the classical CPT measurements

| | R-Squared Regression Value |
|---|-----------------------------------|
| q_t vs D_{50} | 0.08 |
| f_s vs D_{50} | 0.31 |
| $\Delta(T)_{\max}$ vs D_{50} <i>HKN Site</i> | 0.74 |
| $\Delta(T)_{\max}$ vs D_{50} <i>Additional Site</i> | 0.85 |

Table 13: Regression analyses between mean grain size, the temperature measurements and the classical CPT measurements for the HKN site

| | D_{50} |
|-------------------|--|
| q_t | <p>q_t vs Lab Tests D_{50} for $\Delta(T)_{max}$</p>  <p>$y(x) = 0.02 \cdot x + 0.15$ R-Squared: 0.08 & adjR-Squared: -0.01</p> <p>D50 Data Best fit</p> |
| f_s | <p>f_s vs Lab Tests D_{50} for $\Delta(T)_{max}$</p>  <p>$y(x) = 0.05 \cdot x + 0.14$ R-Squared: 0.31 & adjR-Squared: 0.24</p> <p>D50 Data Best fit</p> |
| $\Delta(T)_{max}$ | <p>$\Delta(T)_{max}$ vs Lab Tests D_{50}</p>  <p>$y(x) = 0.08 \cdot x + 0.14$ R-Squared: 0.74 & adjR-Squared: 0.72</p> <p>D50 Data Best fit</p> |

8. Conclusions & Recommendations

In this final chapter, the main conclusions of this research are addressed for different aspects of the research project. Firstly, general conclusions are given regarding the T-CPT potentials and its limitations. Then, recommendations for further work are provided in the closing of this conclusion chapter and report.

8.1. Conclusions On The T-CPT Potentials & Limitations

Up until today, the strongest potential of the T-CPT is still in determining thermal conductivity through temperature decay tests that can be used to calibrate the derived CPT correlations by Vardon (2019) used to determine continuous heat capacity and thermal conductivity profiles of soils.

Regarding the T-CPT potentials in predicting soil parameters involved in the heat transfer such as the soil bulk density, the heat capacity and thermal conductivity. The numerical analyses showed the evident link between the soil type, the porosity and the maximum temperature difference reachable for a given heat source. However, it was demonstrated that the T-CPT cannot be used to estimate these soil parameters due to the uncertainties associated with the estimation of the interface friction angle and the estimation of the resulting friction occurring between the cone tip and the soil during cone penetration. The impact of the estimate friction uncertainties on the maximum temperature difference results in a larger maximum temperature difference for pure sand with a porosity value set equal to 0.3 than the actual porosity effect on the maximum temperature difference for pure sand. Additionally, the maximum temperature difference requires approximately a meter of cone penetration, depending on the heat source magnitude, with constant friction occurring on the cone tip. This is by far the biggest limitation of the T-CPT since such conditions are most of the time not encountered in a real situation due to the more or less high variability of the soil. As a result, the T-CPT cannot be used for site investigation in order to estimate soil properties involved in the heat transfer occurring between the cone tip and the soil.

The database analysis showed that the T-CPT use is limited to Sandy soils to Silty Clay soils due to the low stresses generating low friction value and therefore low heat source in the clayish soil layers. The numerical investigations and database analysis are both giving the same conclusions regarding the influences of the soil texture on the maximal cone tip temperature. The database analysis showed strong correlations between the particle size distribution of sands and the maximal cone tip temperature as well as the temperature gradient recorded once the maximal temperature reached. Although, it is assumed that the correlations found are site-specific, depending on different parameters discussed in the discussions chapter. This possible potential of the T-CPT is concluded to be highly limited by the fact that the maximal cone tip temperature is not reached in a controlled manner and may never be reached depending on the soil vertical variability.

Thin soil layers are not easily detected using the sleeve friction measurements. The sleeve friction measures average friction over 130 mm for a standard cone penetrometer resulting in the smoothing of the soil friction. Past research showed the great ability of pore pressure sensor located on the cone tip to detect thin soil layer strata (Tom Lunne, Peter K. Robertson, 1997; M M Ahmadi and Robertson, 2005). The numerical investigations performed in this research project on multi-layer soil system shows significant thermal behaviour of the cone tip compared to homogenous soil layer configuration. However, the database analysis performed does not contain such soil strata (thin clay and sand layers). In conclusions, the pore pressure sensor located on the cone tip of the cone penetrometer is still, up today, the sensor offering the best accuracy for thin soil layers detections.

8.2. Recommendations & Future Work

8.2.1. Recommendations for future numerical modelling investigations

Numerical model investigations did not take into account any mechanical interactions. As a result, no solid study was performed to estimate the heat generated by friction. The study of the heat generated and dissipated is of interest for a better understanding of soil behaviour. To do so, a FEM would not be adequate since this method does not cope with large strain occurring during cone penetration. Investigations using MPM method and elastoplastic soil models are recommended in order to capture the friction generated by the cone penetration. Moreover, the numeral investigations were performed assuming the soil is solid. This simplification does not allow to study the effect of the particle geometry such as the grain size, the coefficient of uniformity, the roundness and sphericity. These geometrical features are thought to be of significant matter for the contact surface between particles for heat transfer occurring in sandy soils.

8.2.2. Recommendations on the database results

Despite the good correlation observed between temperature features and particle size distribution, the particle size distribution using the temperature measurements recorded using the T-CPT are not thought to be as straightforward as it seems. As explained in the discussion chapter, the in-situ stresses are thought to influence the relationships found with the regression analyses. Further database analyses should be undertaken at different site locations to better estimate the in-situ stresses effect as well as the potential of the T-CPT in predicting particle size distribution without destructive sampling methods and laboratory tests.

The T-CPT should be deployed on more homogeneous soils in order to assess its potentials. Additionally, the T-CPT should be deployed in all soils, such as clay and peat, and over consolidated clay in order to study the different thermal behaviour of the cone tip. Plus, it would be interesting to study the cone tip thermal behaviour in contractive and dilative soil with pore pressure measurements as well in order to assess any possible potential of the T-CPT.

9. References

- Ahmadi, M M and Robertson, P. K. (2005) 'Thin-layer effects on the CPT qc measurement', *Canadian Geotechnical Journal*, (January 2011). doi: 10.1139/t05-036.
- Ahmadi, M. M. and Robertson, P. K. (2005) 'Thin-layer effects on the CPT qcmeasurement', *Canadian Geotechnical Journal*, 42(5), pp. 1302–1317. doi: 10.1139/t05-036.
- Akrouch, G. A. *et al.* (2016) 'Thermal Cone Test to Determine Soil Thermal Properties', *Journal of Geotechnical and Geoenvironmental Engineering*, 142(3), p. 04015085. doi: 10.1061/(asce)gt.1943-5606.0001353.
- Appelo, C. A. J. *et al.* (2018) 'PHT3D : A Reactive Multicomponent Transport Model for Porous Laser-Induced Media DyeLIFTM : A Saturated New Direct-Push Fluorescence Sensor System for Chlorinated Solvent DNAPL and Non-Naturally Fluorescing NAPLs'. doi: 10.1111/gwmr.12296.
- Arshad, M. I. *et al.* (2014) 'Experimental study of cone penetration in silica sand using digital image correlation', *Géotechnique*. Thomas Telford Ltd, 64(7), pp. 551–569.
- ASTM (2014) *Standard test method for determination of thermal conductivity of soil and soft rock by thermal needle probe procedure, TA - TT -*. West Conshohocken, Pa.: ASTM.
- Bratton, W. L. and Bianchi, J. C. (1996) 'Surface mounted pH sensor for cone penetration testing'. Google Patents.
- Bratton, W. and Rooney, D. J. (1998) 'In situ oxidation reduction potential measurement of soils and ground water'. Google Patents.
- Burns, S. E. and Mayne, P. W. (1998) 'Penetrometers for soil permeability and chemical detection, geosystems engineering group', *School of Civil and Environmental Engineering, Georgia Institute of Technology Atlanta, Georgia*, pp. 30332–30355.
- Campanella, R. and Ap-, A. N. (1993) 'A New Approach to Measuring Dilatancy in Saturated Sands ° T', 16(4).
- Campanella, R. G. and Kokan, M. J. (1993) 'A new approach to measuring dilatancy in saturated sands', *Geotechnical Testing Journal*. ASTM International, 16(4), pp. 485–495.
- Carslaw, H. S. and Jaeger, J. C. (2003) *Conduction of heat in solids. LK -* <https://tudelft.on.worldcat.org/oclc/840381097>. 2nd ed., TA - TT -. 2nd ed. New York SE - 510 blz. ; .. cm.: Oxford University Press.
- Chen, R. P. *et al.* (2010) 'Measurement of electrical conductivity of pore water in saturated sandy soils using time domain reflectometry (TDR) measurements', 206, pp. 197–206. doi: 10.1139/T09-088.

Conshohocken, W. (1996) 'Standard Test Method for Performing Electronic Friction Cone and Piezocone Penetration Testing of Soils 1', *Current*, 04(January), pp. 1–20. doi: 10.1520/D5778-12.agreed.

Diego, S. (2001) 'Xenon has been the subject of considerable recent interest as a gamma-ray detector medium, including its use in ionization and proportional detectors, and as a scintillator. Its high atomic number (', 248(2), pp. 289–294.

Douwes Dekker, D. M. (1984) *Soil mechanics for engineering purposes, Part I and II - lecture book*.

Falagush, O., McDowell, G. R. and Yu, H.-S. (2015) 'Discrete element modeling of cone penetration tests incorporating particle shape and crushing', *International Journal of Geomechanics*. American Society of Civil Engineers, 15(6), p. 4015003.

Farouki, O. T. (1981) 'Thermal properties of soils', pp. 110–120. doi: 10.4236/ojss.2011.13011.

Fourier, J. B. (1822) *Analytical theory of heat*. Edited by A. Freeman. New York: Dovan Publications.

Fugro Netherlands Marine (2019) *Fugro Document No. P903749/03: Geological Ground Model Hollandse Kust (noord) Wind Farm Zone Geological Ground Model Hollandse Kust (noord) Wind Farm Zone Dutch Sector , North Sea*.

Gouda Geo-Equipment BV. (2019) *Magnetometer Cone (MagCone)*.

Haigh, S. K. (2008) 'Thermal Conductivity Of Sands', *Heat and Mass Transfer/Waerme- und Stoffuebertragung*, 44(10), pp. 1241–1246. doi: 10.1007/s00231-007-0357-1.

Han, F. *et al.* (2018) 'Effects of Interface Roughness, Particle Geometry, and Gradation on the Sand–Steel Interface Friction Angle', *Journal of Geotechnical and Geoenvironmental Engineering*, 144(12), p. 04018096. doi: 10.1061/(asce)gt.1943-5606.0001990.

Hebeler, G. L., Martinez, A. and Frost, J. D. (2018) 'Interface response-based soil classification framework', *Canadian Geotechnical Journal*, 55(12), pp. 1795–1811. doi: 10.1139/cgj-2017-0498.

Houlsby, G. T. and Hitchman, R. (1988) 'Calibration chamber tests of a cone penetrometer in sand', *Geotechnique*, 38(I), pp. 39–44.

Houlsby, G. T. and Ruck, B. M. (1998) 'Interpretation of Signals from an Acoustic Cone Penetrometer', pp. 1075–1080.

Hryciw, R. D., Ghalib, A. M. and Raschke, S. A. (1998) 'In situ soil characterization using Vision Cone Penetrometer (VisCPT)', *Proc. 1st IC on Site Characterization, Atlanta*, 2, pp. 1081–1086.

Jaeger, J. (2011) ‘Conduction of Heat in an Infinite Region Bounded Internally by a Circular Cylinder of a Perfect Conductor’, *Australian Journal of Physics*, 9(2), p. 167. doi: 10.1071/ph560167.

Jia, R. *et al.* (2013) ‘Interpretation of density profile of seabed sediment from nuclear density cone penetration test results’, *Soils and Foundations*. Elsevier, 53(5), pp. 671–679. doi: 10.1016/j.sandf.2013.08.005.

Jia, R. *et al.* (2019) ‘In Situ Determination of Density Profiles in Complex Strata Using the Nuclear Density Cone Penetrometer’, 2019.

Kulhawy, F. H. and Mayne, P. W. (1990) *Manual on estimating soil properties for foundation design*.

Kurup, P. *et al.* (2017) ‘A Review of Technologies for Characterization of Heavy Metal Contaminants’, *Indian Geotechnical Journal*. Springer India, 47(4), pp. 421–436. doi: 10.1007/s40098-016-0214-6.

Kurup, P. U. (2006) ‘Innovations in cone penetration testing’, in *Site and Geomaterial Characterization*, pp. 48–55.

Kurup, P. U. *et al.* (2007) ‘Electronic Nose – Membrane Interface Probe for Geoenvironmental Site Characterization’, 132(9), pp. 1133–1142.

Lengkeek, Arny; de Greef, J.; Joosten, S. (2018) ‘CPT based unit weight estimation extended to soft organic soils and peat’, *Cone Penetration Testing 2018*, (July). doi: 10.1201/9780429505980.

Lightner, E. M. and Purdy, C. B. (1995) ‘Cone penetrometer development and testing for environmental applications’, in *Proc., Int. Symp. on Cone Penetration Testing*, pp. 41–48.

Lin, J. *et al.* (1995) ‘Laser fluorescence excitation-emission matrix (EEM) probe for cone penetrometer pollution analysis’, in *Optical Sensors for Environmental and Chemical Process Monitoring*, pp. 70–79.

van der Linden, T. I. (2016) *Influence of Multiple Thin Soft Layers on the Cone Resistance in Intermediate Soils*. Technical Univeristy of Delft.

Looijen, P. *et al.* (2018) ‘Fibre optic cone penetrometer’, *Cone Penetration Testing 2018: Proceedings of the 4th International Symposium on Cone Penetration Testing*. Edited by Hicks, Pisano, and Peuchen. Delft: Delft University of Technology, pp. 407–409.

Lubking, P. (1997) *Soft Soil Correlaties- 374590. Tech. rep.* Delft, The Netherlands.

Mao, W. *et al.* (2018) ‘High Frequency Acoustic Emissions Observed during Model Pile Penetration in Sand and Implications for Particle Breakage Behavior’, *International Journal of Geomechanics*, 18(11), p. 04018143. doi: 10.1061/(ASCE)GM.1943-5622.0001287.

Marton, R., Taylor, L. and Wilson, K. (1988) 'Development of an In-Situ Subsurface Radioactivity Detection System-the Radcone', *Waste Management*, 88.

Massarsch, K. R. (1986) 'Acoustic penetration testing', in *Proceeding of the 4th Geotechnical Seminar, Field Instrumentation and In-Situ Measurements, Nanyang Tech. Inst., Singapore*.

Mathworks, C. (2019) *Curve Fitting Toolbox™ User's Guide R 2019 a*.

Mccall, W. *et al.* (2018) 'Evaluation and application of the optical image profiler (OIP) a direct push probe for photo - logging UV - induced fluorescence of petroleum hydrocarbons', *Environmental Earth Sciences*. Springer Berlin Heidelberg, 77(10), pp. 1–15. doi: 10.1007/s12665-018-7442-2.

Menge, P. and Van Impe, W. (1995) 'The application of acoustic emission testing with penetration testing', in *Proceedings of the International Symposium on Cone Penetration Testing (CPT'95)*, pp. 49–54.

Meyerhof, G. G. (1974) 'Ultimate bearing capacity of footings on sand layer overlying clay', *Canadian Geotechnical Journal*. NRC Research Press, 11(2), pp. 223–229.

Meyerhof, G. G. (1983) 'Scale effects of ultimate pile capacity', *Journal of Geotechnical Engineering*. American Society of Civil Engineers, 109(6), pp. 797–806.

Mimura, M. (1995) 'Performace of RI Cone Penetrometers in Sand Deposits', in *Proc Int. Symp. on Cone Penetrometer Testing, CPT'95*, pp. 55–60.

Miyamoto, T., F, K. and C, J. (2012) 'Simultaneous measurement of soil water and soil hardness using a modified time domain reflectometry probe and a conventional cone penetrometer', (June), pp. 240–248. doi: 10.1111/j.1475-2743.2012.00391.x.

Morgan, J. C., Adams, J. W. and Ballard, J. H. (1998) 'Field use of a cone penetrometer gamma probe for radioactive-waste detection.', *Field Analytical Chemistry & Technology*. Wiley Online Library, 2(2), pp. 111–115.

Muromachi, T. (1981) 'Cone penetration Testing in Japan, Symposium on Cone Penetration Testing and Experiences', *Geotechnical Engineering Division, ASCE, October, St. Louis*, pp. 76–107.

Netherlands Enterprise Agency (2019) *Hollandse Kust (noord) Wind Farm Zone, Project and Site Description*.

Nozaki, R. and Bose, T. K. (1990) 'Measurement of the dielectric properties of materials by using time domain reflectometry', in *7th IEEE Conference on Instrumentation and Measurement Technology*, pp. 263–269.

Olie, J. J., Van Ree, C. and Bremmer, C. (1992) 'In situ measurement by chemoprobe of

groundwater from in situ sanitation of versatic acid spill', *Geotechnique*. Thomas Telford Ltd, 42(1), pp. 13–21.

Pepper, J. W., Wright, A. O. and Kenny, J. E. (2002) 'In situ measurements of subsurface contaminants with a multi-channel laser-induced fluorescence system', 58, pp. 317–331.

Potyondy, J. G. (1961) 'Skin Friction Between Various Soils and', *Géotechnique*, 11(4), pp. 339–353.

Raschke, S. A. and Hryciw, R. D. (1997) 'Vision cone penetrometer for direct subsurface soil observation', *Journal of geotechnical and geoenvironmental engineering*. American Society of Civil Engineers, 123(11), pp. 1074–1076.

Rees, S. W. *et al.* (2000) 'Ground heat transfer effects on the thermal performance of earth-contact structures', *Renewable & sustainable energy reviews*, 4(3), pp. 213–265. doi: 10.1016/S1364-0321(99)00018-0.

Robertson, P. K. (2010) 'Soil behaviour type from the CPT: an update', *Proceedings of the Second Symposium on Cone Penetration Testing*, (May), p. 8 p. doi: 10.1093/oxrep/grh008.

Robertson, Peter K. and Cabal, K. L. (2010) 'Estimating soil unit weight from CPT', *Proceedings of the 2nd International Symposium on Cone Penetration Testing*, (May), p. 8 pp.

Robertson, P.K. and Cabal, K. L. (2010) 'Guide to Cone Penetration Testing for Geo-Environmental Engineering', *Gregg Drilling & Testing, Inc.*, pp. 1–85.

Rossabi, J. *et al.* (2000) 'Field tests of a DNAPL characterization system using cone penetrometer-based Raman spectroscopy', *Groundwater Monitoring & Remediation*. Wiley Online Library, 20(4), pp. 72–81.

Shibata, T. (1994) 'Use of RI-cone penetrometer in foundation engineering', in *Proc. 13th Int. Conf. on Soil Mech. and Found.*, pp. 147–150.

SHIBATA, T. *et al.* (1992) 'Moisture measurement by neutron moisture cone penetrometer: design and application', *Soils and foundations*. The Japanese Geotechnical Society, 32(4), pp. 58–67.

Silva, M. F. and Bolton, M. D. (2004) 'Centrifuge penetration tests in saturated layered sands', pp. 377–384.

Smits, F. P. (1977) 'Sonderen in zand - een theoretische basis voor analyse van de conusweerstand', in *Proceedings of FUGRO Sondeersymposium*, pp. 31–42.

Sully, J. P. (1988) 'In situ density measurement with nuclear cone penetrometer', *Proc. ISOPT-1*, 2, pp. 1001–1005.

Tom Lunne, Peter K. Robertson, J. J. M. P. (1997) *Cone Penetration Testing in Geotechnical*

Practice. Blackie Academic and Professional.

Tringale, P. T. and Mitchell, J. K. (1982) 'An acoustic cone penetrometer for site investigation', in *Proceeding of the Second European Symposium on Penetration Testing (ESOPT II)*, pp. 909–914.

Upadhyaya, S. K. *et al.* (1982) *Cone index prediction equations for Delaware soils*.

Vardon, P. J. (2018) 'Thermal Cone Penetration Test (T-CPT) Thermal Cone Penetration Test (T-CPT)', (June).

Vardon, P. J. (2019) 'Heat capacity and thermal conductivity', 2019(January).

Vardon, P. J., Baltoukas, D. and Peuchen, J. (2018) 'Interpreting and validating the thermal cone penetration test (T-CPT)', *Géotechnique*, (August), pp. 1–13. doi: 10.1680/jgeot.17.P.214.

Vaz, C. M. P., Bassoi, L. H. and Hopmans, J. W. (2001) 'Contribution of water content and bulk density to field soil penetration resistance as measured by a combined cone penetrometer-TDR probe', *Soil and Tillage Research*, 60(1–2), pp. 35–42. doi: 10.1016/S0167-1987(01)00173-8.

Villet, W. C. B., Mitchell, J. K. and Tringale, P. T. (1981) 'Acoustic emissions generated during the quasi-static cone penetration of soils', *Acoustic Emissions in Geotechnical Engineering Practice*. ASTM International, pp. 174–193.

Wiertsema & Partners (2016) *Magnetometer Cone Penetration Testing*.

Wijk, W. R. van (1963) *Physics of plant environment*. LK - <https://tudelft.on.worldcat.org/oclc/1660671>, North-Holland Books TA - TT -. Amsterdam: North-Holland Pub. Co.;

Woeller, D. J. *et al.* (1991) 'Penetration testing for arctic soil and permafrost conditions', in *Proceedings of the Geotechnical Engineering Congress, Boulder, Colo*, pp. 10–12.

Yoon, H.-K., Jung, S.-H. and Lee, J.-S. (2011) 'Characterisation of subsurface spatial variability using a cone resistivity penetrometer', *Soil Dynamics and Earthquake Engineering*. Elsevier, 31(7), pp. 1064–1071.

Yoon, H. *et al.* (2009) 'Electrical Resistivity and Cone Tip Resistance Monitoring by Using Cone Resistivity Penetrometer', 1, pp. 168–171.

Yu, X. and Drnevich, V. P. (2004) 'Soil water content and dry density by time-domain reflectometry', *Journal of Geotechnical and Geoenvironmental Engineering*. American Society of Civil Engineers, 130(9), pp. 922–934.

Zhang, Q. *et al.* (2007) 'Detection of Deeply Buried UXO Using CPT Magnetometers', 45(2), pp. 410–417.

Zuidberg, H. M. (1988) 'Advanced in situ measurements', in *Proc. of 2nd International Symposium on Field Measurements in Geomechanics*.

Appendix I Add-On Sensors for Cone Penetration Testing

Extensive Literature Review on Add-on Sensors for Cone Penetration Testing

ABSTRACT: The widely used cone penetration test (CPT) allows in-situ measurements of soil behaviour during continuous penetration. The traditional sensors incorporated in a cone penetrometer are for measuring cone resistance, sleeve friction, pore pressure and inclination. Many supplementary sensors have been studied and tried in research settings and in practice. Examples are sensors for natural gamma radiation, electrical resistivity and time domain reflectometry. None have made it to routine practice.

This paper presents a review of CPT add-on sensors that (1) allow continuous penetration at 20 mm/s, (2) robust, have no external moving parts, and (3) offer the potential for broad geotechnical value, not limited to special applications only. The review considers recent advances in electronics, sensor technology and data processing systems.

Keywords: Cone Penetration Test; Add-on sensors; In-situ testing; Soil investigation; Geotechnical engineering;

1. GENERAL INTRODUCTION

CPTu Principle:

The Cone Penetration Test (CPT) is considered as one of the most used tools for in situ for soil investigation in geotechnical engineering. The CPT principle is a simple procedure defined in the ASTM D5778 – 12 (Conshohocken, 1996), which consists of a penetrometer cone tip with a 60° angle and a projected cone based area (A_c) of 10 cm² (or 15 cm², depending on the cone model) penetrating through the soil at a constant penetration test of 20 mm/s. During the cone penetrometer penetration, the force applied on the conical point required to penetrate the soil is recorded by electrical methods at different resolution (20 to 10 mm interval readings) depending on the maximal resolution capacity of the cone penetrometer used. The cone resistance, q_c is often used directly in soil characterization and obtained dividing the recorded force by the cone base area (A_c). The second measurement made during CPT via a friction sleeve present directly behind the cone tip. As the force applied on the cone tip, the force exerted on the sleeve is measured by electrical methods. The sleeve friction resistance, f_s , is obtained by dividing the measured axial force exerted on the sleeve by the surface area of the sleeve friction, A_{ft} of 150 cm² for a 10 cm² cone (225 cm² for a 15 cm² cone).

Nowadays, recording the pore water pressure at the u_2 location during the continuous cone penetration using an electronic pressure transducer as an add-on sensor on the classic CPT has become a common practice, and is commonly called piezocone penetration test (CPTu). The record of the pore pressure offers several advantages such as allowing the correction of the pore water pressure acting on the cone geometry during the continuous cone penetration, mainly to correct

and normalized the cone tip resistance used for soil characterisation (especially in soft clays and silts). Additionally, CPTu can be used for a to determine the soil permeability and increase the soil type identification reliability by halting the cone penetration at the desired depth and recording the pore pressure decay over time (pore pressure dissipation test).

Inclinometers are also included in modern cones to record the vertical deviation of the cone penetrometer during penetration. The vertical deviation should not exceed 2 degrees and check should be made on pushrods straightness. This check is of great use to avoid any damage to equipment, and obviously, ass the verticality of the tests.

The classical CPT sensors are for measuring cone resistance, q_c , sleeve friction, f_s , pore pressure, u , and inclination. These measurements are commonly used in order to identify the soil type during site investigation using Soil Behaviour Type charts (Tom Lunne, Peter K. Robertson, 1997). Additionally, a great number of semi-empirical correlations have been developed to estimate engineering geotechnical soil parameters from the traditional sensors incorporated in a cone penetrometer. These semi-empirical correlations allow Geotechnical engineers to estimate geotechnical soil parameters important for designing such as the soil density (and relative density for sandy soil), the over-consolidation ratio, the friction angle, the permeability, the undrained shear strength, the coefficient of consolidation, some stiffness soil parameters and others. The different reliabilities for each correlation depend on the type of soil and are presented by Robertson (2010; 2016).

The Review's focus:

Apart from the piezometer probe, multiples sensors have been implemented without making it to routine practice. An exhaustive review of existing CPT add-on sensors is undertaken to aim to inventory any major add-on sensors developed to date. This paper consists in reviewing and introducing the CPT probes (the test procedure, the soil characteristics measured and derived, the advantages and possible limitations of each CPT sensor developed up today), respecting the following conditions: (1) continuous penetration at 20 mm/s, (2) robust, have no external moving parts, and (3) offer the potential for broad geotechnical value, not only limited to special applications only. The review considers recent advances in electronics, sensor technology and data processing systems. The following list of CPT add-on sensors have been investigated:

- Acoustic Sensor (Microphone)
- Video Sensor (VisCPT)
- Electrical Resistivity Sensor (ERT & CRP)
- Time Domain Reflectometry Sensor (TDR)
- Radioisotope Sensors (NM & ND)
- Multi-Friction & Multi-Piezo-Friction Sensors (MPFP)
- Temperature Sensor (Thermocouples & T-CPT)
- Magnetometer Sensor (MagCone)
- Optical Fiber Sensors (FO)
- pH & Redox Potential Sensors
- Laser-Induced Fluorescence Sensor (LIF)
- Integrated Optoelectronic Chemical Sensor

2. GENERAL OVERVIEW

The CPT add-on sensor review starts with a general overview in the form of a table detailing the penetration mode, the add-on sensor measurements and derived soil characteristics, and the available works of literature.

| Add-on Sensor | | Penetration Mode | Soil Characteristics | | Available Literature |
|--|--|------------------|--|--|--|
| | | | Measured | Derived | |
| Acoustic (Microphone) | | Continuous | -Acoustic Emission Activity [kHz] | -Stratigraphy Transition -Changes in Relative Density | Villet (1981), Muromachi (1981), Tringale (1982), Massarsch (1986), Menge (1995), Houlsby (1998), Mao (2018) |
| Video (VisCPT) | | Continuous | -Direct Soil Observation | -Stratigraphy Transition -Clay Fissure Detection -Clay & Sand Seam Detection -Particle Size Analysis -Soil Contaminant | Raschke (1997), Hryciw (1998) |
| Electrical Resistivity Sensors | Electrical Resistivity Tomography (ERT) | Halted | -Soil Resistivity -Pore Water Resistivity | -Porosity -Density | Zuidberg (1988), Campanella (1993) |
| | Cone Resistivity Penetrometer (CRP) | Continuous | -Soil Electrical Resistivity | -Subsurface Spatial Variation -Thin Soil Layering Detection -Sand Dilatancy Characteristics -Relative Density -Soil Contaminant (acidic & NAPL spills) | Campanella (1993), Yoon (2009, 2011) |
| Time-Domain Reflectometry (TDR) | | Halted | -Permittivity -Soil Electrical Conductivity | -Water Content -Dry density -Porosity -Spatial Distribution of The Volumetric Water Content | Upadhyaya (1982), Nozaki (1990), Lightner (1995), Vaz (2001), Yu (2004), Chen (2010) |

| Add-on Sensor | | Penetration Mode | Soil Characteristics | | Available Literature |
|--|----------------------|---|---|---|--|
| | | | Measured | Derived | |
| Multi-Piezo-Friction Sensor (MPFP) | | Continuous | -Friction On Texturized Sleeve -Pore Pressure | -Soil Type Classification | Hebeler (2018) |
| pH, Electrical Conductivity & Redox Potential Sensor (ORP or ChemiCone) | | Halted Continuous for the pH sensor only | -Electron & Hydrogen ions activity -pH -Electrical conductivity | -Soil Oxidation -Soil Contaminants (acid & base spills) | Olie (1992), Bratton (1996; 1998), Woeller (1991) |
| Magnetometer (MagCone) | | Continuous | -Magnetic Field | -Unexploded Bomb Detection (UXB/UXO), -Existing Underground Structures Detection (driving depth of pile foundations, sheet pile lengths, the position of anchors & power cables) | Zhang (2007), Wiertsema & Partners (2016), Gouda Geo-Equipment BV (2019), |
| Radioisotope Sensors (NM & ND) | | Halted | -Radioactive Energy Photons Dissipation -Soil Atomic Density | -Density -Porosity -Water Content -Stratigraphy Transition -Liquefaction Potential | Marton (1988), Sully (1988), Shibata (1992; 1994), Mimura (1995), Jia (2013, 2019) |
| Temperature Sensors | Thermocouples | Halted | -Temperature Variations | -Soil Chemical Activity (Methane Generation & Biological activity) -Permafrost Depth | Woeller (Woeller <i>et al.</i> , 1991), Burns (1998) |
| | T-CPT | Halted | -Temperature Decay | -Thermal Conductivity -Initial Soil Temperature | Akrouch (Akrouch <i>et al.</i> , 2016), Vardon (Vardon, 2018; Vardon <i>et al.</i> , 2018) |

| Add-on Sensor | Penetration Mode | Soil Characteristics | | Available Literature |
|--|------------------|---|--|---|
| | | Measured | Derived | |
| Fiber Optic (FO) | Continuous | -Cone Resistance with High-Frequency (500 Hz) & Lower Temperature Sensitivity | -Thin Soil Layers Better Detected | Looijen (2018) |
| Laser-Induced Fluorescence Sensor (LIF) | Continuous | -Soil Fluorescence | -Soil Contaminants: Petroleum Hydrocarbons & Aromatic Hydrocarbons | Lin (1995), Burns (Burns and Mayne, 1998), Rossabi (2000), Pepper (2002), Kurup (2006; 2007, 2017), Appelo (2018) |
| Integrated Optoelectronic Chemical Sensor | Continuous | -In-situ Chemical Concentration by Wave Interference | -Soil Contaminants: Ammonia, pH & BTEX | Burns (Burns and Mayne, 1998), Mccall (2018) |
| Gamma Radiation & Neutron Sensors (RadCone) | Halted | -In-situ Uranium Detection By Na(Tl) Crystal Detector | -Radioactive Soil Contaminants | Marton (Marton <i>et al.</i> , 1988), Morgan (1998), Diego (2001), |

3. DISCUSSION

Acoustic Sensors:

Tringale and Mitchell (1982) designed a cone penetrometer with a microphone placed into the tip measuring the acoustic response with depth and the cone resistance as well as the sleeve friction. Massarsch (1986) improved the concept by implementing a highly sensitive acoustic sensor working in a much higher frequency range in order to avoid the problem of acoustic noise generated from the mechanical penetration equipment. The test procedure does not differ from the procedure of a classical cone penetration test, while the cone is pushed through the soil at the standard continuous penetration rate, the classic CPT measurements such as the cone tip resistance and the sleeve friction are recorded as well as the acoustic emission.

The acoustic sensor is an add-on sensor with high potential in addition to the cone penetration, pore pressures and sleeve friction measurements to improve soil identification. The results obtained using such a design gave remarkable information regarding the layering and the transition between two different materials. Menge and van Impe (1995) showed, by using calibration tests, that the detection of layers was significantly more evident using acoustic response than the cone resistance q_c . Massarsch proved by field tests that even thin layers of sand or silt (less than 1mm) can be recognized by such a design. The Acoustic sensor finds limitation in noise pollution. Also, acoustic emission depends on the sand structure, microstructure for which only a small database is available.

Video Sensors (VisCPT):

The VisCPT probe consists of two cameras (one low-magnification and one high-magnification camera) installed and an embedded lighting system in a housing camera housing unit, which is placed above the sleeve friction and the cone tip CPT features (Error! Reference source not found.). The VisCPT probe presents a larger outer diameter (51 mm) than the usual CPT probe and pushrods outer diameter. The test procedure does not differ from the procedure of a classical cone penetration test, while the cone is pushed through the soil at the standard continuous penetration rate, the classic CPT measurements such as the cone tip resistance and the sleeve friction are recorded as well as the continuous in-field image recording (Raschke and Hryciw, 1998).

The video sensor installed on the CPT removes the main limitation of the CPT which is the impossibility to directly observe the soil. Thus, the VisCPT offers the advantage to observe and identify geological features that are too small to be observed and detected using conventional CPT such as changes in stratigraphy, location of soil layers, fine soil layering, and small-scale soil anomalies such as clay veins, sand lenses and fissures, etc.

The identification of small-scale soil anomalies using the VisCPT relies on encountering the actual existing geological features, not witnessing them does not exclude the possibility of their existence on the investigated site. Moreover, the rare deployment of such a probe induces a small database, limiting the VisCPT performance evaluation.

Electrical Resistivity Sensors (ERT & CRP):

The latest designs include a resistivity module in cone penetrometers, allowing to dispense with another resistivity probe for the water. However, the water samples must be analysed afterwards in a laboratory to determine its resistivity. Using a soil resistivity probe and a water resistivity probe, the penetration is stopped every 0.2m while resistivity measurements are taken. In the meanwhile, a water resistivity probe is penetrated, and at every 0.2m of soil penetration, a water sample is taken into a chamber for pore water resistivity measurements (Zuidberg, 1988; Campanella and Kokan, 1993).

The ERT probe offers the advantage to derive the porosity and the density in a more consistent way. However, the test necessitates determining extra information such as the water resistivity, the fines and clays contents from laboratory tests on samples. The assumption on soil type need to be made and the cone penetration must be halted every 0.2 m. All these conditions make the ERT a time-consuming in-situ test. Nevertheless, the ERT is a less direct method to measure soil density since it relies on three measurements that are: electrical resistivity of the soil (R) with one probe, electrical resistivity of pore water with a second probe and laboratory calibration of electrical resistivity to soil porosity on samples. None of these two methods gives the exact soil unit, even though the measurements obtained from the ERT are more representatives.

The Cone Resistivity Penetrometer (CRP) probe design embeds an electrical resistance component made of inner electrode welded with high voltage and high current and external electrode welded with low voltage and low current cable. The electrical resistivity module is placed at the cone tip for better soil-probe contact. The test procedure does not differ from the procedure of a classical cone penetration test, while the cone is pushed through the soil at the standard continuous penetration rate, the classic CPT measurements such as the cone tip resistance and the sleeve friction are recorded as well as the continuous in-field soil electrical resistivity (Campanella and Ap-, 1993; Yoon et al., 2009; Yoon, Jung and Lee, 2011).

The CRP probe offers the advantage to detect thin layered soils with a higher resolution during continuous cone penetration tests. Additionally, the CRP probe can clearly detect the densification effects of the sandy soils.

Time Domain Reflectometry Sensors (TDR):

The probe consists of two parallel steel wires (conductor and ground) implemented either in the cone tip or the sleeve friction apparatus (Error! Reference source not found.). The TDR probe implemented in the cone tip was found to be a more suitable location due to the better probe-soil contact. The test procedure consists of halting the cone penetration at the desired depth interval and measuring the TDR measurements were recorded.

The TDR probe offers the advantage to measure in a simultaneous way the permittivity and the electrical conductivity of a material, and to derive the water content of the material relying on the good relationship between both during a CPT as well as the classic CPT measurements (qc, fs, u). Miyamoto (2012) showed the ability of the TDR probe method to satisfactory predict the spatial distribution of the volumetric water content and the ability to detect contaminated soils. In order to derive the soil porosity using the TDR probe method, the specific gravity of soil grains, G_s , needs

to be determined from samples by laboratory tests. Which makes the TDR probe method, not a direct method to derive parameters. Secondly, the TDR probe was found sensitive to change in temperature, hence a correction for the temperature effect must be applied. Thirdly, the test procedure required to halt the cone penetration to record the TDR measurements, which, depending on the desired depth interval, makes the TDR test procedure time-consuming. Moreover, the water content is often found underestimated nearby the soil surface using the TDR probe method (Miyamoto, F and C, 2012).

Magnetometer Sensor:

The magnetometer probe is mounted on top of a CPT made of high-grade non-magnetic steel. The magnetometer sensor is used to measure the strength and direction of the magnetic field. The disturbance in the magnetic field-tested induced by ferromagnetic material is detectable using a magnetometer probe attached to a classic CPT/CPTu. The magnetic disturbance creates a small alternating magnetic field which is recorded by the magnetometer probe as the CPT is pushed through the soil and collecting the usual CPT/CPTu data. Once electronically amplified and processed, the results are addressed in geophysical surveys, such as magnetotellurics and magnetic surveys (Gouda Geo-Equipment BV., 2019).

The magnetometer cone offers several advantages over other geophysical magnetic survey methods. Firstly, the test is undertaken without any pre-drilling or any operations. Secondly, the test provides both geotechnical and magnetic measurement data in one single test procedure. Providing a continuous measurement of both the magnetic field and the soil behaviour (classic CPT/CPT(u) data), the magnetometer cone penetration test offers different potential such as Unexploded Bomb/Ordnance surveys (UXB/UXO), or the determination of the driving depth of pile foundation, sheet piles length, anchors locations, cables and pipes locations. The result of the survey allows the production of 3 dimensions representative model of site hazard identified. The interpretation of the encountered magnetic field anomaly must be undertaken by an experienced operator. This is even more important for the unexploded bomb/ordnance surveys, that must, by law, be supervised by qualified geophysicist with suitable experience to undertake the survey within its limitations. Moreover, the cone penetrometer is, by itself, a ferromagnetic object influencing the magnetic field under the rig. Therefore, only the influence of the cone penetrometer is recorded during the first four meters of penetration. To solve this issue, a preliminary scan using a hand-carried magnetometer should be planned, especially in case of risk of buried bombs.

Multi-Friction & Multi-Piezo-Friction Sensors (MFP & MPFP):

The first design generation (MFP) included four extra independent friction sleeve sensors. These sleeves can be equipped with different roughness characteristics. The second-generation device (MPFP) included five additional pore pressure sensors to the set of multiple sleeve friction sensors. The recent studies undertaken by Hebelier (2018) showed the necessity of only one extra texturized sleeve friction. The test procedure does not differ from the procedure of a classical cone penetration test, while the cone is pushed through the soil at the standard continuous penetration rate, the classic CPT measurements such as the cone tip resistance and the sleeve friction are recorded as well as extra sleeve friction sensors with increasing surface roughness.

The MFP offers higher confidence in the use of the friction reading using only one extra textured sleeve reading ($R_{max} = 0.50$ mm) along the probe's shaft. High level of confidence for sandy, silty, clayey mixture classification boundaries. The proposed new classification system tends to overcome the main issue of the existing CPT-based classification systems, that rely on parameters depending on each other (normalization of f_s , u_2 and q_{net}) that can lead to distortion in the soil classification.

The classification results gave good results for silica sands, sandy, silty, clayey mixtures and calcareous deposits. A better soil classification using Qtn-MFP chart for silica sands, sandy, silty, clayey mixtures was found than if using Q_t - B_q , Q_t - U_2 and Qtn-Fr charts. Plus, the Qtn-MFP chart offers the advantage to separate calcareous and cemented materials from uncemented and silica-based materials. The main limitation of the Multi-Friction & Multi-Piezo-Friction Sensors is its recent introduction. A larger database is required in OC clays and gravels to improve the classification boundaries. The Qtn-Fr chart gives better soil identification of OC fine-grained layers, mostly due to the small database currently available.

Radioisotope Sensors (NDT):

To date, two different nuclear sensors have been developed, the neutron moisture probe (NM) for measuring water content profile and the nuclear density probe (ND) for measuring the soil density. The NM sensor is based on the fact that neutrons are slowed down in presence of the hydrogen and therefore, to measure the water content of the soil if all the hydrogen is in the form of water. The nuclear density probe (ND) for measuring soil density based on the energy level of the emitted photons from the source and the detected photons entering the detector after irradiation of the soil mass. The test procedure does not offer the possibility to undertake radioactive measurement in a continuous way. Therefore, at the standard continuous penetration rate, the classic CPT measurements such as the cone tip resistance and the sleeve friction are recorded, and at the desired depths the cone penetration is halted and the radioactive energy dissipation of the photons depending on the energy level of the photons and the atomic density of the soil encountered are recorded using nuclear sensors.

Using a nuclear density test (NDT) in combination with a CPT/CPTU allows clear identification of the layering thanks to the density profile obtained from the NDT offering the advantage to measure the soil density and the water content in a more "direct way" than with ERT probe. Additionally, the use of NDT seems to be significantly useful for identification of the peat layer. Density and water contents result from in-situ measurements using NDT match extremely well with results measured in the laboratory on samples. Unlike using ERT probes, the greater diameter used for the design of the NDT (44mm diameter for NDT compared to 36mm diameter for ERT) seems to create greater disturbances and hence densification of the loose sand around the probe. Plus, this combined to the smaller soil volume tested in the NDT measurement compared to the soil volume tested with ERT result in the ERT giving more representative in situ densities. The NDT tends to over predict the best estimate (4% higher on average). Other studies proved the need for a correction factor on the NDT measurements (between 0.95 and 1.03, depending on soil type and location). Moreover, the use of nuclear probes is limited in practice due to the radioactivity of the probe requiring the accord of the right authorities and to the necessity to halt the cone penetration to undertake the nuclear measurements (Tom Lunne, Peter K. Robertson, 1997).

Temperature Sensor (Thermocouples & Thermal CPT):

The first temperature sensors added on a CPT probe were the Thermocouple sensors. Preliminary, they were incorporated to CPT probe and used to aid in calibration CPT corrections. The sensors were then deployed to detect permafrost layers and soil contaminants that generate heat due to chemical or biological activity (Woeller et al., 1991).

The T-CPT probe includes a temperature sensor on the cone tip of the CPT. To date, 2 different T-CPT prototypes have been deployed and used. Both cones have a radius of 18 mm, the T-CPT prototypes developed by FUGRO differ by the location of the temperature sensor installed on the probe and the internal voids (the second cone presenting a smaller void close to the cone tip). The T-CPT Cone Prototype 1 has its temperature sensor located above the cone tip, further away from the outer diameter of the probe than the T-CPT Prototype 2. The T-CPT Cone Prototype 2 has its temperature sensor located closer to the cone tip and its outer surface. The T-CPT implies pushing the cone penetrometer through the soil and continuously measuring the cone resistance, sleeve friction as well as the temperature generated by friction. At a selected temperature difference, the cone penetration is stopped, and the dissipation of the heat generated during the cone penetration is recorded (no heat source required).

The main advantage of the T-CPT is the probe robustness compared to the commonly used needle probe test extremely fragile. The T-CPT offers the advantage to get in-situ thermal conductivity test in deep and strong soil which was not doable using a needle probe. Secondly, the test offers the advantage to derive the thermal conductivity value and the initial temperature of the soil in-situ and with good reliability. The T-CPT test is limited to point measurements, no continuous profile can be derived using this approach. Secondly, the interpretation model developed to derive the heat capacity of the soil using temperature decay record cannot be used due to lack of reliability (Vardon, Baltoukas and Peuchen, 2018). Thirdly, the temperature decay test required is time-consuming (500 s) and the interpretation model developed requires a temperature difference between the cone tip and the initial soil temperature of minimum 3 degrees to be used reliably, which is hardly reachable in soft soil such clay and organic soil.

Fiber Optic Sensors (FO):

The FO penetrometer prototype respects the standards given by the ASTM D5778 – 12 (Conshohocken, 1996), only differing by the replacement of the classical electric strain-gauges by the fibre optical sensors. The test procedure does not differ from the procedure of a classical cone penetration test, while the cone is pushed through the soil at the standard continuous penetration rate, the classic CPT measurements such as the cone tip resistance, the sleeve friction and pore pressure are recorded using the FO sensors.

The FO sensors offer many advantages such as a smaller difference in the zero-load reading before and after testing, a better precision allowing to distinguish changes in qc measurements as small as 0.07 kPa (10g). Moreover, the FO sensors offer data acquisition at higher frequency (500 Hz instead of the 2 Hz allowed by the classical CPT), which allows detecting very thin soil layers with more accuracy. Plus, FO sensors have proved their smaller sensitivity than classic electric strain-gauges to temperature shock. Research, as part of the FO cone penetrometer future development, is currently ongoing to fit a temperature sensor in the FO cone penetrometer to target heat flux and

to provide a correction for transient temperature effects on the CPT measurements. The actual FO sensors range for measuring qc and fs restrict the use of such sensors for soft soils only. Moreover, the FO cone penetrometers are available only recently and no consistent database or feedback is currently available to judge the full performances of the FO sensors on the field. Additionally, the performance tests undertaken focused on the qc-sensor, the result for the test performance undertaken on the fs-sensor are unknown. To date, FO pore pressure and inclination sensors have not been developed yet but are part of the future development of the FO sensors.

pH, Electrical Conductivity & Redox Potential Sensors (ORP or ChemiCone):

The probe design includes a pH electrode, an ORP sensor, references electrodes, and a temperature sensor. The electrodes are implemented laterally on the side of the penetrometer and above the cone tip. This location allows the electrodes to be in acceptable effective contact with the soil and to be protected from damaging impacts and the high pressure occurring at the cone tip during CPT. The signals recorded by the electrodes are then transmitted to a transducer and then to a microprocessor to store and retrieval of data. (Bratton and Bianchi, 1996; Bratton and Rooney, 1998). The test procedure does require halted penetration to measure the ORP and the electrical conductivity, the pH profile can be measured continuously during the cone penetration without stopping the test.

The main advantages of the probe are the in-situ measurements of ORP and pH within the most accurate and lowest in-situ economic costs to soil contamination investigation compared to classical method requiring sampling and laboratory tests that are time and economical highly costly. Plus, the direct measurement of the oxidation using the ORP electrode offers the advantage to directly measure the oxidation of the soil and avoid distortion of actual soil characteristics by exposure of samples required for laboratory testing to airborne oxygen. The main limitations of the probe are the possibility to miss the soil contaminant due to the test procedure which requires to absorb some contaminant into a measuring cell. Additionally, the measuring cell requires to be cleaned after using it in order to eliminate any cross-contamination. The high-temperature sensitivity of the pH sensor makes the addition of a temperature sensor mandatory for correction and the low abrasion resistance of the pH sensor can be problematic. All in all, these limitations make the probe not convenient to be used in-situ.

Laser-Induced Fluorescence Sensor (LIF):

The LIF probe design embeds four main components that are an excitation system (laser and Raman shifter), an optical delivery system, a sample interface and a detection system (Pepper, Wright and Kenny, 2002). The LIF probe deployed on a cone penetrometer allows recording continuously, at a standard penetration rate, the classical CPT data as well as the soil fluorescence.

The soil fluorescence response allows detecting the most common fuel soil contaminants such as petroleum hydrocarbons and aromatic hydrocarbons. However, the LIF sensor is limited to detect fluorescing pollutants and does not detect common chemical contaminants such as chlorinated hydrocarbons (TCE & PCE) since these contaminants do not fluoresce when exposed to the laser light.

Integrated Optoelectronic Chemical Sensor:

The optoelectronic chemical probe design includes the glass waveguide, the polymeric coating, the laser light source, and a data processing system. The optoelectronic chemical sensor is embedded in a stainless steel housing respecting the standard CPT diameter (35 mm) and 100 mm long (Burns and Mayne, 1998). The test procedure does not differ from the standard continuous CPT, only the fluid sampling system which requires to halt the CPT penetration.

The optoelectronic chemical probe offers the possibility to detect a wide variety of chemical such as the detection of benzene, toluene, ethylbenzene and xylene (BTEX chemicals) in both gaseous and aqueous phases. Additionally, the optoelectronic probe, and more precisely the polymeric coating can be rapidly adapted to detect other chemicals such as chlorinated hydrocarbons or dissolved metals. However, the probe is limited by its robustness which needs improvement to withstand the CPT standard.

Gamma Radiation & Neutron Sensors (RadCone):

The RadCone probe design consists of nuclear instrumentation module (NIM) components used for signal processing, a for power supply, and a multichannel analyser (Marton, Taylor and Wilson, 1988). Deployed on a CPT, the classical data can be obtained as well as the nuclear contamination of the soil at the desired depths.

The gamma radiation sensors offer in-situ reconnaissance of gamma-emitting particles in soils in real-time for radioactivity profiles during the site investigation. Plus, the probe offers the advantage to be non-radioactive, which simplifies its deployment compared to nuclear density or water content probes. However, the gamma probe requires to halt the cone penetration to take radioactivity measurements.

4. CONCLUDING REMARKS

Many of the CPT add-on sensors did not make it as a routine due to both, the specificity of the extra measurements offered, the probe cost and to practical reasons (i.e. derogation required for nuclear probes, tests requiring halting the cone penetration for some time). The last CPT add-on sensor advancements seem to direct the research in the development of CPT capable of higher frequency data recording offering the advantage to be less sensitive to temperature changes (FO sensors). The expectations addressed in the past regarding the development of new nuclear sensor less costly and non-radioactive (which would not require special derogation for deployment), have not been reached. The future technological advancements might help to provide a non-contaminating and cheaper nuclear probe.

The Fiber Optic and the Multi-Piezocone Friction Sensors give interesting promises in the improvement of the soil investigation and in the development of more reliable and more accurate sensors. Their potentials should be investigated into depth to increase their database and confirm their promises. Interests are shown by the industry to implement gravimeters into CPT probe as add-on sensors to record gravitation acceleration which allows the derivation of the soil in-situ density (Lacoste, 2002). Improvement still needs to be made to build more compact probes that could be deployed on a cone penetrometer.

References:

- Akrouch, G. A. et al. (2016) 'Thermal Cone Test to Determine Soil Thermal Properties', *Journal of Geotechnical and Geoenvironmental Engineering*, 142(3), p. 04015085. doi: 10.1061/(asce)gt.1943-5606.0001353.
- Appelo, C. A. J. et al. (2018) 'PHT3D : A Reactive Multicomponent Transport Model for Porous Laser-Induced Media DyeLIF TM : A Saturated New Direct-Push Fluorescence Sensor System for Chlorinated Solvent DNAPL and Non-Naturally Fluorescing NAPLs'. doi: 10.1111/gwmr.12296.
- Bratton, W. L. and Bianchi, J. C. (1996) 'Surface mounted pH sensor for cone penetration testing'. Google Patents.
- Bratton, W. and Rooney, D. J. (1998) 'In situ oxidation reduction potential measurement of soils and ground water'. Google Patents.
- Burns, S. E. and Mayne, P. W. (1998) 'Penetrometers for soil permeability and chemical detection, geosystems engineering group', *School of Civil and Environmental Engineering, Georgia Institute of Technology Atlanta, Georgia*, pp. 30332–30355.
- Campanella, R. and Ap-, A. N. (1993) 'A New Approach to Measuring Dilatancy in Saturated Sands ° T', 16(4).
- Campanella, R. G. and Kokan, M. J. (1993) 'A new approach to measuring dilatancy in saturated sands', *Geotechnical Testing Journal. ASTM International*, 16(4), pp. 485–495.
- Chen, R. P. et al. (2010) 'Measurement of electrical conductivity of pore water in saturated sandy soils using time domain reflectometry (TDR) measurements', 206, pp. 197–206. doi: 10.1139/T09-088.
- Conshohocken, W. (1996) 'Standard Test Method for Performing Electronic Friction Cone and Piezocone Penetration Testing of Soils 1', *Current*, 04(January), pp. 1–20. doi: 10.1520/D5778-12.agreed.
- Diego, S. (2001) 'Xenon has been the subject of considerable recent interest as a gamma-ray detector medium, including its use in ionization and proportional detectors, and as a scintillator. Its high atomic number (', 248(2), pp. 289–294.
- Gouda Geo-Equipment BV. (2019) Magnetometer Cone (MagCone). Available at: <https://www.gouda-geo.com/products/cpt-equipment/special-modules-for-cpt/magnetometer-cone-magcone> (Accessed: 22 February 2019).
- Hebeler, G. L., Martinez, A. and Frost, J. D. (2018) 'Interface response-based soil classification framework', *Canadian Geotechnical Journal*, 55(12), pp. 1795–1811. doi: 10.1139/cgj-2017-0498.
- Houlsby, G. T. and Ruck, B. M. (1998) 'Interpretation of Signals from an Acoustic Cone Penetrometer', pp. 1075–1080.
- Hryciw, R. D., Ghalib, A. M. and Raschke, S. A. (1998) 'In situ soil characterization using Vision Cone Penetrometer (VisCPT)', *Proc. 1st IC on Site Characterization, Atlanta*, 2, pp. 1081–1086.

- Jia, R. et al. (2013) 'Interpretation of density profile of seabed sediment from nuclear density cone penetration test results', *Soils and Foundations*. Elsevier, 53(5), pp. 671–679. doi: 10.1016/j.sandf.2013.08.005.
- Jia, R. et al. (2019) 'In Situ Determination of Density Profiles in Complex Strata Using the Nuclear Density Cone Penetrometer', 2019.
- Kurup, P. et al. (2017) 'A Review of Technologies for Characterization of Heavy Metal Contaminants', *Indian Geotechnical Journal*. Springer India, 47(4), pp. 421–436. doi: 10.1007/s40098-016-0214-6.
- Kurup, P. U. (2006) 'Innovations in cone penetration testing', in *Site and Geomaterial Characterization*, pp. 48–55.
- Kurup, P. U. et al. (2007) 'Electronic Nose – Membrane Interface Probe for Geoenvironmental Site Characterization', 132(9), pp. 1133–1142.
- Lacoste, M. (2002) Micro-g LaCoste Borehole Gravity Survey Services. Available at: <http://www.microglacoste.com/bhg.htm> (Accessed: 22 May 2007).
- Lightner, E. M. and Purdy, C. B. (1995) 'Cone penetrometer development and testing for environmental applications', in *Proc., Int. Symp. on Cone Penetration Testing*, pp. 41–48.
- Lin, J. et al. (1995) 'Laser fluorescence excitation-emission matrix (EEM) probe for cone penetrometer pollution analysis', in *Optical Sensors for Environmental and Chemical Process Monitoring*, pp. 70–79.
- Looijen, P. et al. (2018) 'Fibre optic cone penetrometer', *Cone Penetration Testing 2018: Proceedings of the 4th International Symposium on Cone Penetration Testing*. Edited by Hicks, Pisano, and Peuchen. Delft: Delft University of Technology, pp. 407–409.
- Mao, W. et al. (2018) 'High Frequency Acoustic Emissions Observed during Model Pile Penetration in Sand and Implications for Particle Breakage Behavior', *International Journal of Geomechanics*, 18(11), p. 04018143. doi: 10.1061/(ASCE)GM.1943-5622.0001287.
- Marton, R., Taylor, L. and Wilson, K. (1988) 'Development of an In-Situ Subsurface Radioactivity Detection System-the Radcone', *Waste Management*, 88.
- Massarsch, K. R. (1986) 'Acoustic penetration testing', in *Proceeding of the 4th Geotechnical Seminar, Field Instrumentation and In-Situ Measurements*, Nanyang Tech. Inst., Singapore.
- Mccall, W. et al. (2018) 'Evaluation and application of the optical image profiler (OIP) a direct push probe for photo - logging UV - induced fluorescence of petroleum hydrocarbons', *Environmental Earth Sciences*. Springer Berlin Heidelberg, 77(10), pp. 1–15. doi: 10.1007/s12665-018-7442-2.
- Menge, P. and Van Impe, W. (1995) 'The application of acoustic emission testing with penetration testing', in *Proceedings of the International Symposium on Cone Penetration Testing (CPT'95)*, pp. 49–54.

- Mimura, M. (1995) 'Performace of RI Cone Penetrometers in Sand Deposits', in Proc Int. Symp. on Cone Penetrometer Testing, CPT'95, pp. 55–60.
- Miyamoto, T., F, K. and C, J. (2012) 'Simultaneous measurement of soil water and soil hardness using a modified time domain reflectometry probe and a conventional cone penetrometer', (June), pp. 240–248. doi: 10.1111/j.1475-2743.2012.00391.x.
- Morgan, J. C., Adams, J. W. and Ballard, J. H. (1998) 'Field use of a cone penetrometer gamma probe for radioactive-waste detection.', *Field Analytical Chemistry & Technology*. Wiley Online Library, 2(2), pp. 111–115.
- Muromachi, T. (1981) 'Cone penetration Testing in Japan, Symposium on Cone Penetration Testing and Experiences', *Geotechnical Engineering Division, ASCE*, October, St. Louis, pp. 76–107.
- Nozaki, R. and Bose, T. K. (1990) 'Measurement of the dielectric properties of materials by using time domain reflectometry', in *7th IEEE Conference on Instrumentation and Measurement Technology*, pp. 263–269.
- Olie, J. J., Van Ree, C. and Bremmer, C. (1992) 'In situ measurement by chemoprobe of groundwater from in situ sanitation of versatic acid spill', *Geotechnique*. Thomas Telford Ltd, 42(1), pp. 13–21.
- Pepper, J. W., Wright, A. O. and Kenny, J. E. (2002) 'In situ measurements of subsurface contaminants with a multi-channel laser-induced fluorescence system', 58, pp. 317–331.
- Raschke, S. A. and Hryciw, R. D. (1997) 'Vision cone penetrometer for direct subsurface soil observation', *Journal of geotechnical and geoenvironmental engineering*. American Society of Civil Engineers, 123(11), pp. 1074–1076.
- Raschke, S. A. and Hryciw, R. D. (1998) 'Vision Cone Penetrometer For Direct Subsurface Soil Observation', *Journal of Geotechnical and Geoenvironmental Engineering*, 123(November 1997), pp. 1074–1076.
- Robertson, P. K. (2016) 'Cone penetration test (CPT)-based soil behaviour type (SBT) classification system — an update', *Canadian Geotechnical Journal*, 53(12), pp. 1910–1927. doi: 10.1139/cgj-2016-0044.
- Robertson, P. K. and Cabal, K. . (2010) 'Guide to Cone Penetration Testing for Geo-Environmental Engineering', *Gregg Drilling & Testing, Inc.*, pp. 1–85.
- Rossabi, J. et al. (2000) 'Field tests of a DNAPL characterization system using cone penetrometer-based Raman spectroscopy', *Groundwater Monitoring & Remediation*. Wiley Online Library, 20(4), pp. 72–81.
- Shibata, T. (1994) 'Use of RI-cone penetrometer in foundation engineering', in *Proc. 13th Int. Conf. on Soil Mech. and Found.*, pp. 147–150.
- SHIBATA, T. et al. (1992) 'Moisture measurement by neutron moisture cone penetrometer: design and application', *Soils and foundations*. The Japanese Geotechnical Society, 32(4), pp. 58–67.

- Sully, J. P. (1988) 'In situ density measurement with nuclear cone penetrometer', Proc. ISOPT-1, 2, pp. 1001–1005.
- Tom Lunne, Peter K. Robertson, J. J. M. P. (1997) *Cone Penetration Testing in Geotechnical Practice*. Blackie Academic and Professional.
- Tringale, P. T. and Mitchell, J. K. (1982) 'An acoustic cone penetrometer for site investigation', in *Proceeding of the Second European Symposium on Penetration Testing (ESOPT II)*, pp. 909–914.
- Upadhyaya, S. K. et al. (1982) Cone index prediction equations for Delaware soils.
- Vardon, P. J. (2018) 'Thermal Cone Penetration Test (T-CPT) Thermal Cone Penetration Test (T-CPT)', (June).
- Vardon, P. J., Baltoukas, D. and Peuchen, J. (2018) 'Interpreting and validating the thermal cone penetration test (T-CPT)', *Géotechnique*, (August), pp. 1–13. doi: 10.1680/jgeot.17.P.214.
- Vaz, C. M. P., Bassoi, L. H. and Hopmans, J. W. (2001) 'Contribution of water content and bulk density to field soil penetration resistance as measured by a combined cone penetrometer-TDR probe', *Soil and Tillage Research*, 60(1–2), pp. 35–42. doi: 10.1016/S0167-1987(01)00173-8.
- Villet, W. C. B., Mitchell, J. K. and Tringale, P. T. (1981) 'Acoustic emissions generated during the quasi-static cone penetration of soils', *Acoustic Emissions in Geotechnical Engineering Practice*. ASTM International, pp. 174–193.
- Wiertsema & Partners (2016) *Magnetometer Cone Penetration Testing*. Available at: www.wiertsema.nl.
- Woeller, D. J. et al. (1991) 'Penetration testing for arctic soil and permafrost conditions', in *Proceedings of the Geotechnical Engineering Congress*, Boulder, Colo, pp. 10–12.
- Yoon, H.-K., Jung, S.-H. and Lee, J.-S. (2011) 'Characterisation of subsurface spatial variability using a cone resistivity penetrometer', *Soil Dynamics and Earthquake Engineering*. Elsevier, 31(7), pp. 1064–1071.
- Yoon, H. et al. (2009) 'Electrical Resistivity and Cone Tip Resistance Monitoring by Using Cone Resistivity Penetrometer', 1, pp. 168–171.
- Yu, X. and Drnevich, V. P. (2004) 'Soil water content and dry density by time-domain reflectometry', *Journal of Geotechnical and Geoenvironmental Engineering*. American Society of Civil Engineers, 130(9), pp. 922–934.
- Zhang, Q. et al. (2007) 'Detection of Deeply Buried UXO Using CPT Magnetometers', 45(2), pp. 410–417.
- Zuidberg, H. M. (1988) 'Advanced in situ measurements', in *Proc. of 2nd International Symposium on Field Measurements in Geomechanics*.

Appendix II Thermal Soil Engineering Parameter Values in function of the Soil Type & Soil Porosity according to Farouki (1981)

| Soil Fraction | | Soil Bulk Density [kg/m ³] | | | | | | | | |
|---------------|------|--|------|------|------|------|------|------|------|------|
| | | Porosity, n: | | | | | | | | |
| Sand | Clay | 0.1 | 0.2 | 0.3 | 0.4 | 0.5 | 0.6 | 0.7 | 0.8 | 0.9 |
| 1 | 0 | 2494 | 2327 | 2161 | 1995 | 1829 | 1662 | 1496 | 1330 | 1163 |
| 0.9 | 0.1 | 2493 | 2327 | 2160 | 1994 | 1828 | 1662 | 1496 | 1329 | 1163 |
| 0.8 | 0.2 | 2492 | 2326 | 2160 | 1994 | 1828 | 1661 | 1495 | 1329 | 1163 |
| 0.7 | 0.3 | 2491 | 2325 | 2159 | 1993 | 1827 | 1661 | 1495 | 1329 | 1163 |
| 0.6 | 0.4 | 2490 | 2324 | 2158 | 1992 | 1827 | 1661 | 1495 | 1329 | 1163 |
| 0.5 | 0.5 | 2489 | 2323 | 2158 | 1992 | 1826 | 1660 | 1494 | 1329 | 1163 |
| 0.4 | 0.6 | 2488 | 2323 | 2157 | 1991 | 1826 | 1660 | 1494 | 1328 | 1163 |
| 0.3 | 0.7 | 2487 | 2322 | 2156 | 1991 | 1825 | 1659 | 1494 | 1328 | 1163 |
| 0.2 | 0.8 | 2487 | 2321 | 2156 | 1990 | 1825 | 1659 | 1494 | 1328 | 1163 |
| 0.1 | 0.9 | 2486 | 2320 | 2155 | 1989 | 1824 | 1659 | 1493 | 1328 | 1162 |
| 0 | 1 | 2485 | 2319 | 2154 | 1989 | 1824 | 1658 | 1493 | 1328 | 1162 |

| Soil Fraction | | Specific Heat Capacity [J/kg·K] | | | | | | | | |
|---------------|------|---------------------------------|------|------|------|------|------|------|------|------|
| | | Porosity, n: | | | | | | | | |
| Sand | Clay | 0.1 | 0.2 | 0.3 | 0.4 | 0.5 | 0.6 | 0.7 | 0.8 | 0.9 |
| 1 | 0 | 1072 | 1414 | 1755 | 2097 | 2439 | 2781 | 3123 | 3464 | 3806 |
| 0.9 | 0.1 | 1078 | 1419 | 1760 | 2101 | 2443 | 2784 | 3125 | 3466 | 3807 |
| 0.8 | 0.2 | 1084 | 1425 | 1765 | 2106 | 2446 | 2786 | 3127 | 3467 | 3808 |
| 0.7 | 0.3 | 1091 | 1430 | 1770 | 2110 | 2450 | 2789 | 3129 | 3469 | 3808 |
| 0.6 | 0.4 | 1097 | 1436 | 1775 | 2114 | 2453 | 2792 | 3131 | 3470 | 3809 |
| 0.5 | 0.5 | 1103 | 1442 | 1780 | 2118 | 2457 | 2795 | 3133 | 3471 | 3810 |
| 0.4 | 0.6 | 1110 | 1447 | 1785 | 2122 | 2460 | 2798 | 3135 | 3473 | 3810 |
| 0.3 | 0.7 | 1116 | 1453 | 1790 | 2127 | 2464 | 2800 | 3137 | 3474 | 3811 |
| 0.2 | 0.8 | 1122 | 1458 | 1795 | 2131 | 2467 | 2803 | 3139 | 3476 | 3812 |
| 0.1 | 0.9 | 1129 | 1464 | 1800 | 2135 | 2471 | 2806 | 3142 | 3477 | 3813 |
| 0 | 1 | 1135 | 1470 | 1804 | 2139 | 2474 | 2809 | 3144 | 3478 | 3813 |

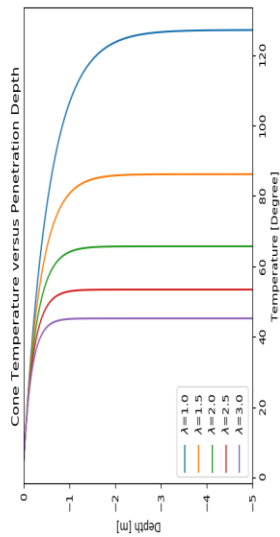
| Soil Fraction | | Volumetric Heat Capacity [MJ/m ³ ·K] | | | | | | | | |
|---------------|------|---|------|------|------|------|------|------|------|------|
| | | Porosity, n: | | | | | | | | |
| Sand | Clay | 0.1 | 0.2 | 0.3 | 0.4 | 0.5 | 0.6 | 0.7 | 0.8 | 0.9 |
| 1 | 0 | 2.16 | 2.38 | 2.60 | 2.82 | 3.04 | 3.26 | 3.48 | 3.70 | 3.92 |
| 0.9 | 0.1 | 2.18 | 2.39 | 2.61 | 2.83 | 3.05 | 3.27 | 3.49 | 3.70 | 3.92 |
| 0.8 | 0.2 | 2.19 | 2.41 | 2.63 | 2.84 | 3.06 | 3.27 | 3.49 | 3.71 | 3.92 |
| 0.7 | 0.3 | 2.21 | 2.42 | 2.64 | 2.85 | 3.07 | 3.28 | 3.50 | 3.71 | 3.93 |
| 0.6 | 0.4 | 2.22 | 2.44 | 2.65 | 2.86 | 3.08 | 3.29 | 3.50 | 3.71 | 3.93 |
| 0.5 | 0.5 | 2.24 | 2.45 | 2.66 | 2.87 | 3.09 | 3.30 | 3.51 | 3.72 | 3.93 |
| 0.4 | 0.6 | 2.26 | 2.47 | 2.68 | 2.88 | 3.09 | 3.30 | 3.51 | 3.72 | 3.93 |
| 0.3 | 0.7 | 2.27 | 2.48 | 2.69 | 2.90 | 3.10 | 3.31 | 3.52 | 3.73 | 3.93 |
| 0.2 | 0.8 | 2.29 | 2.50 | 2.70 | 2.91 | 3.11 | 3.32 | 3.52 | 3.73 | 3.93 |
| 0.1 | 0.9 | 2.31 | 2.51 | 2.71 | 2.92 | 3.12 | 3.32 | 3.53 | 3.73 | 3.94 |
| 0 | 1 | 2.32 | 2.52 | 2.73 | 2.93 | 3.13 | 3.33 | 3.53 | 3.74 | 3.94 |

| Soil Fraction | | Thermal Conductivity [W/m·K] | | | | | | | | |
|---------------|------|------------------------------|------|------|------|------|------|------|------|------|
| | | Porosity, n: | | | | | | | | |
| Sand | Clay | 0.1 | 0.2 | 0.3 | 0.4 | 0.5 | 0.6 | 0.7 | 0.8 | 0.9 |
| 1 | 0 | 6.45 | 4.96 | 3.81 | 2.92 | 2.24 | 1.72 | 1.32 | 1.02 | 0.78 |
| 0.9 | 0.1 | 5.86 | 4.55 | 3.53 | 2.74 | 2.13 | 1.65 | 1.28 | 1.00 | 0.77 |
| 0.8 | 0.2 | 5.33 | 4.18 | 3.28 | 2.57 | 2.02 | 1.58 | 1.24 | 0.97 | 0.76 |
| 0.7 | 0.3 | 4.84 | 3.84 | 3.04 | 2.41 | 1.91 | 1.52 | 1.20 | 0.95 | 0.76 |
| 0.6 | 0.4 | 4.40 | 3.53 | 2.83 | 2.26 | 1.81 | 1.45 | 1.17 | 0.93 | 0.75 |
| 0.5 | 0.5 | 4.00 | 3.24 | 2.62 | 2.12 | 1.72 | 1.39 | 1.13 | 0.91 | 0.74 |
| 0.4 | 0.6 | 3.63 | 2.97 | 2.43 | 1.99 | 1.63 | 1.34 | 1.09 | 0.90 | 0.73 |
| 0.3 | 0.7 | 3.30 | 2.73 | 2.26 | 1.87 | 1.55 | 1.28 | 1.06 | 0.88 | 0.73 |
| 0.2 | 0.8 | 3.00 | 2.51 | 2.10 | 1.75 | 1.47 | 1.23 | 1.03 | 0.86 | 0.72 |
| 0.1 | 0.9 | 2.73 | 2.30 | 1.95 | 1.65 | 1.39 | 1.18 | 0.99 | 0.84 | 0.71 |
| 0 | 1 | 2.48 | 2.12 | 1.81 | 1.54 | 1.32 | 1.13 | 0.96 | 0.82 | 0.70 |

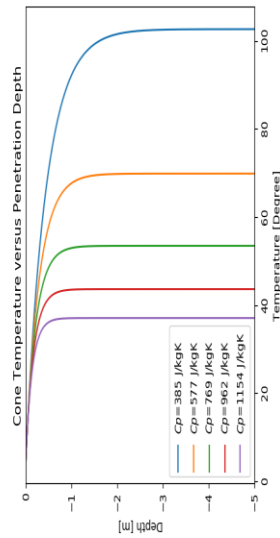
| Soil Fraction | | Thermal Diffusivity [mm ² /s] | | | | | | | | |
|---------------|------|--|------|------|------|------|------|------|------|------|
| | | Porosity, n: | | | | | | | | |
| Sand | Clay | 0.1 | 0.2 | 0.3 | 0.4 | 0.5 | 0.6 | 0.7 | 0.8 | 0.9 |
| 1 | 0 | 2.41 | 1.51 | 1.00 | 0.70 | 0.50 | 0.37 | 0.28 | 0.22 | 0.18 |
| 0.9 | 0.1 | 2.18 | 1.38 | 0.93 | 0.65 | 0.48 | 0.36 | 0.27 | 0.22 | 0.17 |
| 0.8 | 0.2 | 1.97 | 1.26 | 0.86 | 0.61 | 0.45 | 0.34 | 0.27 | 0.21 | 0.17 |
| 0.7 | 0.3 | 1.78 | 1.15 | 0.80 | 0.57 | 0.43 | 0.33 | 0.26 | 0.21 | 0.17 |
| 0.6 | 0.4 | 1.61 | 1.06 | 0.74 | 0.54 | 0.41 | 0.31 | 0.25 | 0.20 | 0.17 |
| 0.5 | 0.5 | 1.46 | 0.97 | 0.68 | 0.50 | 0.38 | 0.30 | 0.24 | 0.20 | 0.17 |
| 0.4 | 0.6 | 1.32 | 0.88 | 0.63 | 0.47 | 0.36 | 0.29 | 0.23 | 0.19 | 0.17 |
| 0.3 | 0.7 | 1.19 | 0.81 | 0.59 | 0.44 | 0.34 | 0.28 | 0.23 | 0.19 | 0.16 |
| 0.2 | 0.8 | 1.08 | 0.74 | 0.54 | 0.41 | 0.33 | 0.26 | 0.22 | 0.19 | 0.16 |
| 0.1 | 0.9 | 0.97 | 0.68 | 0.50 | 0.39 | 0.31 | 0.25 | 0.21 | 0.18 | 0.16 |
| 0 | 1 | 0.88 | 0.62 | 0.47 | 0.36 | 0.29 | 0.24 | 0.21 | 0.18 | 0.16 |

Appendix III Simplified Cone Tip / Soil Heat Transfer Analytical Solution

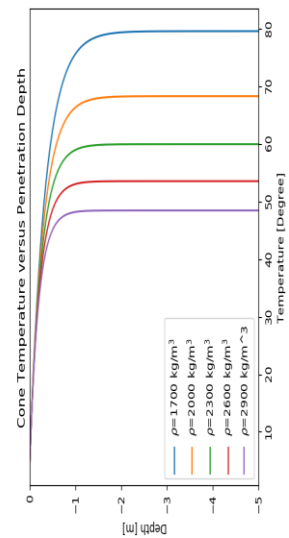
Thermal Conductivity Influence:



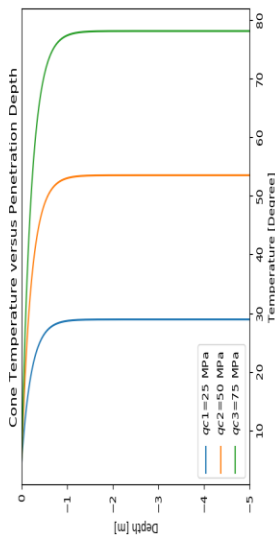
Heat Capacity Influence:



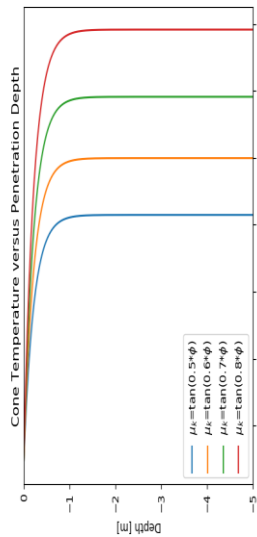
Soil Density Influence:



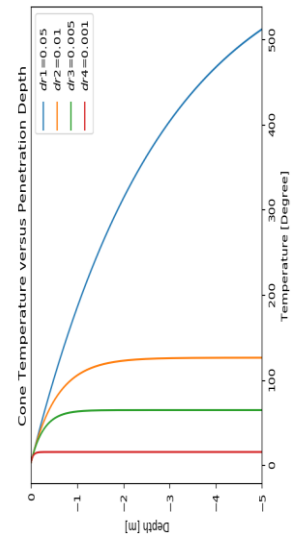
Cone Tip Resistance Influence:



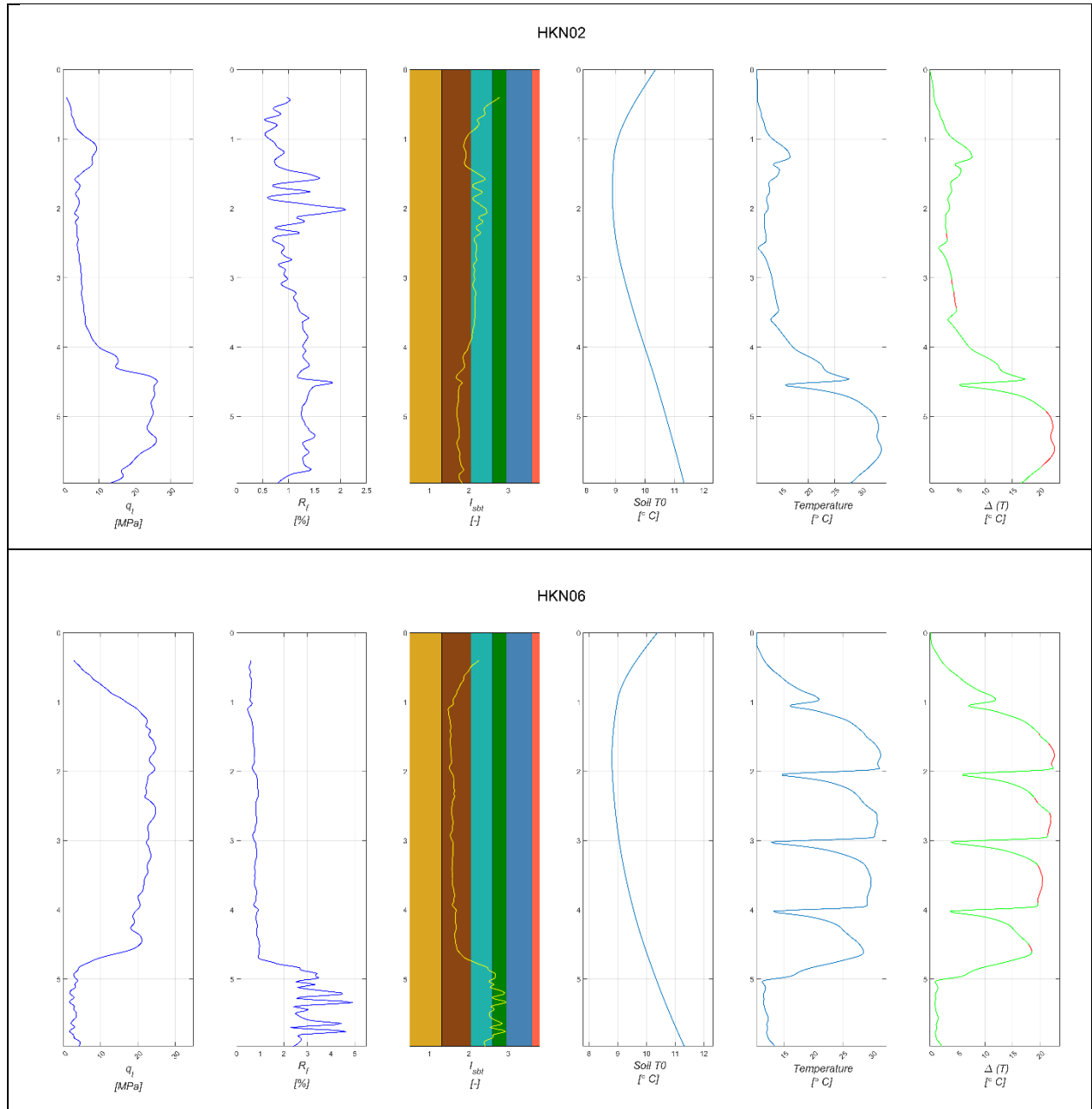
Kinetic Coefficient of Friction Influence:



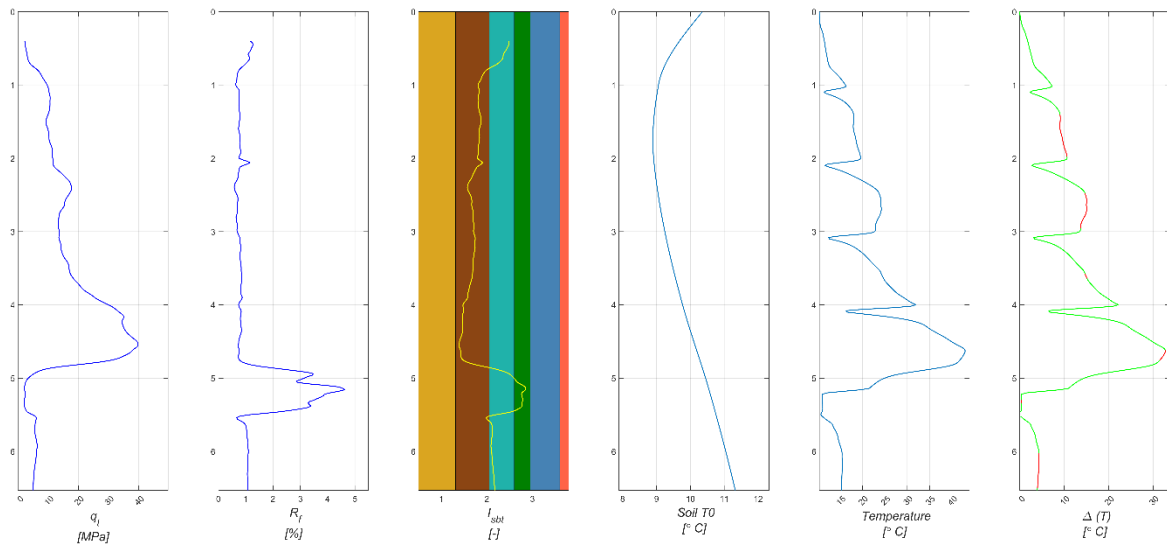
Friction Factor Influence:



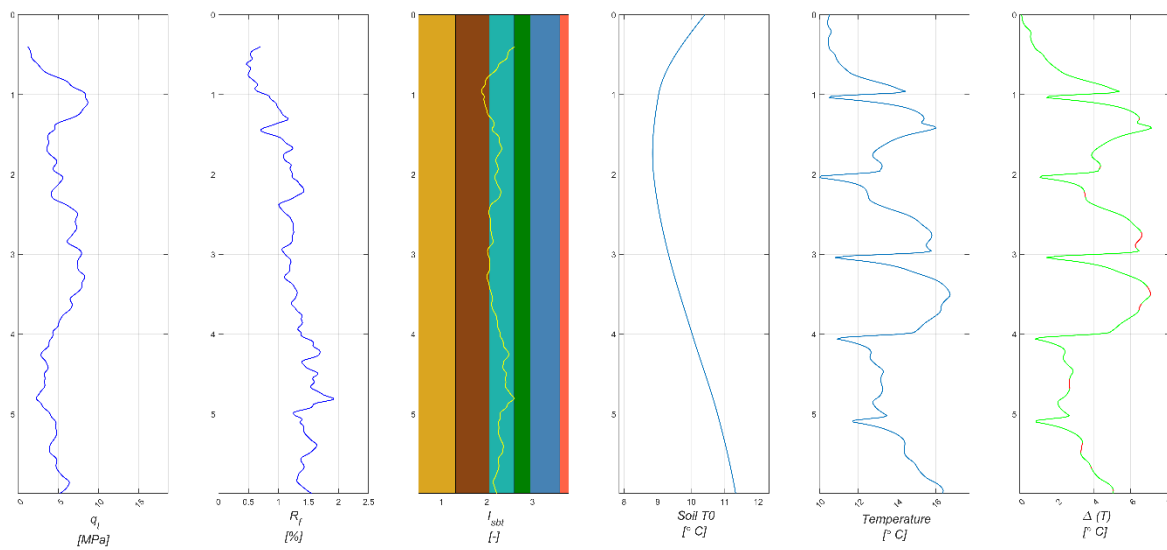
Appendix IV HKN Site T-CPT Profiles



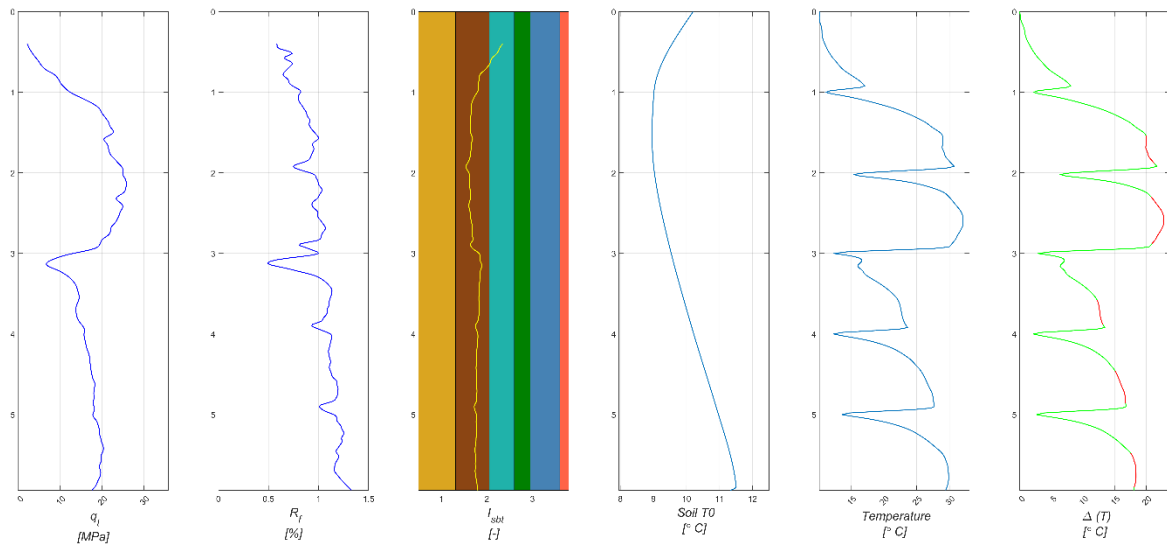
HKN09



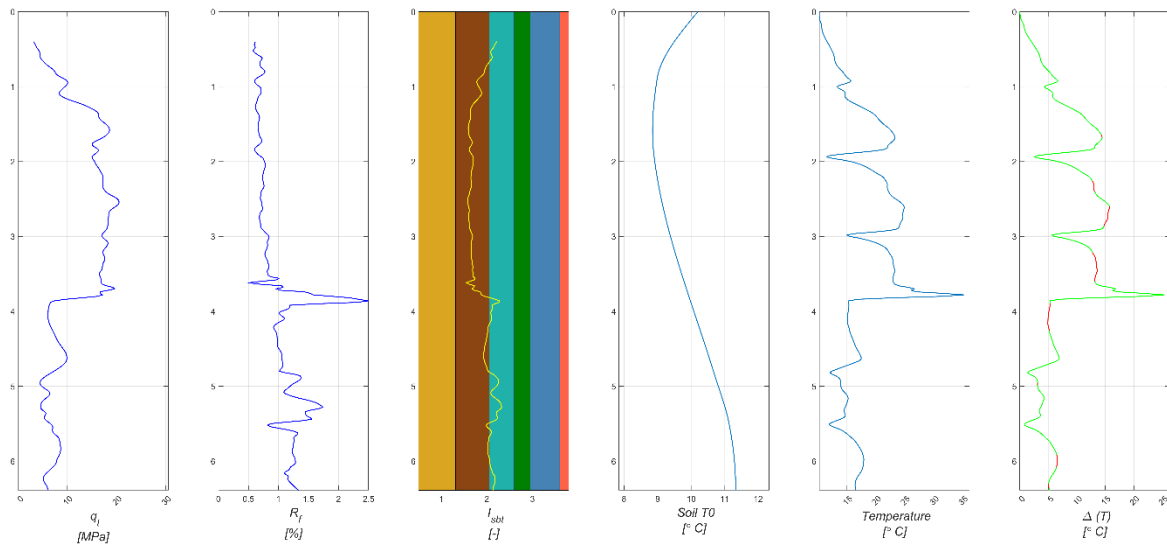
HKN10



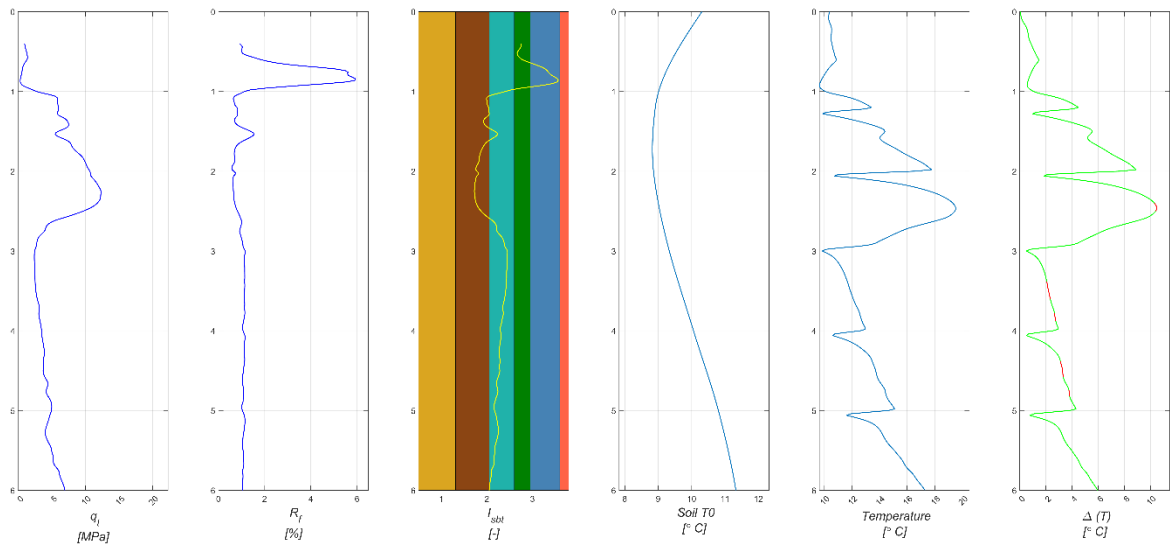
HKN21



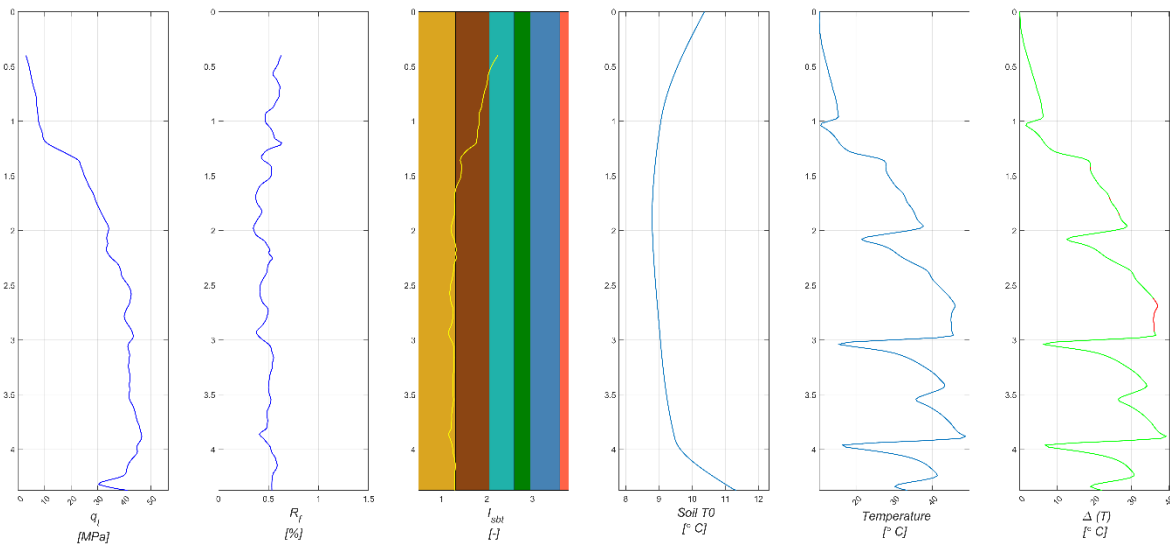
HKN25

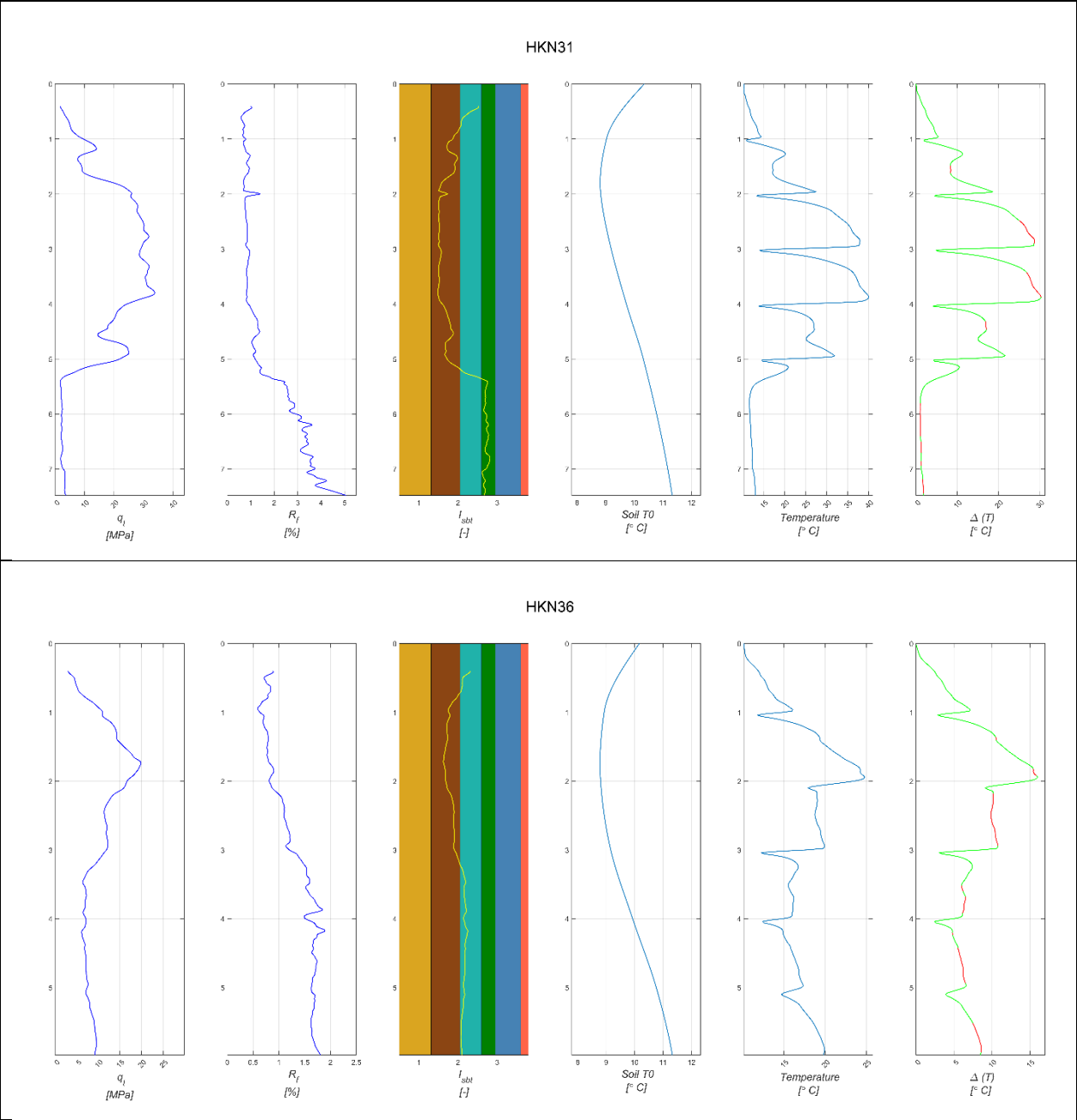


HKN26

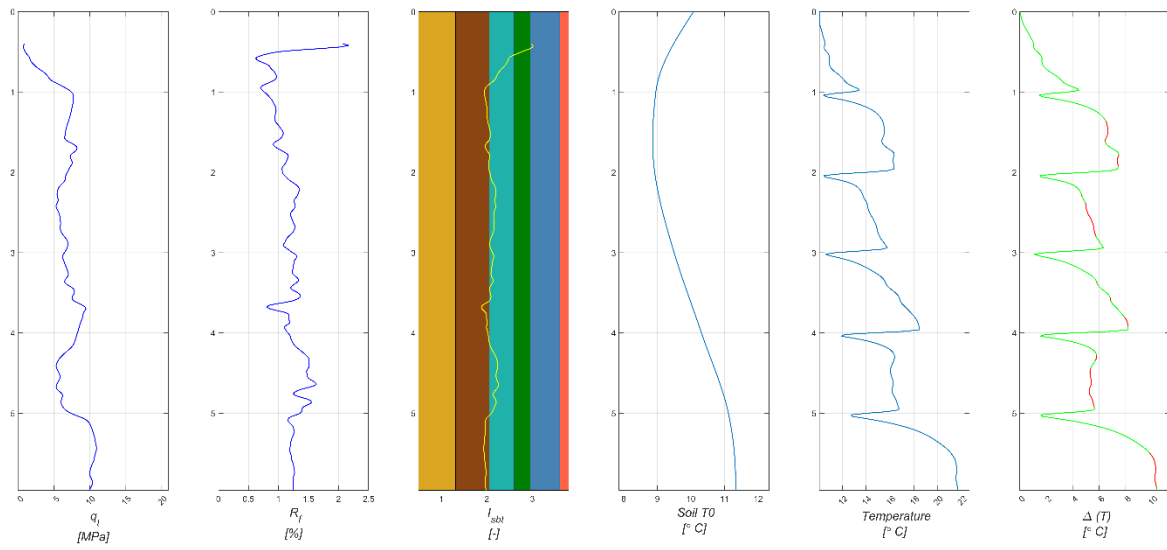


HKN27

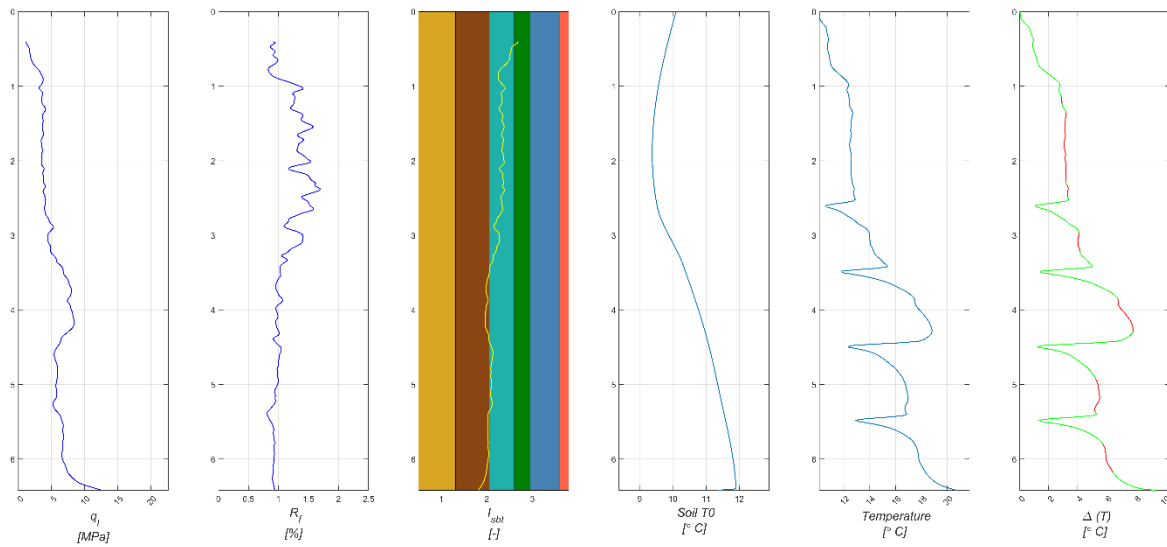




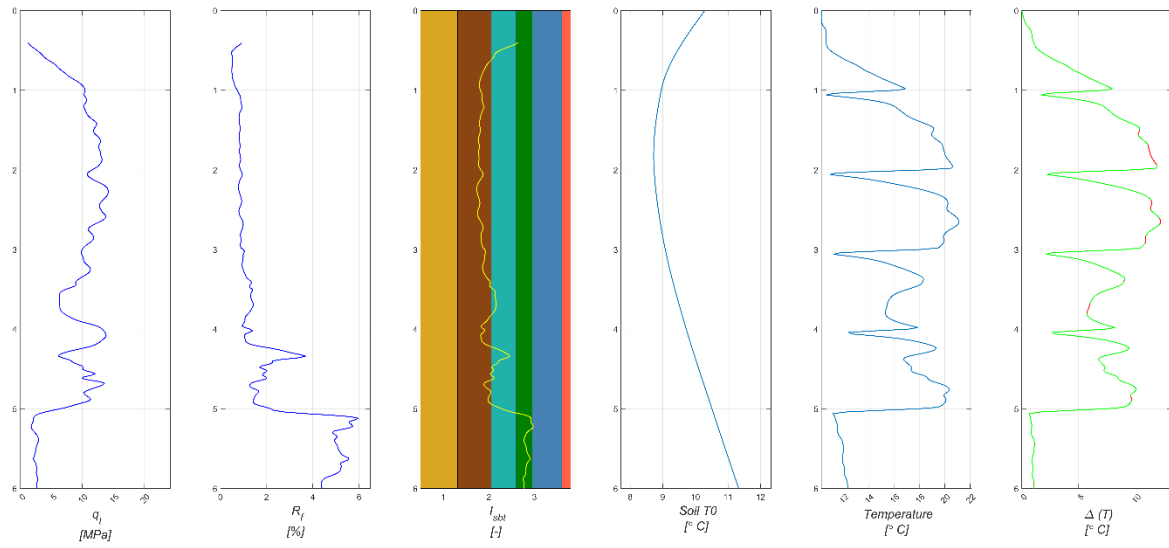
HKN38



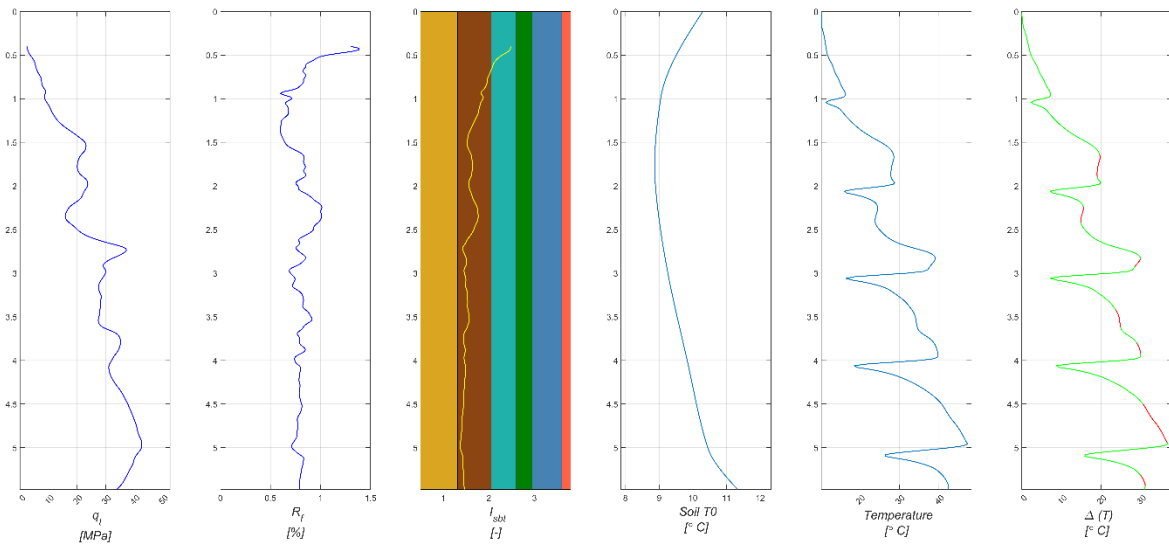
HKN41



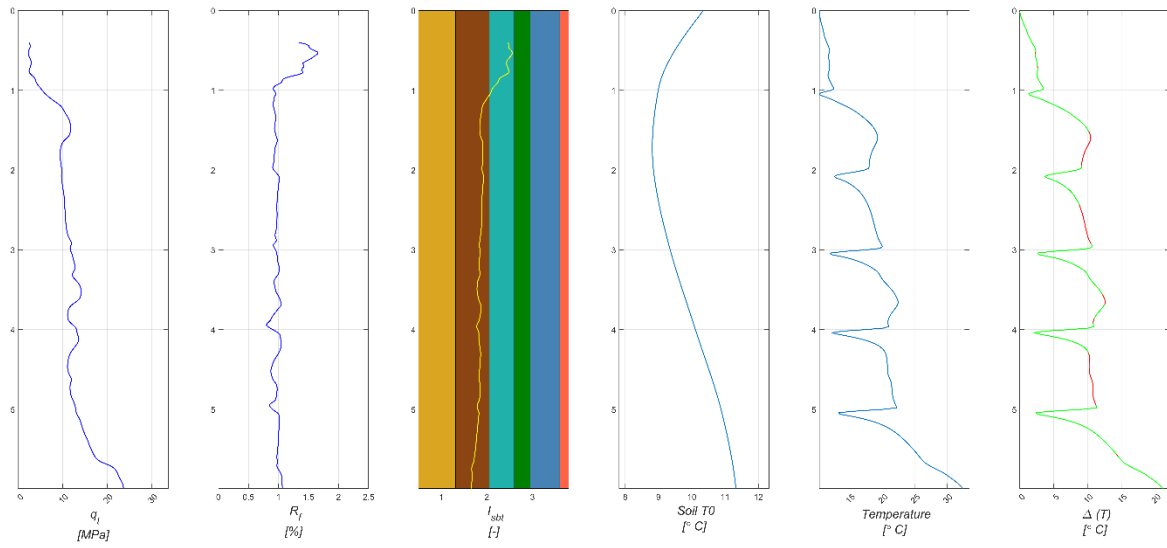
HKN46



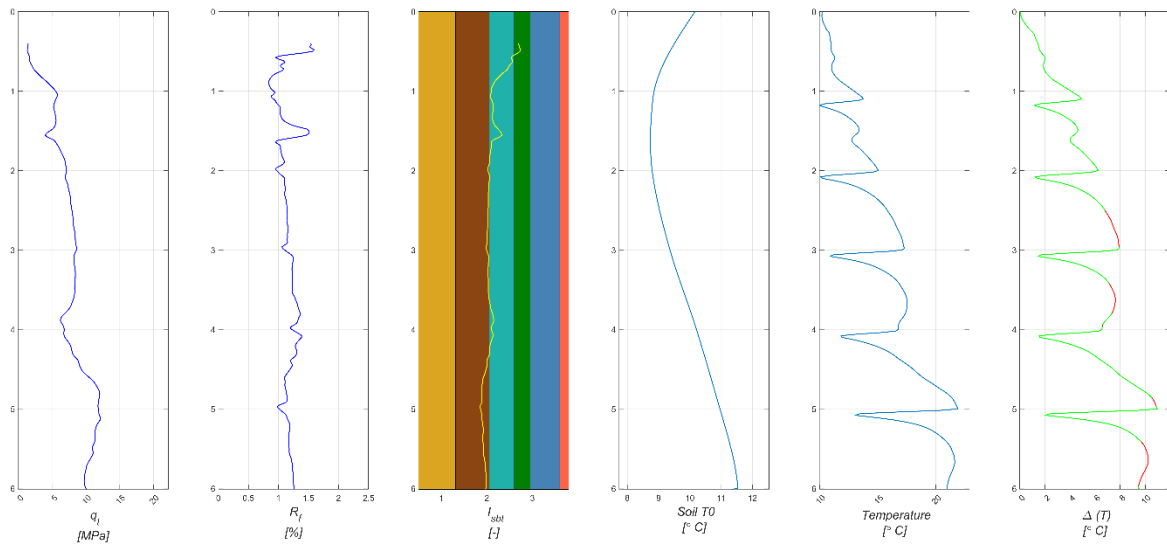
HKN47



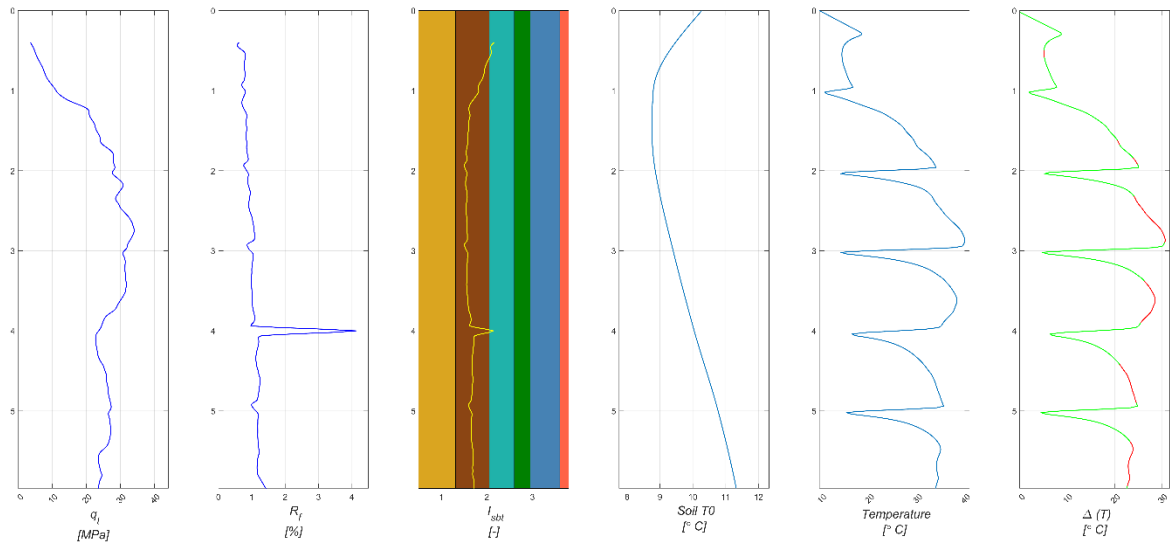
HKN48



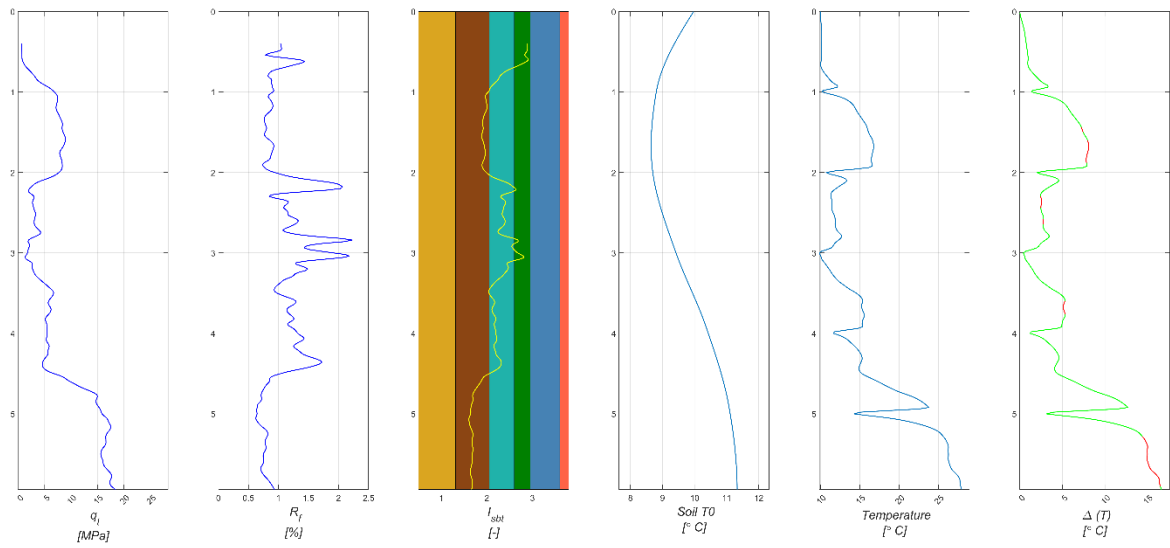
HKN56



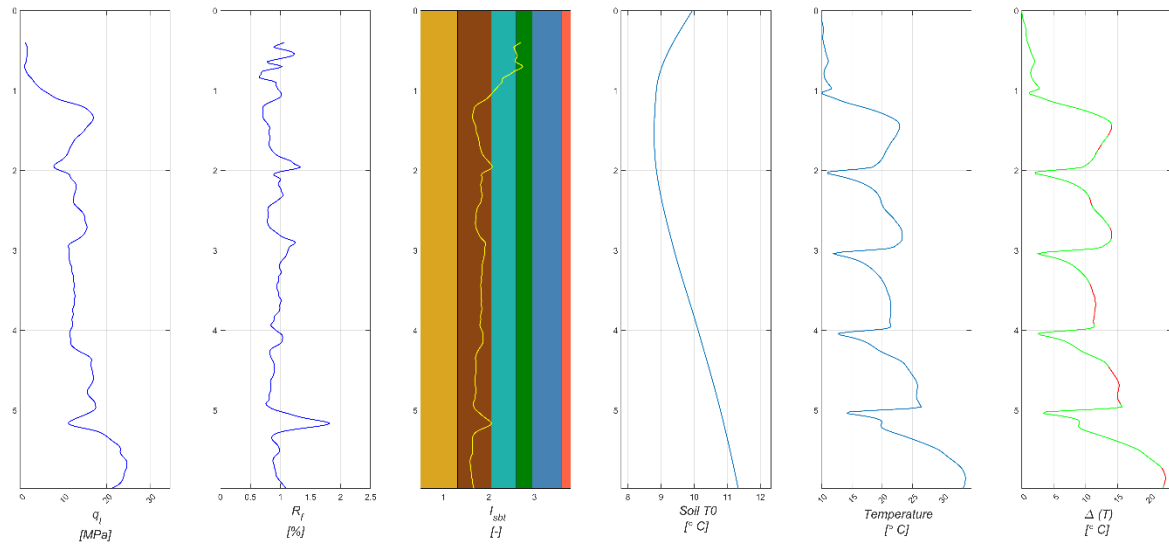
HKN58



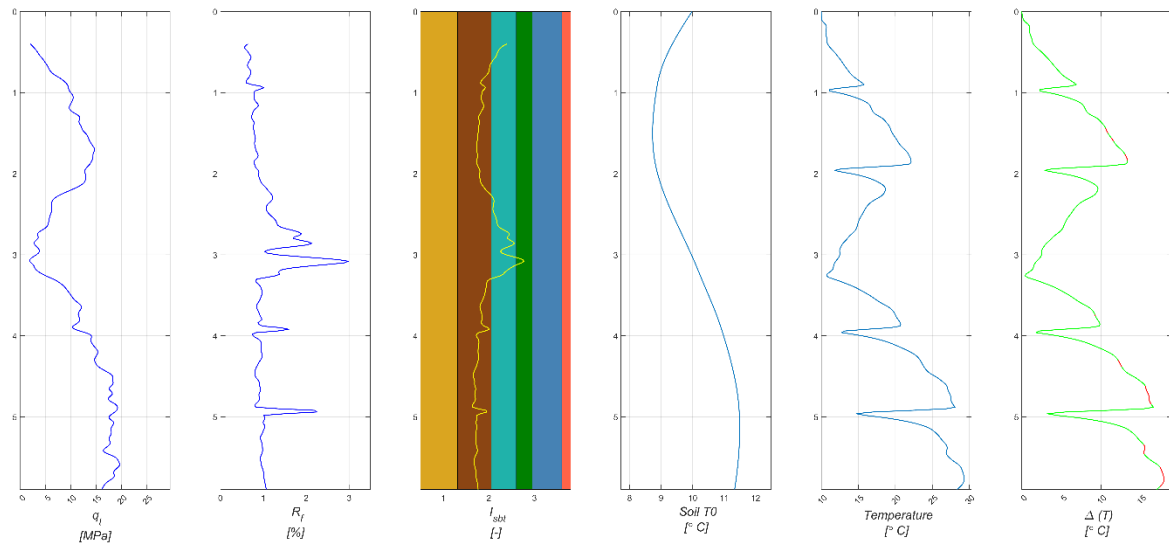
HKN61



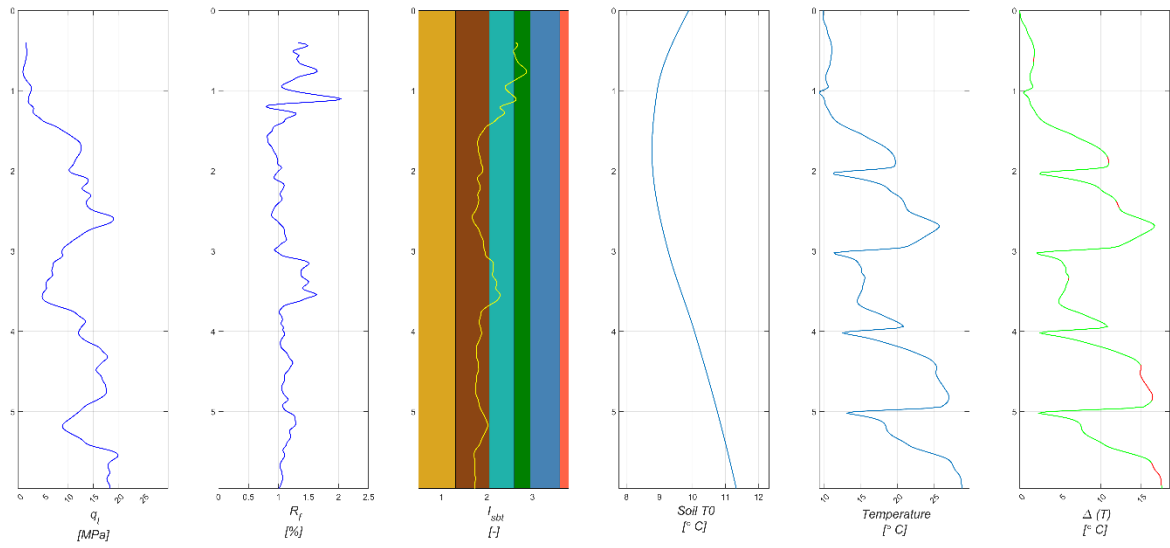
HKN65



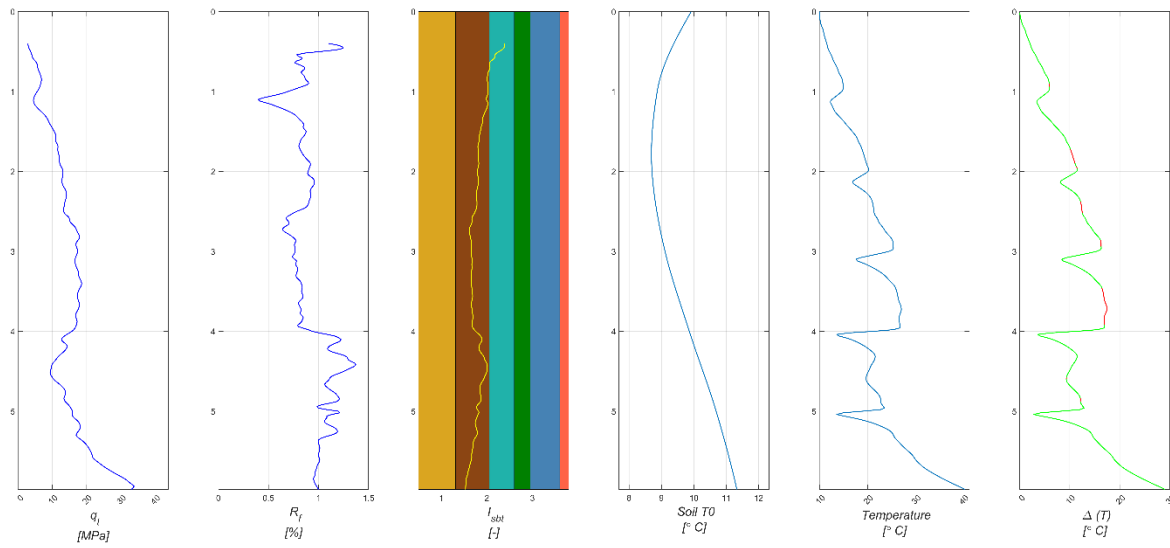
HKN67



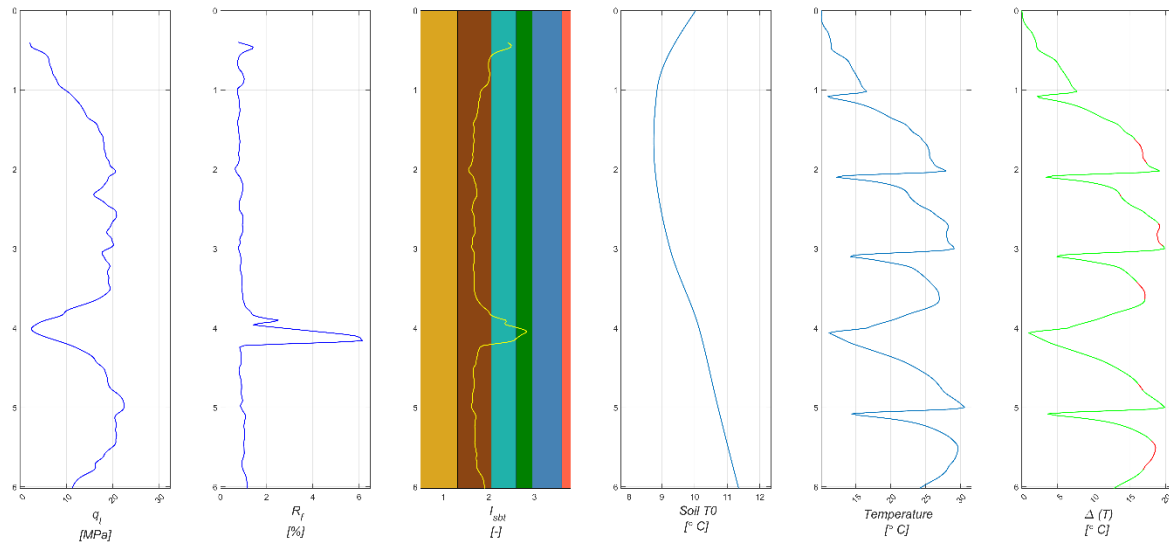
HKN70



HKN72



HKN75



The figure displays four scatter plots arranged in a 2x2 grid, showing the relationship between the initial residual difference ($\Delta T_{\text{initial}}$) versus the final residual difference (q_t) and the distance (D) for different diameters ($D10$, $D50$, $D60$, and $D90$). Each plot includes a linear regression line and statistical data.

Top Left Plot (D10):

- Y-axis: $\Delta T_{\text{initial}}$ vs q_t Residuals
- X-axis: $D10$ [mm]
- Regression equation: $y(x) = 3.5086 \cdot x + 5.1034$
- R-Squared: 0.0368
- Legend: $\Delta T_{\text{initial}}$ vs q_t D10 (blue dots), Best fit (red line)

Top Right Plot (D50):

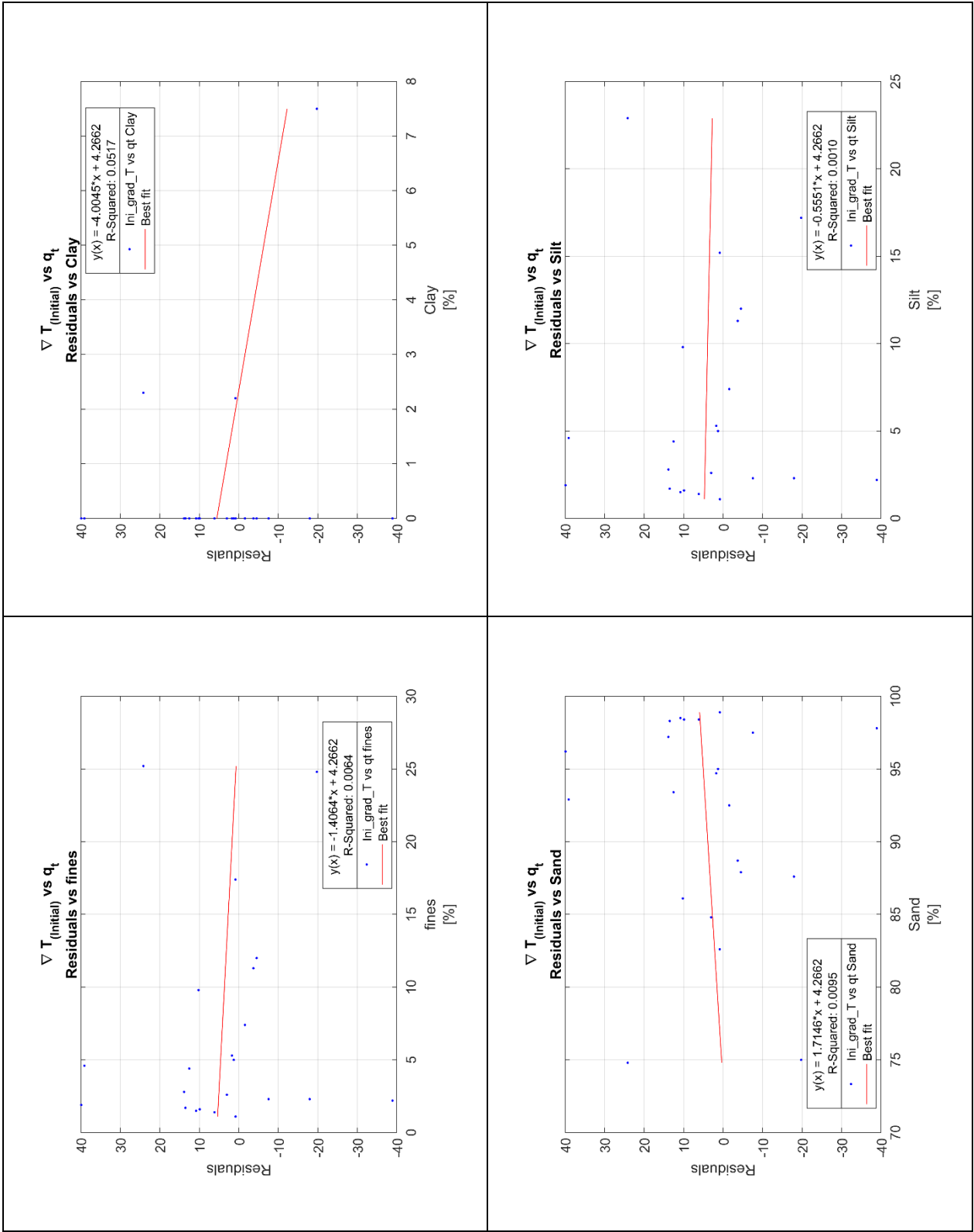
- Y-axis: $\Delta T_{\text{initial}}$ vs q_t Residuals
- X-axis: $D50$ [mm]
- Regression equation: $y(x) = 9.5508 \cdot x + 4.2662$
- R-Squared: 0.2939
- Legend: $\Delta T_{\text{initial}}$ vs q_t D50 (blue dots), Best fit (red line)

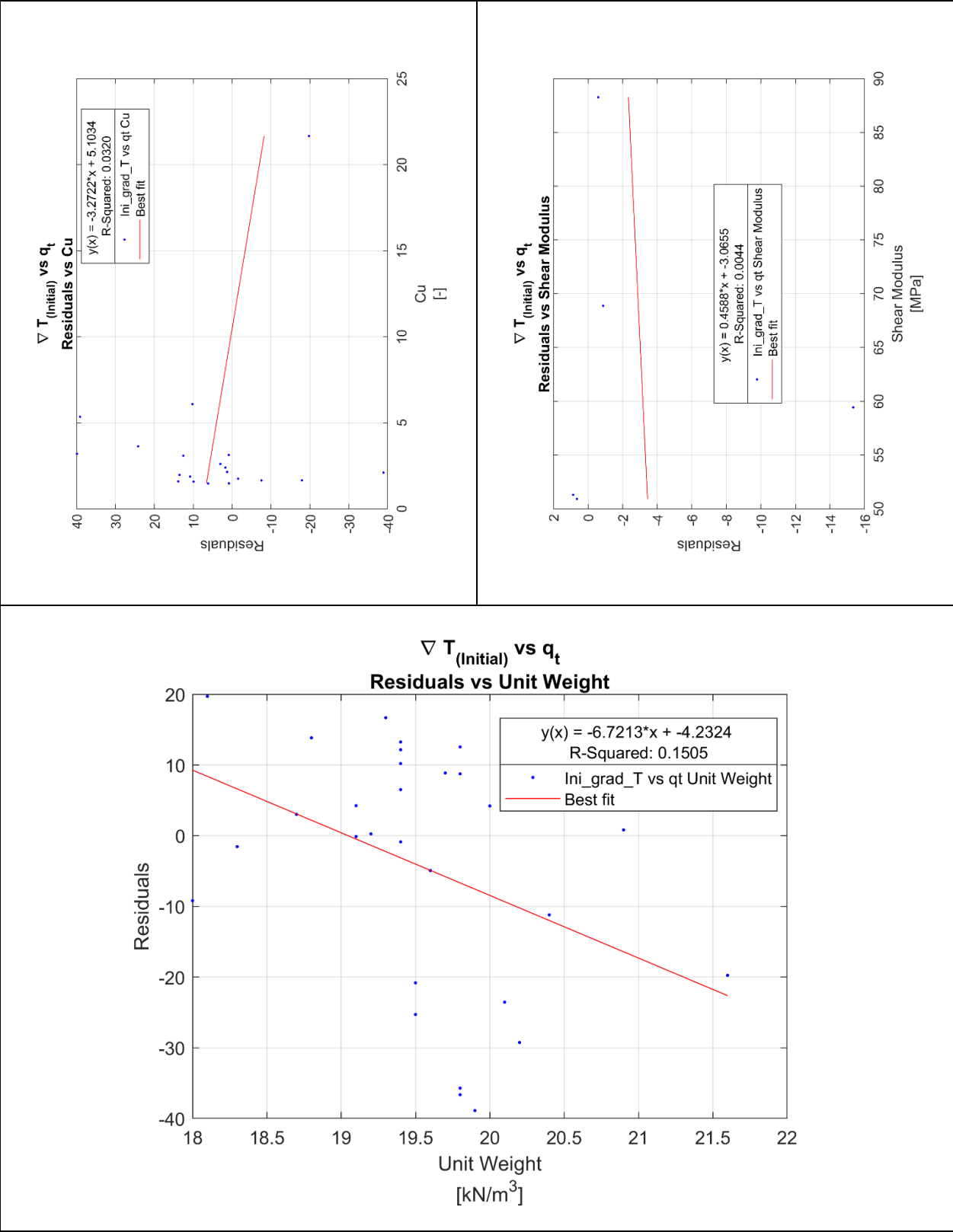
Bottom Left Plot (D60):

- Y-axis: $\Delta T_{\text{initial}}$ vs q_t Residuals
- X-axis: $D60$ [mm]
- Regression equation: $y(x) = 10.5201 \cdot x + 4.2662$
- R-Squared: 0.3566
- Legend: $\Delta T_{\text{initial}}$ vs q_t D60 (blue dots), Best fit (red line)

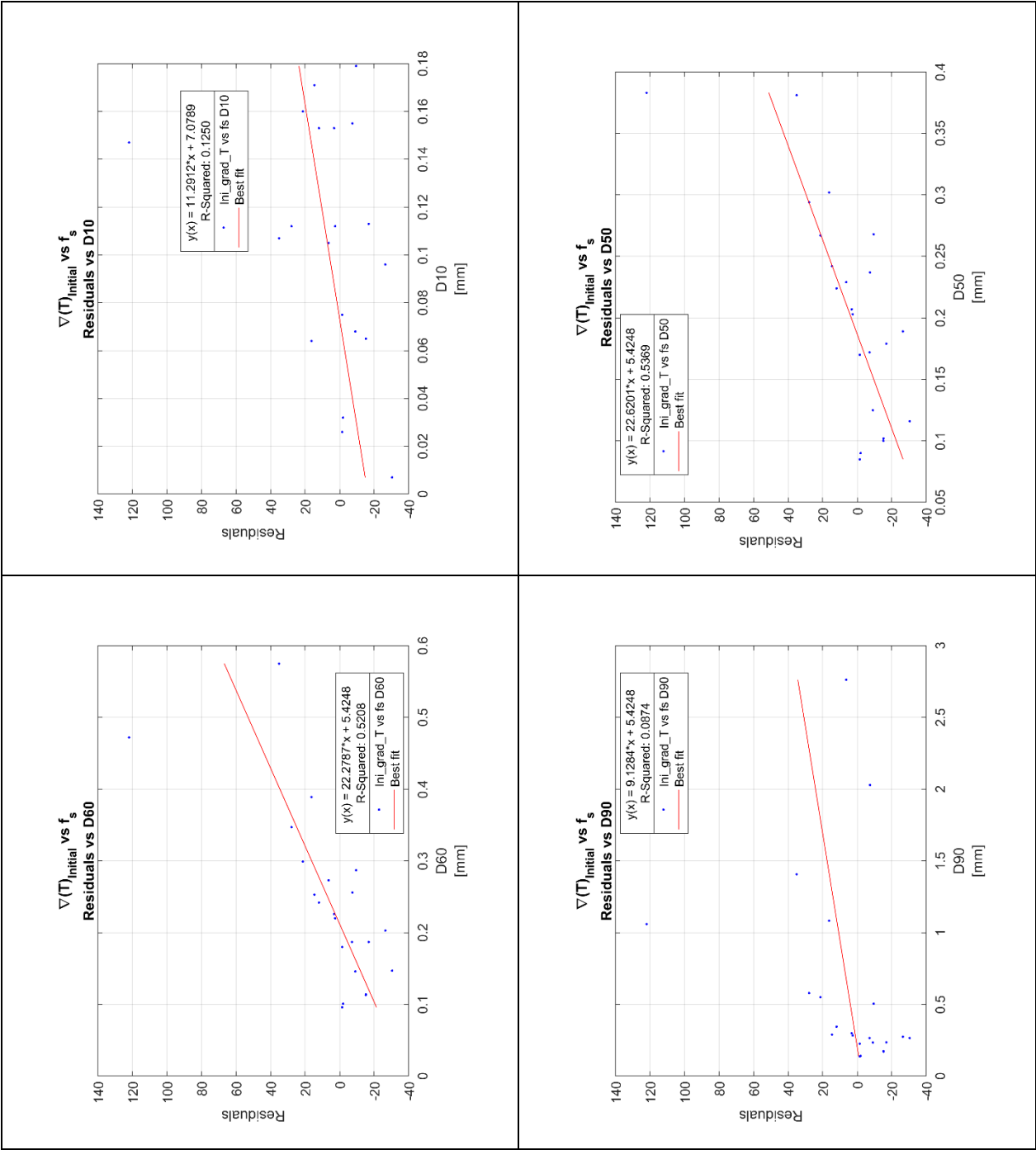
Bottom Right Plot (D90):

- Y-axis: $\Delta T_{\text{initial}}$ vs q_t Residuals
- X-axis: $D90$ [mm]
- Regression equation: $y(x) = 2.6029 \cdot x + 4.2662$
- R-Squared: 0.0218
- Legend: $\Delta T_{\text{initial}}$ vs q_t D90 (blue dots), Best fit (red line)





Appendix VI $\nabla(T)_{\text{Initial}}$ vs f_s Regression Residuals Investigation



$\nabla(T)_{\text{Initial}}$ vs f_s

Residuals vs D60

$y(x) = 22.2787 \cdot x + 5.4248$

R-Squared: 0.5206

Ini_grad_T vs f_s D60

Best fit

$\nabla(T)_{\text{Initial}}$ vs f_s

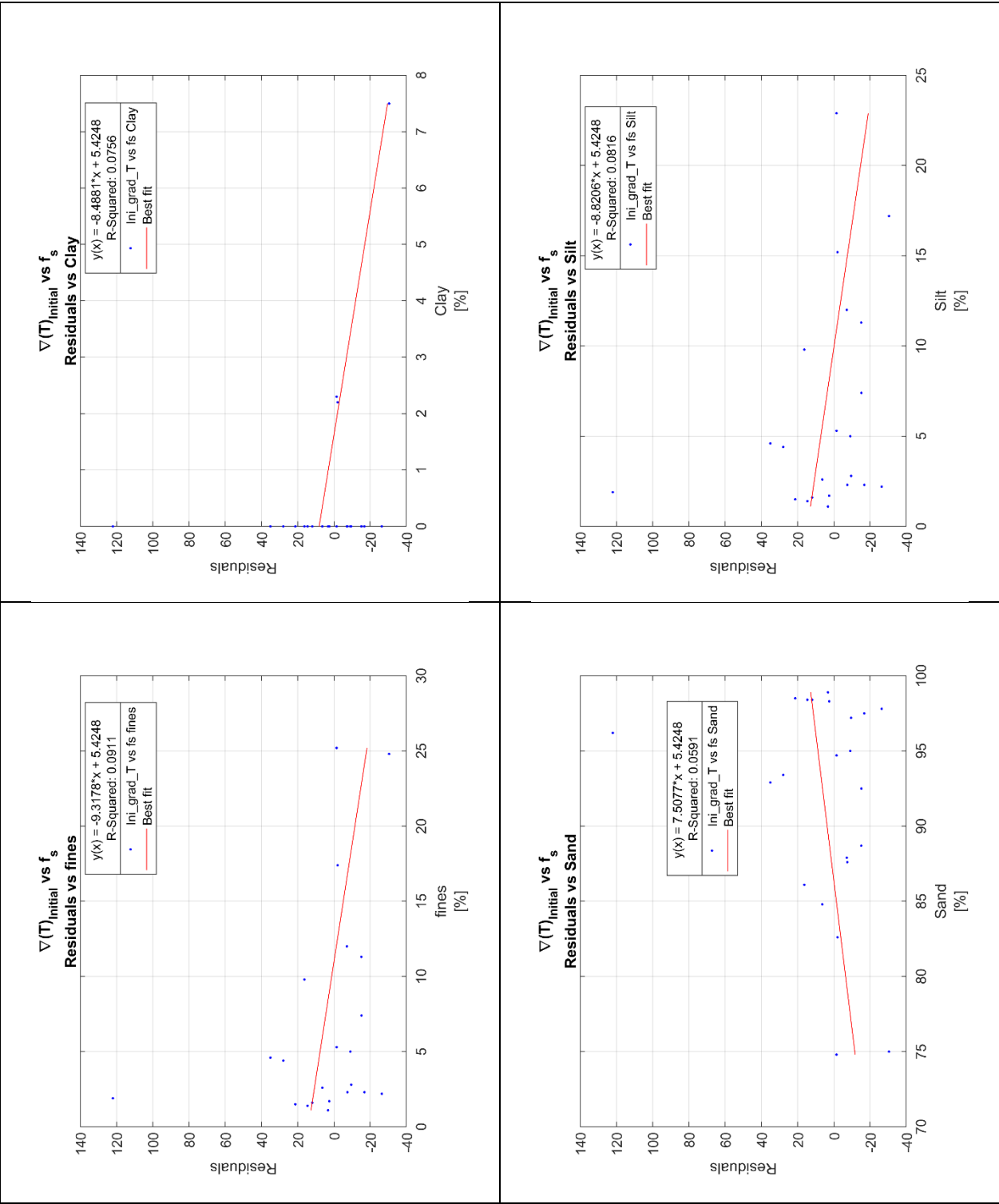
Residuals vs D90

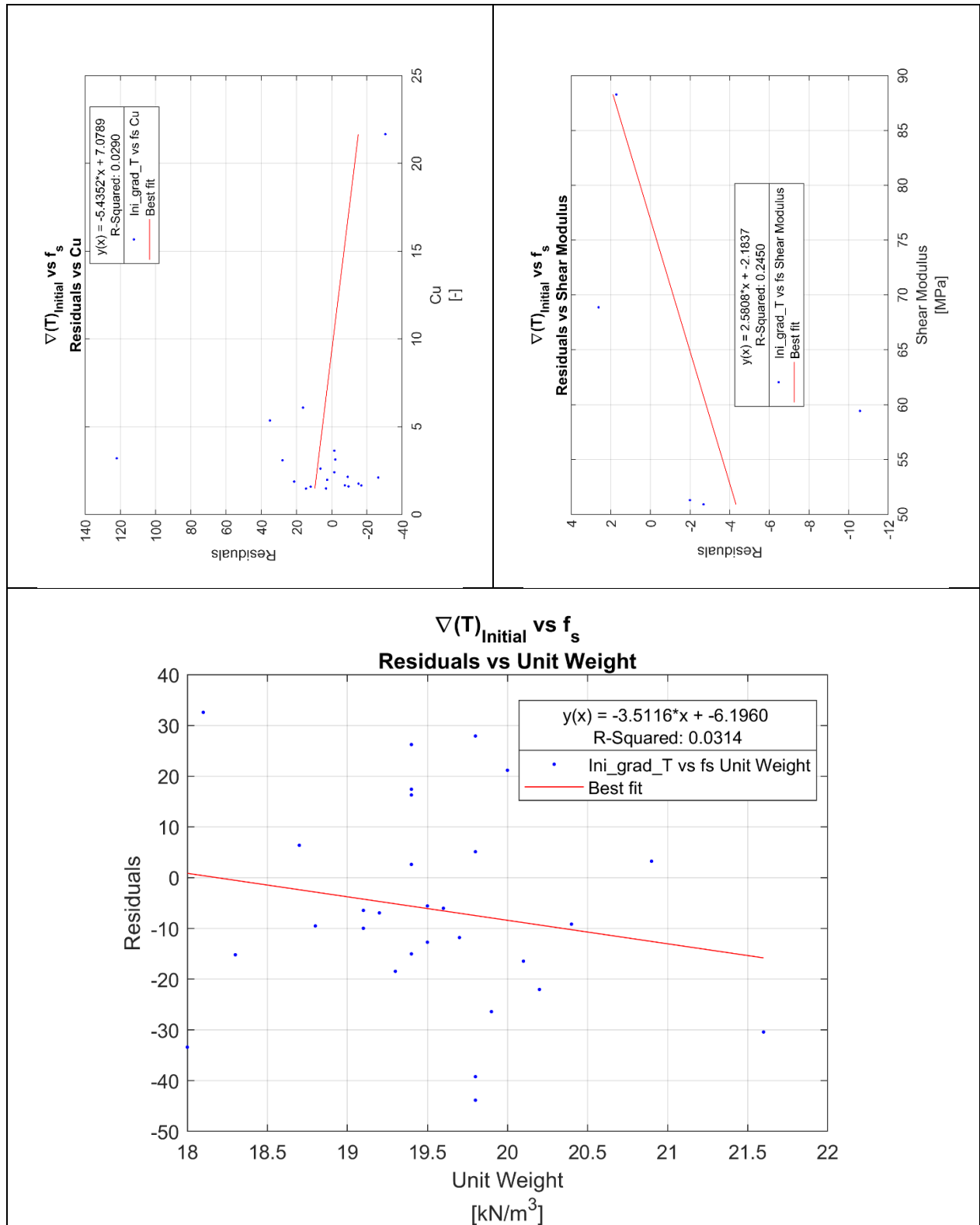
$y(x) = 9.1284 \cdot x + 5.4248$

R-Squared: 0.0874

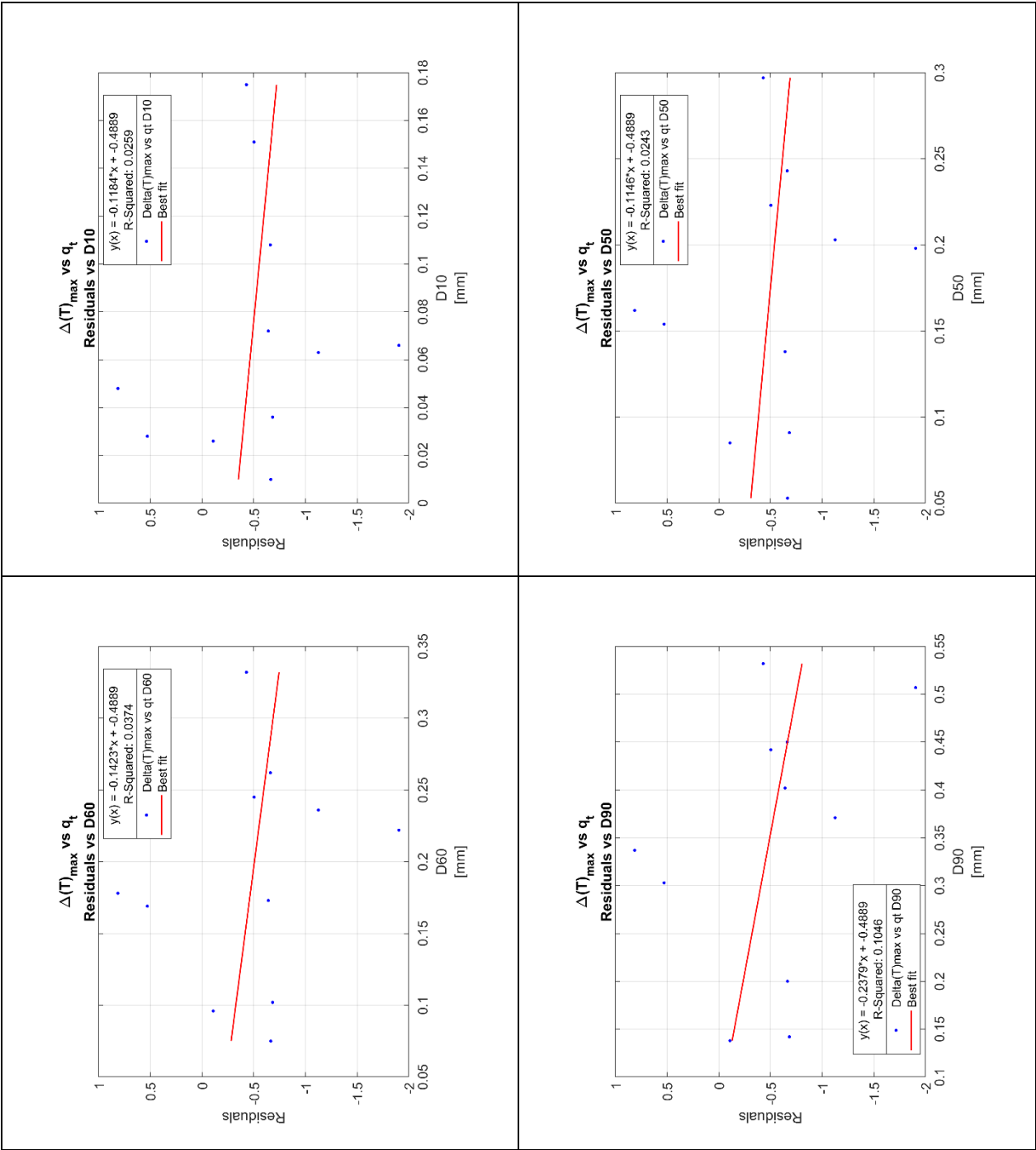
Ini_grad_T vs f_s D90

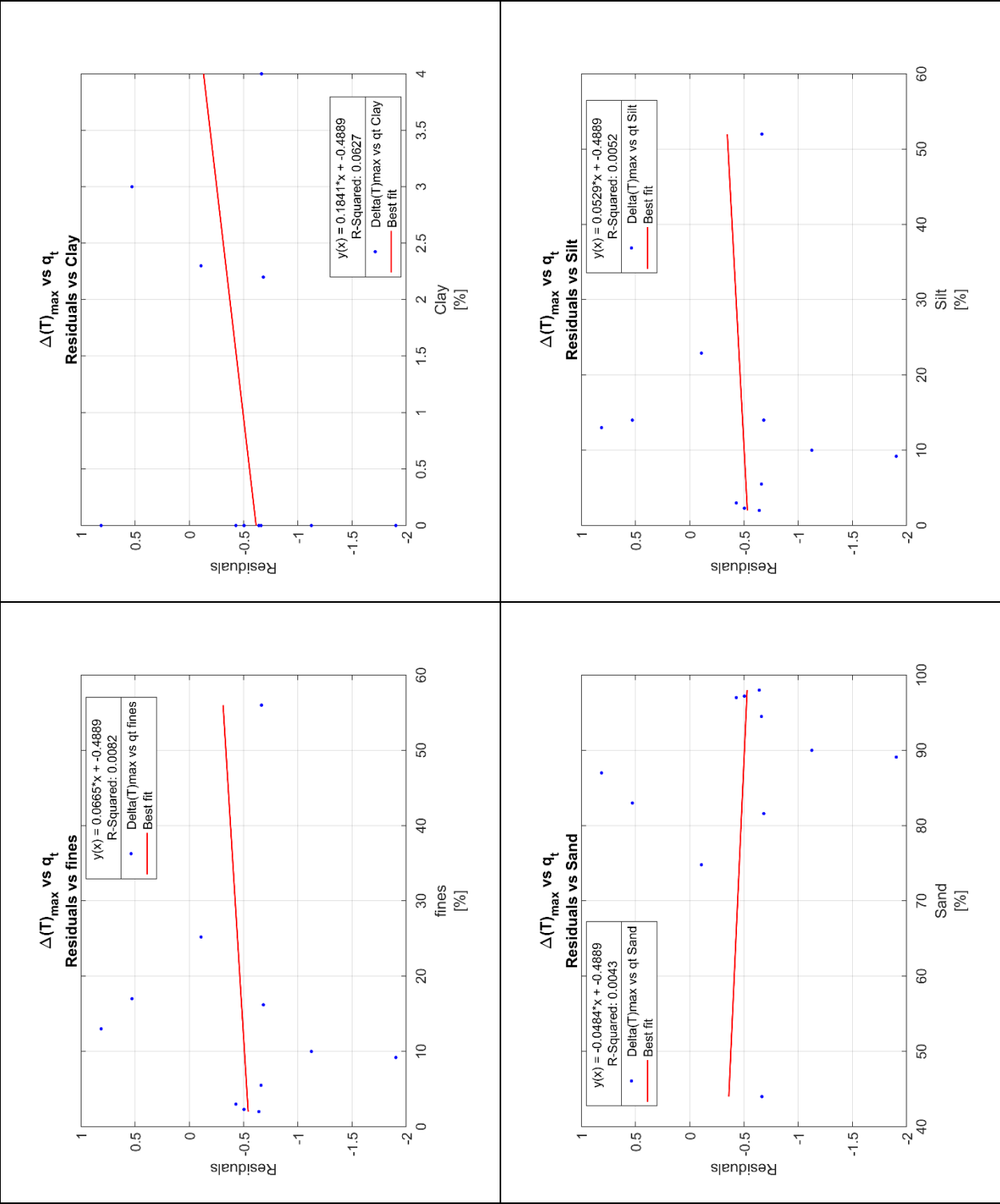
Best fit

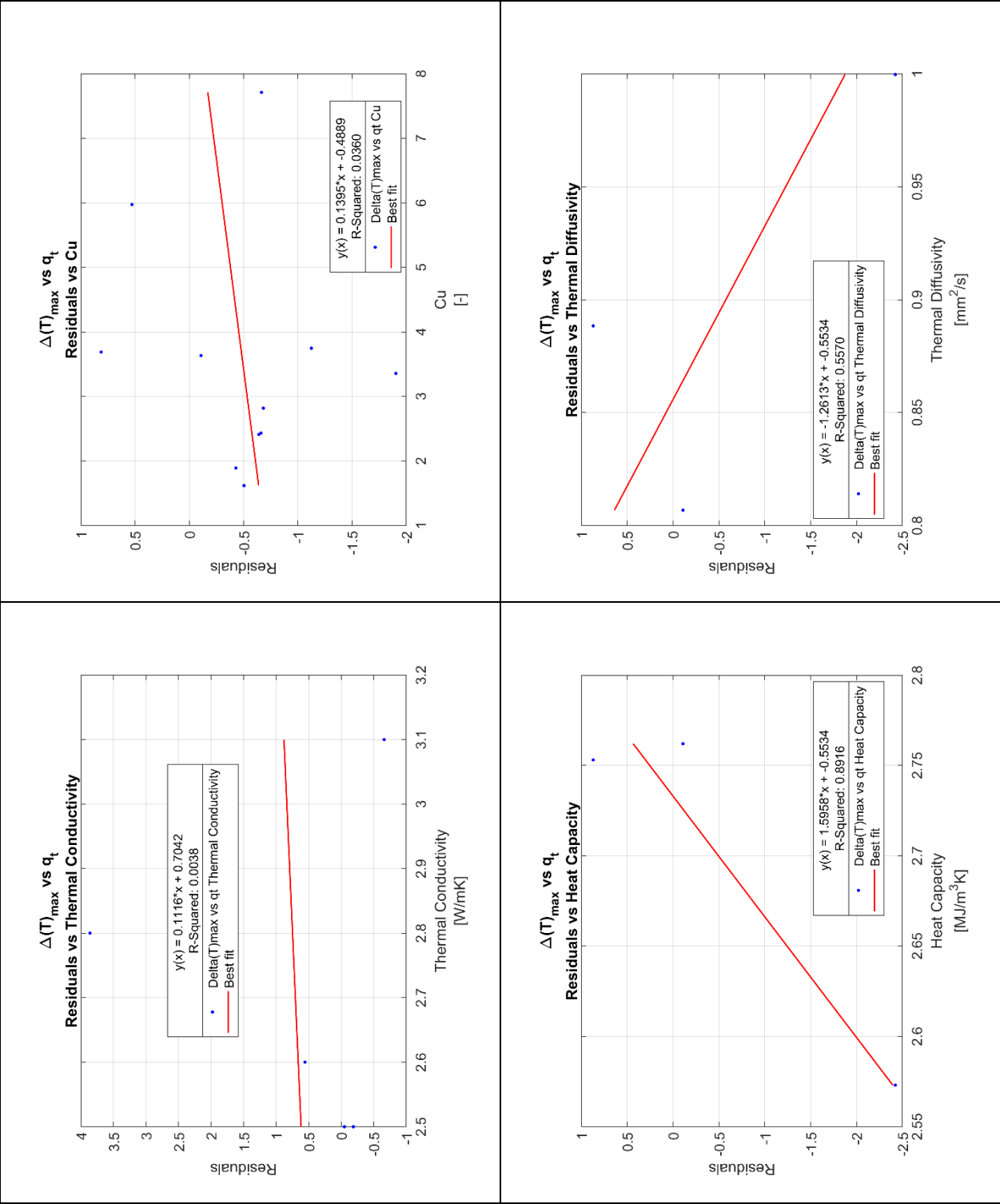


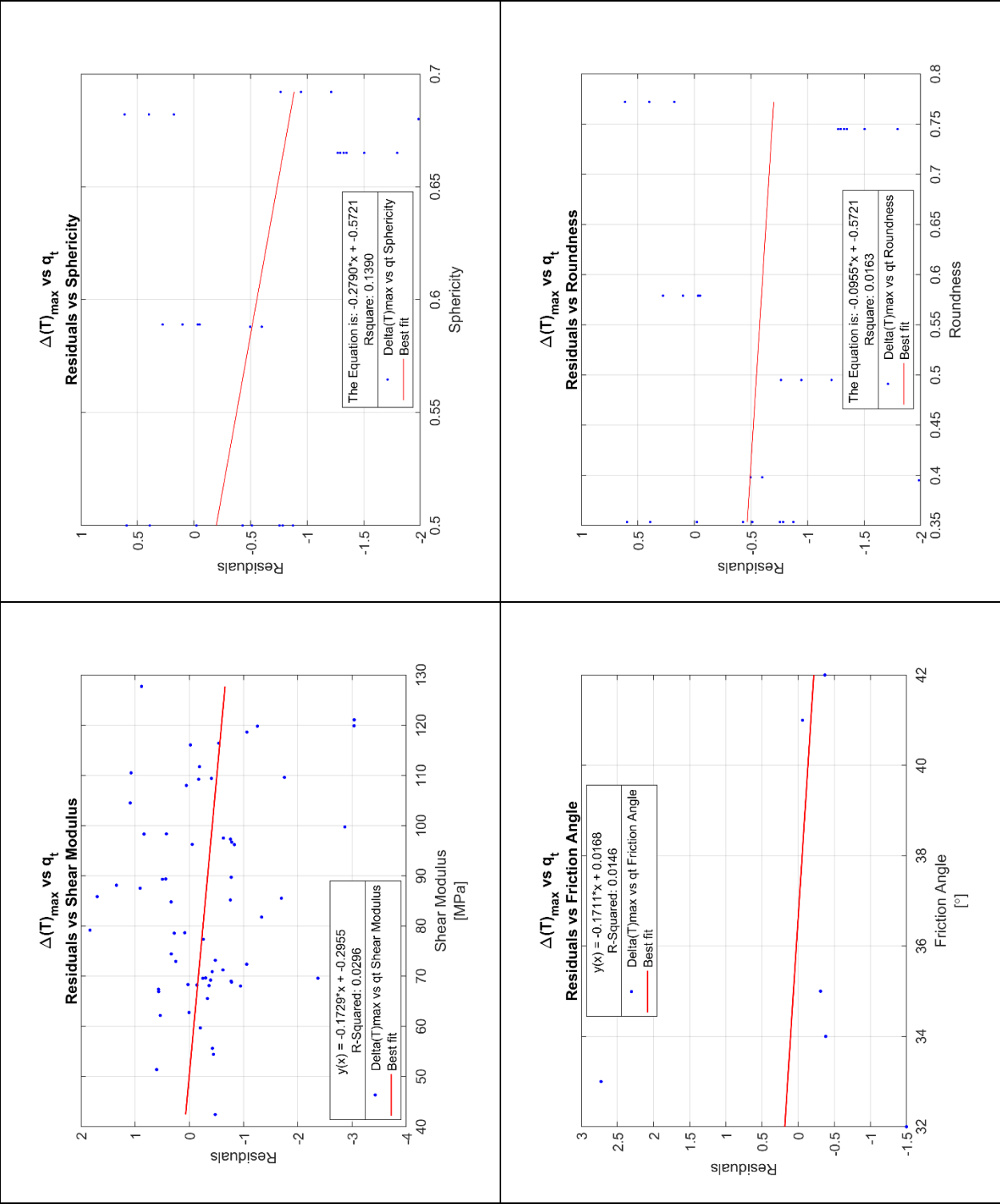


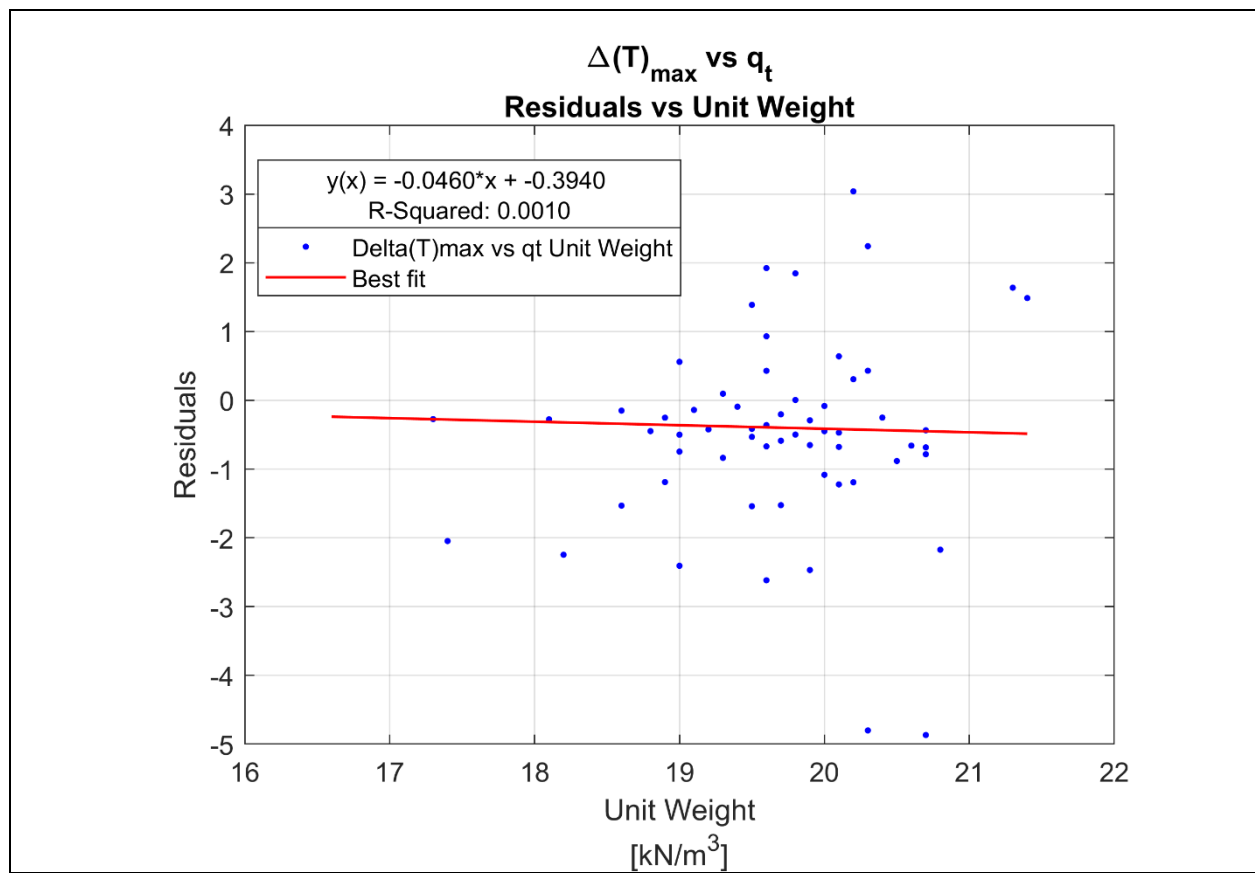
Appendix VII $\Delta(T)_{\max}$ vs q_t Regression Residuals Investigation











The figure displays four scatter plots arranged in a 2x2 grid, each showing the relationship between $\Delta(T)_{\max}$ (Y-axis) and f_s (X-axis) for different values of D (D10, D50, D60, D90). The Y-axis for all plots is labeled "Residuals" and ranges from -8 to 6. The X-axis is labeled " D [mm]" and ranges from 0 to 0.18 for D10, 0.05 to 0.3 for D50, 0.05 to 0.35 for D60, and 0.1 to 0.55 for D90. Each plot includes a linear regression line (red) and a legend box with the following information:

- Equation: $y(x) = \text{coefficient} \cdot x + \text{intercept}$
- R-Squared value
- Data series: Delta(T)max vs fs D[Value]
- Best fit line

Top Left Plot (D10):

- Equation: $y(x) = 47.5866x + -4.5383$
- R-Squared: 0.4251
- Data series: Delta(T)max vs fs D10
- Best fit line

Top Right Plot (D50):

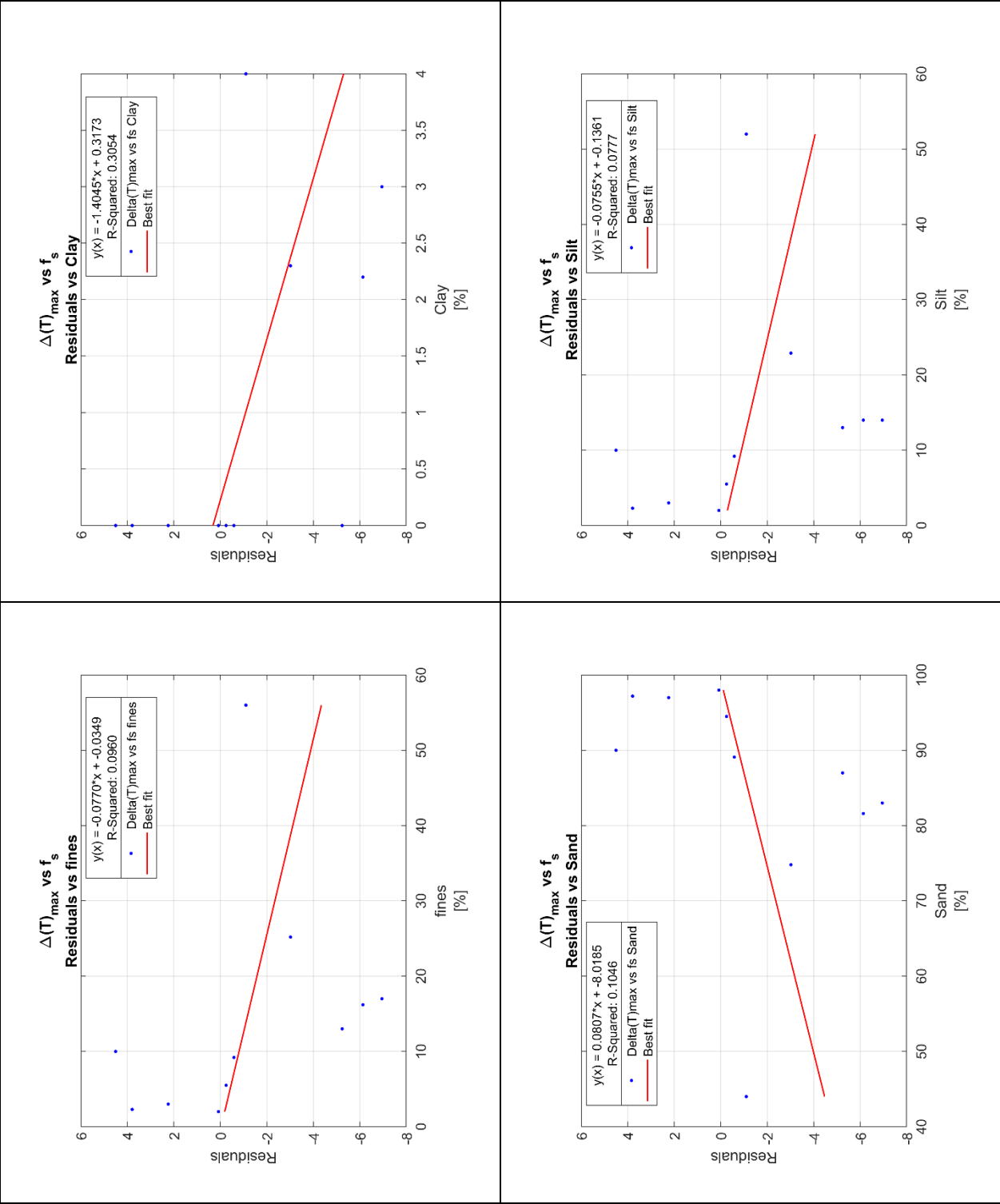
- Equation: $y(x) = 29.1915x + -6.0526$
- R-Squared: 0.3116
- Data series: Delta(T)max vs fs D50
- Best fit line

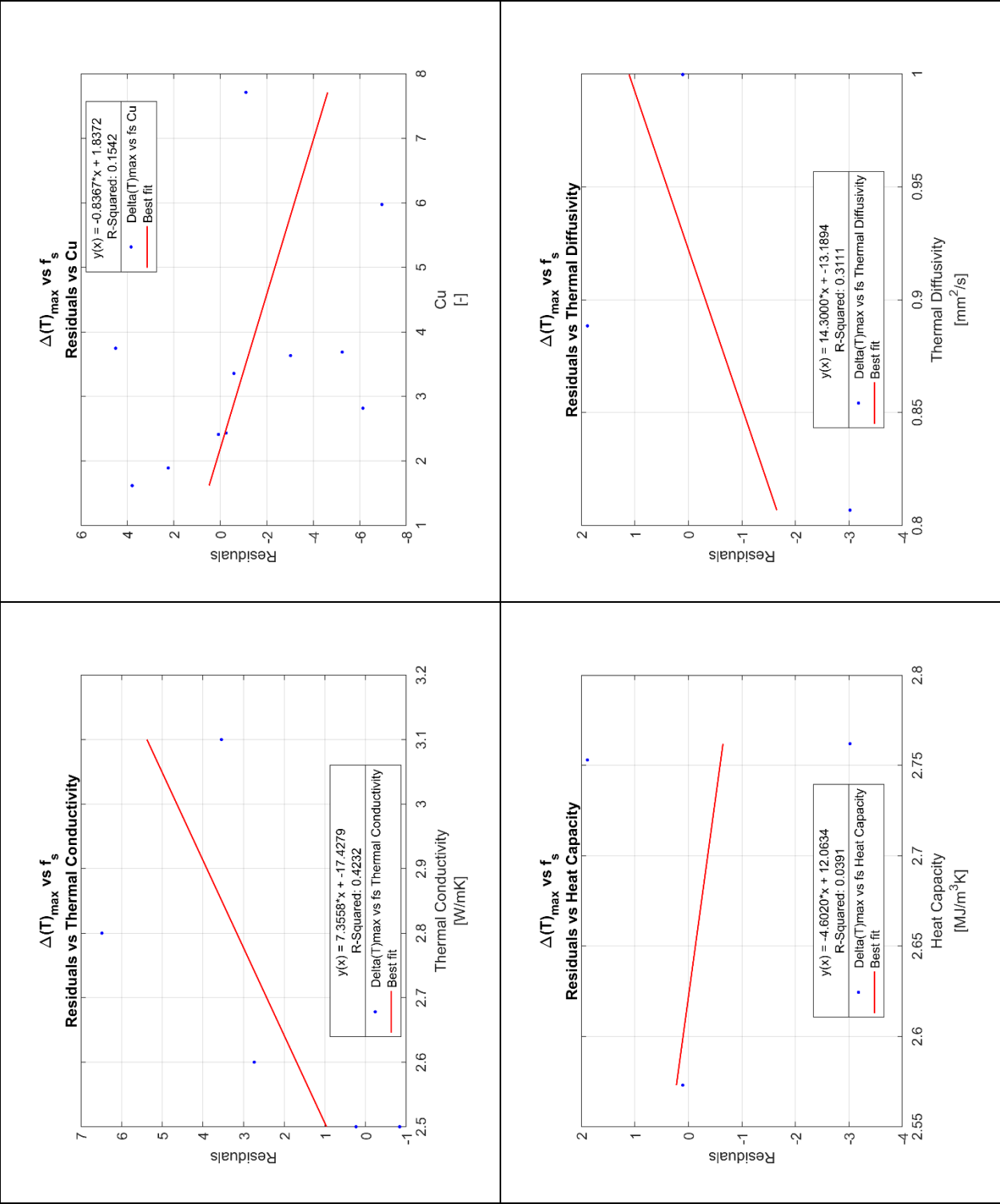
Bottom Left Plot (D60):

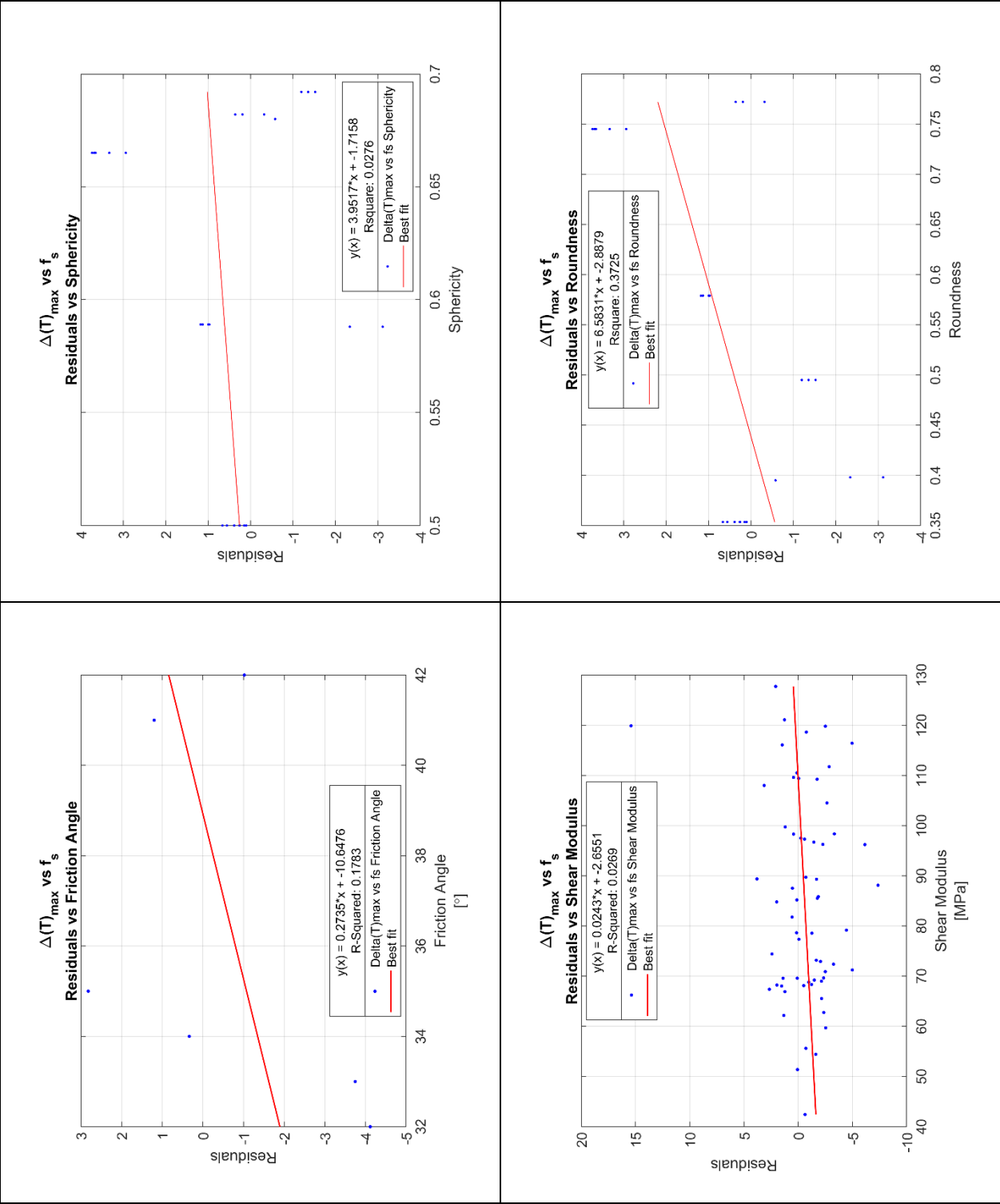
- Equation: $y(x) = 29.8242x + -6.8176$
- R-Squared: 0.3706
- Data series: Delta(T)max vs fs D60
- Best fit line

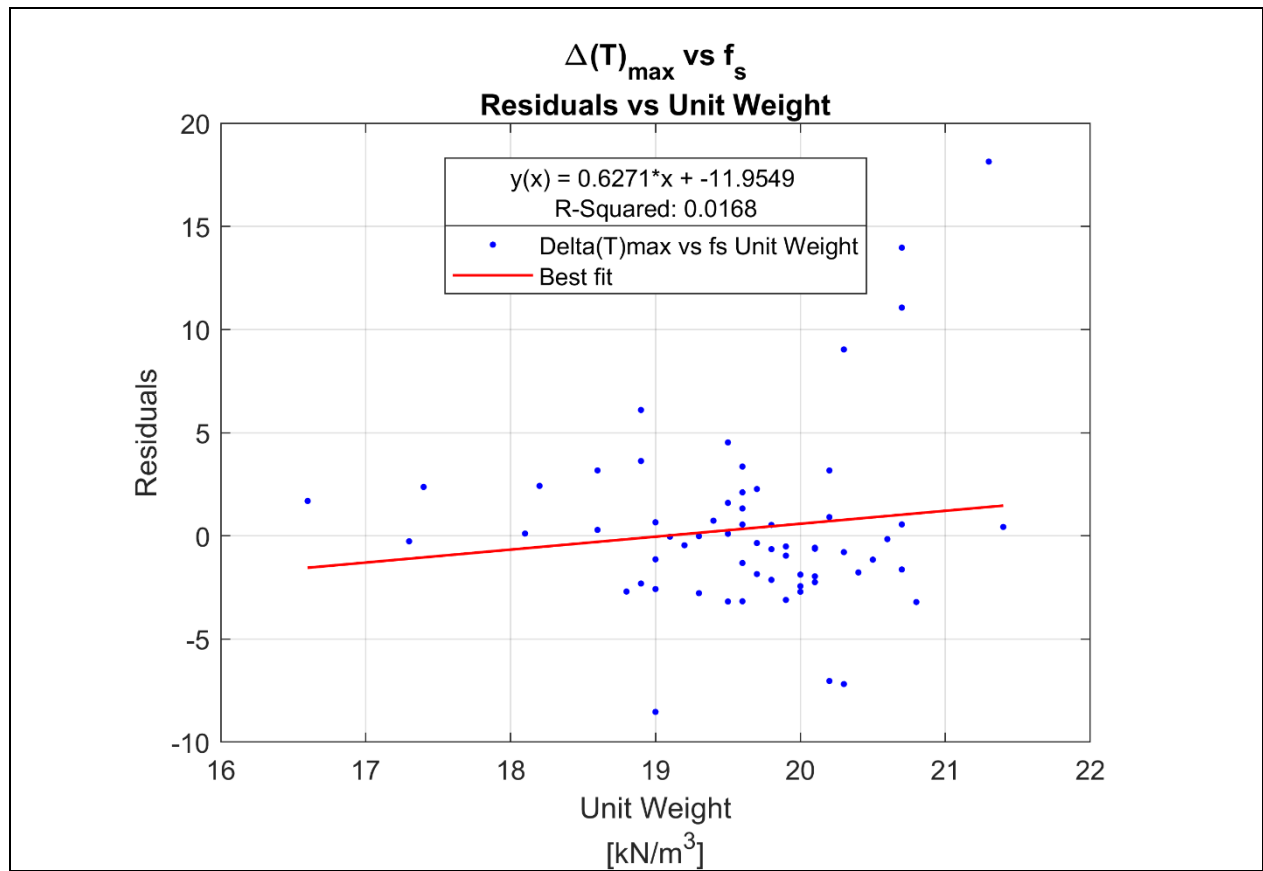
Bottom Right Plot (D90):

- Equation: $y(x) = 16.5501x + -6.9045$
- R-Squared: 0.3531
- Data series: Delta(T)max vs fs D90
- Best fit line

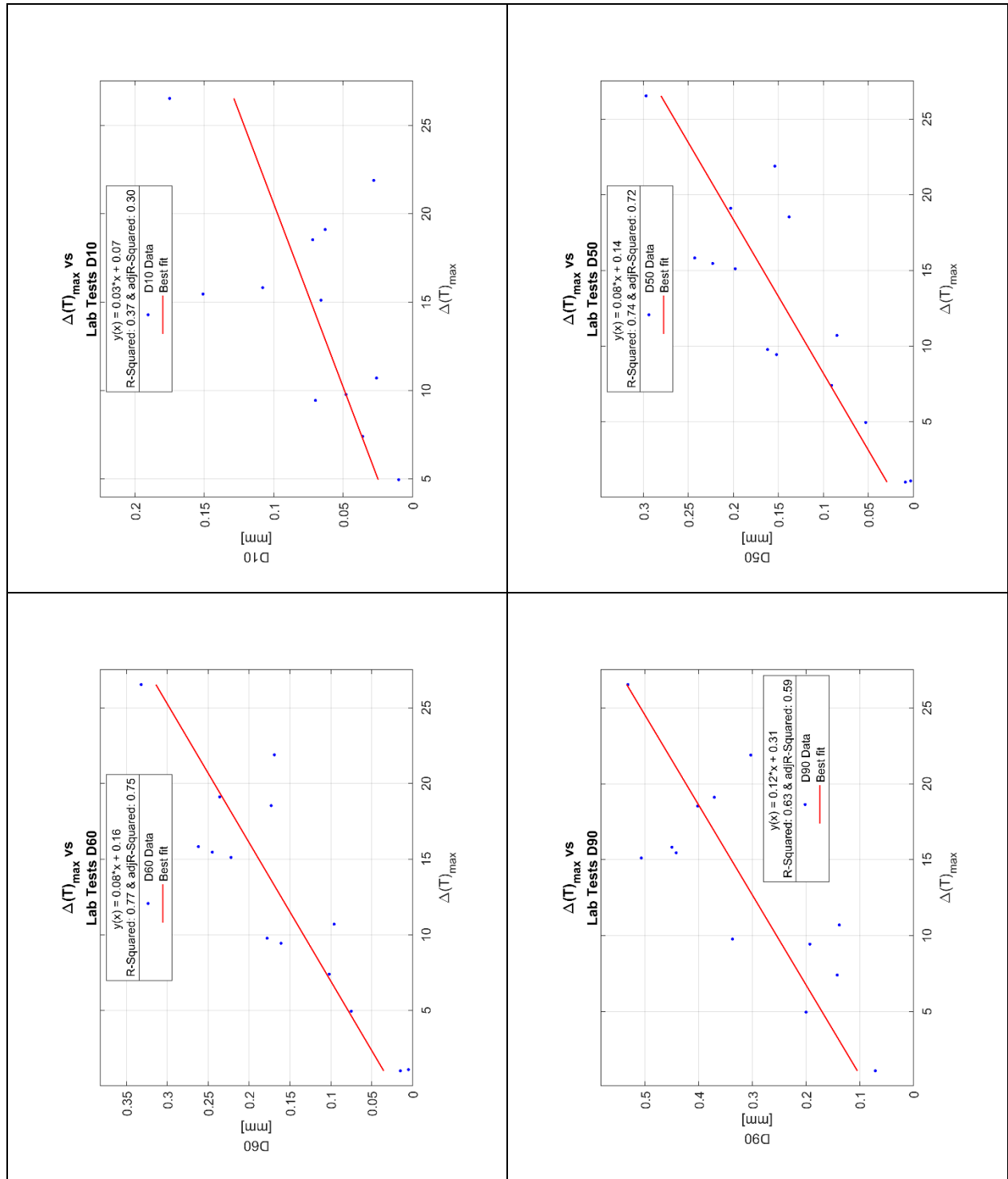


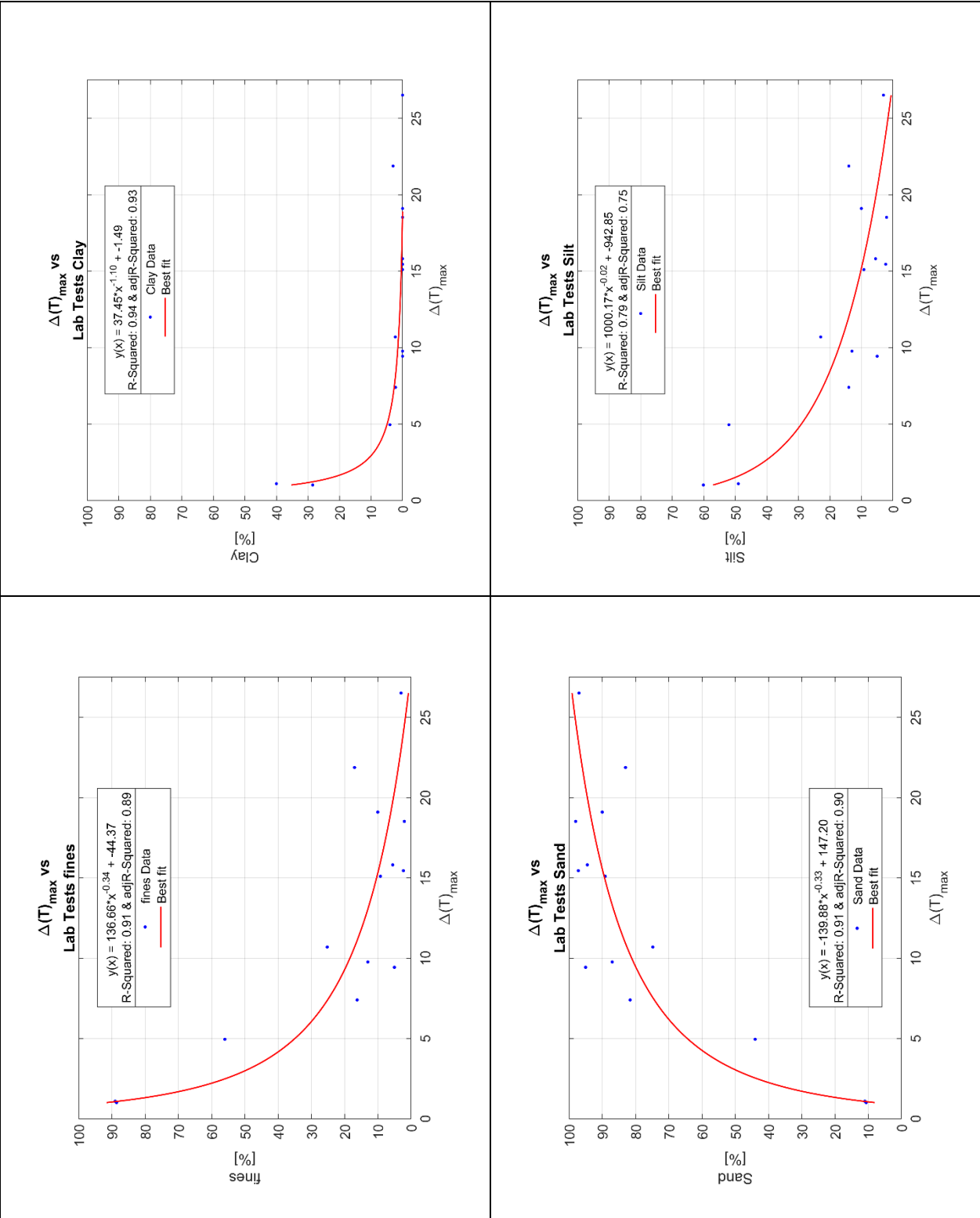


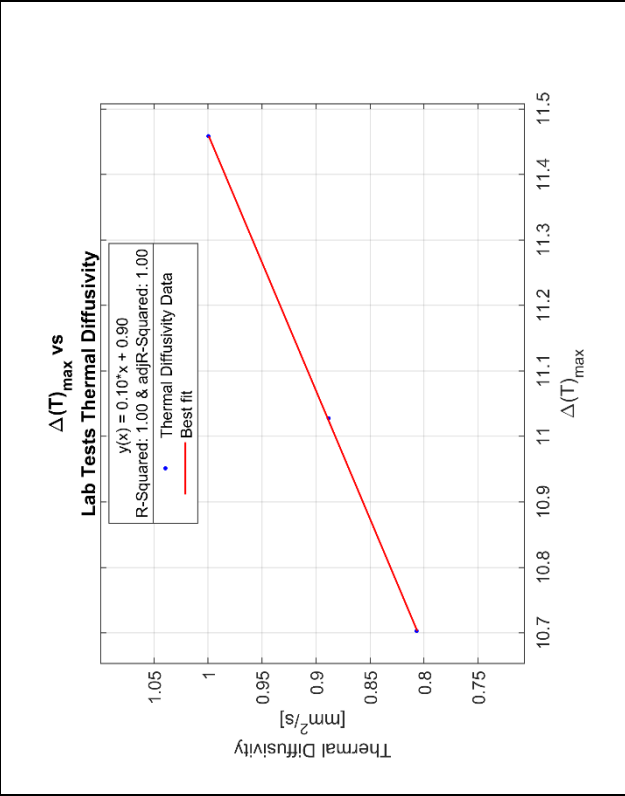
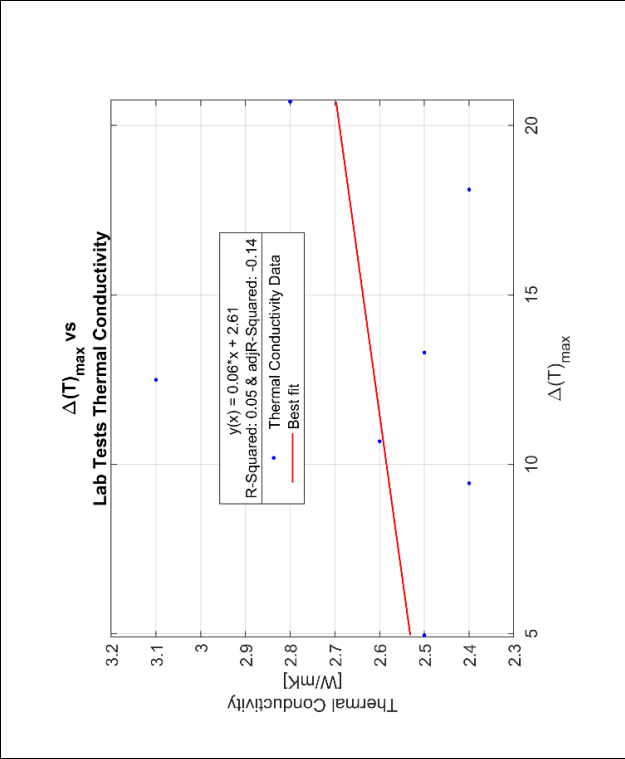
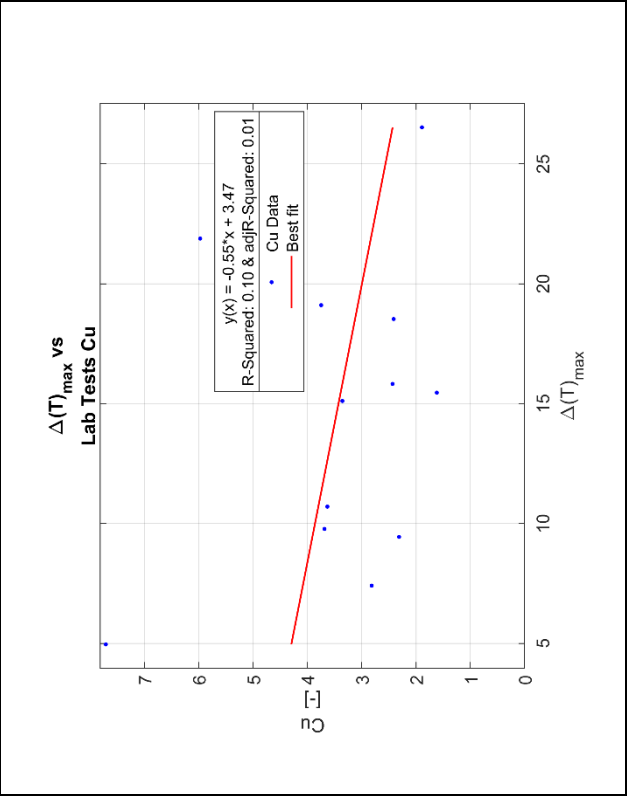
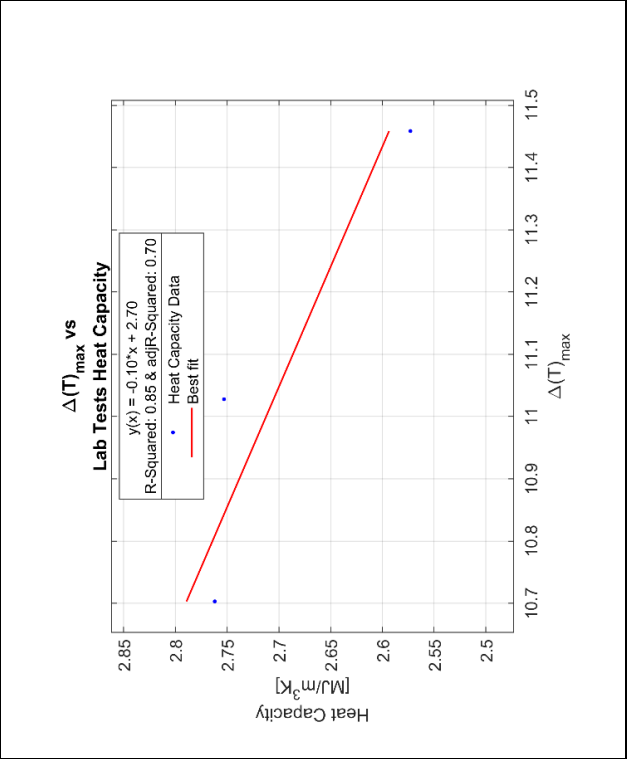


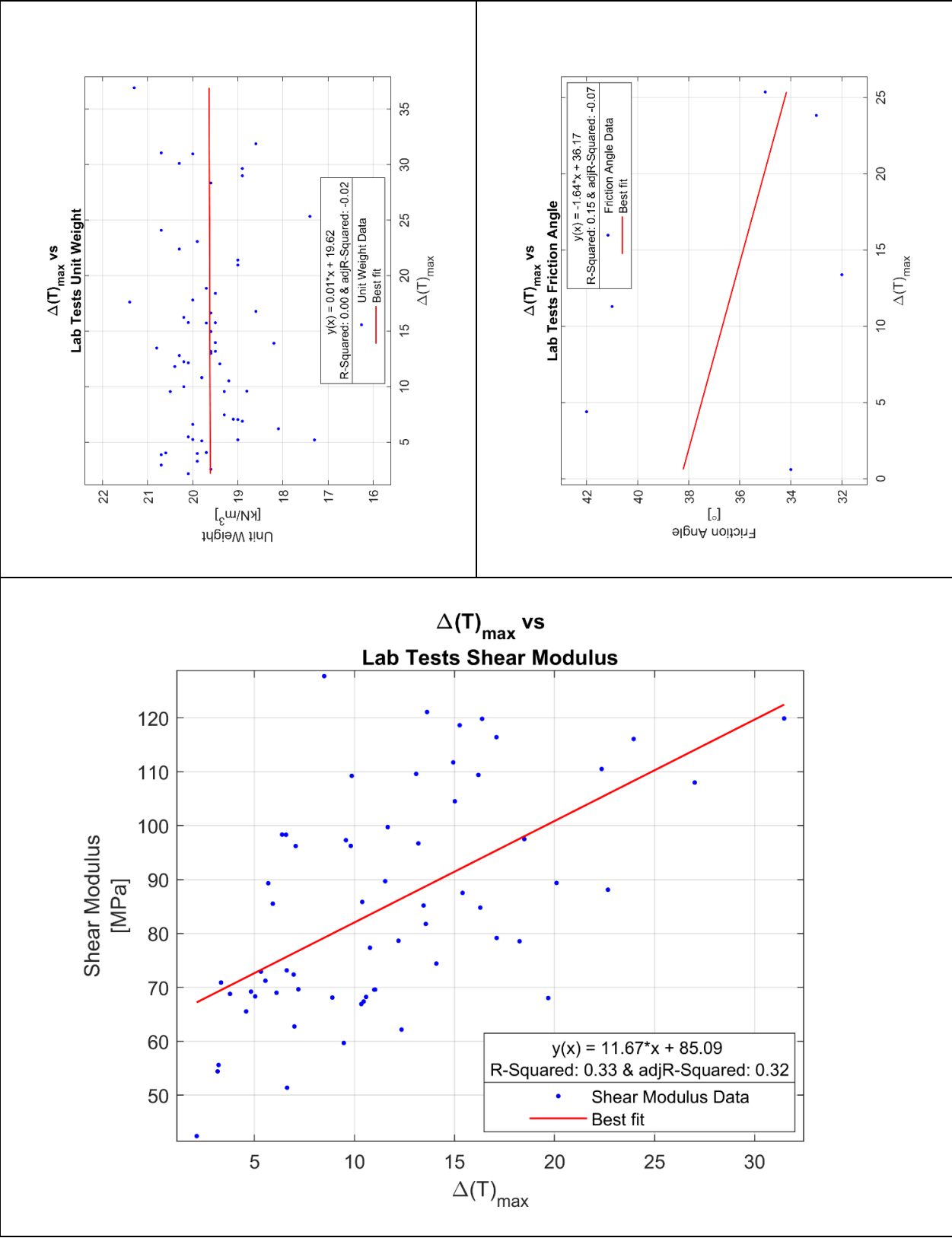


Appendix IX $\Delta(T)_{\max}$ vs Laboratory & SCPT Tests Regression Investigation

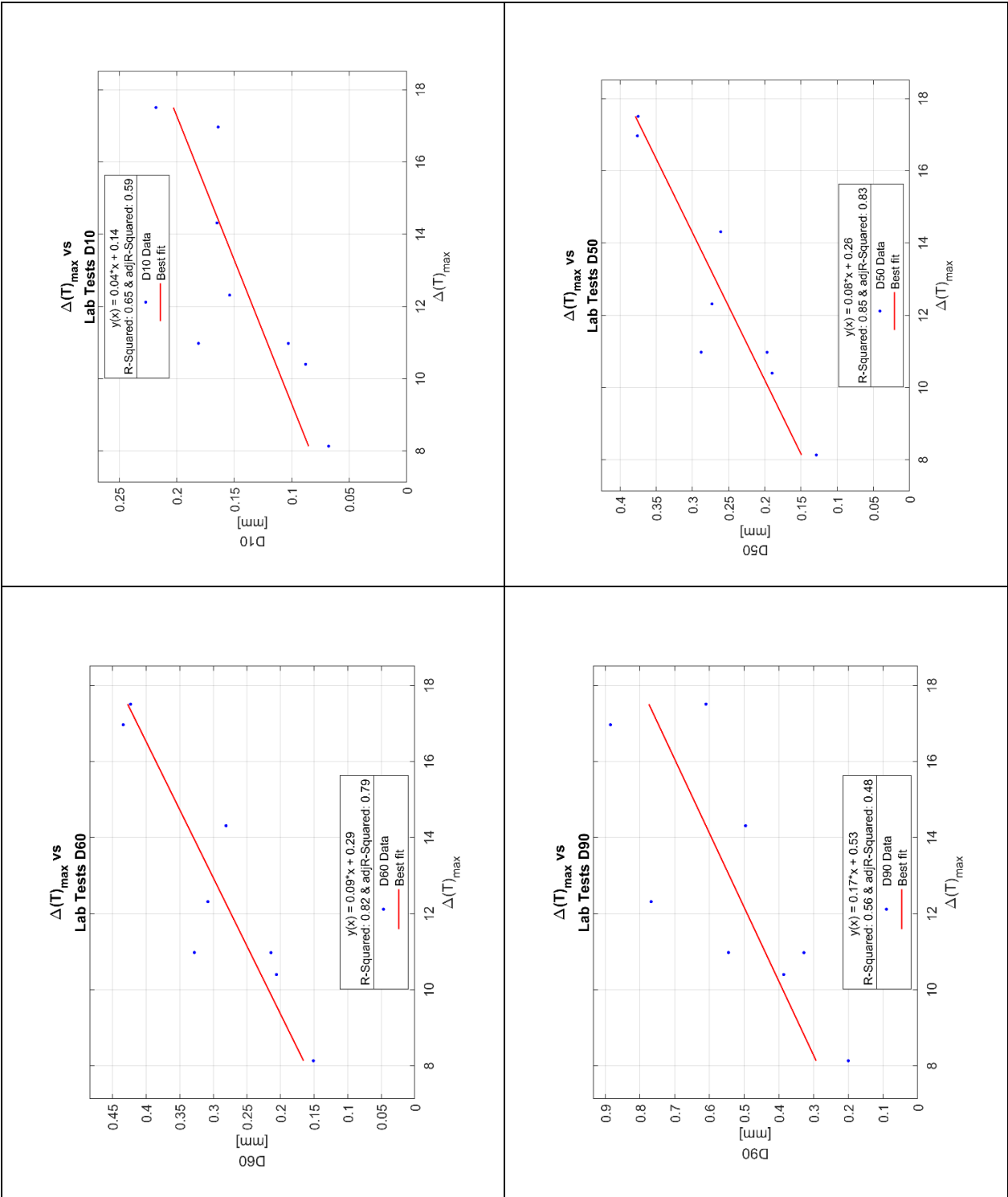


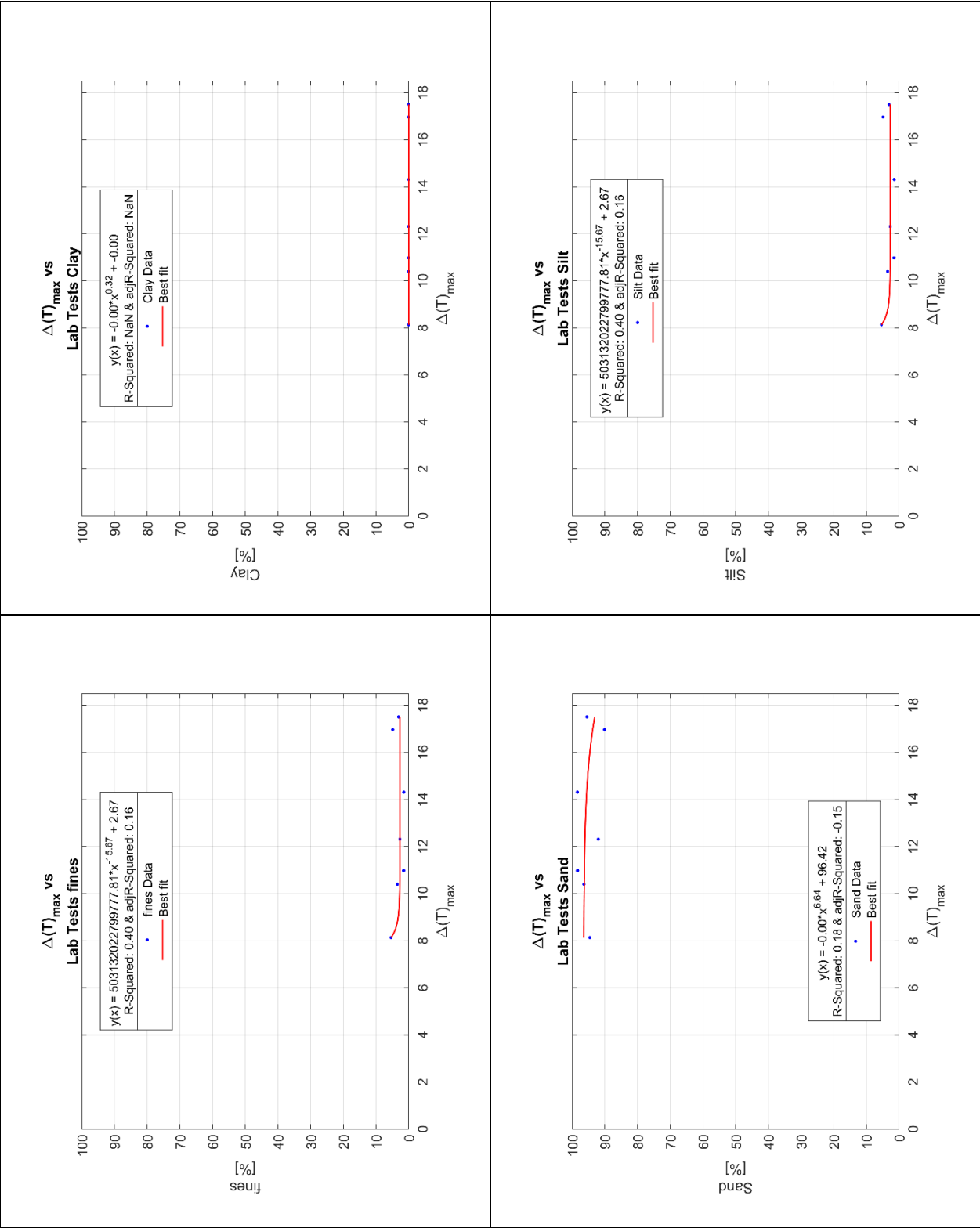


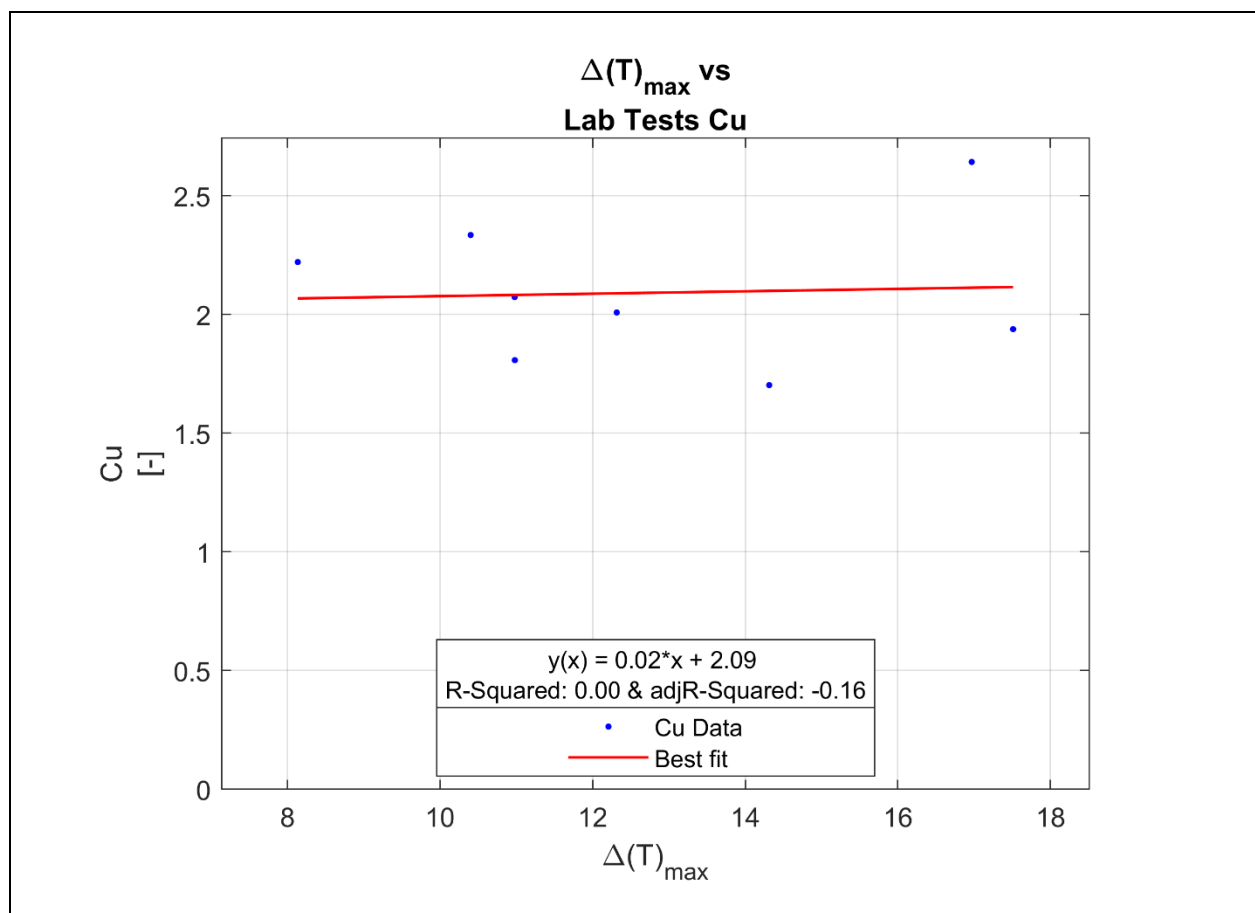




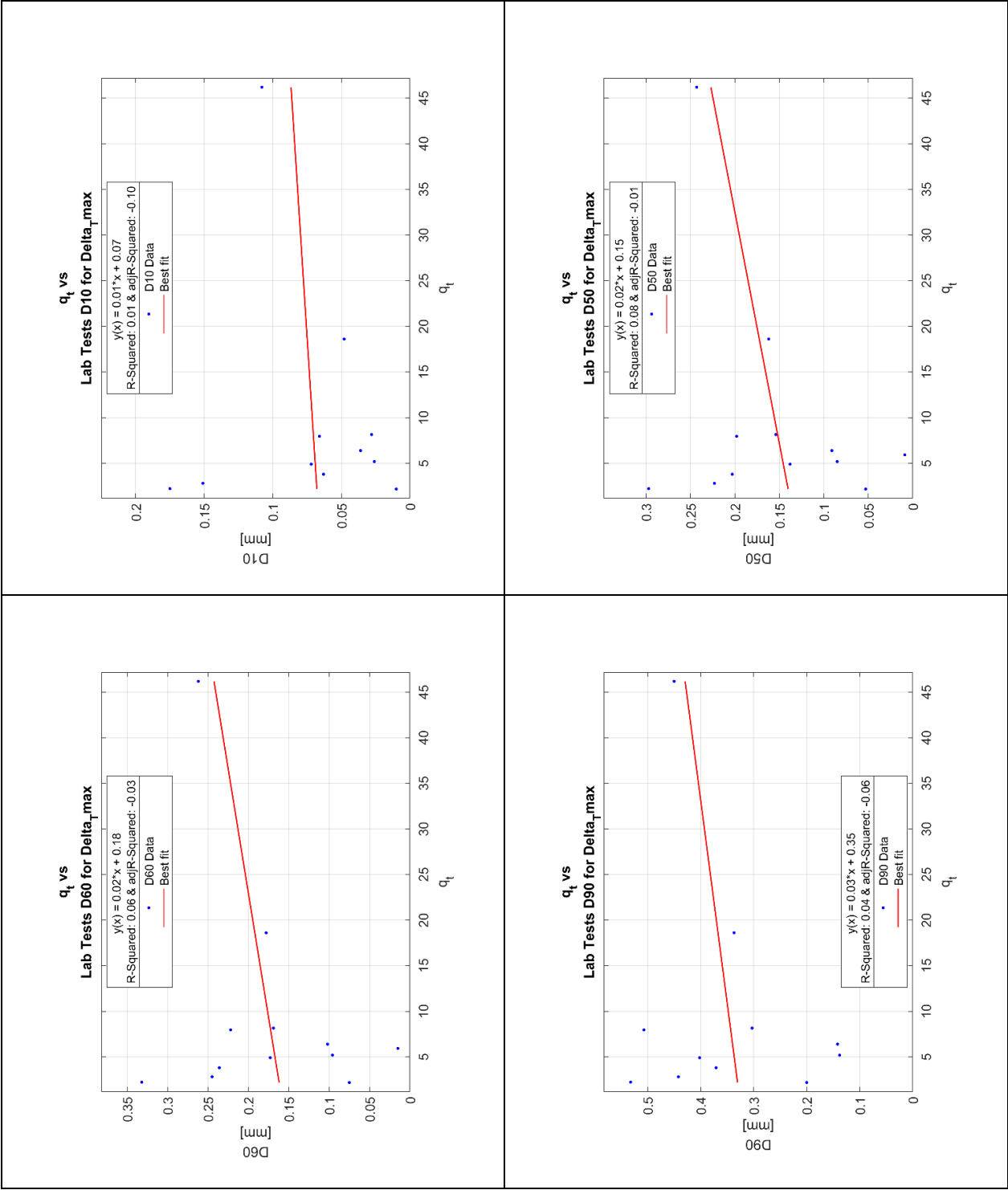
Appendix X $\Delta(T)_{\max}$ vs Laboratory Tests Regression Investigation From Additional Database







Appendix XI Cone Tip Resistance, q_t , vs Particle Size Distribution



Appendix XII Sleeve Friction, f_s , vs Particle Size Distribution

